

TRIPLE-BOND METATHESIS WITH GROUP 6 NITRIDO COMPLEXES: THE
IMPORTANCE OF LIGAND IDENTITY AND THE DEVELOPMENT OF XXX
PINCER LIGANDS

by

Eric Scott Wiedner

A dissertation submitted in partial fulfillment
of the requirements for the degree of
Doctor of Philosophy
(Chemistry)
in The University of Michigan
2009

Doctoral Committee:

Associate Professor Melanie S. Sanford, Co-Chair
Assistant Professor Marc J. A. Johnson, Co-Chair
Professor Mark M. Banaszak Holl
Professor Richard M. Laine

© Eric Scott Wiedner

All Rights Reserved
2009

Acknowledgements

There are a number of people I would like to thank for their support in helping me get to this point. First I would like to thank Professor Marc Johnson for the opportunity to work in his lab. His ideas and chemical insight were always welcome and appreciated, and helped guide my research focus to improve the chemistry that I was investigating. I have learned a lot about being a scientist over the last several years, and Marc has played an important role in the process. I would also like to thank my committee members (Professors Banaszak Holl, Laine, and Sanford) for their direction and perspectives on my research. I would also like to thank Professor Sanford for the opportunity to rotate in her lab, which was very enjoyable and made my decision on which lab to join very difficult.

The Johnson group members were the people I saw most on a day to day basis. Robyn Gdula was always full of energy and helped me to feel welcome when I first joined the lab. I shared many lunches with her at NYPD, and her trips to Espresso Royale helped start me down the path towards the coffee addiction that I now enjoy so much. Steve Caskey was a great deskmate and always set a great example of how to do science well. Once I realized he isn't actually a scary person, I found he had a great sense of humor, and his jokes always caught me off guard. Michael Stewart was an amazing labmate and friend. He always went out of his way to teach me about synthetic techniques, glovebox maintenance (which could fill an entire thesis chapter itself!), and more. Additionally, Michael was very generous with the metal complexes he made, and let me use a wide variety of them for various experiments. I had many great conversations with Michael on topics ranging from Michigan football to how a *good* glovebox should be built. Andrea Geyer was always fun to work with, especially during our first year when she fed me leftovers on a regular basis. Because our projects overlapped quite a bit, we were always bouncing chemistry ideas off of each other, and I know that we both benefited from it. I also want to thank Andrea for giving me an excuse to eat at Wendy's far more often than I should have. Marisa Macnaughtan is quite an interesting person, and always had very different ideas on topics ranging from politics to how to make Grubbs' catalyst (her lab-coat extraction was unorthodox but quite effective!). She was great at helping keep up my morale, and for helping with the many paper-cuts that I acquired in the lab. Meghan Wagner was always good spirited and fun to work with. Brannon Gary was extremely helpful in teaching me how to perform DFT calculations; without his help my DFT work would have taken three times longer. Yi-Joon (EJ) Ahn was always pleasant and fun to talk to, and the lab undergrads were fun to work with, including Rob Dood, Barry Leonard, Tim Tseng, Ryan Pakula, Nicola Kuhlman, Jason Wu, Michael Holland, and Joel Goodman.

A lot of other friends throughout the department made my time at Michigan very memorable. Mike Bury, Cornelius "Corn" Kristalyn, and Ben Thompson were fantastic housemates. Coincidentally, my beer drinking and video game playing probably reached

their peak when I lived with them at Woodbury. Kami Hull was always fun to go to the bar with, while Allison Dick and Trisha Duffey always stomped me at Dance Dance Revolution. Anna Merkle, Corinne Sulok, and Deidra Gerlach always listened if I wanted to complain about something, and were really helpful in proofreading my thesis and listening to practice talks. A number of other people were also good friends, including Valerie Cwynar, Lopa Desai, Tim DeVries, Dipannita Kalyani, Becky Kelly, Josie Nakhla, Bob Rarig, and Leilani Zart.

The technical staff members were all incredibly helpful. Chris Kojiro and Eugenio Alvarado provided me with a lot of NMR assistance, and it was very pleasurable to work with them during my time as the NMR GSI. I am thankful to Jeff Kampf for refining all of my X-ray crystal structures, and to Jim Windak for running a number of MS on air-sensitive samples. Roy Wentz is a terrific glassblower and always found time to seal my air-sensitive elemental samples. Rich Giszczak was very helpful with whatever problem I brought to him, and Patti Fitzpatrick was invaluable in her assistance with ordering lab supplies.

I would also like to thank Professor Harvest Collier, my undergraduate research advisor at University of Missouri-Rolla. He introduced me to research very early in my career by letting me join his labs just after my freshman year. His endless optimism about chemistry was extremely contagious, and laid the groundwork for me to persevere in graduate school.

I would like to thank my family for the tremendous support they have given me. My parents Terry and Carol have always encouraged me in everything I have done, even though they may not have completely understood what I was actually doing. They have always been there when I have needed them, and I will never be able to thank them enough. My parents-in-law, Dr. David and Karen Deeter, are also wonderful, and I thank them for taking me into their family and for all of the support they have given. Finally, I would like to thank my wife Susan for her strength, support, encouragement, and patience. I can always share a laugh with her when it is needed most, and her fantastic cooking keeps me very well fed. She has been my best friend throughout the most difficult parts of grad school, which has made a world of difference for me.

Table of Contents

Acknowledgements.....	ii
List of Figures	vii
List of Schemes.....	ix
List of Tables	xii
List of Appendices	xiii
List of Abbreviations	xiv
Chapter 1: Overview of Triple Bond Metathesis, XXX Pincer Ligands, and Electronically Tunable Pincer Ligands.....	1
1.1 Triple Bond Metathesis Overview	1
1.2 Early Hetero- and Homogeneous ACM Catalysts	6
1.3 Tungsten Alkylidyne ACM Catalysts	7
1.4 Molybdenum Alkylidyne ACM Catalysts	9
1.5 Mo ACM Catalysts via Mo(N[R]Ar) ₃	12
1.6 Mo ACM Catalysts via N≡[Mo] Complexes	15
1.7 Applications of ACM.....	17
1.8 Nitrile–Alkyne Cross Metathesis	21
1.9 Trianionic (XXX) Pincer Ligands	24
1.10 Electronic Tuning of Pincer Ligands	29
1.11 Thesis Goals.....	32
1.12 References.....	33
Chapter 2: Nitrile-Alkyne Cross Metathesis with Group 6 Nitride Complexes	37
2.1 Introduction.....	37
2.2 Substrate Scope of [W]≡N Catalysts	37
2.3 Arylene Ethynylene Macrocycles via NACM	41
2.4 Design of Mo NACM Catalysts.....	44
2.5 Protonolysis of N≡Mo(NMe ₂) ₃	46
2.6 Protonolysis of N≡Mo(N[R]Ar) ₃	52
2.7 ACM Studies of Mo Nitride Complexes	54
2.8 NACM Studies of Mo Nitride Complexes.....	56
2.9 Conclusions.....	60

2.10 Experimental	61
2.10.1 Methods.....	61
2.10.2 Materials	62
2.10.3 Synthetic Procedures.....	64
2.10.4 Substrate Compatibility Studies with 2.1	72
2.10.5 Additional Protonolysis Reactions.....	79
2.10.6 ACM Studies.....	81
2.10.7 NACM Concentration Studies with 2.23	83
2.10.8 Attempted NACM with [Mo] Complexes	84
2.11 References.....	87
 Chapter 3: Design and Synthesis of Trianionic (XXX) Pincer Ligands.....	89
3.1 Introduction.....	89
3.2 Bis-Imidazole Ligand.....	91
3.3 Trianion Generation.....	95
3.4 Monoanion Generation	99
3.5 Synthesis of XXX Precursors Containing Three Acidic Protons	101
3.6 Conclusions.....	106
3.7 Experimental	107
3.7.1 Methods.....	107
3.7.2 Materials	108
3.7.3 Synthetic Procedures.....	109
3.7.4 Other Reactions.....	117
3.8 References.....	132
 Chapter 4: Synthesis and Theoretical Investigations of Zr Complexes Containing a Charge-Versatile XXX Pincer Ligand	134
4.1 Introduction.....	134
4.2 Ancillary Ligand Substitution.....	135
4.3 Peripheral <i>N</i> -atom Alkylation	140
4.4 Peripheral <i>N</i> -atom Borylation	142
4.5 Peripheral <i>N</i> -atom Silylation.....	145
4.6 Other Silylation Pathways.....	150
4.7 Computational Investigations	152
4.8 Conclusions.....	159
4.9 Experimental	160
4.9.1 Methods.....	160
4.9.2 Materials	161
4.9.3 Synthetic Procedures.....	161
4.9.4 Silylation Reactions	168
4.9.5 Other Reactions.....	173
4.9.6 Computational Details	177
4.10 References.....	178

Chapter 5: Conclusions and Future Directions	179
5.1 Conclusions.....	179
5.2 Nitrile-Alkyne Cross Metathesis.....	180
5.3 XXX Pincer Ligand Development.....	181
5.4 Future Directions	183
5.5 References.....	186
Appendices.....	187

List of Figures

Figure 1.1. Mo complexes observed or isolated from Furstner's ACM system.	13
Figure 1.2. Arylene-ethynylene macrocycles synthesized via ACM.	20
Figure 1.3. Milstein's 3,5-lutidine PCP ligand.	30
Figure 2.1. W-NACM catalysts.	38
Figure 2.2. Unsuccessful substrates for macrocycle formation.	41
Figure 2.3. 50 % thermal ellipsoid plot of 2.18	49
Figure 2.4. 50 % thermal ellipsoid plot of 2.21	51
Figure 2.5. Statistical equilibrium mixture of ACM with 1-phenyl-1-butyne.	54
Figure 2.6. Design of NACM test reaction.	56
Figure 2.7. Conversion to NACM products catalyzed by 2.23	57
Figure 2.8. Catalyst reaction pathways in NACM with 2.22	58
Figure 2.9. Literature complexes tested for NACM.	60
Figure 3.1. Monodentate vs. tridentate ligand coordination in NACM transition state.	89
Figure 3.2. Comparison of known and proposed Ru alkylidyne complexes.	90
Figure 3.3. Proposed use of 1,3-bis(4,5-diaryl-1 <i>H</i> -imidazol-2-yl)benzene molecules as XXX pincer ligands.	91
Figure 4.1. 50 % thermal ellipsoid plot of the molecular anion of 4.3	137
Figure 4.2. 50 % thermal ellipsoid plot of the molecular anion of 4.4	138
Figure 4.3. 50 % thermal ellipsoid plot 4.6	141
Figure 4.4. 50 % thermal ellipsoid plot of 4.12	147

Figure 4.5. 50 % thermal ellipsoid plots of the front views showing the planarity of 4.6 and the non-planarity of 4.12	148
Figure 4.6. Structures modeled by computation.	152
Figure 4.7. Effect of χ_P on $\Delta q(\text{Zr})$	155
Figure 4.8. Pictorial description of the D-A stabilization energy ($\Delta E_{i \rightarrow j^*}^{(2)}$).....	157
Figure 4.9. Assigned Lewis structure for NBO calculations.	157
Figure 4.10. Effect of χ_P on Δ D-A stabilization energy.....	158

List of Schemes

Scheme 1.1. Triple–bond metathesis reactions.....	1
Scheme 1.2. Possible ACM mechanisms.....	2
Scheme 1.3. Formation of azametalacyclobutadiene species.	5
Scheme 1.4. Formation of a Ti azametalacycle.	5
Scheme 1.5. Synthesis of tungsten alkylidyne complexes.....	7
Scheme 1.6. Synthesis of alkyl-alkoxide neopentylidyne complexes.	8
Scheme 1.7. Synthesis of molybdenum alkylidyne complexes.	10
Scheme 1.8. Molybdenum alkylidyne formation through Mo≡Mo bond scission.	11
Scheme 1.9. Cummins' molybdenum alkylidyne synthesis.	12
Scheme 1.10. Moore's reductive recycle strategy.	14
Scheme 1.11. Reactions of Mo nitride complexes with alkynes.	15
Scheme 1.12. Routes to obtain Mo nitride complexes.....	17
Scheme 1.13. Tandem RCAM – Lindlar reduction to give cyclic Z-alkenes.....	17
Scheme 1.14. RCAM step in total synthesis of epothilone C.....	18
Scheme 1.15. Poly(arylene-ethylene)'s via ACM.	19
Scheme 1.16. Carbazole macrocycle synthesis via precipitation-driven ACM.....	21
Scheme 1.17. Known W alkylidyne and nitride complex interconversions.	22
Scheme 1.18. Effect of alkoxide donor strength on relative energies of W nitride and alkylidyne complexes.....	23
Scheme 1.19. Schrock's XXX ligands.....	24

Scheme 1.20. Bercaw's XXX pincer ligand.	25
Scheme 1.21. Veige's XXX pincer ligand.	26
Scheme 1.22. Veige's [NCN] ³⁻ Hf complexes.	27
Scheme 1.23. Redox active ONO pincer ligand.	28
Scheme 1.24. Redox active NNN pincer ligand.	28
Scheme 1.25. Sequential protonation of Rh(SNS)(CO).	31
Scheme 1.26. Redox state switching induced through pincer ligand deprotonation.	32
Scheme 2.1. Synthesis of an arylene ethynylene tetramer using NACM.	42
Scheme 2.2. Formation of silicon-containing macrocycles by NACM.	44
Scheme 2.3. Synthesis of 2.13	46
Scheme 2.4. Protonolysis of 2.13 with HOSiPh ₃	47
Scheme 2.5. Protonolysis of 2.13 with HOSiPh ₂ ^t Bu.	48
Scheme 2.6. Protonolysis of 2.13 with HOCPh ₂ Me.	48
Scheme 2.7. Protonolysis of 2.13 with substituted phenols.	50
Scheme 2.8. Protonolysis of N≡Mo(N[^t Bu]Ar) ₃ with HOSiPh ₃	52
Scheme 2.9. Protonolysis of N≡Mo(N[ⁱ Pr]Ar) ₃ with HOSiPh ₂ ^t Bu.	53
Scheme 3.1. Synthesis of imidazole 3.3	92
Scheme 3.2. Known pincer ligand transmetalation from Zr to Rh.	93
Scheme 3.3. Zr mediated activation of 3.3	93
Scheme 3.4. Attempted XXX transmetalation from 3.6	95
Scheme 3.5. Synthesis of imidazoles NCN-X-H ₂	96
Scheme 3.6. Tri-lithiation followed by deuterium quenching.	97
Scheme 3.7. Tri-anion formation using a Grignard reagent.	98

Scheme 3.8. Synthesis of potential LXL precursors NCN-X-Me ₂	100
Scheme 3.9. Lithiation to give an LXL precursor 3.17	101
Scheme 3.10. Attempted synthesis of desired 2,5-bisimidazole-pyrrole.	102
Scheme 3.11. Paal-Knorr synthesis of 3.12	103
Scheme 3.12. Attempted dione formation with an N-protected imidazole.	104
Scheme 3.13. Synthesis of an NNN-H ₃ ligand precursor.	106
Scheme 4.1. Interaction of XXX ligand with Lewis acids (LA).	134
Scheme 4.2. Ancillary ligand substitution of 4.1	136
Scheme 4.3. Synthesis of 4.4	138
Scheme 4.4. Halide metathesis to give 4.5	139
Scheme 4.5. N-atom methylation to give 4.6	140
Scheme 4.6. N-atom borylation with BH ₃ •SMe ₂ to give 4.7	143
Scheme 4.7. N-atom borylation with BF ₃ •Et ₂ O to give 4.9	144
Scheme 4.8. N-atom silylation of 4.3 with TMSI.	146
Scheme 4.9. N-atom silylation with TMSOTf.	149
Scheme 4.10. Silyl group cleavage with [TBA]Cl.	150
Scheme 4.11. Alternative silylation pathway.	151
Scheme 5.1. Use of NNN-Tl ₃ as a pincer ligand transfer reagent.	184
Scheme 5.2. Possible effect of NNN size on metathesis reactivity.	185

List of Tables

Table 2.1. Nitrile substrates tolerated in NACM.	39
Table 2.2. Catalyst deactivation modes (indicated by Y) with incompatible substrates. ..	40
Table 2.3. Catalytic ACM of 1-phenyl-1-butyne.....	55
Table 2.4. NACM studies with 2.23	84
Table 3.1. Results of tri-lithiation reactions.....	97
Table 4.1. Calculated Gibbs energy of C ₁ and C _{2v} structures.	153
Table 4.2. Natural charges <i>q</i> of the inner coordination sphere calculated by NPA.	154
Table 4.3. D-A stabilization energies in units of kcal mol ⁻¹	159

List of Appendices

Appendix

1 Crystallographic Data for $\text{N}\equiv\text{Mo}(\text{OCPh}_2\text{Me})_3(\text{NHMe}_2)$	188
2 Crystallographic Data for $\text{N}\equiv\text{Mo}(\text{OAr})_3(\text{NHMe}_2)$ ($\text{Ar} = 2,6\text{-}^i\text{Pr}_2\text{C}_6\text{H}_3$).	200
3 Crystallographic Data for $[\text{TBA}]_2[\text{Zr}(\text{XXX})\text{Cl}_3]$	211
4 Crystallographic Data for $[\text{TBA}]_2[\text{Zr}(\text{XXX})\text{Br}_3]$	222
5 Crystallographic Data for $\text{Zr}(\text{LXL-Me}_2)\text{Cl}_3$	235
6 Crystallographic Data for $\text{Zr}(\text{LXL}-(\text{SiMe}_3)_2)\text{ClI}_2$	248
7 Atomic Coordinates for Geometry Optimized Computational Structures.....	265

List of Abbreviations

ACM	alkyne cross-metathesis
AM	alkyne-metathesis
Anal	elemental analysis
Ar	aryl
br	broad
^t Bu	CMe ₃
<i>n</i> -Bu	(CH ₂) ₃ CH ₃
C ₆ D ₆	benzene- <i>d</i> ₆
Calcd	calculated
CD ₂ Cl ₂	dichloromethane- <i>d</i> ₂
CDCl ₃	chloroform- <i>d</i>
cm ⁻¹	wavenumber
Cp	cyclopentadienyl
Cy	cyclohexyl
d	day(s), doublet
DFT	density functional theory
DME	1,2-dimethoxyethane
DMF	N,N-dimethylformamide
DMSO	dimethylsulfoxide
D-A	donor - acceptor

EI MS	electron impact mass spectrometry
Et	ethyl
EtCN	propionitrile
Et ₂ O	diethyl ether
equiv	equivalent(s)
g	grams
G	Gibbs energy
GC/MS	gas chromatography mass spectrometry
GOF	goodness of fit
¹ H	proton
h	hour(s)
HRMS	high-resolution mass spectroscopy
Hz	hertz
kcal	kilocalorie(s)
LXL	monoanionic, monoanionic pincer ligand
lp	lone pair of electrons
lp*	non-Lewis lone pair of electrons
m	multiplet
M	molar, mega
MALDI	matrix-assisted-laser-desorption-ionization
Me	methyl
MeCN	acetonitrile
mg	milligrams

min	minute(s)
mL	milliliters
mol	moles
mmol	millimoles
NACM	nitrile-alkyne cross metathesis
NBO	natural bond orbital
NCN	nitrogen-carbon-nitrogen pincer ligand
NMR	nuclear magnetic resonance
NNN	nitrogen-nitrogen-nitrogen pincer ligand
NPA	natural population analysis
ORTEP	oak ridge thermal ellipsoid plot
OTf	OSO ₂ CF ₃
q	quartet, atomic charge
Ph	phenyl
POSS	polyhedral oligomeric silsesquioxane
ppm	parts per million
ⁱ Pr	CH(Me) ₂
py	pyridine
R	alkyl
s	singlet
t	triplet
TBA	tetra- <i>n</i> -butyl ammonium
THF	tetrahydrofuran

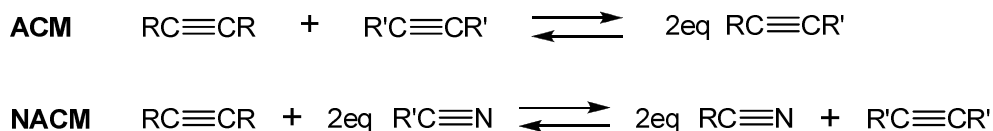
TMA	tetramethylammonium
TMS	trimethylsilyl
TOF	time-of-flight
XRD	x-ray diffraction
XXX	trianionic, trianionic pincer ligand
°C	degrees Celsius
Å	angstroms
δ	chemical shift in ppm downfield from zero
Δ	algebraic difference
$\Delta v_{1/2}$	peak width at half height
μL	microliter(s)
χ_{P}	Pauling electronegativity
\equiv	triple bond

Chapter 1

Overview of Triple Bond Metathesis, XXX Pincer Ligands, and Electronically Tunable Pincer Ligands

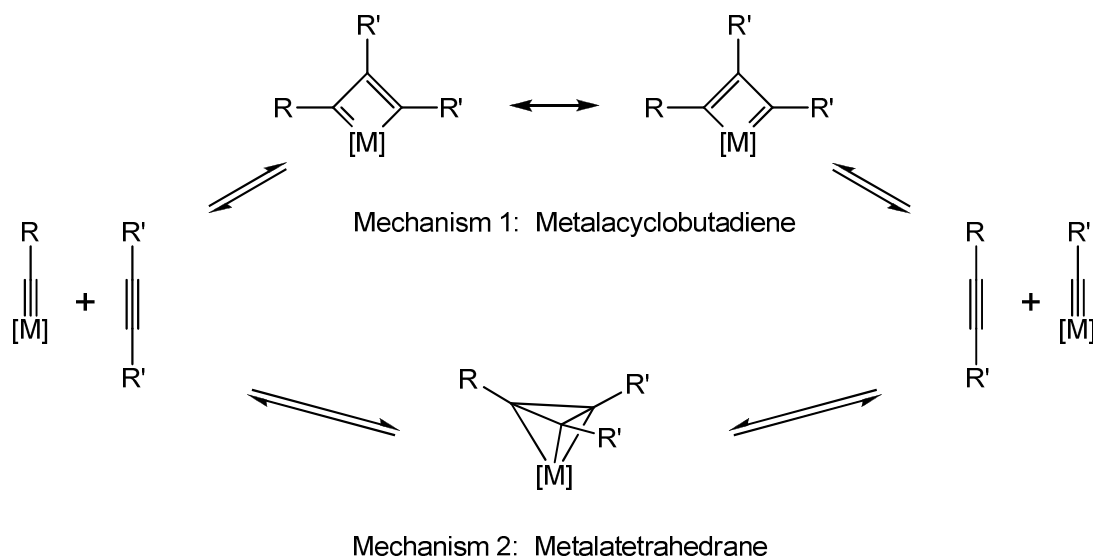
1.1 Triple Bond Metathesis Overview

Catalytic–triple bond metathesis is a growing field that has found application in both natural product and conjugated macrocycle synthesis.¹⁻⁵ The most common form of triple–bond metathesis is alkyne cross metathesis (ACM), in which two organic alkyne fragments are interconverted to yield a new C-C triple bond (Scheme 1.1). A drawback to ACM is the need for the desired substrate to possess a preexisting alkyne functional group. As nitrile functional groups are typically more readily introduced than alkyne groups,⁶⁻⁸ nitrile alkyne cross metathesis (NACM) is an appealing process in which an organic nitrile and an alkyne are metathesized to give a new alkyne and a new nitrile species (Scheme 1.1). Both ACM and NACM are equilibrium processes, and so a driving force is required to achieve complete conversion to the desired product species.



Scheme 1.1. Triple–bond metathesis reactions.

ACM is typically catalyzed by Group 6 (Mo, W) alkylidyne species, which can be generated *in situ* or used as discrete complexes. Two plausible mechanisms have been proposed for ACM. In the first mechanism, the metal alkylidyne complex undergoes a [2+2] cycloaddition with an alkyne to generate a metalacyclobutadiene intermediate; subsequent [2+2] cycloreversion yields a new alkyne and a new alkylidyne complex (Scheme 1.2).⁹ A second possible mechanism is the formation of a metalatetrahedrane intermediate, which then breaks up to give the new alkyne and alkylidyne complex.¹⁰



Scheme 1.2. Possible ACM mechanisms.

Both metalacyclobutadiene^{11, 12} and metalatetrahedrane^{10, 13} complexes have been isolated; some examples of the former are active for ACM, while no examples of the latter have been shown to catalyze ACM.¹⁴ Theoretical calculations on the model system $\text{HC}\equiv\text{MoCl}_3 + \text{HC}\equiv\text{CH}$ reveal that the parallel approach of the alkyne to the alkylidyne group is symmetry-allowed, leading to the formation of a metalacyclobutadiene

complex.¹⁵ However, the corresponding perpendicular approach leading to a metalatetrahedrane was found to be symmetry-forbidden, indicating that such a pathway would have a high energy barrier.¹⁵ The same study also found the metalatetrahedrane $\text{Mo}(\eta^3\text{-C}_3\text{H}_3)\text{Cl}_3$ to be 52 kJ mol^{-1} more stable in energy than the corresponding metalacyclobutadiene $\text{Mo}(\eta^2\text{-C}_3\text{H}_3)\text{Cl}_3$,¹⁵ suggesting that metalatetrahedrane complexes may be catalyst deactivation products in ACM systems. On the other hand, some metalacyclobutadienes are active ACM catalysts. As such, it is currently accepted that ACM proceeds through a metalacyclobutadiene intermediate.

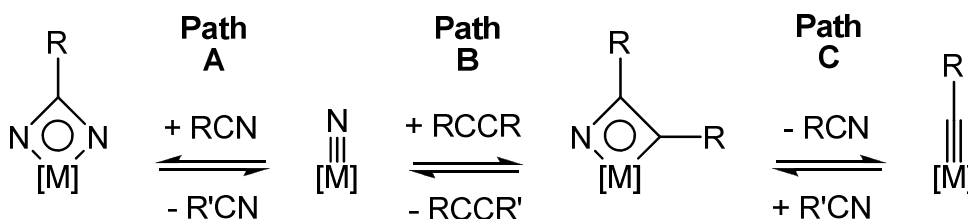
Most ACM catalysts have the general formula $\text{RC}\equiv\text{M}(\text{OR}')_3$ with $\text{M} = \text{Mo}, \text{W}$. For these catalysts, several important reactivity trends have been noted. First, a more Lewis acidic metal center corresponds to an increase in the rate of ACM.¹⁴ One manner of raising the metal acidity is to use a less donating alkoxide ligand. This effect is noted both computationally¹⁶ and experimentally, as $\text{RC}\equiv\text{Mo}(\text{OC}(\text{CF}_3)_2\text{Me})_3$ is active for ACM while $\text{RC}\equiv\text{Mo}(\text{OCMe}_3)_3$ is not.¹⁷ A second method to increase the metal acidity is to use a less electronegative metal while retaining the same alkoxide identity. For example, $\text{RC}\equiv\text{W}(\text{OCMe}_3)_3$ catalyzes ACM while the corresponding Mo complex does not.^{17, 18} The lower acidity for Mo relative to W also results in Mo catalysts displaying a higher tolerance of polar functional groups.⁴ Finally, the decreased spatial extent of the Mo 4d orbitals relative to the W 5d orbitals results in a higher activation barrier for metalacyclobutadiene formation with Mo than with W given the same ligand set.¹⁶

Typically ACM is limited to internal alkyne substrates. In some instances terminal alkynes can undergo ACM,¹⁹ however the turnover numbers are very low. One proposed reason for the failure of terminal alkynes to undergo ACM is that degenerate

metathesis occurs, thus preventing productive ACM.¹⁷ A second obstacle is the formation of catalytically inactive deprotonated metalacyclobutadiene species, of which a variety have been isolated for both Mo and W.^{17, 20} Additionally, both terminal alkynes and internal alkynes can be polymerized by alkylidyne complexes. Steric factors are important in the polymerization side reaction, as both smaller alkoxide ligands and smaller alkynes lead to larger amounts of polymerization products.^{11, 19} The composition of the poly(alkyne) products remain elusive, leading to uncertainty in the polymerization mechanism. Current theories for polymer formation include a ring expansion mechanism,²¹ a bimolecular mechanism,²² and the presence of trace alkylidene complexes, which are known to polymerize alkynes.^{19, 23, 24}

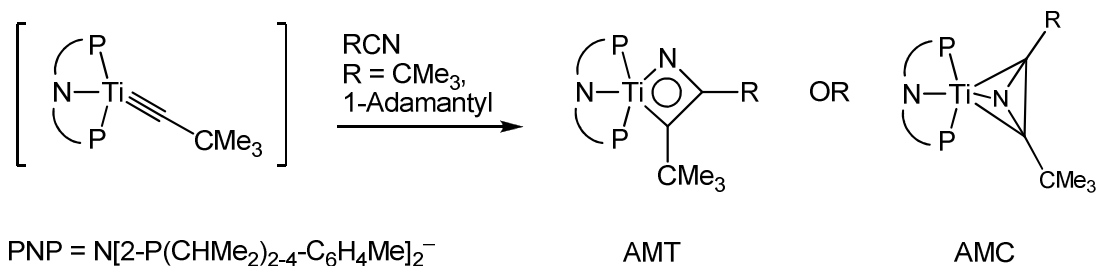
Azametallacyclobutadiene species can also be formed as unobserved intermediates in a variety of reactions (Scheme 1.3). Complexes $\text{N}\equiv\text{W}(\text{O}^t\text{Bu})_3$,²⁵ $\text{N}\equiv\text{Mo}(\text{OC}(\text{CF}_3)_2\text{Me})_3$,²⁶ and $\text{N}\equiv\text{Mo}(\text{OC}(\text{CF}_3)_3)_3(\text{NCMe})$ ²⁶ have been shown to react with ¹⁵N labeled nitriles to generate the corresponding ¹⁵N≡[M] complexes. The mechanism is assumed to proceed through a diazametallacyclobutadiene intermediate, which is not observed (Path A, Scheme 1.3). Monoazametallacyclobutadiene intermediates can be formed through reaction of either a metal nitride complex with an alkyne (Path B)²⁷ or a metal alkylidyne complex with a nitrile (Path C).²⁸⁻³² The ancillary ligand identity has been found to influence the relative thermodynamic stability of W and Mo nitride and alkylidyne complexes. Strong alkoxide donors typically favor the more oxidizing nitride ligand over the alkylidyne ligand.³³ Conversely, weak alkoxide ligands favor the less oxidizing alkylidyne ligand over the nitride ligand.³³ For a given ligand set, if there is a large energy difference between the alkylidyne and nitride complexes, then no

equilibrium between the two species can be established. However, if the energies of the alkylidyne and nitride complexes are close enough to allow reversible interconversion, then NACM is possible.^{34, 35}



Scheme 1.3. Formation of azametallacyclobutadiene species.

While a wide variety of metallacyclobutadienes have been isolated, there are no examples of Group 6 azametallacyclobutadiene complexes. In one case, an azametallacyclobutadiene (AMC) was formed and isolated from the reaction between a transient Ti alkylidyne complex with a nitrile (Scheme 1.4).³⁶ An X-Ray structure could not be obtained to definitively exclude the possibility of an azametallatetrahedrane (AMT) structure. Support for the AMC geometry came from DFT calculations which found it to be the more stable isomer by 40 kcal / mol.³⁶ Additionally, the calculated ¹⁵N NMR chemical shift of δ 676 ppm matched well to the experimental chemical shift of δ 672.6 ppm (reference to NH₃(l) at 0 ppm).³⁶



Scheme 1.4. Formation of a Ti azametallacycle.

1.2 Early Hetero- and Homogeneous ACM catalysts

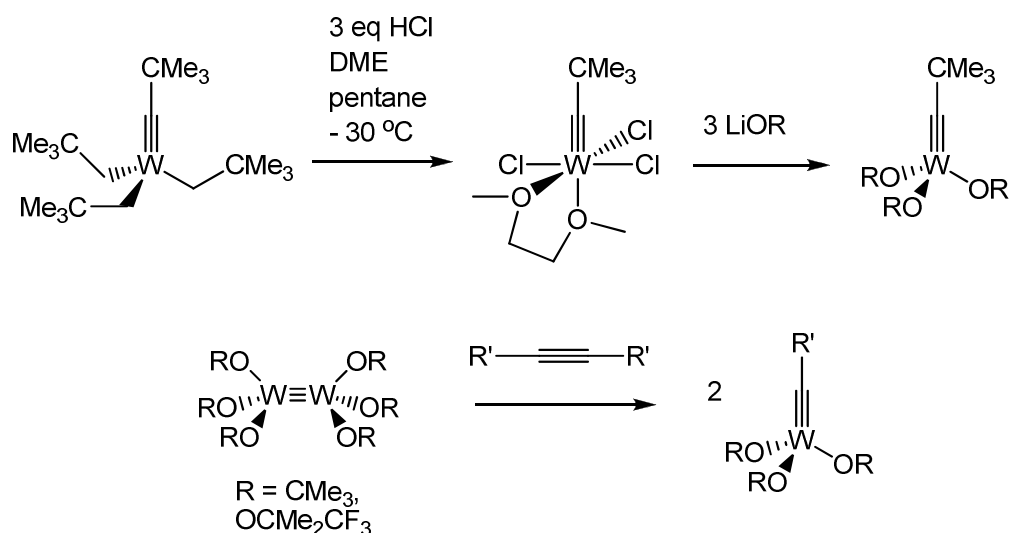
The first ACM catalysts were heterogeneous silica-supported tungsten oxide species.^{37, 38} These systems operated in a continuous flow reactor over a temperature range of 100–500 °C. Large amounts of aromatic byproducts were formed through a cyclotrimerization pathway, making these heterogeneous catalysts impractical for selective alkyne formation. The active species in these systems were proposed to be surface metal alkylidyne species, though no evidence has been reported to support this claim.

In 1974, Mortreaux and Blanchard extended ACM to the homogeneous phase with the discovery that an *in-situ* combination of Mo(CO)₆ and phenol gave an active ACM catalyst.³⁹ Later studies indicated that more acidic phenols can be used to generate more reactive catalyst mixtures.^{1, 40} The functional group tolerance of the system is high, with groups such as acetates, nitriles, amides, and sulfones being tolerated, among others.^{1, 40} As the catalyst precursors are inexpensive, commercial, and can be weighed directly in air, the Mo(CO)₆ system is quite convenient for use by organic chemists. However, low activity and high operating temperatures (140–150 °C) somewhat limit the system's utility. Additionally, the inability to identify the actual catalyst species makes systematic optimization difficult.

Some years later, an analogous W(CO)₆ catalyst mixture was discovered.⁴¹ The tungsten system is less attractive for ACM as it requires higher catalyst loadings and operating temperatures than the molybdenum system. Furthermore, the range of compatible functional groups is greatly reduced in the tungsten system.

1.3 Tungsten Alkylidyne ACM Catalysts

The first well-defined ACM catalyst was reported by Schrock in 1981.¹⁸ Schrock's original synthesis, shown in Scheme 1.5, involved treatment of $\text{Me}_3\text{CC}\equiv\text{W}(\text{CH}_2\text{CMe}_3)_3$ with HCl in the presence of DME to give $\text{Me}_3\text{CC}\equiv\text{WCl}_3(\text{DME})$. Subsequent treatment of $\text{Me}_3\text{CC}\equiv\text{WCl}_3(\text{DME})$ with a variety of lithium alkoxides led to isolation of a variety of neopentylidyne complexes, $\text{Me}_3\text{CC}\equiv\text{W}(\text{OR})_3$. An improved synthetic route was later discovered in which internal alkynes promote W-W triple-bond scission in $\text{W}_2(\text{OR})_6$ complexes (Scheme 1.5).^{42, 43}

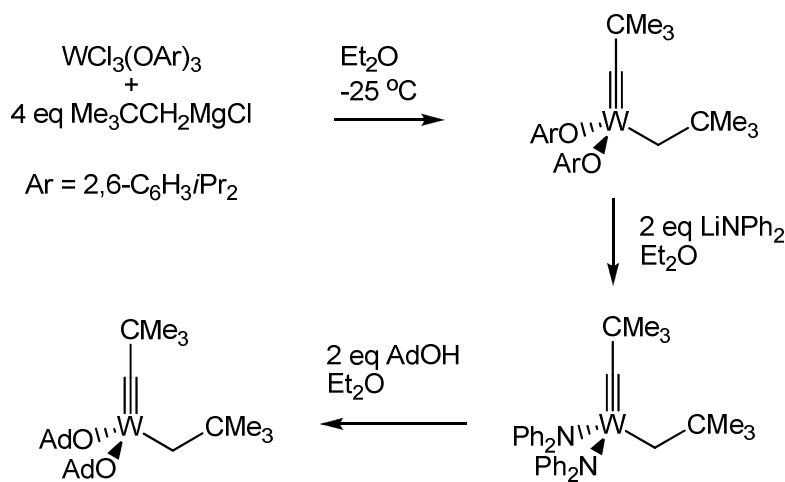


Scheme 1.5. Synthesis of tungsten alkylidyne complexes.

The prototypical catalyst $\text{Me}_3\text{CC}\equiv\text{W}(\text{OCMe}_3)_3$, which is now commercially available, is far more active than the early ill-defined ACM systems. At $25\text{ }^\circ\text{C}$, unsymmetrical internal alkynes are metathesized to an equilibrium of the unsymmetrical alkyne and the corresponding symmetrical alkyne in less than 4 hours.¹⁸ Catalysts

containing fluorinated *tert*-butoxide ligands $\text{OCMe}_n(\text{CF}_3)_{n-1}$ display even faster rates of ACM, with a higher degree of fluorination corresponding to a higher rate of metathesis.¹⁷ The size of the alkoxide ligand was found to be important as ligands smaller than *tert*-butoxide yield higher amounts of alkyne polymerization products relative to ACM products.¹¹ Despite the high catalytic activity, these alkylidyne complexes are highly sensitive to moisture, oxygen, and are incompatible with polar functional groups including thioethers, thiophenes, alcohols, amines, and crown ethers.^{2,4}

More recently, Schrock has reported a class of tungsten alkylidyne complexes containing mixed alkyl-alkoxide ancillary ligands.⁴⁴ As shown in Scheme 1.6, treatment of $\text{WCl}_3(\text{OAr})_3$ ($\text{Ar} = 2,6\text{-diisopropylphenoxide}$) with neopentyl Grignard leads to the formation of $\text{Me}_3\text{CC}\equiv\text{W}(\text{CH}_2\text{CMe}_3)(\text{OAr})_2$. Subsequent treatment with $\text{LiNPh}_2\cdot\text{Et}_2\text{O}$ and 1-adamantanol (HOAd) generates $\text{Me}_3\text{CC}\equiv\text{W}(\text{CH}_2\text{CMe}_3)(\text{OAd})_2$.



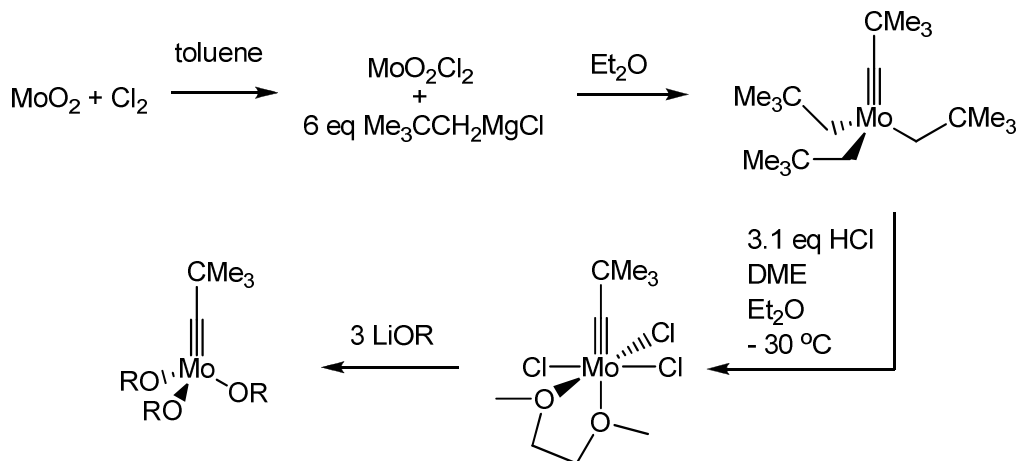
Scheme 1.6. Synthesis of alkyl-alkoxide neopentylidyne complexes.

The bis-aryloxide complex is a poor ACM catalyst as it requires more than 24 hours at room temperature to reach an equilibrium mixture of ACM products and generates large amounts of alkyne polymerization products. In the presence of 3-hexyne, the aryloxide catalyst exists predominantly at a metalacyclobutadiene resting state. Sluggish cycloreversion from the metalacyclobutadiene could account for both the slow ACM rate and the observed alkyne polymerization. Conversely, the bis-adamantoxide complex undergoes more rapid ACM, with an equilibrium mixture of products being observed in less than three hours at room temperature. The adamantoxide catalyst has a propylidyne resting state, indicating that cycloreversion from the metalacycle is rapid. The effect of the alkyl ligand on the functional group compatibility has not been reported at the present time.

1.4 Molybdenum Alkylidyne ACM Catalysts

Shortly after his initial report on the synthesis of W neopentylidyne complexes, Schrock reported a similar synthesis for the lighter congener $\text{Me}_3\text{CC}\equiv\text{Mo}(\text{CH}_2\text{CMe}_3)_3$.⁴⁵ Similar ligand substitutions allowed for the isolation of a variety of complexes with the form $\text{Me}_3\text{CC}\equiv\text{Mo}(\text{OR})_3$ (Scheme 1.7). Unlike the case of tungsten, the complex $\text{Me}_3\text{CC}\equiv\text{Mo}(\text{OCMe}_3)_3$ reacts very slowly with internal alkynes at room temperature. Use of $-\text{OCMe}_2\text{CF}_3$ as the alkoxide ligand improves the rate of metathesis for smaller alkynes, but the rates for larger alkynes such as 3-heptyne are still rather slow. Neopentylidyne complexes containing the alkoxide $-\text{OCMe}(\text{CF}_3)_2$ are even more active for ACM, with 3-heptyne being metathesized rapidly at room temperature. The complexes $\text{RC}\equiv\text{Mo}(\text{OAr})_3$ ($\text{OAr} = 2,6\text{-diisopropylphenoxide}$) were also found to be

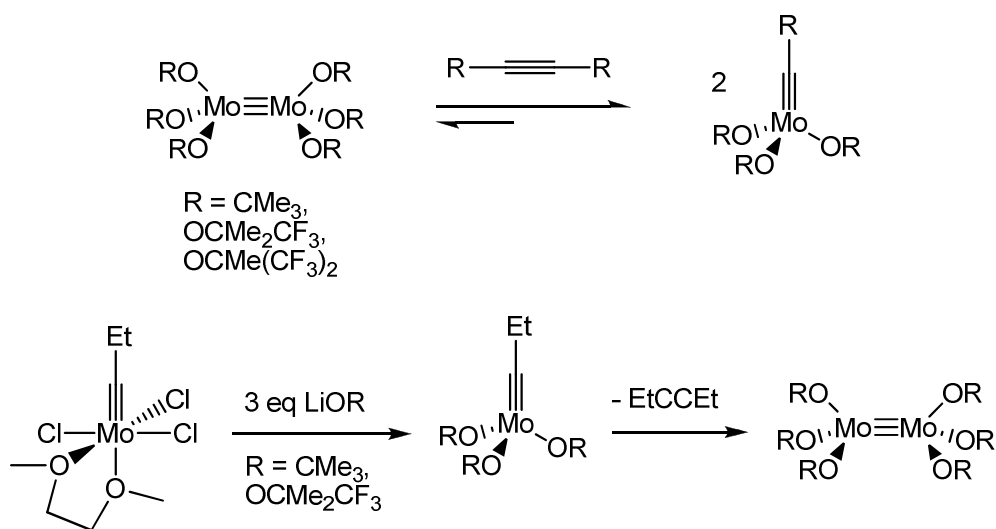
highly active ACM catalysts, with equilibrium mixtures formed in less than five minutes at room temperature.⁴⁵ For $\text{RC}\equiv\text{Mo}(\text{OAr})_3$, only the neopentylidyne complex ($\text{R} = \text{CMe}_3$) is a solid, while the propylidyne complex ($\text{R} = \text{Et}$) is reported to be an oil.¹⁷



Scheme 1.7. Synthesis of molybdenum alkylidyne complexes.

Unlike the tungsten analogue, $\text{Me}_3\text{CC}\equiv\text{Mo}(\text{CH}_2\text{CMe}_3)_3$ is not amenable to isolation on a large scale as the yields are low and purification is difficult. Dimolybdenum complexes $\text{Mo}_2(\text{OR})_6$ were originally thought to be unreactive towards triple-bond scission with alkynes, as no alkylidyne complexes were observed upon treatment with symmetrical internal alkynes.⁴⁶ Recently, Geyer discovered that $\text{Mo}_2(\text{OR})_6$ complexes do indeed catalyze ACM of unsymmetrical alkynes at temperatures ranging from 25–45 °C.⁴⁷ Heating the reaction mixtures to 75–85 °C allowed for the spectroscopic observation of the complexes $\text{PhC}\equiv\text{Mo}(\text{OR})_3$ ($\text{R} = \text{OCMe}_3, \text{OCMe}_2\text{CF}_3$), though the pure alkylidynes could not be isolated (Scheme 1.8). When $\text{R} = \text{OCMe}(\text{CF}_3)_2$, no buildup of an alkylidyne complex was observed, suggesting that only a trace amount of an alkylidyne complex is formed. The complexes $\text{Mo}_2(\text{OR})_6$ and $\text{R}'\text{C}\equiv\text{Mo}(\text{OR})_3$ were

concluded to exist in equilibrium, with more donating alkoxides displaying greater conversion to the benzyldiyne complex. This trend makes intuitive sense as stronger alkoxide donors should facilitate the formal Mo(III) to Mo(VI) oxidation. Additionally, the equilibrium lies much further to the right for the analogous W system (Scheme 1.5), since W is less electronegative than Mo and therefore easier to oxidize.

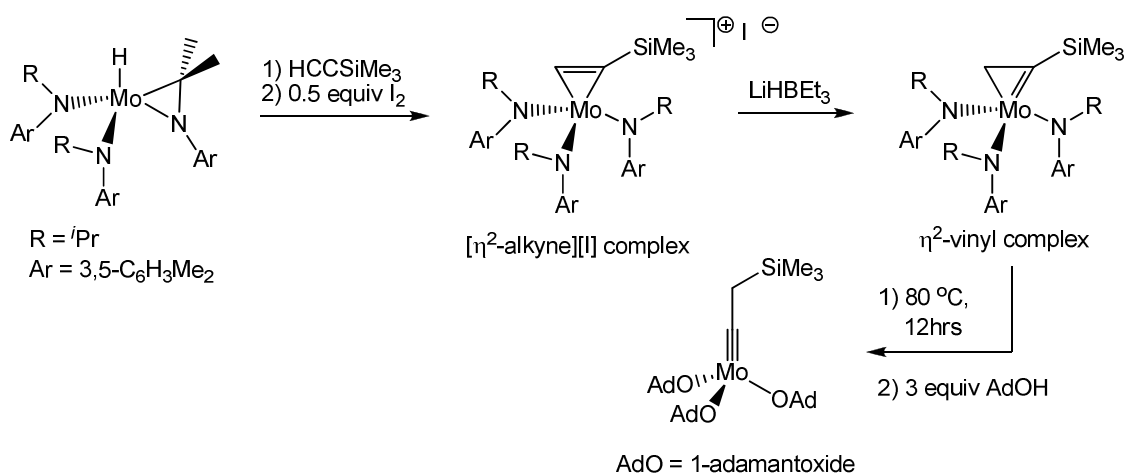


Scheme 1.8. Molybdenum alkylidyne formation through Mo≡Mo bond scission.

When the propylidyne complex $\text{EtC}\equiv\text{MoCl}_3(\text{DME})$ was treated with LiOR ($\text{R} = \text{OCMe}_3, \text{OCMe}_2\text{CF}_3$), complexes $\text{EtC}\equiv\text{Mo}(\text{OR})_3$ were formed and subsequently reacted bimolecularly at low temperatures to yield $\text{Mo}_2(\text{OR})_6$ (Scheme 1.8).⁴⁷ No Mo≡Mo bond formation was observed when more highly fluorinated alkoxides were employed, though the isolated alkylidynes retained a DME ligand that likely prevented further reaction. These observations illustrate the subtle influence that sterics can have on the reactivity of these complexes, as the neopentylidyne complex $\text{Me}_3\text{CC}\equiv\text{Mo}(\text{OCMe}_3)_3$ has never been reported to undergo self-reaction to give $\text{Mo}_2(\text{OR})_6$.

1.5 Mo ACM Catalysts via Mo(N[R]Ar)₃

Other synthetic routes to molybdenum ACM catalysts have been reported. In 2000, Cummins reported a multi-step synthesis of Me₃SiCH₂C≡Mo(OAd)₃ (OAd = 1-adamantoxide).⁴⁸ Beginning with their previously reported molybdaziridine-hydride complex,⁴⁹ they found that introduction of trimethylsilylacetylene formed a paramagnetic η²-alkyne complex that was isolated as the [(η²-RCCR')Mo(N[ⁱPr(Ar)₃][I)] salt following oxidation by 0.5 equiv I₂. Reduction with LiHBEt₃ afforded an η²-vinyl complex, which rearranged at 80 °C to give an alkylidyne tris-amido complex. Finally, protonolysis with 1-adamantanol yielded the alkylidyne tris-adamantoxide complex (Scheme 1.9). The adamantoxide complex is active for ACM at room temperature, though few details on rates or substrate scope were given.⁴⁸ Given the tedious synthesis and reactive nature of the molybdaziridine hydride (which reacts with N₂),⁴⁹ Cummins' ACM catalyst has not found widespread use.



Scheme 1.9. Cummins' molybdenum alkylidyne synthesis.

Cummins' related molybdenum tris-anilide complex $\text{Mo}(\text{N}[\text{tBu}]\text{Ar})_3$ ⁵⁰ was later found by Furstner to give an active ACM mixture upon activation with CH_2Cl_2 and other geminal dihalides.^{51, 52} These ACM mixtures displayed good yields of metathesis products when heated at 80 °C. A wide range of functional groups were tolerated, though secondary amides and substrates containing acidic protons remained problematic.⁵² The complexes $\text{ClMo}(\text{N}[\text{tBu}]\text{Ar})_3$ and $\text{HC}\equiv\text{Mo}(\text{N}[\text{tBu}]\text{Ar})_3$ were observed spectroscopically in the *in situ* generated catalyst mixtures and their identities were confirmed through independent synthesis (Figure 1.1). Pure samples of $\text{ClMo}(\text{N}[\text{tBu}]\text{Ar})_3$ displayed catalytic activity comparable to the catalyst mixture, while the $\text{HC}\equiv\text{Mo}(\text{N}[\text{tBu}]\text{Ar})_3$ surprisingly displayed very sluggish rates of ACM. When $\text{Mo}(\text{N}[\text{tBu}]\text{Ar})_3$ was activated with CH_2Cl_2 in the presence of alkynes, complexes $\text{Mo}_2\text{Cl}_2(\text{N}[\text{tBu}]\text{Ar})_4$ and $\text{MoCl}_2(\text{NAr})(\text{N}[\text{tBu}]\text{Ar})_2$ were isolated and crystallographically characterized (Figure 1.1). The former displayed no ACM activity, while the latter was slightly superior to the *in situ* generated catalyst mixture.

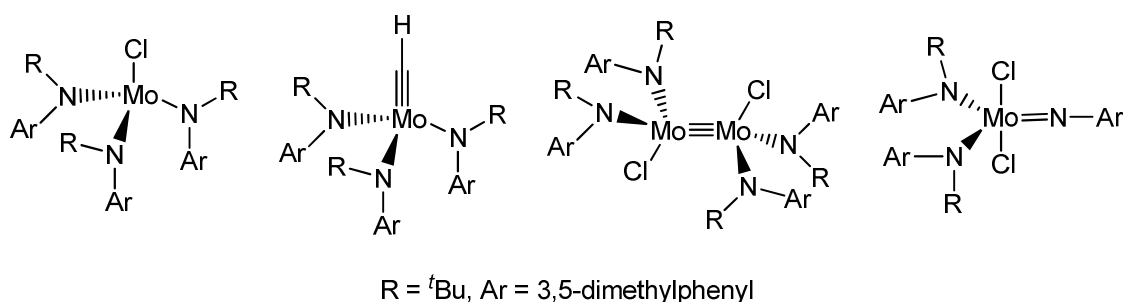
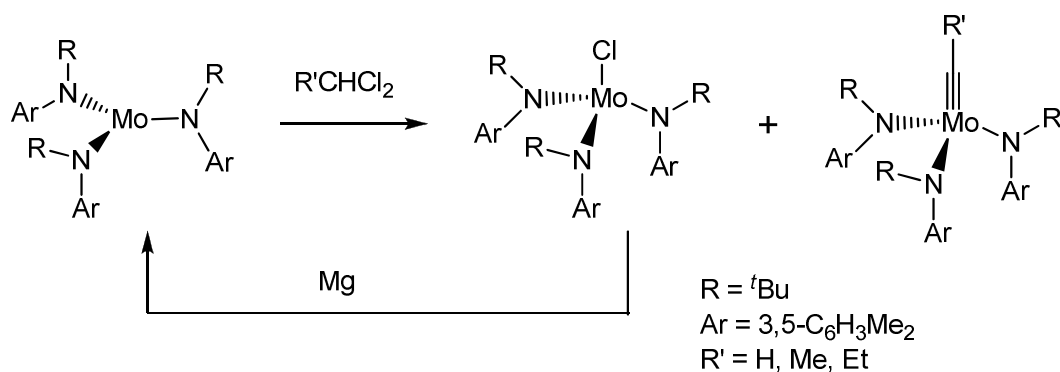


Figure 1.1. Mo complexes observed or isolated from Furstner's ACM system.

Moore improved upon Furstner's system by introducing a "reductive recycle" strategy in which $\text{Mo}(\text{N}[\text{tBu}]\text{Ar})_3$ is activated with a geminal dihalide in the presence of

magnesium.⁵³ Both $\text{ClMo}(\text{N}[\text{tBu}]\text{Ar})_3$ and $\text{RC}\equiv\text{Mo}(\text{N}[\text{tBu}]\text{Ar})_3$ are formed from the initial activation, but $\text{ClMo}(\text{N}[\text{tBu}]\text{Ar})_3$ is selectively reduced back to $\text{Mo}(\text{N}[\text{tBu}]\text{Ar})_3$ (Scheme 1.10). In this way, the reaction could be driven to give high yields of the alkylidyne complexes. Subsequent alcoholysis gives *in situ* mixtures that are active catalysts for ACM. While Moore's system is appealing as a ready source of molybdenum alkylidyne species, the route suffers from irreproducibility as a variety of factors, such as Mg particle size, can have drastic effects on the success of the reaction.



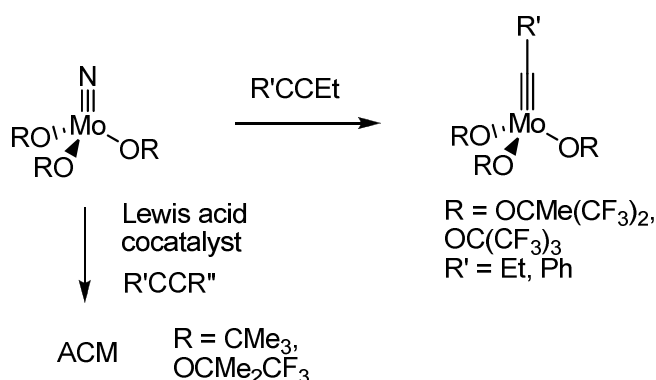
Scheme 1.10. Moore's reductive recycle strategy.

Moore later made a heterogeneous ACM catalyst by impregnating $\text{EtC}\equiv\text{Mo}(\text{N}[\text{tBu}]\text{Ar})_3$ onto silica.²² The resulting catalyst was determined to have a surface composition of $\text{EtC}\equiv\text{Mo}(\text{N}[\text{tBu}]\text{Ar})_n(\text{OSi})_{3-n}$ and was found to rapidly catalyze ACM at room temperature. Thiophenes and methyl benzoate groups were tolerated, though an extended functional group compatibility study was not reported. The catalyst is recyclable for at least three cycles and does not give alkyne polymerization products, which suggests a bimolecular mechanism for the polymerization reaction. Moore later reported homogeneous analogues using a variety of incompletely condensed polyhedral

oligomeric silsesquioxanes (POSS).⁵⁴ A range of ACM activity was observed with different POSS's, though functional group tolerance was not reported.

1.6 Mo ACM catalysts via N≡[Mo] complexes

In 2006, our group reported that molybdenum alkylidyne complexes could be accessed from molybdenum nitride complexes N≡Mo(OR)₃ (R = CMe(CF₃)₂, C(CF₃)₃) by treatment with 3-hexyne at 95 °C.²⁷ Addition of DME to the reaction mixture containing EtC≡Mo(OCMe(CF₃)₂)₃ allowed for the isolation of the alkylidyne complex as its DME adduct (Scheme 1.11). Later Geyer reported the similar preparation of the analogous benzylidyne complex by using 1-phenyl-1-butyne.⁴⁷ Additionally, Geyer discovered that solutions of N≡Mo(OR)₃ (R = CMe(CF₃)₂, C(CF₃)₃) effectively catalyze ACM at room temperature without prior generation of the alkylidyne ligand, presumably through formation of trace unobserved alkylidyne species.

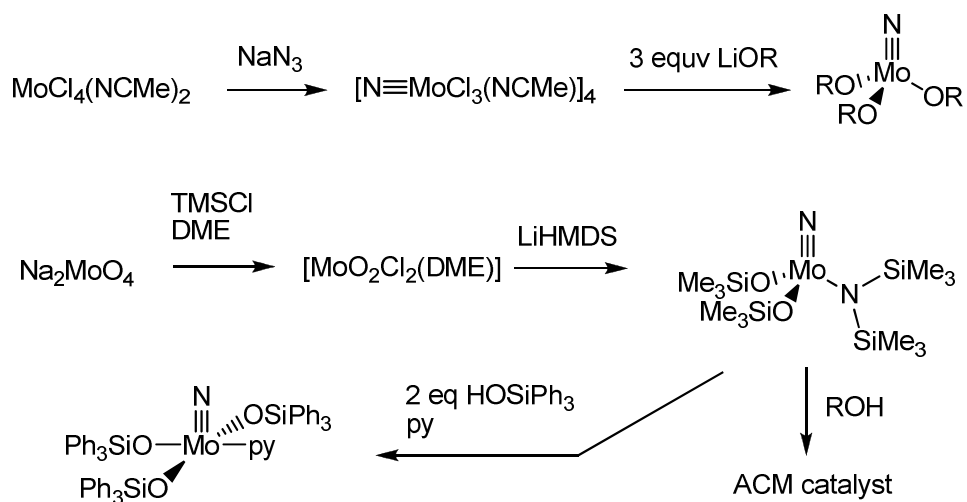


Scheme 1.11. Reactions of Mo nitride complexes with alkynes.

As heavily fluorinated alkoxide ligands are quite expensive, catalysts utilizing less fluorinated alkoxides were desired. Geyer found that the combination of a Lewis

acid co-catalyst and $\text{N}\equiv\text{Mo}(\text{OR})_3$ ($\text{R} = \text{CMe}_3, \text{CMe}_2\text{CF}_3$) gave an active ACM catalyst (Scheme 1.11).⁴⁷ A wide variety of Lewis acids were screened, with MgBr_2 and MgI_2 being among the most active. No buildup of alkylidyne complexes was observed, suggesting only trace alkylidyne formation. The role of the Lewis acid was not elucidated, but likely acts as a lone pair acceptor from either the nitride or alkoxide ligands.

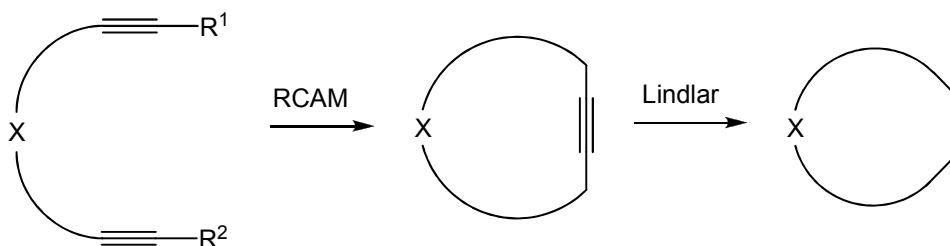
The typical method for preparation of $\text{N}\equiv\text{Mo}(\text{OR})_3$ species involves the reaction of $\text{MoCl}_4(\text{NCMe})_2$ with an azide, such as NaN_3 , to give an intermediate species $[\text{N}\equiv\text{MoCl}_3(\text{NCMe})]_4$. Subsequent treatment with LiOR leads to formation of the desired nitride complexes (Scheme 1.12).^{26, 55, 56} Seeking to avoid the use of potentially explosive azides, Furstner reported in 2009 the use of $\text{N}\equiv\text{Mo}(\text{OSiMe}_3)_2(\text{N}[\text{SiMe}_3]_2)$ as a precursor for ACM.⁵⁷ The parent nitride complex, which is synthesized under relatively mild conditions (Scheme 1.12), underwent alcoholysis with a variety of fluorinated alcohols, phenols, and silanols to give an active *in situ* ACM catalyst mixture at 80 °C. Of the alcohols screened, HOSiPh_3 gave the best results, with the ring-closing alkyne metathesis (RCAM) of their benchmark dialkyne being complete within 1.5 hours. Though a mixture of molybdenum species were observed spectroscopically, only $\text{N}\equiv\text{Mo}(\text{OSiPh}_3)_3(\text{py})$ could be isolated upon addition of pyridine to the *in situ* mixture. The pyridine adduct was only slightly less reactive than the *in situ* generated catalyst mixture. Additionally, the pyridine adduct was found to be tolerant of both pyridine and thiophene substrates, which are typically challenging functional groups in ACM.



Scheme 1.12. Routes to obtain Mo nitride complexes.

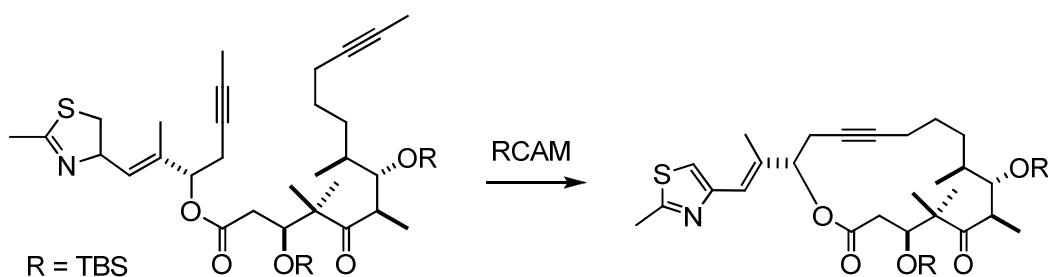
1.7 Applications of ACM

Though not as common as with olefin metathesis,^{58, 59} applications for the construction of complex molecules using ACM have been of interest. One such tool is ring-closing alkyne metathesis (RCAM), in which a diyne substrate is metathesized to give a cyclic alkyne product (Scheme 1.13). The alkyne functionality can then be transformed further to other functional groups such as *Z*-alkenes (Lindlar reduction).⁵² Because the latter transformations proceed stereoselectively, RCAM offers an advantage over the corresponding ring-closing olefin metathesis reaction, which typically yields mixtures of *E*- and *Z*-isomers.



Scheme 1.13. Tandem RCAM – Lindlar reduction to give cyclic *Z*-alkenes.

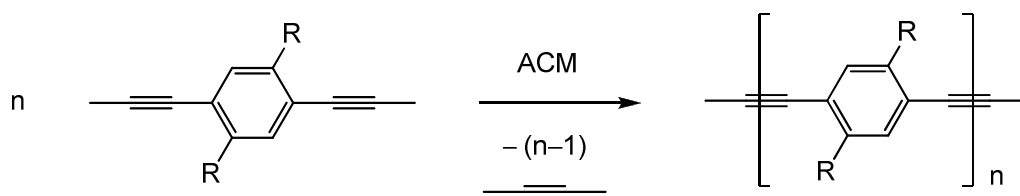
RCAM has been mediated by a variety of ACM catalysts. Original reports of RCAM employed $\text{Mo}(\text{CO})_6 / \text{ROH}$ and $\text{RCW}(\text{OCMe}_3)_3$ catalysts.^{40, 60-63} However, the usefulness of RCAM was attenuated by the limited functional group compatibility of the catalysts. Furstner later reported that his *in situ* $\text{Mo}(\text{N}[\text{tBu}]\text{Ar})_3 / \text{CH}_2\text{Cl}_2$ catalyst also efficiently mediated RCAM.^{4, 64} Due to the higher functional group tolerance of $\text{Mo}(\text{N}[\text{tBu}]\text{Ar})_3$, Furstner was able to employ RCAM in a late stage step in the total synthesis of epothilone C (Scheme 1.14), which is a member of a family of chemotherapy drugs.⁵² This ring-closing is particularly interesting as the substrate contains challenging thiophene and pyridyl functional groups. As described previously, $\text{Mo}(\text{N}[\text{tBu}]\text{Ar})_3$ is quite synthetically challenging, and so Furstner recently described the use of the less synthetically challenging but similarly functional group tolerant $\text{N}\equiv\text{Mo}(\text{OSiMe}_3)_2(\text{N}[\text{SiMe}_3]_2) / \text{HOSiPh}_3$ as an *in situ* catalyst for RCAM.⁵⁷



Scheme 1.14. RCAM step in total synthesis of epothilone C.

A second application for ACM is in the synthesis of conjugated arylene-ethynylene polymers and macrocycles. In the case of polymer synthesis, a 1,4-diyne (Scheme 1.15) undergoes ACM to yield a poly(arylene-ethynylene) (PAE), in which the polymer backbone is fully conjugated. PAE's display favorable optical properties that

make them attractive for use in applications such as LED displays.⁶⁵ The most common method of PAE synthesis is via Pd-catalyzed cross coupling, which can lead to problems with end group ambiguity, defect structures, and separation of the PAE from Pd and P byproducts.⁶⁶ Polymerizations via ACM using $\text{RC}\equiv\text{W}(\text{OCMe}_3)_3$ and $\text{Mo}(\text{CO})_6 / \text{ROH}$ were able to avoid the typical problems associated with PAE synthesis, and a variety of structures could be obtained.^{65, 67, 68}



Scheme 1.15. Poly(arylene-ethynylene)'s via ACM.

ACM of diyne substrates can also give macrocyclic structures as shown in Figure 1.2.³ A variety of ring sizes have been synthesized via ACM, depending on the substitution pattern of the diyne. Because ACM is an equilibrium process, macrocycle formation via ACM leads to formation of a thermodynamic product, which often allows for high conversions to a given macrocycle.⁶⁹ Contrarily, Pd-catalyzed cross coupling reactions lead to kinetic products and subsequently very low yields of the desired macrocycle, as the C-C bond formation is irreversible. Initial ACM synthesis used the catalysts $\text{RCW}(\text{OCMe}_3)_3$ and $\text{Mo}(\text{CO})_6 / \text{ROH}$, but still often gave low yields due to the lack of a driving force to force the equilibrium towards the desired product.⁶⁹

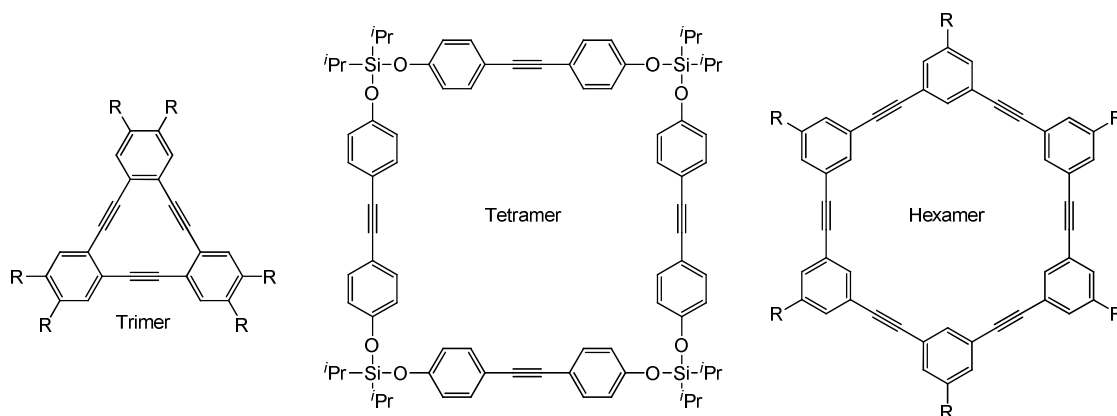
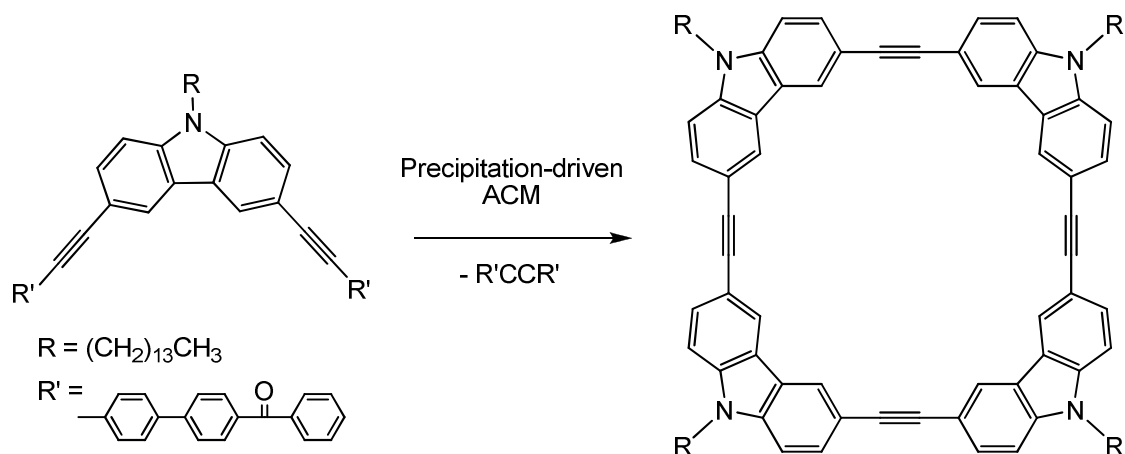


Figure 1.2. Arylene-ethynylene macrocycles synthesized via ACM.

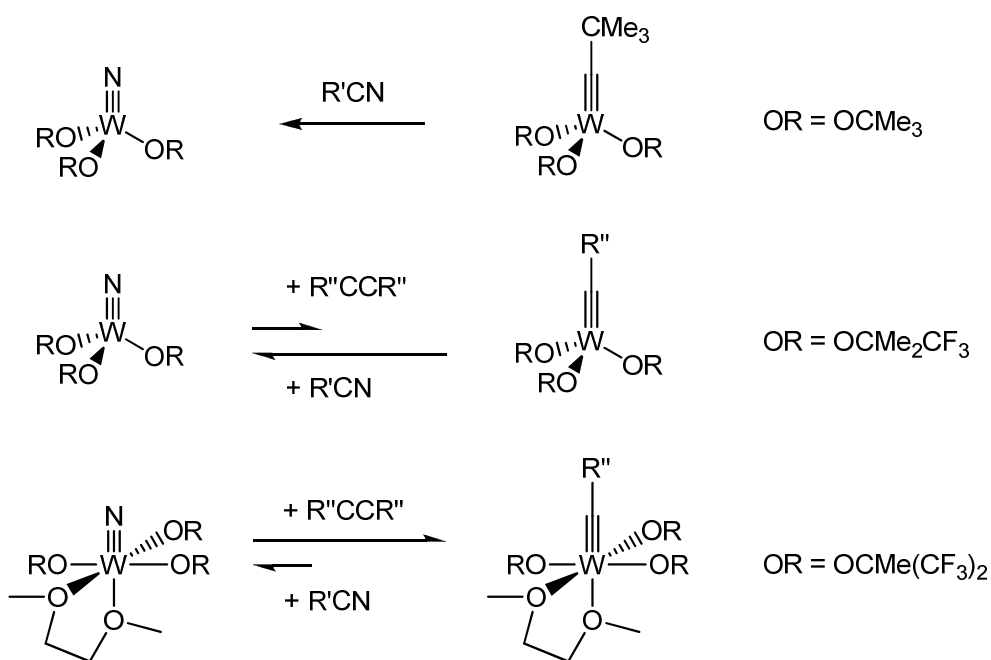
Using his reductive-recycle catalyst, Moore investigated a vacuum-driven strategy to remove 2-butyne as it was formed during the course of the ACM reaction.⁷⁰ This approach led to successful high-yield syntheses of hexameric macrocycles (Figure 1.2) and the corresponding pentameric macrocycles. However, the vacuum-driven ACM strategy only worked well on a milligram scale. Moore next investigated a precipitation-driven ACM strategy in which the typical 1-propynyl group was replaced with a large benzoylbiphenyl acetylene group.⁷⁰ The insoluble bis-benzoylbiphenyl acetylene product readily precipitates from the reaction solution, which allowed for high conversions to a tetrameric carbazole macrocycle (Scheme 1.16). Later Moore demonstrated that the carbazole tetramer could also be synthesized using the same strategy with his homogeneous Mo-POSS ACM catalyst.⁵⁴ These macrocycles are potentially useful materials, as nanofibril films of the carbazole tetramer have been employed in the detection of explosives *via* fluorescence quenching.⁷¹



Scheme 1.16. Carbazole macrocycle synthesis via precipitation-driven ACM.

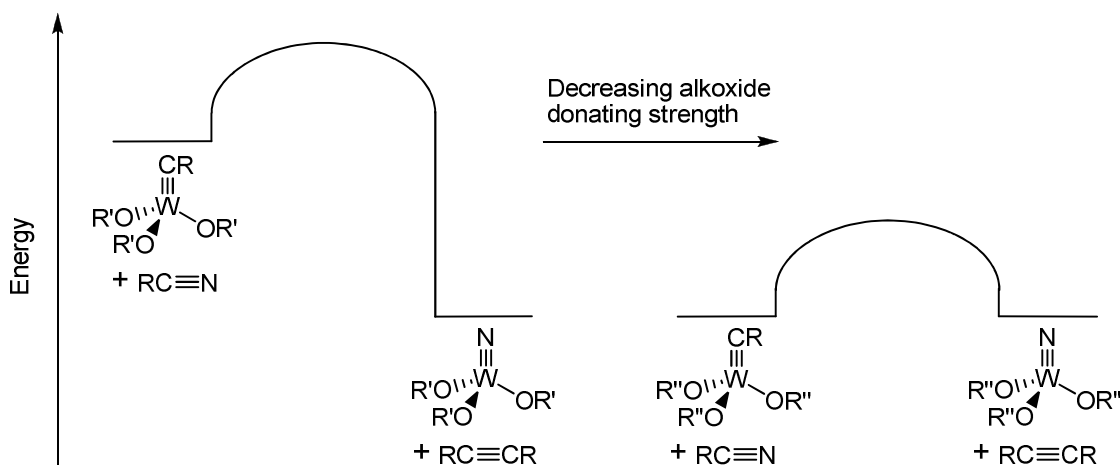
1.8 Nitrile–Alkyne Cross Metathesis

Schrock's alkylidyne complex $Me_3CC\equiv W(OCMe_3)_3$ is known to react irreversibly with nitriles to give the nitride complex $N\equiv W(OCMe_3)_3$ (Scheme 1.17).²⁸ The discovery of reversible NACM was first made in our lab by Gdula, who demonstrated that $N\equiv W(OCMe(CF_3)_2)_3(DME)$ will *reversibly* interconvert into the corresponding alkylidyne complex in the presence of alkynes at 95 °C.⁵⁶ This observation allowed for the development of catalytic NACM.^{34, 35} By employing a “sacrificial” alkyne, *e.g.* 3-hexyne, nitriles RCN were transformed into their corresponding alkyne species RCCEt and RCCR.



Scheme 1.17. Known W alkylidyne and nitride complex interconversions.

Further studies in our lab by Geyer demonstrated that $\text{N}\equiv\text{W}(\text{OCMe}_2\text{CF}_3)_3$ was also an active NACM catalyst.^{34, 35, 47} Mechanistic studies determined that the alkoxide ligand identity affected the position of the equilibrium between the nitride and alkylidyne complexes (Scheme 1.17). When $\text{OR} = \text{OCMe}_2\text{CF}_3$, the nitride complex is favored over the alkylidyne complex. However, the alkylidyne complex was favored over the nitride complex when $\text{OR} = \text{OCMe}(\text{CF}_3)_2$. Because the nitride ligand is more oxidizing than the alkylidyne ligand,³³ decreasing the alkoxide donor strength has the net effect of stabilizing the alkylidyne complex relative to its corresponding nitride complex (Scheme 1.18). Therefore NACM is only observed within a limited range of ancillary ligand donor strengths, as both the nitride and alkylidyne complexes must be thermally accessible from each other.

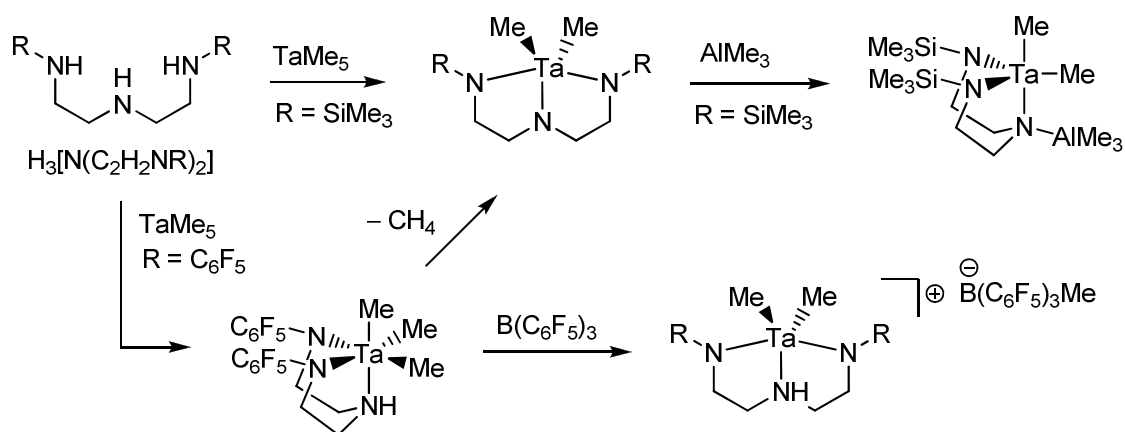


Scheme 1.18. Effect of alkoxide donor strength on relative energies of W nitride and alkylidyne complexes.

Chapter 2 discusses the functional group tolerance of the current W NACM catalysts. As expected from a Lewis acidic W catalyst, a variety of functional groups will be shown to be problematic. Since Mo ACM displays a wider range of functional group tolerance than their W counterparts, one can reasonably expect a Mo NACM catalyst to exhibit the same trend. However, NACM with Mo poses several challenges. First, the requisite alkylidyne to nitride transformation has never been observed for Mo.^{47, 56} This lack of reactivity is attributed both to the greater barrier to metalacycle formation for Mo relative to W,¹⁶ and to the greater electronegativity of Mo, which causes alkylidyne ligation to be more favorable than nitride ligation.³³ Finally, the tendency of Mo alkylidyne complexes to form Mo₂(OR)₆ species can lead to a deactivation pathway for NACM, as the dimolybdenum complexes do not react with nitriles.⁴⁷ Therefore, discovery of a Mo NACM catalyst will require these obstacles to be overcome or avoided.

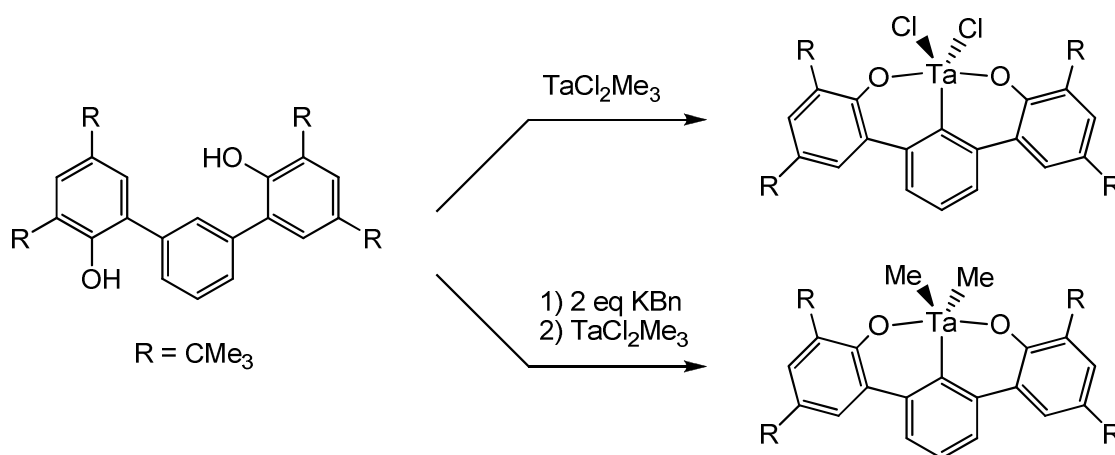
1.9. Trianionic (XXX) Pincer Ligands

As discussed in Chapter 3, our lab became interested in the use of trianionic (XXX) pincer ligands. At the time the current work was begun, only one bulky XXX pincer ligand had been reported, while several others have been reported since. The previously known example was an $\text{H}_3[\text{N}(\text{C}_2\text{H}_4\text{NR})_2]$ triamido ligand from the Schrock group (Scheme 1.19).⁷² Metalation of $\text{H}_3[\text{N}(\text{C}_2\text{H}_4\text{NR})_2]$ ($\text{R} = \text{SiMe}_3, \text{C}_6\text{F}_5$) occurred with TaMe_5 to give $\text{Ta}[\text{N}(\text{C}_2\text{H}_4\text{NR})_2]\text{Me}_2$ (Scheme 1.19), in which the $\text{N}(\text{C}_2\text{H}_4\text{NR})_2$ ligand adopts a meridional pincer geometry. In the case of $\text{R} = \text{C}_6\text{F}_5$, the intermediate complex $\text{Ta}[\text{HN}(\text{C}_2\text{H}_4\text{NR})_2]\text{Me}_3$ could be isolated prior to the final ligand deprotonation. The lack of rigidity in the pincer ligand allowed it to adopt a facial geometry upon reaction of the central amido group with AlMe_3 ($\text{R} = \text{SiMe}_3$). However, addition of a methyl group abstractor to $\text{Ta}[\text{HN}(\text{C}_2\text{H}_4\text{NR})_2]\text{Me}_3$ led to $[\text{Ta}[\text{HN}(\text{C}_2\text{H}_4\text{NR})_2]\text{Me}_2]^+$, in which the ligand retained a pincer geometry. Schrock also reported the closely related $\text{Ta}[\text{N}(\text{C}_6\text{H}_4\text{NSiMe}_3)_2]\text{Me}_2$ complex, in which the ligand C_2H_4 linkers have been replaced by 1,2- C_6H_4 linkers.⁷²



Scheme 1.19. Schrock's XXX ligands.

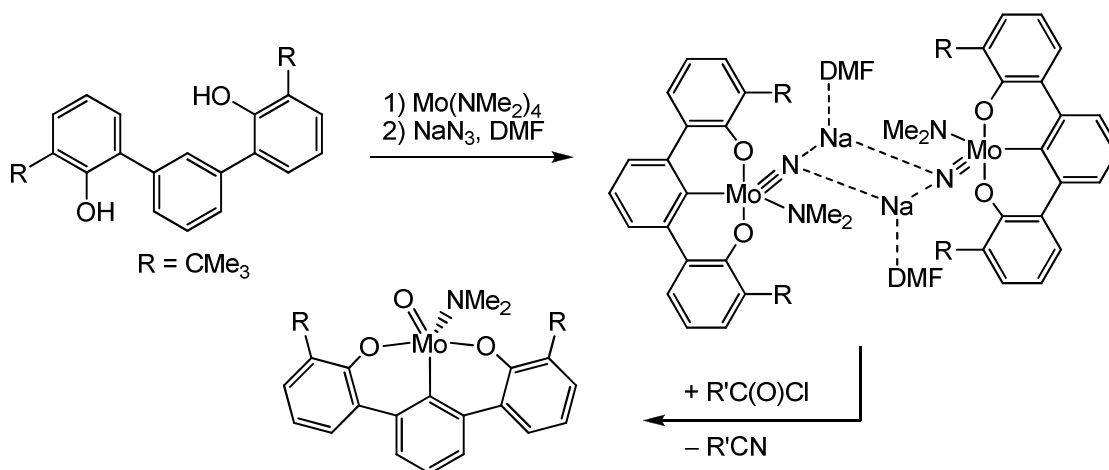
In 2007, Bercaw reported an $[\text{OCO}]^{3-}$ ligand based on a 1,3-bis(2'-hydroxyphenyl)benzene framework (Scheme 1.20).^{73, 74} The ligand underwent σ -bond metathesis with $\text{TaCl}_2(\text{Me})_3$ to give the complex $\text{Ta}(\text{OCO})\text{Cl}_2$ with 3 equiv of CH_4 as the byproduct. An intermediate complex preceding the CH activation was characterized and found to possess an agostic CH bond *trans* to the lone remaining methyl ligand. Heating the intermediate to 90 °C led to the formation of the fully trianionic ligand. A second metalation route involved deprotonation of the phenols with KBn , followed by salt metathesis with $\text{TaCl}_2(\text{Me})_3$, with subsequent σ -bond metathesis leading to $\text{Ta}(\text{OCO})\text{Me}_2$. In this instance, the CH activation occurred readily at room temperature, likely due to the presence of two *cis* methyl ligands in the proposed intermediate trialkyl species.



Scheme 1.20. Bercaw's XXX pincer ligand.

In 2008, Veige reported a similar phenolic ligand that was activated through reaction with $\text{Mo}(\text{NMe}_2)_4$ yielding $\text{Mo}(\text{OCO})(\text{NMe}_2)(\text{NHMe}_2)_2$.⁷⁵ Subsequent treatment of this Mo(IV) complex lead to the formation of a dimeric molybdenum nitride complex

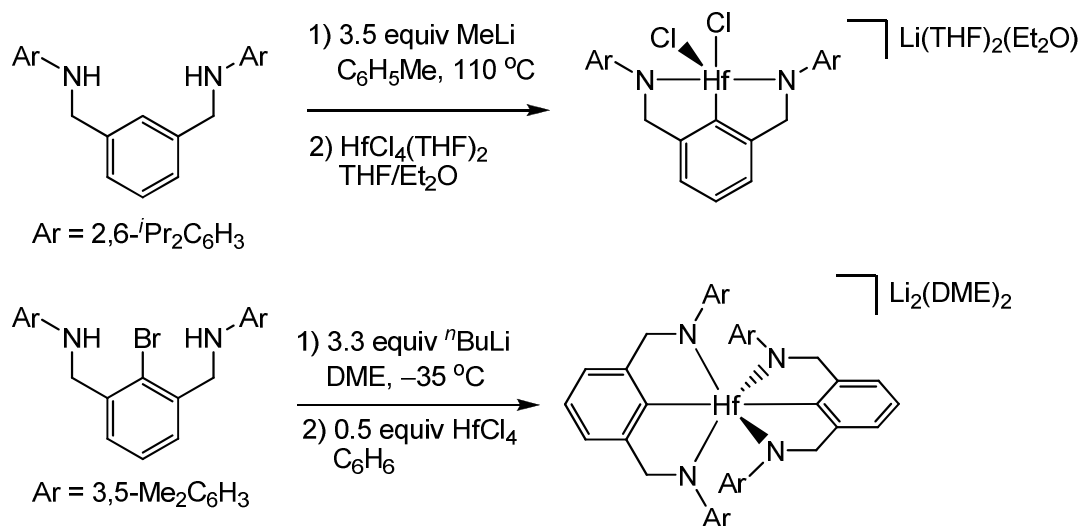
(Scheme 1.21). No triple bond metathesis activity was reported for the dimeric nitride complex, as the -NMe_2 *cis* to the nitride ligand likely prevents approach of organic substrates. The dimer was later shown to be nucleophilic, with initial substitution occurring at the nitride ligand to generate imide complexes.⁷⁶ Utilizing the nucleophilic nitride ligand, Veige reported that treatment of the dimer complex with acyl chloride substrates leads to the extrusion of a new nitrile and formation of a Mo oxo complex.⁷⁶ Similar N-atom transfer reactions have previously been employed to synthesize nitriles,^{77, 78} with Cummins demonstrating a complete cycle for incorporation of dinitrogen into the product nitrile.⁷⁹



Scheme 1.21. Veige's XXX pincer ligand.

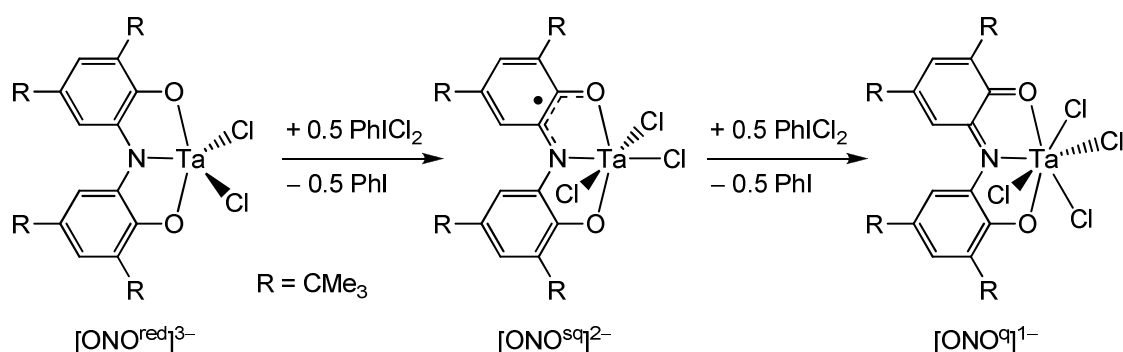
Veige also reported a pair of hafnium complexes containing NCN^{3-} ligands as shown in Scheme 1.22.⁸⁰ Each ligand was first isolated as the corresponding $[\text{NCN-Li}_3]_2$ complex prior to undergoing salt metathesis with HfCl_4 . Depending on the pendant aryl group identity, different structures were observed. When the group was bulky (Ar = 2,6-ⁱPr₂C₆H₃), a single NCN ligand was coordinated to Hf, with the Ar groups nearly

perpendicular to the ligand backbone in the solid state. With the smaller group Ar = 3,5-Me₂C₆H₃, two NCN ligands were coordinated to Hf, and each ligand was nearly planar.



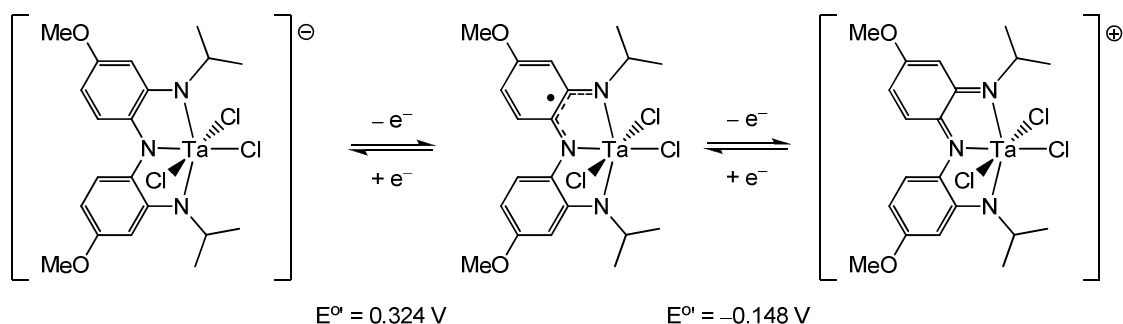
Scheme 1.22. Veige's [NCN]³⁻ Hf complexes.

Heyduk has reported a redox-active pincer ligand with an ONO framework (Scheme 1.23).⁸¹ In its fully reduced state, the pincer is formally an XXX pincer ligand. The complex TaCl₂(ONO^{red}) underwent sequential one-electron oxidations with PhICl₂ to give the complexes TaCl₃(ONO^{sq}) and TaCl₄(ONO^q) in which the ONO ligand exists in its semiquinone (sq) and quinone (q) oxidized states, respectively (Scheme 1.23). In the same study, the bridging imide complex [(Ta(ONO^{red})(py)-μ-NAr]₂ was found to extrude ArN=NAr upon treatment with PhICl₂. This latter transformation presumably proceeds through an initial oxidation of the ONO ligand as Ta is already in its highest oxidation state.



Scheme 1.23. Redox active ONO pincer ligand.

Shortly after his report of a redox active ONO pincer ligand, Heyduk reported a closely related NNN pincer ligand.⁸² Methoxy groups were introduced into the aryl backbone in order to increase the reducing ability of the ligand. Upon isolation of TaCl₃(NNN^{sq}) with the NNN ligand in its semiquinone form (Scheme 1.24 center), cyclic voltammetry studies revealed that reversible one-electron reduction and oxidation were both possible, giving the reduced and quinone forms respectively. The small potential gap ($\Delta E^{\circ'} = 0.5$ V) relating the three oxidation states indicates that all three should be readily accessible. The redox-active NNN ligand then allowed for nitrene transfer from an organic azide to Ta(V), a process which requires an input of 2 e⁻ into the azide group.



Scheme 1.24. Redox active NNN pincer ligand.

1.10 Electronic Tuning of Pincer Ligands

As described previously in the current chapter, the ancillary ligand donor strength can have a direct and significant effect on the metathesis reactivity of Group 6 nitride and alkylidyne complexes. Pincer ligand donation strength is commonly tuned by introducing electron-withdrawing or electron-donating groups into the pincer backbone. This often requires the synthesis of a wide variety of ligand precursors, which can be tedious.⁸³ A novel approach is to introduce a Lewis basic site into the pincer backbone that does not coordinate to the metal center. Subsequent interaction of the basic site with a Lewis acid can pull electron density away from the metal center, thus changing its reactivity. Examples of electronically tunable pincer ligands are sparse and currently limited to late transition metals.

Milstein introduced a PCP pincer ligand in which the central phenyl ring has been replaced with a 3,5-lutidine ring (Fig 1.3).⁸⁴ The outer pyridyl nitrogen atom was able to react with Lewis acids, with the BEt_3 and PdCl_2 adducts being reported. Incorporation of electron withdrawing *para* substituents is known to cause a downfield shift for the C_{ipso} chemical shift in the ^{13}C NMR spectrum as a result of decreased electron density at the C_{ipso} atom.^{85, 86} A similar effect is observed upon Lewis acid coordination to Milstein's PCP ligands, with both the BEt_3 and PdCl_2 adducts displaying deshielded C_{ipso} chemical shifts relative to the parent complex.⁸⁴ The reduction in electron density at C_{ipso} is expected to make the arylidene ring a weaker donor ligand, which in turn reduces the electron density at Pd. This effect is indeed observed, as Lewis acid coordination causes the ^{31}P NMR resonances to shift downfield as a result of increased donation to Pd.

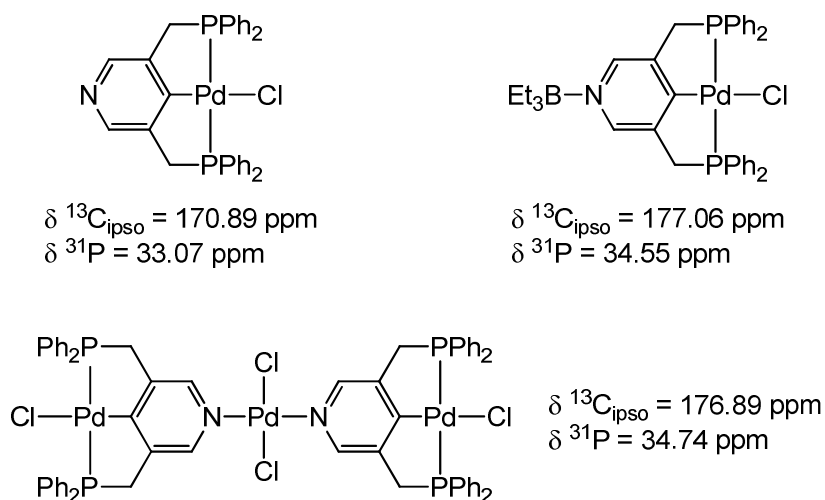
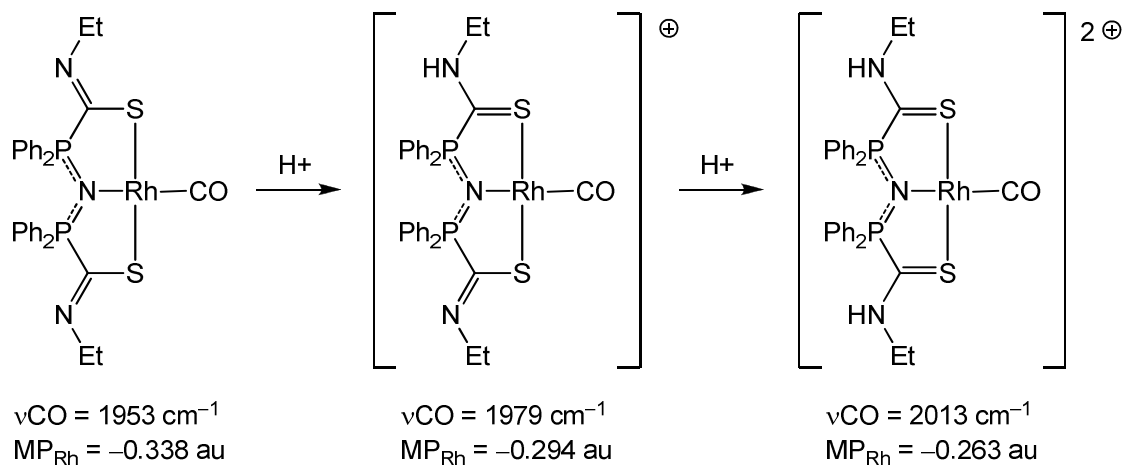


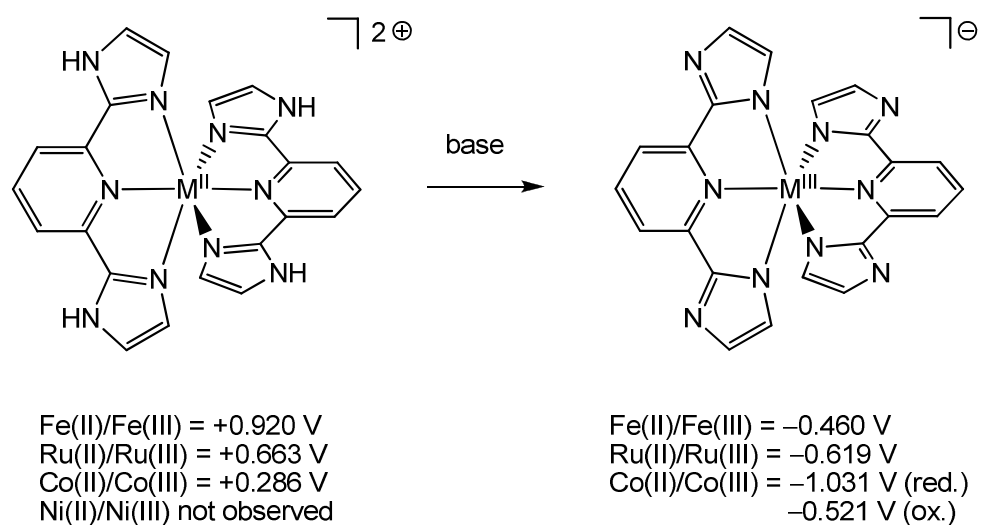
Figure 1.3. Milstein's 3,5-lutidine PCP ligand.

Cauzzi recently reported a zwitterionic Rh(SNS)(CO) complex as shown in Scheme 1.25.⁸⁷ The imine-N atoms of the SNS pincer are available for Lewis acid interaction, and the sequential protonation of each was demonstrated. Increasing protonation was found to increase $\nu(\text{CO})$ from 1953 cm^{-1} for Rh(SNS)(CO) to 2013 cm^{-1} for $[\text{Rh}(\text{H}_2\text{SNS})(\text{CO})]^{2+}$. The change in CO stretching intensity corresponds to a reduction in electron density at Rh as a result of weaker donation from the thione ligand relative to the original thiolate ligand. Computationally derived Mulliken populations confirmed the decreasing Rh electron density (Scheme 1.25). The rate of oxidative addition of MeI by $[\text{Rh}(\text{H}_2\text{SNS})(\text{CO})]^{1+}$ was found to be three orders of magnitude slower than the parent Rh(SNS)(CO). Double protonation led to an even slower rate of MeI oxidative addition by $[\text{Rh}(\text{H}_2\text{SNS})(\text{CO})]^{2+}$, though the rate was not determined.



Scheme 1.25. Sequential protonation of Rh(SNS)(CO).

Williams has demonstrated that deprotonation of 2,6-bis-imidazolylpyridine pincer ligands in complexes $[\text{M}^{\text{II}}(\text{H}_2\text{NCN})_2]^{2+}$ leads to spontaneous metal oxidation, yielding complexes $[\text{M}^{\text{III}}(\text{NCN})_2]^{1-}$ (Scheme 1.26).^{88, 89} A result of increased N-atom donor strength, the deprotonation-induced spontaneous oxidation was observed for Fe, Ru, and Co complexes, but not for Ni. Cyclic voltammetry indicated a large drop in the $\text{M}^{\text{II}}/\text{M}^{\text{III}}$ oxidation potential, with the protonated complexes undergoing reversible oxidation at positive potential and the deprotonated complexes being reversibly oxidized at negative potentials. The protonated Fe(II) complex displayed spin-crossover behavior with $\mu_{\text{eff}} = 3.6 \mu_{\text{B}}$ at room temperature and $\mu_{\text{eff}} \approx 0 \mu_{\text{B}}$ at 200 K. Conversely, the deprotonated Fe complex was confirmed to be low spin Fe(III) with $\mu_{\text{eff}} = 1.9 \mu_{\text{B}}$.⁸⁹



Scheme 1.26. Redox state switching induced through pincer ligand deprotonation.

1.11 Thesis Goals

The long-term goal of the current work is to develop NACM for use in organic synthesis. The first half of Chapter 1 will discuss the substrate scope of current W NACM catalysts,^{34, 35} along with the application of NACM in the synthesis of conjugated macrocycles.³⁵ In the second half of Chapter 2, the synthesis of thermally robust Mo nitride complexes is discussed, along with their concurrent NACM reactivity. Chapter 3 will describe the design and synthesis of XXX pincer ligands intended to facilitate NACM, as well as the challenges associated with their ligation to early transition metals. In Chapter 4, XXX-Zr complexes are utilized to investigate the ability of a new XXX ligand to undergo post-ligation electronic tuning. An understanding of the degree of electronic tuning possible will be useful to apply to future NACM catalysts containing similar XXX ligands.

1.12 References

1. Bunz, U. H. F.; Kloppenburg, L., *Angew. Chem., Int. Ed.* **1999**, *38*, 478-481.
2. Zhang, W.; Moore, J. S., *Advanced Synthesis & Catalysis* **2007**, *349*, 93-120.
3. Zhang, W.; Moore, J. S., *Angew. Chem., Int. Ed.* **2006**, *45*, 4416-4439.
4. Furstner, A.; Davies, P. W., *Chem. Commun.* **2005**, 2307-2320.
5. Schrock, R. R.; Czekelius, C., *Advanced Synthesis & Catalysis* **2007**, *349*, 55-77.
6. Patai, S., *The Chemistry of the Carbon-Carbon Triple Bond*. John Wiley & Sons: Chichester, 1978 Part 1.
7. Tyrrell, E., Alkynes. In *Comprehensive Organic Functional Group Transformations II*, 1 ed.; Katritzky, A. R., Taylor, R. J. K., Ed. Elsevier: Amsterdam; Boston, 2005; Vol. 1, pp 1083 - 1176.
8. In *The Chemistry of the Cyano Group*, 1st ed.; Rappaport, Z., Ed. John Wiley & Sons: London, 1970.
9. Katz, T. J.; McGinnis, J., *J. Am. Chem. Soc.* **1975**, *97*, 1592-1594.
10. Schrock, R. R.; Pedersen, S. F.; Churchill, M. R.; Ziller, J. W., *Organometallics* **1984**, *3*, 1574-1583.
11. Churchill, M. R.; Ziller, J. W.; Freudenberger, J. H.; Schrock, R. R., *Organometallics* **1984**, *3*, 1554-1562.
12. Freudenberger, J. H.; Schrock, R. R.; Churchill, M. R.; Rheingold, A. L.; Ziller, J. W., *Organometallics* **1984**, *3*, 1563-1573.
13. Schrock, R. R.; Murdzek, J. S.; Freudenberger, J. H.; Churchill, M. R.; Ziller, J. W., *Organometallics* **1986**, *5*, 25-33.
14. Schrock, R. R., *Acc. Chem. Res.* **1986**, *19*, 342-348.
15. Woo, T.; Folga, E.; Ziegler, T., *Organometallics* **1993**, *12*, 1289-1298.
16. Zhu, J.; Jia, G.; Lin, Z., *Organometallics* **2006**, *25*, 1812-1819.
17. McCullough, L. G.; Schrock, R. R.; Dewan, J. C.; Murdzek, J. C., *J. Am. Chem. Soc.* **1985**, *107*, 5987-5998.
18. Wengrovius, J. H.; Sancho, J.; Schrock, R. R., *J. Am. Chem. Soc.* **1981**, *103*, 3932-3934.
19. Mortreux, A.; Petit, F.; Petit, M.; Szymanskabuzar, T., *J. Mol. Catal. A-Chem.* **1995**, *96*, 95-105.
20. Freudenberger, J. H.; Schrock, R. R., *Organometallics* **1986**, *5*, 1411-1417.
21. Zhang, W.; Kraft, S.; Moore, J. S., *J. Am. Chem. Soc.* **2004**, *126*, 329-335.
22. Weissman, H.; Plunkett, K. N.; Moore, J. S., *Angew. Chem., Int. Ed.* **2006**, *45*, 585-588.
23. Strutz, H.; Dewan, J. C.; Schrock, R. R., *J. Am. Chem. Soc.* **1985**, *107*, 5999-6005.
24. Masuda, T.; Sasaki, N.; Higashimura, T., *Macromolecules* **1975**, *8*, 717-721.
25. Chisholm, M. H.; Delbridge, E. E.; Kidwell, A. R.; Quinlan, K. B., *Chem. Commun.* **2003**, 126-127.
26. Gdula, R. L.; Johnson, M. J. A.; Ockwig, N. W., *Inorg. Chem.* **2005**, *44*, 9140-9142.
27. Gdula, R. L.; Johnson, M. J. A., *J. Am. Chem. Soc.* **2006**, *128*, 9614-9615.
28. Freudenberger, J. H.; Schrock, R. R., *Organometallics* **1986**, *5*, 398-400.
29. Chisholm, M. H.; Folting, K.; Lynn, M. L.; Tiedtke, D. B.; Lemoigno, F.; Eisenstein, O., *Chemistry-a European Journal* **1999**, *5*, 2318-2326.

30. Chisholm, M. H.; Folting-Streib, K.; Tiedtke, D. B.; Lemoigno, F.; Eisenstein, O., *Angew. Chem., Int. Ed. Engl.* **1995**, *34*, 110-112.
31. Tonzetich, Z. J.; Lam, Y. C.; Müller, P.; Schrock, R. R., *Organometallics* **2007**, *26*, 475-477.
32. Fischer, H.; Hofmann, P.; Kreissl, F. R.; Schrock, R. R.; Schubert, U.; Weiss, K., *Carbyne Complexes*. VCH Publishers: New York, 1988; p 235.
33. Nugent, W. A.; Mayer, J. M., *Metal-Ligand Multiple Bonds*. John Wiley & Sons: New York, 1988; p 26-29.
34. Geyer, A. M.; Gdula, R. L.; Wiedner, E. S.; Johnson, M. J. A., *J. Am. Chem. Soc.* **2007**, *129*, 3800-3801.
35. Geyer, A. M.; Wiedner, E. S.; Gary, J. B.; Gdula, R. L.; Kuhlmann, N. C.; Johnson, M. J. A.; Dunietz, B. D.; Kampf, J. W., *J. Am. Chem. Soc.* **2008**, *130*, 8984-8999.
36. Bailey, B. C.; Fout, A. R.; Fan, H. J.; Tomaszewski, J.; Huffman, J. C.; Gary, J. B.; Johnson, M. J. A.; Mindiola, D. J., *J. Am. Chem. Soc.* **2007**, *129*, 2234-2235.
37. Pennella, F.; Banks, R. L.; Bailey, G. C., *Chem. Commun.* **1968**, 1548-&.
38. Moulijn, J. A.; Boelhouw, C.; Reitsma, H. J., *Journal of Catalysis* **1972**, *25*, 434-459.
39. Mortreux, A.; Blanchard, M., *Journal Of The Chemical Society-Chemical Communications* **1974**, 786-787.
40. Grela, K.; Ignatowska, J., *Org. Lett.* **2002**, *4*, 3747-3749.
41. Kloppenburg, L.; Bunz, U. H. F., *J. Organomet. Chem.* **2000**, *606*, 13-15.
42. Freudenberger, J. H.; Pedersen, S. F.; Schrock, R. R., *Bulletin De La Societe Chimique De France* **1985**, 349-352.
43. Listemann, M. L.; Schrock, R. R., *Organometallics* **1985**, *4*, 74-83.
44. Tonzetich, Z. J.; Lam, Y. C.; Muller, P.; Schrock, R. R., *Organometallics* **2007**, *26*, 475-477.
45. McCullough, L. G.; Schrock, R. R., *J. Am. Chem. Soc.* **1984**, *106*, 4067-4068.
46. Strutz, H.; Schrock, R. R., *Organometallics* **1984**, *3*, 1600-1601.
47. Geyer, A. M. Development and Investigation of NW(OR)₃, NMo(OR)₃, and Mo₂(OR)₆ Complexes for Triple-Bond Metathesis. University of Michigan, Ann Arbor, 2009.
48. Tsai, Y. C.; Diaconescu, P. L.; Cummins, C. C., *Organometallics* **2000**, *19*, 5260-5262.
49. Tsai, Y. C.; Johnson, M. J. A.; Mindiola, D. J.; Cummins, C. C.; Klooster, W. T.; Koetzle, T. F., *J. Am. Chem. Soc.* **1999**, *121*, 10426-10427.
50. Laplaza, C. E.; Johnson, M. J. A.; Peters, J. C.; Odom, A. L.; Kim, E.; Cummins, C. C.; George, G. N.; Pickering, I. J., *J. Am. Chem. Soc.* **1996**, *118*, 8623-8638.
51. Furstner, A.; Mathes, C.; Lehmann, C. W., *J. Am. Chem. Soc.* **1999**, *121*, 9453-9454.
52. Furstner, A.; Mathes, C.; Lehmann, C. W., *Chemistry-a European Journal* **2001**, *7*, 5299-5317.
53. Zhang, W.; Kraft, S.; Moore, J. S., *Chem. Commun.* **2003**, 832-833.
54. Cho, H. M.; Weissman, H.; Wilson, S. R.; Moore, J. S., *J. Am. Chem. Soc.* **2006**, *128*, 14742-14743.
55. Chan, D. M. T.; Chisholm, M. H.; Folting, K.; Huffman, J. C.; Marchant, N. S., *Inorg. Chem.* **1986**, *25*, 4170-4174.

56. Gdula, R. L. Design and Synthesis of Highly Active Group 6 Metal Catalysts for use in Triple-Bond Metathesis. University of Michigan, Ann Arbor, 2006.
57. Bindl, M.; Stade, R.; Heilmann, E. K.; Picot, A.; Goddard, R.; Furstner, A., *J. Am. Chem. Soc.* **2009**, *131*, 9468-9470.
58. Grubbs, R. H., *Handbook of Metathesis*. Wiley-VCH: Weinheim, 2003; Vol. 2 - Applications in Organic Synthesis, p 510.
59. Grubbs, R. H., *Handbook of Metathesis*. Wiley-VCH: Weinheim, 2003; Vol. 3 - Applications in Polymer Synthesis, p 442.
60. Furstner, A.; Guth, O.; Rumbo, A.; Seidel, G., *J. Am. Chem. Soc.* **1999**, *121*, 11108-11113.
61. Furstner, A.; Seidel, G., *J. Organomet. Chem.* **2000**, *606*, 75-78.
62. Furstner, A.; Stelzer, F.; Rumbo, A.; Krause, H., *Chemistry-A European Journal* **2002**, *8*, 1856-1871.
63. Sashuk, V.; Ignatowska, J.; Grela, K., *Journal of Organic Chemistry* **2004**, *69*, 7748-7751.
64. Furstner, A.; Radkowski, K.; Grabowski, J.; Wirtz, C.; Mynott, R., *Journal of Organic Chemistry* **2000**, *65*, 8758-8762.
65. Brizius, G.; Pschirer, N. G.; Steffen, W.; Stitzer, K.; zur Loye, H. C.; Bunz, U. H. F., *J. Am. Chem. Soc.* **2000**, *122*, 12435-12440.
66. Goodson, F. E.; Wallow, T. I.; Novak, B. M., *J. Am. Chem. Soc.* **1997**, *119*, 12441-12453.
67. Ge, P. H.; Fu, W.; Herrmann, W. A.; Herdtweck, E.; Campana, C.; Adams, R. D.; Bunz, U. H. F., *Angew. Chem., Int. Ed.* **2000**, *39*, 3607-3610.
68. Kloppenburg, L.; Song, D.; Bunz, U. H. F., *J. Am. Chem. Soc.* **1998**, *120*, 7973-7974.
69. Zhang, W.; Moore, J. S., *J. Am. Chem. Soc.* **2005**, *127*, 11863-11870.
70. Zhang, W.; Moore, J. S., *J. Am. Chem. Soc.* **2004**, *126*, 12796-12796.
71. Naddo, T.; Che, Y. K.; Zhang, W.; Balakrishnan, K.; Yang, X. M.; Yen, M.; Zhao, J. C.; Moore, J. S.; Zang, L., *J. Am. Chem. Soc.* **2007**, *129*, 6978-6979.
72. Schrock, R. R.; Lee, J.; Liang, L. C.; Davis, W. M., *Inorg. Chim. Acta* **1998**, *270*, 353-362.
73. Agapie, T.; Bercaw, J. E., *Organometallics* **2007**, *26*, 2957-2959.
74. Agapie, T.; Day, M. W.; Bercaw, J. E., *Organometallics* **2008**, *27*, 6123-6142.
75. Sarkar, S.; Carlson, A. R.; Veige, M. K.; Falkowski, J. M.; Abboud, K. A.; Veige, A. S., *J. Am. Chem. Soc.* **2008**, *130*, 1116-1117.
76. Sarkar, S.; Abboud, K. A.; Veige, A. S., *J. Am. Chem. Soc.* **2008**, *130*, 16128-16129.
77. Van Tamelen, E. E., *Acc. Chem. Res.* **1970**, *3*, 361-367.
78. Clough, C. R.; Greco, J. B.; Figueroa, J. S.; Diaconescu, P. L.; Davis, W. M.; Cummins, C. C., *J. Am. Chem. Soc.* **2004**, *126*, 7742-7743.
79. Curley, J. J.; Sceats, E. L.; Cummins, C. C., *J. Am. Chem. Soc.* **2006**, *128*, 14036-14037.
80. Koller, J.; Sarkar, S.; Abboud, K. A.; Veige, A. S., *Organometallics* **2007**, *26*, 5438-5441.
81. Zarkesh, R. A.; Ziller, J. W.; Heyduk, A. F., *Angew. Chem., Int. Ed.* **2008**, *47*, 4715-4718.
82. Nguyen, A. I.; Blackmore, K. J.; Carter, S. M.; Zarkesh, R. A.; Heyduk, A. F., *J. Am. Chem. Soc.* **2009**, *131*, 3307-3316.

83. van de Kuil, L. A.; Luitjes, H.; Grove, D. M.; Zwikker, J. W.; van der Linden, J. G. M.; Roelofsen, A. M.; Jenneskens, L. W.; Drenth, W.; van Koten, G., *Organometallics* **1994**, *13*, 468-477.
84. Weisman, A.; Gozin, M.; Kraatz, H. B.; Milstein, D., *Inorg. Chem.* **1996**, *35*, 1792-1797.
85. Bromilow, J.; Brownlee, R. T. C.; Craik, D. J.; Sadek, M.; Taft, R. W., *J. Org. Chem.* **1980**, *45*, 2429-2438.
86. Bromilow, J.; Brownlee, R. T. C.; Lopez, V. O.; Taft, R. W., *J. Org. Chem.* **1979**, *44*, 4766-4770.
87. Delferro, M.; Tegoni, M.; Verdolino, V.; Cauzzi, D.; Graiff, C.; Tiripicchio, A., *Organometallics* **2009**, *28*, 2062-2071.
88. Stupka, G.; Gremaud, L.; Bernardinelli, G.; Williams, A. F., *Dalton Trans.* **2004**, 407-412.
89. Carina, R. F.; Verzeznassi, L.; Bernardinelli, G.; Williams, A. F., *Chem. Commun.* **1998**, 2681-2682.

Chapter 2:

Nitrile-Alkyne Cross Metathesis with Group 6 Nitride Complexes

2.1. Introduction

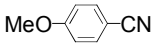
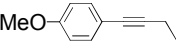
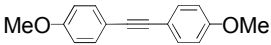
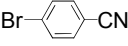
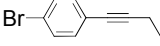
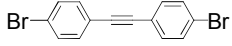
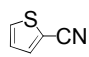
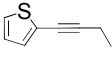

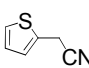
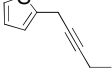
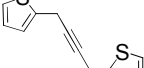
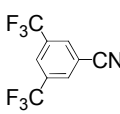
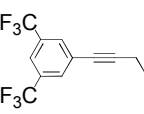
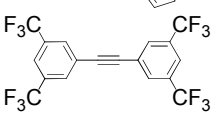
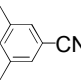
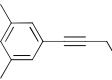
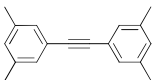
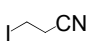
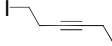
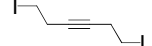
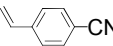
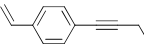
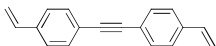
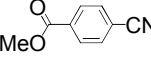
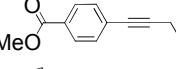
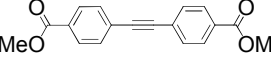
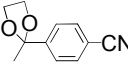
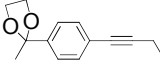
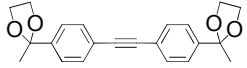
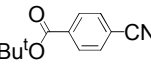
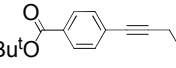
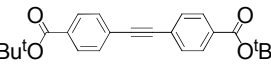
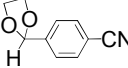
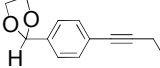
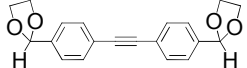
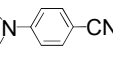
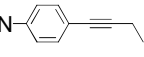
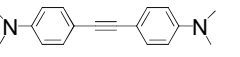
Nitrile-alkyne cross metathesis (NACM) is a convenient method to form a new carbon-carbon triple bond from a pre-existing carbon-nitrogen triple bond. The actual synthetic utility of NACM is dependent on the tolerance of the catalyst for a diverse array of functional groups. In Chapter 1, NACM was successfully demonstrated with W nitride catalysts, but the functional group tolerance of the systems remained unknown. Therefore the substrate tolerance of the W catalysts will be addressed in this chapter, along with the application of NACM in the synthesis of arylene ethynylene macrocycles.

As described in Chapter 1, Mo-based ACM catalysts are typically tolerant of a wider variety of functional groups than W-based ACM catalysts. The inability of current Mo complexes to catalyze NACM will be addressed along with strategies to overcome the inherent obstacles associated with Mo. Finally, new complexes will be synthesized and tested for NACM activity.

2.2 Substrate Scope of [W]≡N Catalysts

Previous studies have determined the optimized reaction conditions for NACM reactions with complexes **2.1** and **2.2** (Figure 2.1).^{1,2} Use of 3-hexyne as an inexpensive “sacrificial” alkyne allows for the facile initiation of the NACM cycle. For a given nitrile

Table 2.1. Nitrile substrates tolerated in NACM.

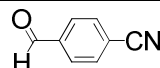
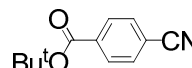
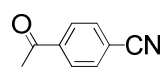
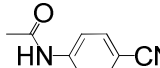
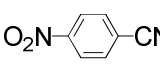
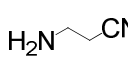
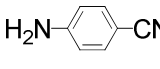
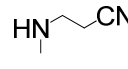
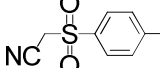
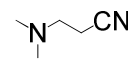
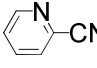
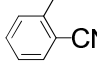
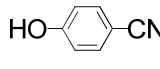
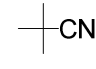
Entry	Starting Nitrile	Products (% Yield)		Time (h)	3-hexyne (equiv)		
		Unsymmetrical Alkyne	Symmetrical Alkyne				
1			11 18 ^a		81 61 ^a	8 31 ^a	1.0 1.0 ^a
2			0		100	15	2.0
3			19		41	11	2.0
4			0		75	22	2.0
5			5		95	25	2.0
6			<5		>95	24	2.0
7			40		33	6	2.0
8			34		64	13	1.6
9			76		24	24	3.0
10			19 58 ^a		23 12 ^a	11 25 ^a	1.0 1.0 ^a
11			43 ^a		6 ^a	20 ^a	2.0 ^a
12			4 25 ^a		0 0 ^a	12 25 ^a	1.0 1.0 ^a
13			69		13	18	2.0

NMR conversions. Conditions: toluene-*d*₈, 95 °C, 20 equiv of nitrile, catalyst **2.1** unless otherwise noted. ^a Catalyst **2.2**.

As seen in Table 2.2, a variety of polar functional groups were shown to be incompatible with NACM catalyzed by **2.1**. Three modes of reaction failure were identified: deactivation of the tungsten nitride complex, deactivation of the alkylidyne complex, and failure to undergo NACM without catalyst deactivation. In all cases,

catalyst deactivation was determined through addition of anisonitrile (4-methoxybenzonitrile) to the reaction mixture – lack of NACM reactivity with anisonitrile indicated catalyst deactivation. Ketone (entry 2), pyridyl (entry 6), and protic (entries 4, 7, 9-11) groups were found to immediately deactivate the nitrile complex **2.1**; in these reactions, no propionitrile formation was observed, indicating deactivation of the nitrile complex prior to reaction with 3-hexyne. Various other substrates (entries 1, 3, 5, 8, 12) led to deactivation of the alkylidyne complex, as a stoichiometric amount of propionitrile was formed. Bulky substrates (entries 13-14) proved too large to undergo metathesis, but did not cause catalyst deactivation.

Table 2.2. Catalyst deactivation modes (indicated by Y) with incompatible substrates.

Entry	Starting Nitrile	Cat. Decomp.		Entry	Starting Nitrile	Cat. Decomp.	
		[W]N	[W]CEt			[W]N	[W]CEt
1		N	Y	8		N	Y
2		Y		9		Y	
3		N	Y	10		Y	
4		Y		11		Y	
5		N	Y	12		N	Y
6		Y		13		N	N
7		Y		14		N	N

Overall, **2.1** displays a relatively low tolerance of polar functional groups, especially relative to Schrock's ACM catalyst $\text{Me}_3\text{CC}\equiv\text{W}(\text{OCMe}_3)_3$.^{3, 4} Some of the functional group intolerance likely stems from the Lewis acidic tungsten center, which tends to react with polar functional groups. Additionally, the high operating temperatures required for NACM likely led to more rapid catalyst deactivation.

2.3 Arylene Ethynylene Macrocycles via NACM

The utility of NACM in the preparation of arylene ethynylene macrocycles was next investigated, as these macrocycles often display interesting optical properties but can be challenging to make (Chapter 1). Initial studies focused on the dicyanobenzene substrates shown in Figure 2.2. NACM reactions of 1,2-dicyanobenzene (**2.3**) and 4,5-dimethylphthalonitrile (**2.4**) were found to proceed very slowly with no discernible product being formed. The slightly larger substrate 4,5-dimethoxyphthalonitrile (**2.5**) did not display any NACM activity. Clearly these *ortho*-dinitriles are too sterically hindered to undergo efficient NACM.

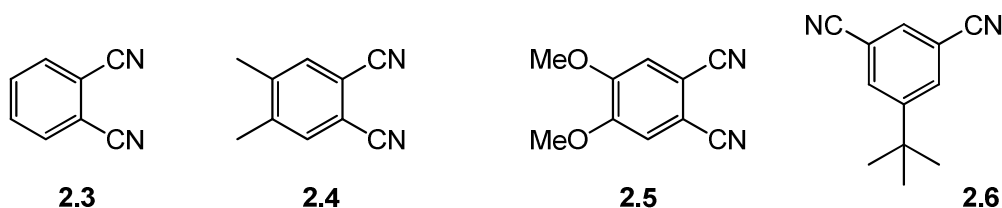
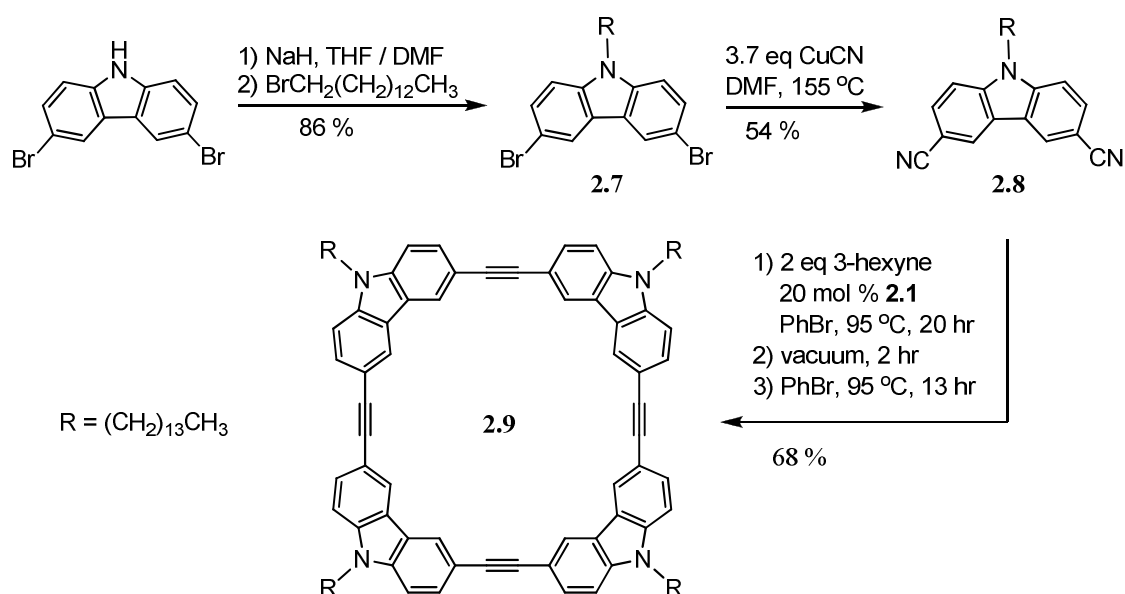


Figure 2.2. Unsuccessful substrates for macrocycle formation.

The less hindered 5-*tert*-butylisophthalonitrile (**2.6**) was active for NACM catalyzed by **2.1**. However, NACM with **2.6** was not selective for macrocycle formation,

as a large number of product peaks were observed in the ^1H NMR spectrum. Attempts to drive the reaction towards selective macrocycle formation through *in vacuo* removal of 3-hexyne and propionitrile were unsuccessful.

The formation of a tetrameric carbazole-derived macrocycle was next targeted. As shown in Scheme 2.1, synthesis of the desired substrate was straightforward. Deprotonation of 3,6-dibromocarbazole with NaH followed by reaction with 1-tetradecylbromide led to the formation of 3,6-dibromo-*N*-tetradecylcarbazole (**2.7**) in 86 % isolated yield. Rosenmund-von Braun coupling of **2.7** with CuCN then gave the desired substrate, 3,6-dicyano-*N*-tetradecylcarbazole (**2.8**), in 54 % isolated yield.



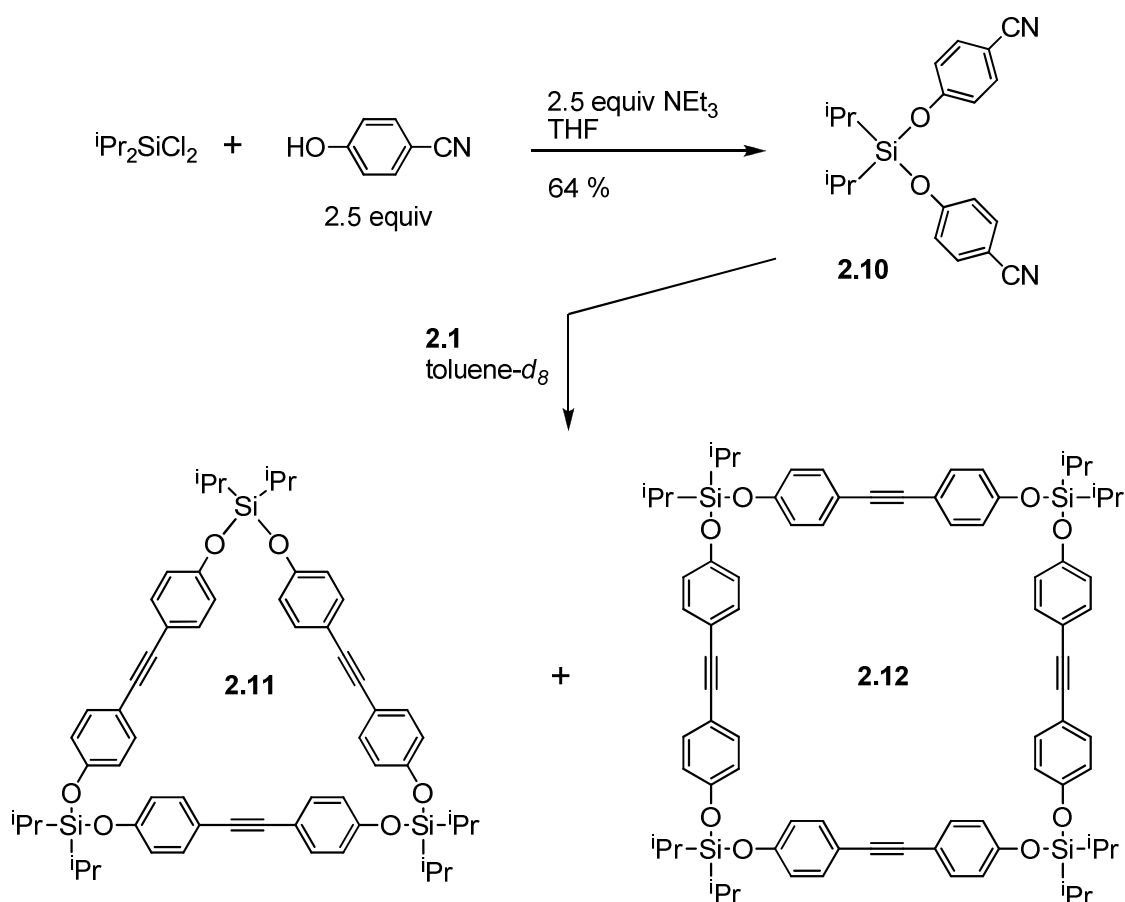
Scheme 2.1. Synthesis of an arylene ethynylene tetramer using NACM.

NACM reactions of **2.8** were found to proceed efficiently using 20 mol % **2.1** and 2 equiv 3-hexyne in bromobenzene. After 20 hours of reaction time, a mixture of **2.9** and other oligomers was formed. Removal of volatile 3-hexyne and propionitrile followed by

ACM of the reaction mixture gave the desired tetrameric arylene ethynylene macrocycle **2.9** in good conversion. Macrocycle **2.9** could be isolated in 68 % yield after workup. Its identity was confirmed through MALDI-TOF mass spectroscopy and comparison of its ^1H and $^{13}\text{C}\{^1\text{H}\}$ NMR spectra to reported values.⁵

Moore's precipitation-driven ACM strategy is the best reported method of synthesizing **2.9**. The current synthesis gives an overall yield (32 %) comparable to Moore's route (42 %)⁵ in three fewer steps; optimization of the reaction conditions to make substrate **2.8** would likely improve the current overall yield. Additionally, Moore's strategy relies on the formation of a large, insoluble alkyne byproduct to drive macrocycle formation, which is atom uneconomical relative to the current byproduct of 3-hexyne. Therefore, the current synthesis of **2.9** highlights that NACM can be more advantageous than ACM.

Given the successful synthesis of a tetrameric macrocycle, we next investigated the ability to form other tetrameric macrocycles *via* NACM. Synthesis of the siloxide substrate **2.10** was readily achieved by condensation of *p*-cyanophenol with diisopropyldichlorosilane in the presence of triethylamine (Scheme 2.2). Extraction of the crude product with Et_2O and subsequent removal of excess *p*-cyanophenol by sublimation afforded **2.10** as a yellow oil in 64 % yield. Studies by Dr. Andrea Geyer indicated that **2.10** does participate in NACM, with both the trimeric (**2.11**) and tetrameric (**2.12**) macrocycles being formed in 33 % conversion each.⁶ The lack of conversion to a single structure is likely the result of the flexibility of the siloxide unit. Preparations of **2.11** and **2.12** via ACM also do not occur selectively, and so the two macrocycles must be separated from each other.⁷



Scheme 2.2. Formation of silicon-containing macrocycles by NACM.

2.4 Design of Mo NACM Catalysts

As seen in Section 2.2, NACM catalysts **2.1** and **2.2** have limited functional group tolerance, making their utility somewhat limited. Because Mo ACM catalysts are often more functional group tolerant than W catalysts, we next sought to develop NACM catalysts based on Mo. Chapter 1 discussed some of the challenges in the design of Mo NACM catalysts, including 1) higher barriers to metalacycle formation for Mo relative to

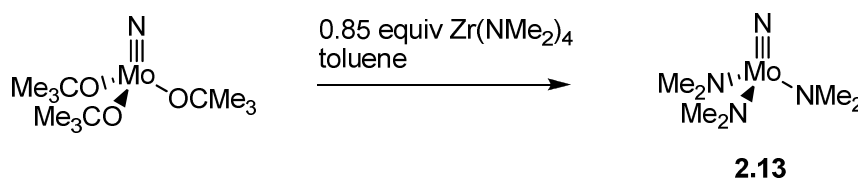
W,⁸ 2) alkylidyne ligation being favored over nitride ligation,⁹ and 3) dimerization of $\text{RC}\equiv\text{Mo}(\text{OR}')_3$ complexes to give $\text{Mo}_2(\text{OR}')_6$ species.⁶

Given that the alkylidyne-to-nitride conversion has never been observed for Mo, the obvious solution is to heat the metathesis mixtures to increasingly higher temperatures until nitride formation occurs. With current Mo systems containing fluorinated alkoxides, this approach was expected to result in catalyst decomposition by either bimolecular decomposition to give $\text{Mo}_2(\text{OR}')_6$ species⁶ or alkoxide C–O bond scission resulting in Mo-oxo species.¹⁰ To prevent these deactivation pathways, we sought to use thermally robust ligands that possess enough steric bulk to prevent bimolecular decomposition.

Not only do the ancillary ligands need to be large and thermally robust, but the donating strength of the ligand must be appropriate to allow reversible interconversion between nitride and alkylidyne ligation. Given the successful conversion of $\text{N}\equiv\text{Mo}(\text{OC}(\text{CF}_3)_2\text{Me})_3$ to $\text{EtC}\equiv\text{Mo}(\text{OC}(\text{CF}_3)_2\text{Me})_3$,¹¹ we chose to use alcohols with a pKa near that of $\text{HOC}(\text{CF}_3)_2\text{Me}$ (pKa = 13.3, H_2O).¹² Phenol (pKa = 9.5, H_2O ; 18.0, DMSO)¹³ and triphenylsilanol (pKa = 16.6, DMSO)¹⁴ were estimated to have an appropriate pKa and therefore were of interest for use as ancillary ligands. Because phenol is rather small, we chose to use phenols containing bulky substituents in the 2,6-positions. Additionally, silanols of the type HOSiPh_2R (R = alkyl) were of interest, as the alkyl substitution would make the corresponding siloxide ligand a stronger donor ligand than triphenylsiloxide.

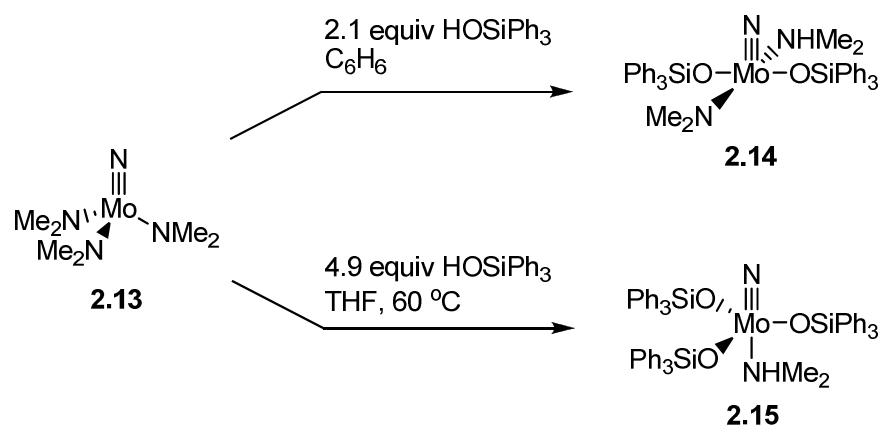
2.5 Protonolysis of $\text{N}\equiv\text{Mo}(\text{NMe}_2)_3$

Protonolysis of Mo-NR_2 bonds was investigated for installation of the desired ancillary ligands. The known complex $\text{N}\equiv\text{Mo}(\text{NMe}_2)_3$ (**2.13**)¹⁵ seemed a good candidate for protonolysis. In a modification of the literature procedure, **2.13** was synthesized by reaction of $\text{N}\equiv\text{Mo}(\text{OCMe}_3)_3$ with $\text{Zr}(\text{NMe}_2)_4$. Complex **2.13** was subsequently isolated in 77 % yield by precipitation from toluene / pentane. The literature procedure uses $\text{Ti}(\text{NMe}_2)_4$, which is purified by distillation and is flammable. Therefore, the advantage in the current synthesis of **2.13** is that $\text{Zr}(\text{NMe}_2)_4$ is readily purified by crystallization.



Scheme 2.3. Synthesis of **2.13**.

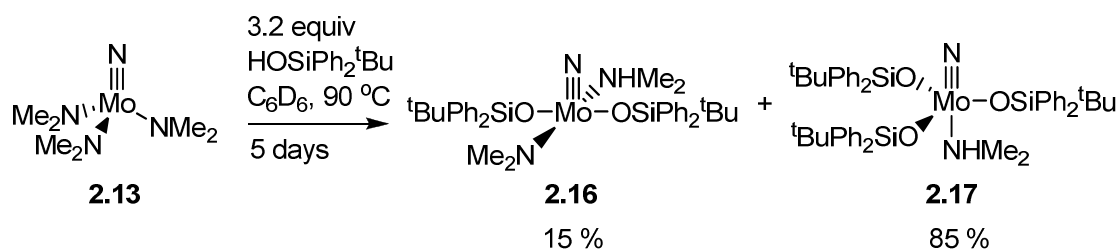
Addition of 2.1 equiv HOSiPh_3 to a benzene solution of **2.13** led to the precipitation of $\text{N}\equiv\text{Mo}(\text{OSiPh}_3)_2(\text{NMe}_2)(\text{NHMe}_2)$ (**2.14**), which was isolated in 93 % yield (Scheme 2.4). The ^1H NMR spectrum of **2.14** displays two methyl resonances each for the $-\text{NMe}_2$ and NHMe_2 ligands, indicating that rotation about the Mo-N bonds is hindered. No crosspeaks between the $-\text{NMe}_2$ and NHMe_2 groups were observed in the 2D NOESY spectrum of **2.14**, suggesting a square pyramidal geometry with *trans* siloxide ligands.



Scheme 2.4. Protonolysis of **2.13** with HOSiPh₃.

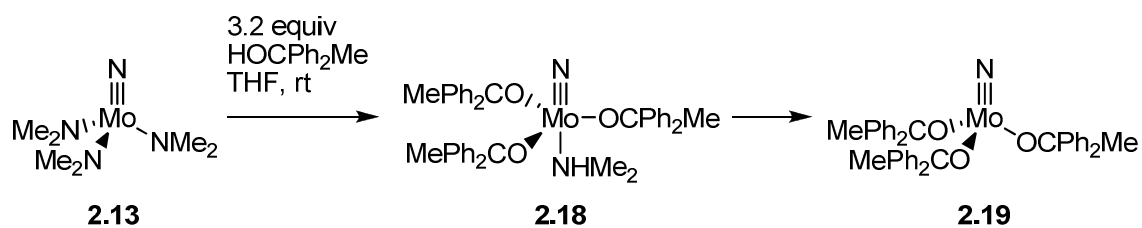
Protonation of the final –NMe₂ ligand proved more challenging. Ultimately, reaction between **2.13** and an excess of HOSiPh₃ in THF at 60 °C led to the formation of N≡Mo(OSiPh₃)₃(NHMe₂) (**2.15**) as shown in Scheme 2.4. Complex **2.15** displayed low solubility in most solvents, except THF and CH₂Cl₂, and hence **2.15** was isolated in 62 % yield containing a small amount of an unknown impurity. A single –OSiPh₃ environment was observed in the ¹H NMR spectrum of **2.15**, indicating either fast exchange of the siloxide ligands or a geometry in which the NHMe₂ ligand is *trans* to the nitride ligand.

Next investigated was HOSiPh₂^tBu,¹⁶ since the corresponding siloxide ligand should be a stronger electron donor than –OSiPh₃, and thus could affect the catalyst resting state in a NACM reaction. When **2.13** was treated with 3.2 equiv of HOSiPh₂^tBu, mixtures of N≡Mo(OSiPh₂^tBu)₂(NMe₂)(NHMe₂) (**2.16**) and N≡Mo(OSiPh₂^tBu)₃(NHMe₂) (**2.17**) were formed. The third protonation step proved quite slow, with only 85 % conversion to **2.17** being observed by ¹H NMR spectroscopy after heating the reaction mixture for 5 days at 90 °C. For this reason, neither **2.16** nor **2.17** was isolated.



Scheme 2.5. Protonolysis of **2.13** with HOSiPh₂^tBu.

The structurally related alcohol HOCPh₂Me was found to react cleanly with **2.13** in THF at room temperature to give N≡Mo(OCPh₂Me)₃(NHMe₂) (**2.18**) as an initial product (Scheme 2.6). However, upon multiple precipitations from toluene / pentane, the NHMe₂ ligand was lost and N≡Mo(OCPh₂Me)₃ (**2.19**) could be isolated in 21 % yield. Unsurprisingly, **2.19** rapidly decomposed at 95 °C to give 1,1-diphenylethene as the only product observed in the ¹H NMR spectrum.



Scheme 2.6. Protonolysis of **2.13** with HOCPh₂Me.

X-ray quality crystals of **2.18** were grown from a toluene / pentane solution at –35 °C. Single-crystal X-ray diffraction analysis revealed that **2.18** crystallizes in the triclinic space group P $\bar{1}$. The dimethylamine ligand is rotationally disordered over two equally occupied positions, and was confirmed to be located *trans* to the nitride ligand. The Mo–N bond for NHMe₂ is very long at 2.606(6) Å and 2.584(6) Å for the two sites.

Additionally, the Mo≡N triple bond is quite long at 1.700(4) Å due to the presence of a σ -donor NMe₂ *trans* to the nitride ligand. This distance is among the longest found for a terminal nitrido complex of Mo.¹⁷

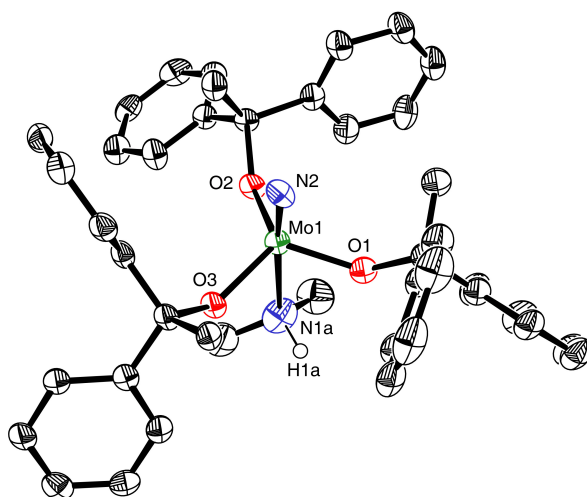
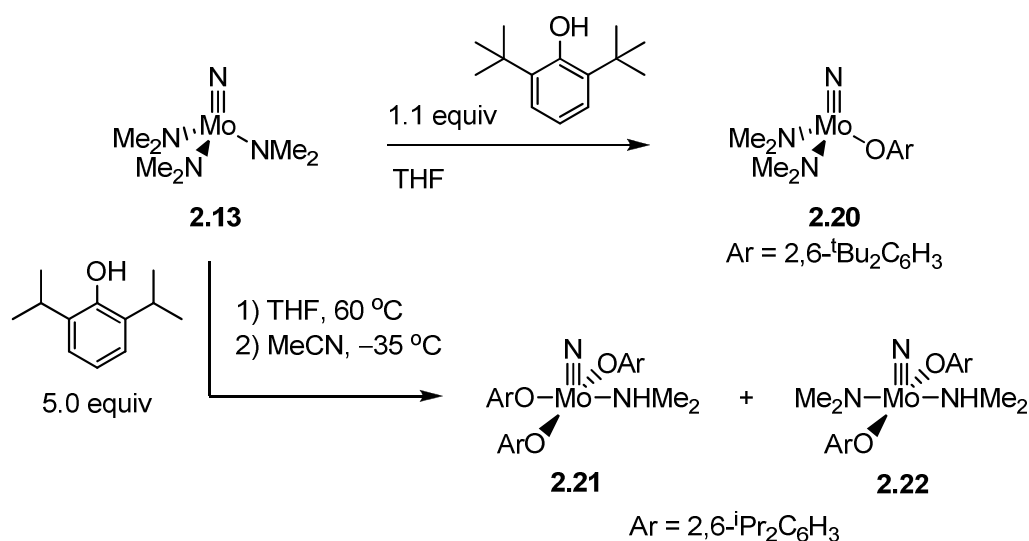


Figure 2.3. 50 % thermal ellipsoid plot of **2.18**. The hydrogen atoms and 1 NMe₂ are omitted for clarity. Selected bond lengths (Å) and angles (deg): Mo1-N2, 1.700(4); Mo1-O1, 1.883(3); Mo1-O2, 1.884(3); Mo1-O3, 1.883(3); Mo1-N1a, 2.606(6); N2-Mo1-O1, 102.18(15); N2-Mo1-O2, 104.09(15); N2-Mo1-O3, 103.01(15); N2-Mo1-N1a, 175.5(2); O1-Mo1-O2, 113.64(12); O1-Mo1-O3, 117.53(12); O2-Mo1-O3, 113.91(12). Complete XRD data can be found in Appendix 1.

Complex **2.13** also reacted readily with bulky substituted phenols. Treatment of **2.13** with 2,6-di-*tert*-butylphenol resulted in a single protonation to give N≡Mo(OAr)(NMe₂)₂ (**2.20**); the inclusion of excess phenol did not lead to further substitution (Scheme 2.7). Washing the crude mixture with cold pentane allowed for the isolation of **2.20** in 81 % yield. The ¹H NMR spectrum for **2.20** displays two broad peaks for the -NMe₂ groups due to hindered rotation. Cooling a toluene-*d*₈ solution of **2.20** to -10 °C resulted in sharpening of the dimethylamido resonances.



Scheme 2.7. Protonolysis of **2.13** with substituted phenols.

As 2,6-di-*tert*-butylphenol proved too large to achieve multiple substitutions, a slightly smaller phenol was next employed. Treatment of **2.13** with an excess of 2,6-diisopropylphenol at 60 °C in THF led to the formation of both $\text{N}\equiv\text{Mo}(\text{OAr})_3(\text{NHMe}_2)$ (**2.21**) and $\text{N}\equiv\text{Mo}(\text{OAr})_2(\text{NMe}_2)(\text{NHMe}_2)$ (**2.22**) at intermediate reaction times (Scheme 2.7). After extended reaction periods (>20hrs), ^1H NMR spectroscopy indicated that **2.22** had been consumed, with **2.21** being the only Mo compound observed. Separation of **2.21** from the remaining phenol proved difficult, as each is highly soluble in nonpolar solvents, including pentane. Ultimately, deep-red crystals of **2.21** were grown slowly from MeCN at -35°C , and **2.21** could be obtained in 85 % yield. Addition of a seed crystal to the solution greatly facilitated the crystal growth of **2.21**. ^1H NMR analysis of crystalline **2.21** revealed the presence of 0.4 equiv of HOAr and 0.1 equiv of **2.22**. The presence of **2.22** in the isolated product was surprising, as no **2.22** was observed in the reaction mixture prior to crystallization. Apparently a mechanism for conversion of **2.21** to **2.22** exists under the crystallization conditions.

X-ray quality crystals of **2.21** were grown from an acetonitrile solution at $-35\text{ }^{\circ}\text{C}$. Single-crystal X-ray diffraction analysis revealed that **2.21** crystallizes in the monoclinic space group $P2_1/n$. The Mo-N triple bond length is typical at $1.6509(10)\text{ \AA}$, and the Mo-NHMe₂ bond length of $2.2859(11)\text{ \AA}$ is much shorter than observed in **2.18** since the NHMe₂ ligand is now bound *cis* to the nitride ligand rather than *trans*. The mutually *trans* aryloxy rings lie approximately in a plane containing the Mo \equiv N bond, while the third aryloxy is approximately orthogonal to the plane. In contrast, only a single aryloxy environment is observed in the solution ¹H NMR spectrum of **2.21** at $25\text{ }^{\circ}\text{C}$.

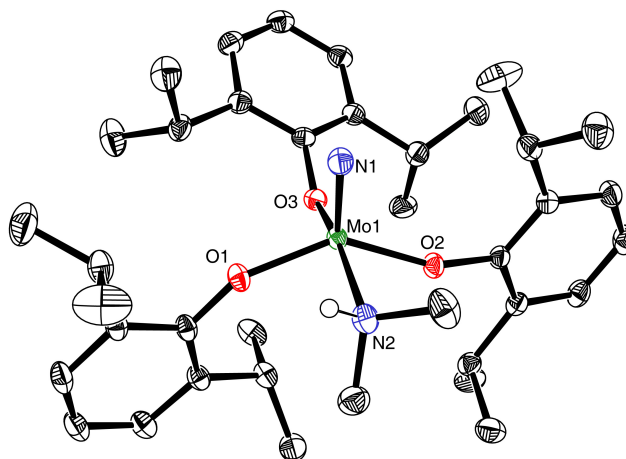


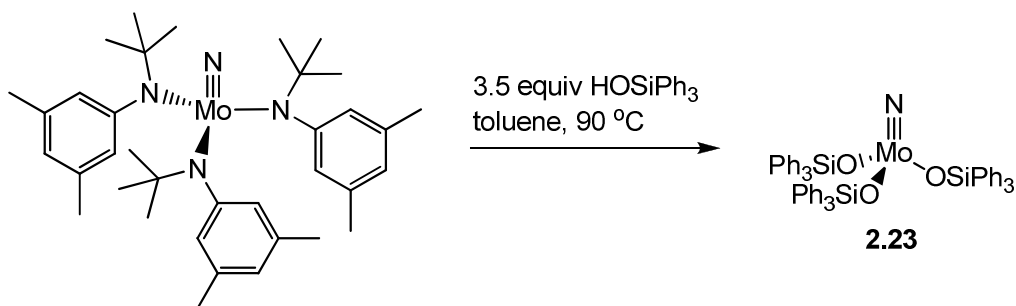
Figure 2.4. 50 % thermal ellipsoid plot of **2.21**. The hydrogen atoms are omitted for clarity. Selected bond lengths (\AA) and angles (deg): Mo1-N1, $1.6509(10)$; Mo1-O1, $1.9292(8)$; Mo1-O2, $1.9206(8)$; Mo1-O3, $1.9333(8)$; Mo1-N2, $2.2859(11)$; N1-Mo1-O1, $103.93(4)$; N1-Mo1-O2, $109.65(4)$; N1-Mo1-O3, $102.35(5)$; N1-Mo1-N2, $92.79(5)$; O1-Mo1-O3, $95.12(4)$; O1-Mo1-N2, $81.34(4)$; O2-Mo1-O3, $92.97(3)$; O2-Mo1-N2, $81.49(4)$. Complete XRD data can be found in Appendix 2.

Of the $\text{N}\equiv\text{Mo}(\text{OR})_3(\text{NHMe}_2)$ complexes isolated, only **2.18** ($\text{R} = \text{CPh}_2\text{Me}$) was found to possess a labile NHMe₂ ligand. The observed NHMe₂ lability of **2.18** is likely a result of stronger σ -donation from the $-\text{OCPh}_2\text{Me}$ ligand relative to $-\text{OSiPh}_3$ (**2.15**) and –

O-2,6-ⁱPr₂C₆H₃ (**2.21**). Therefore, the Mo center of **2.18** is more electron rich and the Mo–NHMe₂ bond is consequently weaker and more labile.

2.6 Protonolysis of N≡Mo(N[R]Ar)₃

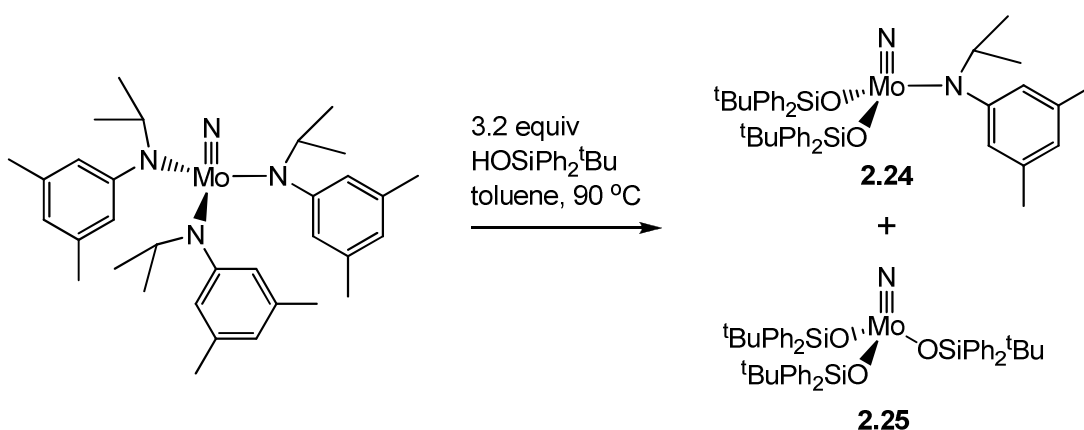
Expecting that a bound NHMe₂ ligand could inhibit triple–bond metathesis reactions of N≡Mo(OR)₃(NHMe₂) complexes, the corresponding base-free complexes N≡Mo(OR)₃ were sought. In this regard, Cummins' complexes N≡Mo(N[R]Ar)₃ (R = ^tBu, ⁱPr; Ar = 3,5-Me₂C₆H₃)^{18, 19} proved useful as the aniline products of protonolysis are likely too large to bind. The *tert*-butyl derivative N≡Mo(N[^tBu]Ar)₃ reacted readily with 3.5 equiv of HOSiPh₃ to give N≡Mo(OSiPh₃)₃ (**2.23**) as the only observable product (Scheme 2.8). The reaction proceeded slowly at room temperature, but was complete within 6 hours at 90 °C in toluene. Separation from the aniline byproducts by precipitation from toluene / pentane afforded **2.23** as a white powder in 51 % yield.



Scheme 2.8. Protonolysis of N≡Mo(N[^tBu]Ar)₃ with HOSiPh₃.

The larger silanol HOSiPh₂^tBu reacted extremely slowly with N≡Mo(N[^tBu]Ar)₃, with only small amounts of substitution observed over 8 days at 90 °C. Use of the smaller isopropyl derivative N≡Mo(N[ⁱPr]Ar)₃ facilitated the reaction greatly. Treatment

of $\text{N}\equiv\text{Mo}(\text{N}[\text{iPr}]\text{Ar})_3$ with 3.2 equiv of $\text{HOSiPh}_2\text{tBu}$ in toluene at room temperature led to the rapid formation of $\text{N}\equiv\text{Mo}(\text{OSiPh}_2\text{tBu})_2(\text{N}[\text{iPr}]\text{Ar})$ (**2.24**) as judged by ^1H NMR spectroscopy (Scheme 2.9). Heating the reaction mixture at $90\text{ }^\circ\text{C}$ resulted in the appearance of $\text{N}\equiv\text{Mo}(\text{OSiPh}_2\text{tBu})_3$ (**2.25**), with a 79 % conversion to **2.25** observed after 3 hours. Further heating of the reaction mixture resulted in negligible change in the product composition. Cooling an acetonitrile solution of the crude mixture to $-35\text{ }^\circ\text{C}$ resulted in the precipitation of a white powder; several sequential precipitations followed by lyophilization from benzene allowed for the isolation of **2.25** as a yellow oil in 59 % yield.



Scheme 2.9. Protonolysis of $\text{N}\equiv\text{Mo}(\text{N}[\text{iPr}]\text{Ar})_3$ with $\text{HOSiPh}_2\text{tBu}$.

The reaction of 2,6-diisopropylphenol with both $\text{N}\equiv\text{Mo}(\text{N}[\text{tBu}]\text{Ar})_3$ and $\text{N}\equiv\text{Mo}(\text{N}[\text{iPr}]\text{Ar})_3$ was very slow. Multiple products were observed by ^1H NMR spectroscopy at all reaction times. Therefore, the 2,6-diisopropyl substitution pattern is shown to be too congested at the $-\text{OH}$ group to allow efficient protonation of the bulky anilide ligands.

2.7 ACM Studies of Mo Nitride Complexes

The ACM activity of the new $N\equiv Mo(OR)_3(L)$ complexes was assessed prior to investigating their NACM activity. Catalytic reactions were performed in C_6D_6 at a catalyst concentration of 5 mg mL^{-1} with 20 equiv 1-phenyl-1-butyne as the substrate. As seen in Scheme 2.10, the ACM products of 1-phenyl-1-butyne are diphenylacetylene and 3-hexyne. The reaction progress was readily monitored by 1H NMR spectroscopy through integration of the Ph group resonances with respect to an internal standard of 1,3,5-trimethoxy benzene. At a statistical equilibrium mixture as shown in Scheme 2.10, the integrations for 1-phenyl-1-butyne and diphenylacetylene would be equivalent.

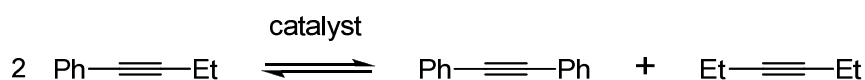


Figure 2.5. Statistical equilibrium mixture of ACM with 1-phenyl-1-butyne.

Of the five tri-alkoxide complexes synthesized, three were active for ACM. The highest activity was observed with $N\equiv Mo(OSiPh_3)_3$ (**2.23**), which catalyzes ACM at room temperature to a reaction equilibrium within 2 hours (Table 2.3). When the ACM mixture was heated to $90\text{ }^\circ\text{C}$, an 80 % conversion to an alkylidyne complex was observed after 16 hours. The complexes $N\equiv Mo(OSiPh_3)_3(NHMe_2)$ (**2.15**) and $N\equiv Mo(O-2,6-{}^iPr_2C_6H_3)_3(NHMe_2)$ (**2.21**), which each contain a basic $NHMe_2$ ligand, were found to require elevated temperatures for ACM to occur. However, equilibrium mixtures were reached rapidly within 1.5-2.5 hours at $75\text{ }^\circ\text{C}$, indicating sufficient lability of the $NHMe_2$ ligand to allow interaction of the Mo center with incoming alkyne substrate.

While $\text{N}\equiv\text{Mo}(\text{OSiPh}_3)_3$ (**2.23**) was found to be a very active ACM catalyst, the related complex $\text{N}\equiv\text{Mo}(\text{OSiPh}_2^t\text{Bu})_3$ (**2.25**) was not active for ACM even at 90 °C. Steric effects of the larger $-\text{OSiPh}_2^t\text{Bu}$ likely increase the activation barrier for metalacycle formation for **2.25** relative to **2.23**, though the magnitude of the effect is currently unknown. Secondly, inductive effects of the ^tBu group should render $-\text{OSiPh}_2^t\text{Bu}$ a stronger electron donor ligand than $-\text{OSiPh}_3$, thus making nitride ligation more favorable than alkylidyne ligation for **2.25**. A pKa value for $\text{HOSiPh}_2^t\text{Bu}$ or similarly substituted silanols has not been reported for comparison to HOSiPh_3 . However, the nearly identical pKa's of HOSiPh_3 (pKa = 16.57, DMSO)¹⁴ and HOCPh_3 (pKa = 16.97, DMSO)¹⁴ suggest that $-\text{OSiPh}_2^t\text{Bu}$ and its carbon analogues should have similar electron donor abilities. Like **2.25**, $\text{N}\equiv\text{Mo}(\text{OCPh}_2\text{Me})_3$ (**2.19**) was inactive for ACM and decomposed at 90 °C with 1,1-diphenylethene being observed as a decomposition product. As $-\text{OCPh}_2\text{Me}$ is smaller than $-\text{OSiPh}_3$, electronic influences also play a role in the inability of **2.19** and **2.25** to catalyze ACM.

Table 2.3. Catalytic ACM of 1-phenyl-1-butyne.^a

Complex	Temp / °C	Time / h ^b	% PhC≡CEt	% PhC≡CPh	% EtC≡CEt
2.15	75	1.5	50	25	25
2.19	75	21.0	100	0	0
2.21	75	2.5	50	25	25
2.23 ^c	RT ^d	2.0	50	25	25
2.25	90	9.0	100	0	0

^a NMR scale reactions with 5 mol % catalyst at catalyst concentration of 10 mg mL⁻¹ in C₆D₆. Product compositions were determined from integration of the ¹H NMR spectrum resonances. ^b Time to reaction completion in hours. ^c 20 mol % catalyst. ^d RT = room temperature.

2.8 NACM Studies of Mo Nitride Complexes

In order to test for NACM activity, the complexes $\text{N}\equiv\text{Mo}(\text{OR})_3(\text{NHMe}_2)$ (**2.15**, **2.21**) and $\text{N}\equiv\text{Mo}(\text{OR})_3$ (**2.23**, **2.25**) were heated in the presence of 10 equiv of 1-phenyl-1-butyne and 10 equiv of anisonitrile. Incorporation of a *p*-methoxyphenyl unit into any one of three possible alkyne products would be evidence for conversion of a metal-alkylidyne species to its corresponding metal-nitride complex. Anisonitrile was chosen as the nitrile substrate for two reasons. First, ^1H NMR spectrum resonances for both the OCH_3 and ArH (*ortho* to MeO) are not typically obscured by other peaks. Secondly, in NACM reactions catalyzed by **2.1**, anisonitrile is more reactive for NACM than most other nitrile substrates (Table 2.1).

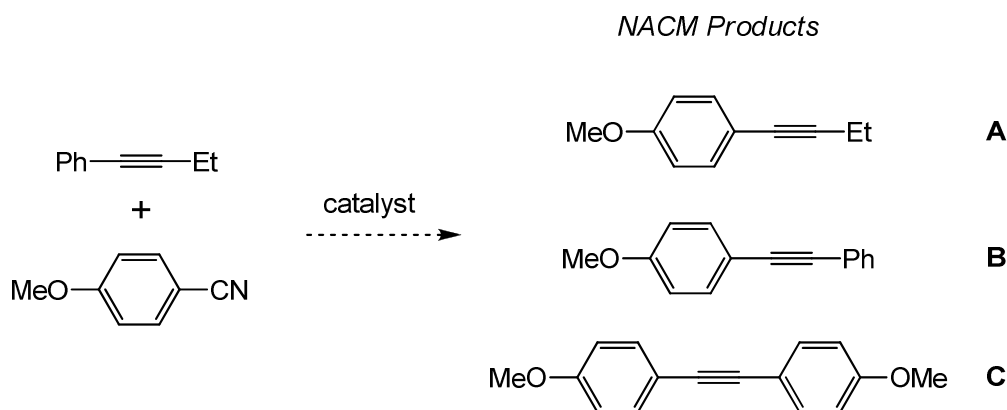


Figure 2.6. Design of NACM test reaction.

During the course of the NACM survey, it was gratifying to discover that $\text{N}\equiv\text{Mo}(\text{OSiPh}_3)_3$ (**2.23**) was active for NACM at 180 – 185 °C in solutions of BrC_6D_5 . Both 1-(but-1-ynyl)-4-methoxybenzene (**A**) and 1-methoxy-4-(phenylethynyl)benzene (**B**) were observed in the ^1H NMR spectrum and their identities were confirmed by GC-

MS and comparison to literature NMR shifts. As seen in Figure 2.7, increasing the catalyst concentration from 20 mg mL⁻¹ (22 mM) to 40 mg mL⁻¹ (42 mM) resulted in higher conversions to NACM products. At a concentration of 40 mg mL⁻¹, NACM is the most rapid and productive with > 20% conversion obtained over 8 hours. At all concentration levels, an alkylidyne species can be observed through appearance of a second *o*-PhH resonance for the siloxide ligand. Catalyst deactivation occurs during the course of the reaction, and so a true equilibrium is never established. The alkylidyne form of the catalyst likely accounts for most of the decomposition, as **2.23** decomposes only slightly upon heating at 180 °C for 16 hours in BrC₆D₅ solution.

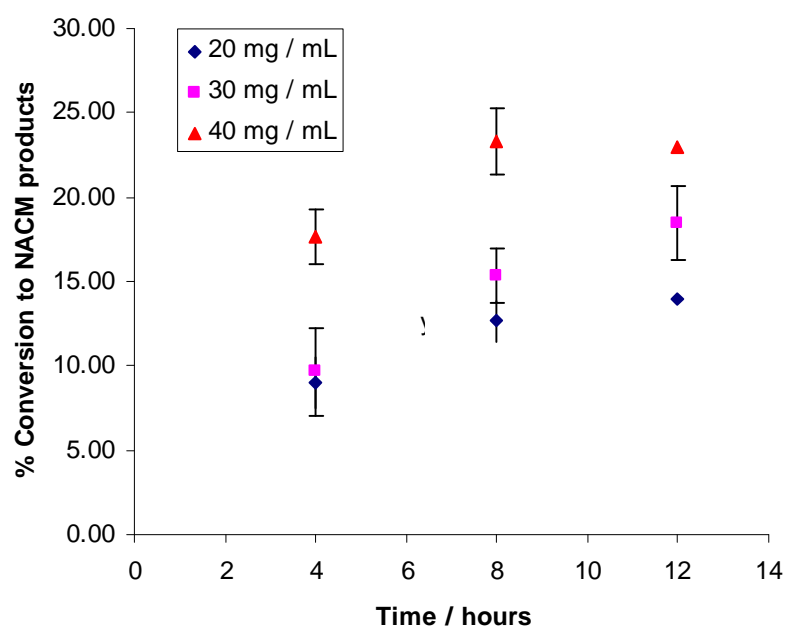


Figure 2.7. Conversion to NACM products catalyzed by **2.23**.

At low catalyst concentrations (20-30 mg mL⁻¹), productive NACM occurred over 12 hours, while at a higher concentration (40 mg mL⁻¹) NACM activity ceased after

8 hours. In all cases, the cessation of NACM activity occurs prior to complete catalyst decomposition, as both the nitride and alkylidyne species were observed in the ^1H NMR spectrum of the NACM–inactive reaction mixtures. The NACM inhibition may arise from the presence of decomposition products in the reaction mixture, though the mode of inhibition is currently unknown. The faster rate of catalyst deactivation at higher concentration is suggestive of an alkylidyne complex bimolecular decomposition pathway, possibly resulting in a $\text{Mo}_2(\text{OR})_6$ species.⁶ However, three separate reaction pathways (I–III) affect the alkylidyne concentration as shown in Figure 2.8, all of which are likely accelerated at increased initial concentrations. Therefore, at higher initial concentrations the nitride-alkylidyne equilibrium may lie further towards an alkylidyne species, thereby increasing the decomposition rate without invoking a bimolecular mechanism. Without a more detailed mechanistic study the factors influencing the mode of catalyst decomposition cannot be elucidated further.

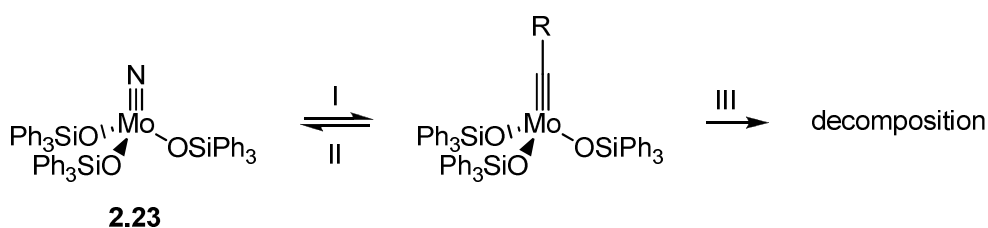


Figure 2.8. Catalyst reaction pathways in NACM with **2.22**.

The other ACM catalysts (**2.15**, **2.21**, and **2.25**) did not display any NACM activity under similar conditions ($185\text{ }^\circ\text{C}$, 40 mg mL^{-1} catalyst concentration). In the case of $\text{N}\equiv\text{Mo}(\text{OSiPh}_3)_3(\text{NHMe}_2)$ (**2.15**), complete complex deactivation occurred after 20 hours, though the decomposition products are unknown. The 2,6-

diisopropylphenoxide complex, $\text{N}\equiv\text{Mo}(\text{OAr})_3(\text{NHMe}_2)$ (**2.21**), was clearly unstable under the reaction conditions, as free HOAr was the only observable phenolic product after 4 hours of reaction. One possible mechanism for the decomposition of **2.21** would be formation of an aryloxy radical *via* homolytic Mo–O bond scission. The complex $\text{N}\equiv\text{Mo}(\text{OSiPh}_2^t\text{Bu})_3$ (**2.25**) was very stable under the reaction conditions, with ACM occurring at the reaction temperature of 180 °C. No alkylidyne formation was observed, suggesting formation of only a trace amount of alkylidyne complex. Given the importance of alkylidyne concentration found for **2.22**, it is not surprising that the trace amounts of alkylidyne species formed from **2.25** are not sufficient to promote NACM.

Other known complexes (Figure 2.9) were also investigated for NACM under the current reaction conditions; as expected, none of these complexes were active for NACM. Complexes **2.28** – **2.30** are all known ACM catalysts,^{6, 11, 20} and accordingly ACM was observed in the current NACM test reactions. The thermal stability of **2.28** and **2.29** was observed to be very low, as only small amounts of nitride complex remained after 4 hours at 185 °C. Decomposition of **2.30** was not readily ascertained from the ¹H NMR spectrum, though the absence of additional ACM upon addition of excess 1-phenyl-1-butyne suggests a lack of alkylidyne species in the reaction mixture. Complexes **2.26** and **2.27** were found to catalyze ACM under the test conditions, which is significant as neither has previously been demonstrated to catalyze ACM without a Lewis acid co-catalyst.⁶ In particular, **2.27** was quite stable under the reaction conditions, though no buildup of an alkylidyne complex was noted, explaining why NACM was not observed.

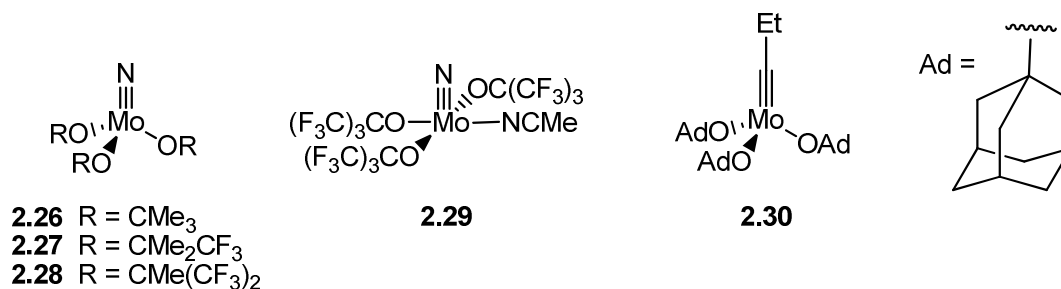


Figure 2.9. Literature complexes tested for NACM.

2.9 Conclusions

Tungsten catalyst **2.1** was found to be an efficient catalyst for effecting NACM using a variety of nitrile substrates. Good functional group compatibility was observed in the absence of very polar groups and protic groups. In a few cases, the less Lewis acidic catalyst **2.2** gave better conversions for some functional groups, such as acetals and ketals. A tetrameric arylene ethynylene macrocycle (**2.9**) was successfully synthesized using NACM catalyzed by **2.1**. Silicon-containing macrocycles (**2.11**, **2.12**) could also be formed through NACM, though not selectively.

A variety of new Mo nitride complexes were synthesized by protonolysis of $N\equiv Mo(N[R]R')_3$ compounds. The size of the amido ligand was found to be important for several reasons. First, in most examples, protonolysis of the small amido ligand $-NMe_2$ led to products containing a strongly bound $NHMe_2$ group, while protonolysis of the larger amido groups allowed for the isolation of base-free complexes. Second, protonation of large amido groups was found to be sensitive to small changes in the amido group size. For example, $HOSiPh_2^tBu$ was slow to protonate the $-N[{}^tBu]Ar$ group, while protonation of the $-N[{}^iPr]Ar$ group was faster.

Four of the new Mo nitride complexes were found to be active for ACM: **2.15**, **2.21**, **2.23**, and **2.25**. Complexes **2.15** and **2.21** required heating prior to the onset of ACM, as the bound NHMe₂ ligand prevents ACM at room temperature. The NHMe₂-free complex **2.23**, an analogue of **2.15**, was found to rapidly catalyze ACM at room temperature. The rates of ACM for **2.15**, **2.21**, and **2.23** are faster than found for *tert*-butoxide derived complexes **2.26-2.29**,⁶ though the challenging syntheses render them less practical. A catalyst with stronger siloxide donor ligands (**2.25**) requires excessive heating for ACM to occur (> 90 °C), making it an unattractive ACM catalyst. The first example of Mo-catalyzed NACM was discovered using **2.23** as a catalyst at 185 °C in BrC₆D₅ solution. Increased catalyst concentration was found to result in greater conversions to NACM products. At a 40 mg mL⁻¹ (42 mM) concentration of **2.23**, a 23 % conversion to NACM products (> 2 turnovers with 10 % **2.23**) was achieved over 8 hours. Decomposition of the alkylidyne complex under the reaction conditions prevented the establishment of reaction equilibrium. Other Mo nitride complexes were found to be inactive for NACM under the same reaction conditions, emphasizing the importance of ancillary ligand identity in triple-bond metathesis.

2.10 Experimental

2.10.1 Methods

All reactions were performed in an atmosphere of dinitrogen, either in a nitrogen-filled MBRAUN Labmaster 130 glove box or by using standard air-free techniques.²¹ ¹H NMR spectra were recorded at 499.909 MHz, 399.967 MHz, or or 300.075 MHz on a Varian Inova 500, Varian Inova 400, Varian MR400, or Varian Inova 300 spectrometer

and referenced to the residual protons in CDCl₃ (7.26 ppm), bromobenzene-*d*₅ (7.18 ppm), C₆D₆ (7.16 ppm), CD₂Cl₂ (5.32 ppm), or toluene-*d*₈ (2.09 ppm). ¹⁹F NMR spectra were recorded at 282.384 MHz on a Varian Inova 300 spectrometer or 376.326 MHz on a Varian Inova 400 spectrometer and were referenced to an external standard of CFC₃ in CDCl₃ (0.00 ppm). ¹³C NMR spectra were recorded at 100.724 MHz on a Varian Inova 400 or Varian MR400 spectrometer and were referenced to naturally abundant ¹³C nuclei in CDCl₃ (77.16 ppm), C₆D₆ (128.06 ppm), toluene-*d*₈ (125.49), or CD₂Cl₂ (54.00 ppm). GC/MS data were collected on a Shimadzu GCMS-QP5000 with a Restek XTI-5 phase column (30m, 0.25 I.D., 0.25 D. F.). HRMS data were collected on a Micromass AutoSpec Ultima with electrospray ionization. MALDI-TOF MS data were collected on a Micromass TofSpec-2E, and EI-MS data were collected on a VG (Micromass) 70-250-S magnetic sector mass spectrometer. Combustion analyses were performed either on a Perkin-Elmer 200 Series II Analyzer or by Midwest Microlabs, LLC.

2.10.2 Materials

All bulk solvents were obtained from VWR scientific. Benzene and CH₂Cl₂ were degassed and dried over 4 Å molecular sieves, and all other solvents used were dried and deoxygenated by the method of Grubbs.²² 3,5-dimethylbenzotrile,²³ 4-(1-(ethylenedioxy)ethyl)benzotrile,²⁴ 4-(1,3-dioxolan-2-yl)benzotrile,²⁵ *t*-butyl-4-cyanobenzoate,²⁶ 3-iodopropionitrile,²⁷ HOSiPh₂^{*t*}Bu,¹⁶ Zr(NMe₂)₄,²⁸ NMo[N(^{*t*}Bu)(3,5-Me₂C₆H₃)]₃,¹⁸ NMo[N(^{*i*}Pr)(3,5-Me₂C₆H₃)]₃,¹⁵ NW(OC(CF₃)₂Me)₃(DME) (**2.1**),¹ NW(OC(CF₃)Me)₃ (**2.2**),¹ 4,5-dimethylphthalonitrile (**2.4**),²⁹ 4,5-dimethoxyphthalonitrile (**2.5**),³⁰ 5-*tert*-butylisophthalonitrile (**2.6**),²³ NMo(O^{*t*}Bu)₃

(2.26),³¹ $\text{NMo}((\text{OC}(\text{CF}_3)\text{Me}_2)_3$ **(2.27)**,³² $\text{NMo}(\text{OC}(\text{CF}_3)_2\text{Me})_3$ **(2.28)**,³³
 $\text{NMo}(\text{OC}(\text{CF}_3)_3)_3(\text{NCMe})$ **(2.29)**,³³ and $\text{EtCMo}(\text{OAd})_3$ (Ad = 1-adamantyl) **(2.30)**²⁰ were
all made according to literature procedures. NMR solvents were obtained from
Cambridge Isotope Laboratories and were dried over 4 Å molecular sieves for at least 24
hours. 1-Bromotetradecane, sodium hydride (60 % in mineral oil), bromobenzene,
copper(I) cyanide, anisonitrile, 3-aminopropionitrile, *p*-aminobenzonitrile, *p*-
dimethylaminobenzonitrile, *p*-nitrobenzonitrile, trimethylacetone, *p*-
hydroxybenzonitrile, 2-cyanopyridine, *p*-toluenesulfonic acid monohydrate, 4-
cyanostyrene, 4-bromostyrene, 4-nitrobenzonitrile, 3-(dimethylamino)propionitrile, 4-
acetylbenzonitrile, N-methyl-β-alaninenitrile, 3-hexyne, 1,2-dicyanobenzene, and 2,6-di-
tert-butylphenol were obtained from Acros. 3,5-bis(trifluoromethyl)benzonitrile was
obtained from Matrix Scientific. 1-phenyl-1-butyne was obtained from GFS Chemicals.
2-thiophenecarbonitrile was obtained from Oakwood Chemicals. Triethylamine, *p*-
bromobenzonitrile, 4-cyano-benzoic acid methyl ester, 2-thiopheneacetonitrile, 3,6-
dibromocarbazole, and 1,3,5-trimethoxybenzene were obtained from Aldrich. 4-
cyanobenzaldehyde, *p*-toluenesulfonyl acetonitrile, and 2,6-diisopropylphenol were
obtained from Alfa Aesar. 1,1-diphenylethanol was obtained from TCI. Triphenylsilanol
and diisopropylchlorosilane were obtained from Gelest. All liquid nitriles and alkynes
were dried for 24 hours using 4 Å molecular sieves. 2-thiopheneacetonitrile was distilled
prior to use. All other reagents were used as received.

2.10.3 Synthetic Procedures

3,6-dibromo-9-tetradecyl-9H-carbazole (2.7). In a glovebox, a solution of THF/DMF (30 mL / 10 mL) was measured into a 250 mL 3-neck flask fitted with a gas adapter, rubber septum, and a solid addition funnel containing NaH (60% in mineral oil, 0.48 g, 12.0 mmol, 1.6 equiv). Under N₂ flow on a Schlenk line, 3,6-dibromocarbazole (2.51 g, 7.72 mmol, 1.01 equiv) was added to the flask, then 1-bromotetradecane (2.28 mL, 7.66 mmol) was added *via* syringe. The resulting solution was cooled to 0 °C, then the NaH was added with stirring. The solution was allowed to warm overnight with stirring, then the volatiles were removed *in vacuo*. The remaining mixture was quenched with 1 M HCl (50 mL). The product was extracted with CHCl₃ (75 mL), and the organic layer was washed with H₂O (3 x 50 mL). The solvent was removed, and the resulting powder was washed with cold pentane (2 x 20 mL) and dried *in vacuo*, yielding white needles of **2.7** (3.45 g, 6.62 mmol, 86 %). ¹H NMR (300 MHz, CD₂Cl₂): δ 8.16 (s, 2H, ArH), 7.57 (d, 2H, ArH, ³J_{H-H} = 8.7 Hz), 7.33 (d, 2H, ArH, ³J_{H-H} = 8.7 Hz), 4.26 (t, 2H, NCH₂, ³J_{H-H} = 7.5 Hz), 1.83 (m, 2H, NCH₂CH₂), 1.23-1.53 (m, 22H, (CH₂)₁₁), 0.88 (t, 3H, CH₃, ³J_{H-H} = 6.6 Hz). ¹³C{¹H} NMR (CDCl₃): δ 139.35, 129.07, 123.50, 123.31, 112.02, 110.46, 43.41, 32.08, 29.83, 29.80, 29.78, 29.73, 29.68, 29.60, 29.52, 29.47, 28.96, 27.34, 22.85, 14.29. Anal. Calcd for C₂₆H₃₅NBr₂: C, 59.90; H, 6.77; N, 2.69. Found: C, 60.06; H, 6.45; N, 2.65.

9-tetradecyl-9H-carbazole-3,6-dicarbonitrile (2.8). In a glovebox, dry DMF (30 mL) was measured into a 100 mL 2-neck flask equipped with a rubber septum and gas adapter. Under N₂ flow on a Schlenk line, **2.7** (3.17 g, 6.08 mmol) and copper(I) cyanide

(2.00 g, 22.3 mmol, 3.7 equiv) were added to the flask. A reflux condenser was fitted under N₂ flow and the solution heated to reflux with stirring for 26 h. The solution was cooled to room temp, then concentrated NH₄OH (20 mL) was added. After stirring for 10 min, the mixture was extracted with CH₂Cl₂ (2 x 50 mL). The combined organics were washed with H₂O (2 x 50 mL) and brine (50 mL), then filtered through a plug of silica to remove solid impurities. The silica plug was washed with CH₂Cl₂ until the filtrate ran colorless. The combined filtrate was concentrated to dryness. The resulting powder was washed with acetone, then dried *in vacuo* yielding **2.8** (1.35 g, 3.26 mmol, 54 %) as a brown powder. ¹H NMR (300 MHz, CDCl₃): δ 8.41 (s, 2H, ArH), 7.79 (d, 2H, ArH, ³J_{H-H} = 8.4 Hz), 7.52 (d, 2H, ArH, ³J_{H-H} = 8.4 Hz), 4.35 (t, 2H, NCH₂, ³J_{H-H} = 6.9 Hz), 1.83-1.90 (m, 2H, -NCH₂CH₂), 1.22-1.33 (m, 22H, (CH₂)₁₁), 0.87 (t, 3H, CH₃, ³J_{H-H} = 6.6 Hz). ¹³C{¹H} NMR (CDCl₃): δ 142.84, 130.40, 125.81, 122.24, 119.92, 110.33, 103.57, 43.90, 32.04, 29.78, 29.76, 29.74, 29.69, 29.60, 29.54, 29.48, 29.39, 28.98, 27.31, 22.81, 14.25. Anal. Calcd for C₂₈H₃₅N₃: C, 81.31; H, 8.53; N, 10.16. Found: C, 80.87; H, 8.41; N, 10.01.

Tetramer (2.9). In a glovebox, complex **2.1** (93.4 mg, 0.112 mmol) and **2.8** (250.5 mg, 0.606 mmol) were weighed into a bomb flask. Bromobenzene (37 mL) and 3-hexyne (0.14 mL, 1.23 mmol) were added, then the bomb flask was sealed and placed in a 95 °C oil bath. After 20 h, the solution was cooled and vacuum was pulled for 2 h to remove volatile products. The bomb flask was sealed and heated for an additional 13 h. The solution was cooled and washed through a plug of silica with CHCl₃ (150 mL). The filtrate was concentrated to dryness, then precipitated from CHCl₃ / pentane at -20 °C.

The mixture was filtered and the precipitate was dried *in vacuo* to give **2.9** (161.1 mg, 0.104 mmol, 69 %) as an off-white powder. ^1H NMR matched the literature values.⁵ MALDI-TOF $[\text{M}/\text{Z}]^+$: 1542.1 ($\text{C}_{112}\text{H}_{140}\text{N}_4$).

4,4'-(diisopropylsilanediyl)bis(oxy)dibenzonitrile (2.10). In a glovebox, 4-cyanophenol (3.29 g, 27.7 mmol, 2.5 equiv) was measured into a 100 mL 2-neck flask and dissolved in THF (40 mL). Triethyl amine (3.86 mL, 27.7 mmol, 2.5 equiv) was then added and the flask fitted with a gas adapter and a rubber septum. Under N_2 flow on a Schlenk line, a liquid addition funnel containing diisopropyldichlorosilane (2.0 mL, 11.1 mmol, 1.0 equiv) was fitted and the flask cooled to 0 °C. The silane was added dropwise to the flask, causing a precipitate to form. After stirring overnight, the volatiles were removed *in vacuo* and the remaining residue was returned to a glovebox. The product was extracted with Et_2O (2 x 30 mL), filtered, and concentrated to dryness. Remaining 4-cyanophenol was then removed *via* sublimation to give **2.10** (2.49 g, 7.11 mmol, 64 %) as a yellow oil. ^1H NMR (400 MHz, CDCl_3): δ 7.55 (d, 4H, *ArH*, $^3J_{\text{H-H}} = 8.7$ Hz), 7.00 (d, 4H, *ArH*, $^3J_{\text{H-H}} = 8.7$ Hz), 1.30 (sep., 2H, $\text{CH}(\text{CH}_3)_2$, $^3J_{\text{H-H}} = 7.4$ Hz), 2.15 (d, 12H, $\text{CH}(\text{CH}_3)_2$, $^3J_{\text{H-H}} = 7.4$ Hz). $^{13}\text{C}\{^1\text{H}\}$ NMR (CDCl_3): δ 158.10, 134.29, 120.51, 118.80, 105.74, 16.84, 12.53. MS $[\text{M}+\text{Na}]^+ = 373$; HRMS calcd for $\text{C}_{20}\text{H}_{22}\text{N}_2\text{O}_2\text{Si}$ 373.1348, found 373.1349.

$\text{NMo}(\text{NMe}_2)_3$ (2.13). Solid $\text{Zr}(\text{NMe}_2)_4$ (1.8886 g, 7.06 mmol, 0.85 equiv) was added to a stirring solution of $\text{NMo}(\text{O}^t\text{Bu})_3$ (2.7373g, 8.31 mmol, 1.0 equiv) in toluene (110 mL). After stirring for 2 hours, the solution was concentrated *in vacuo* to a volume

of *ca.* 25 mL. Pentane (40 mL) was added, and the resulting precipitate was collected by vacuum filtration, washed with pentane, and dried *in vacuo* to give **2.13** (1.1844 g, 4.89 mmol, 59 %) as a yellow powder. The filtrate was concentrated to dryness, then the residue was slurried in pentane (20 mL). The mixture was filtered and the solid was washed with pentane (3 x 5 mL) and dried *in vacuo* to give a second crop of **2.13** (0.3690 g, 1.52 mmol, 18 %). ¹H NMR matched the literature values.¹⁵

NMo(OSiPh₃)₂(NMe₂)(NHMe₂) (2.14). Solid HOSiPh₃ (0.3728 g, 1.349 mmol, 2.1 equiv) was added to a stirring solution of NMo(NMe₂)₃ (0.1554 g, 0.642 mmol, 1.0 equiv) in C₆H₆ (5 mL). The solution immediately changed to a bright yellow color, which faded as a precipitate formed. After stirring 1 hour 15 minutes, pentane (10 mL) was added to the mixture and the precipitate was collected by filtration, washed with pentane (5 mL), and dried *in vacuo* to yield **2.14** (0.4778 g, 0.597 mmol, 93 %) as a pale yellow powder. ¹H NMR (500 MHz, CD₂Cl₂): δ 7.71–7.69 (m, 11H), 7.42–7.34 (m, 16H), 3.68 (s, 3H, –NCH₃), 2.88 (s, 3H, –NCH₃), 2.33 (s, 3H, NHCH₃), 2.32 (s, 3H, NHCH₃), 2.27 (br s, 1H, NHMe₂). ¹³C{¹H} NMR (CD₂Cl₂): δ 138.94, 135.83, 129.92, 128.26, 62.40, 46.88, 40.90. Anal. Calcd for C₄₀H₄₃MoN₃O₂Si₂: C, 64.07; H, 5.78; N, 5.60. Found: C, 64.02; H, 5.75; N, 5.40.

NMo(OSiPh₃)₃(NHMe₂) (2.15). A solid mixture of NMo(NMe₂)₃ (0.1343 g, 0.555 mmol, 1.0 equiv) and HOSiPh₃ (0.4756 g, 1.72 mmol, 3.1 equiv) was dissolved in THF (10 mL) inside of a bomb flask. The flask was placed in a 60 °C oil bath and the reaction solution was stirred for 20 hours. ¹H NMR analysis of an aliquot revealed the

presence of a small amount of remaining **2.14**. Additional HOSiPh₃ (0.2760 g, 1.00 mmol, 1.8 equiv) was added to the reaction solution, which was then stirred at 60 °C for an additional 18 hours. ¹H NMR analysis of a second aliquot revealed the consumption of **2.14**. The reaction solution was pipetted into toluene (60 mL) with vigorous stirring, but no precipitate formed. The solution was concentrated *in vacuo* to a volume of *ca.* 10 mL, resulting in the precipitation of a powder. The solid was collected by vacuum filtration, washed with toluene (3 x 5 mL) and pentane (10 mL), then dried *in vacuo* to yield **2.15** (0.3363 g, 0.343 mmol, 62 %) as a white powder. ¹H NMR analysis revealed the presence of a small amount of HOSiPh₃. The first crop of **2.15** was dissolved in CH₂Cl₂ (10 mL), then Et₂O (8 mL) was added and the solution cooled to –35 °C, resulting in the precipitation of a white powder. The powder was collected by vacuum filtration, washed with toluene (2 x 10 mL) and pentane (2 x 10 mL), then dried *in vacuo* to afford **2.15** (0.2512 g, 0.256 mmol, 46 %). ¹H NMR analysis of the second crop revealed no improvement in purity over the first crop of **2.15**. ¹H NMR (500 MHz, CD₂Cl₂): δ 7.58 (br s, 15H, ArH), 7.29 (br s, 8H, ArH), 7.13 (br s, 15H), 2.54 (br s, 1H, NHMe₂), 1.91 (s, 6H, NH(CH₃)₂). ¹³C{¹H} NMR (CD₂Cl₂): δ 136.85, 136.06, 130.14, 128.23, 41.77. EI/MS [M/Z]⁺: 936.9 (NMo(OSiPh₃)₃).

NMo(OCPh₂Me)₃ (2.19). Solid 1,1-diphenylethanol (0.4588 g, 2.31 mmol, 3.2 equiv) was added to a stirring solution of NMo(NMe₂)₃ (0.1745 g, 0.721 mmol, 1.0 equiv) in THF (12 mL). The solution was stirred for 20 hours, then the volatiles were removed *in vacuo*. The residue was dissolved in toluene (2 mL), then pentane (6 mL) was added to the solution which was then cooled to –35 °C. After 2 days, small colorless

crystals of **2.18** formed on the sides of the crystallization vial, while several large amber blocks had grown at the bottom of the vial. The amber blocks were removed from the mother liquor and rinsed with pentane (1 mL), then they were re-dissolved in a solution of toluene (1.5 mL) and pentane (4 mL), which was then cooled to $-35\text{ }^{\circ}\text{C}$. Colorless clusters precipitated from the solution. The mother liquor was removed *via* pipet and the solid dried *in vacuo* to yield **2.19** (0.1062 g, 0.151 mmol, 21 %) as white flakes. ^1H NMR (400 MHz, C_6D_6): δ 7.32–7.29 (m, 11H), 7.09–7.00 (m, 16H), 2.03 (s, 9H, CH_3). $^{13}\text{C}\{^1\text{H}\}$ NMR (C_6D_6): δ 148.54, 128.28, 127.19, 126.88, 87.74, 29.93. Anal. Calcd for $\text{C}_{42}\text{H}_{39}\text{MoNO}_3$: C, 71.89; H, 5.60; N, 2.00. Found: C, 71.93; H, 5.56; N, 1.84.

NMo(O-2,6- $^t\text{Bu}_2\text{C}_6\text{H}_3$)(NMe $_2$) $_2$ (2.20). Solid 2,6-di-*tert*-butylphenol (0.2783 g, 1.349 mmol, 1.1 equiv) was added to a stirring solution of $\text{NMo}(\text{NMe}_2)_3$ (0.3017 g, 1.246 mmol, 1.0 equiv) in THF (12 mL). After stirring for 5 hours 30 minutes, the volatiles were removed *in vacuo*, then the residue was slurried in cold pentane (4 mL) and cooled to $-35\text{ }^{\circ}\text{C}$. The mixture was filtered and the solid was washed with cold pentane (3 x 1 mL) and dried *in vacuo* to give **2.20** (0.4065 g, 1.008 mmol, 81 %) as a pale yellow powder. ^1H NMR (400 MHz, C_7D_8 , $-10\text{ }^{\circ}\text{C}$): δ 7.36 (d, 2H, *ArH*, $^3J_{\text{H-H}} = 7.8\text{ Hz}$), 6.96 (t, 1H, *ArH*, $^3J_{\text{H-H}} = 7.8\text{ Hz}$), 3.86 (s, 6H, NCH_3), 2.83 (s, 6H, NCH_3), 1.52 (s, 18H, $\text{C}(\text{CH}_3)_3$). $^{13}\text{C}\{^1\text{H}\}$ NMR (C_7D_8 , $-10\text{ }^{\circ}\text{C}$): δ 164.68, 138.62, 120.19, 60.25, 44.20, 35.11, 31.15. Anal. Calcd for $\text{C}_{182}\text{H}_{333}\text{MoN}_3\text{O}$: C, 53.59; H, 8.25; N, 10.42. Found: C, 53.21; H, 8.02; N, 10.22.

NMo(O-2,6-ⁱPr₂C₆H₃)₃(NHMe₂) (2.21). NMo(NMe₂)₃ (0.4150 g, 1.71 mmol, 1.0 equiv) was dissolved in THF (20 mL) inside of a bomb flask. Neat 2,6-diisopropylphenol (2.16 mL, 8.58 mmol, 5.0 equiv) was added to the THF solution. The bomb flask was sealed and heated at 60 °C with stirring for 11 hours 30 minutes. ¹H NMR of an aliquot indicated complete conversion to **2.21**. The solution was concentrated to dryness, then the residue was dissolved in MeCN (3 mL) and cooled to –35 °C. After 14 days no crystals had formed. A seed crystal of **2.21** was added and the solution cooled to –35 °C. After 23 days the mother liquor was removed *via* pipet leaving behind deep red crystals. The crystals were dissolved in C₆H₆ (5 mL) and the solution frozen and lyophilized *in vacuo* to give crude **2.21** (0.4712 g, 1.456 mmol, 85 %) as a deep red powder. ¹H NMR analysis indicated the presence of 0.1 equiv NMo(O-2,6-ⁱPr₂C₆H₃)₂(NMe₂)(NHMe₂) (**2.22**) and 0.4 equiv 2,6-diisopropylphenol. ¹H NMR (500 MHz, C₆D₆): δ 7.14 (d, 6H, ArH (**2.21**), ³J_{H-H} = 7.5 Hz), 7.02 (d, 0.9H, ArH (HOAr), ³J_{H-H} = 7.6 Hz), 6.98 (t, 3H, ArH (**2.21**), ³J_{H-H} = 7.5 Hz), 6.92 (t, 0.4H, ArH (HOAr), ³J_{H-H} = 7.6 Hz), 4.31 (s, 0.4H, OH (HOAr)), 3.94 (s, 0.5H, NCH₃ (**2.22**)), 3.87 (br s, 6H, CHMe₂ (**2.21**)), 2.93 (sep, 0.7H, CHMe₂ (**2.22**), ³J_{H-H} = 6.8 Hz), 2.82 (s, 0.5H, NCH₃ (**2.22**)), 2.39 (sep, 0.7H, CHMe₂ (HOAr), ³J_{H-H} = 6.1 Hz), 2.02 (s, 3H, NHCH₃ (**2.21**)), 2.01 (s, 3H, NHCH₃ (**2.21**)), 1.37 (d, 1.3H, CHCH₃ (**2.22**), ³J_{H-H} = 6.9 Hz), 1.35 (d, 1.3H, CHCH₃ (**2.22**), ³J_{H-H} = 6.9 Hz), 1.29 (d, 36H, CHCH₃ (**2.21**), ³J_{H-H} = 6.8 Hz), 1.14 (d, 4.6H, CHCH₃ (HOAr), ³J_{H-H} = 6.8 Hz). ¹³C{¹H} NMR (C₆D₆, **2.21**): δ 161.09, 138.75, 124.65, 123.81, 42.63, 27.75, 24.81. EI/MS [M/Z]⁺: 643.8 (NMo(O-2,6-ⁱPr₂C₆H₃)₃).

NMo(OSiPh₃)₃ (2.23). Solid NMo[N(CMe₃)(3,5-Me₂C₆H₃)]₃ (0.2889 g, 0.452 mmol, 1.0 equiv) and HOSiPh₃ (0.4392 g, 1.589 mmol, 3.5 equiv) were dissolved in toluene (20 mL) inside of a bomb flask. The flask was heated in a 90 °C oil bath for 5 hours 30 minutes, then cooled. Pentane (25 mL) was added to the solution with vigorous stirring, then the solution was allowed to settle. No precipitate formed over 10 minutes, so additional pentane (5 mL) was added. The solution became cloudy and was allowed to settle overnight. The powder was then collected by vacuum filtration, washed with Et₂O (3 x 15 mL), and dried *in vacuo* to afford **2.22** (0.2146 g, 0.229 mmol, 51 %) as a white powder. ¹H NMR (400 MHz, C₆D₆): δ 7.67 (d, 18H, ArH, ³J_{H-H} = 7.1 Hz), 7.16 (m, ArH), 7.06 (t, 17H, ArH, ³J_{H-H} = 7.5 Hz). ¹³C{¹H} NMR (C₆D₆): δ 135.87, 134.80, 130.45, 128.29. Anal. Calcd for C₅₄H₄₅MoNO₃Si₃: C, 69.28; H, 4.85; N, 1.50. Found: C, 69.04; H, 4.84; N, 1.47.

NMo(OSiPh₂^tBu)₃ (2.25). Solid NMo[N(CHMe₂)(3,5-Me₂C₆H₃)]₃ (0.2777 g, 0.465 mmol, 1.0 equiv) and HOSiPh₂^tBu (0.3837 g, 1.496 mmol, 3.2 equiv) were dissolved in toluene (15 mL) inside of a bomb flask. The flask was heated in a 90 °C oil bath for 10 hours, then the flask was cooled and the volatiles removed *in vacuo*. The resulting oil was dissolved in MeCN (3 mL) and cooled to -35 °C. A semi-solid mass precipitated over several days, then the mother liquor was removed via pipet and the solid rinsed with cold MeCN (2 mL). The solid was re-dissolved in MeCN, and the precipitation procedure was repeated twice more. The resulting solid was dissolved in C₆H₆ (6 mL), then the solution was frozen, lyophilized, and dried *in vacuo* to yield **2.25** (242.2 mg, 0.276 mmol, 59 %) as a dark yellow oil. ¹H NMR (500 MHz, C₆D₆): δ 7.84-

7.82 (m, 12H), 7.18-7.14 (m), 7.13-7.09 (m, 12H), 1.19 (s, 27H). $^{13}\text{C}\{^1\text{H}\}$ NMR (C_6D_6):
 δ 135.71, 134.63, 130.12, 128.15, 27.11, 20.63. EI/MS $[\text{M}/\text{Z}]^+$: 819.9
[$\text{NMo}(\text{OSiPh}_2^t\text{Bu})_3 - \text{CMe}_3$].

2.10.4 Substrate Compatibility Studies with **2.1**

General Procedure: Complex **2.1** and all solid substrates (20 equiv) were added to a J. Young tube and dissolved in toluene- d_8 or bromobenzene- d_5 to give a concentration of 5 mg/mL based on **2.1**. Then 3-hexyne (10 equiv) and liquid substrates (20 equiv) were added to the reaction mixture. An internal standard of 1,3,5-trimethoxybenzene was introduced. The J. Young tube was placed in an oil bath at 95 °C and the reaction was monitored by NMR spectroscopy. Additional 3-hexyne and/or **2.1** were added as necessary to each reaction.

2-thiophenecarbonitrile (Table 2.1, entry #4)

Following the general procedure: Complex **2.1** (3.7 mg, 0.0045 mmol), 2-thiophenecarbonitrile (8.75 μL , 0.094 mmol), and 3-hexyne (5.25 μL , 0.046 mmol) were dissolved in toluene- d_8 (0.74 mL). After 4 h of heating, additional 3-hexyne (5.25 μL , 0.046 mmol) was added. The reaction was further heated for 4 h, at which point ^1H NMR spectroscopy indicated conversion to symmetric alkyne, 1,2-di(thiophen-2-yl)ethyne (26%), and asymmetric alkyne, 2-(but-1-ynyl)thiophene (47%). The volatiles were then removed *in vacuo*. The resulting residue was dissolved in toluene- d_8 (0.74 mL) and heated for 4 h, at which point ^1H NMR spectroscopy indicated conversion to 1,2-di(thiophen-2-yl)ethyne (41%) and 2-(but-1-ynyl)thiophene (19%). The resulting reaction

mixture was washed through a plug of alumina with chloroform and concentrated *in vacuo*. ^1H NMR data agreed with the literature values.^{34, 35} GC/MS [M/Z]⁺ : 136 (C₈H₈S, Rt 4.6 min), 190 (C₁₀H₆S₂, Rt 9.8 min).

3,5-bis(trifluoromethyl)benzonitrile (Table 2.1, entry #5)

Following the general procedure: Complex **2.1** (3.0 mg, 0.0036 mmol), 3,5-bis(trifluoromethyl)benzonitrile (12.0 μL , 0.071 mmol), and 3-hexyne (4.25 μL , 0.037 mmol) were dissolved in toluene-*d*₈ (0.60 mL). After 10 h of heating, additional 3-hexyne (4.25 μL , 0.037 mmol) was added. The reaction was further heated for 11 h, at which point ^1H NMR spectroscopy indicated conversion to symmetric alkyne, 1,2-bis(3,5-bis(trifluoromethyl)phenyl)ethyne (20%), and asymmetric alkyne, 1-(but-1-ynyl)-3,5-bis(trifluoromethyl)benzene (80%). The volatiles were then removed *in vacuo*. The resulting residue was dissolved in toluene-*d*₈ (0.60 mL) and heated for 4 h, at which point ^1H NMR spectroscopy indicated conversion to 1,2-bis(3,5-bis(trifluoromethyl)phenyl)ethyne (95%) and 1-(but-1-ynyl)-3,5-bis(trifluoromethyl)benzene (5%). The resulting reaction mixture was washed through a plug of alumina with chloroform and concentrated *in vacuo*. ^1H NMR (400 MHz, CDCl₃, *symm.*): δ 8.00 (s, 4H, *m-ArH*), 7.89 (s, 2H, *o-ArH*). ^1H NMR (400 MHz, C₆D₅CD₃, *asymm.*): δ 7.56 (s, 2H, *m-ArH*), 7.55 (s, 1H, *o-ArH*), 2.08 (q, 2H, RCH₂CH₃, $^3J_{\text{H-H}} = 7.6$ Hz), 0.99 (t, 3H, RCH₂CH₃, $^3J_{\text{H-H}} = 7.6$ Hz). ^{19}F NMR (CDCl₃, *symm.*): δ -63.45 (s). ^{19}F NMR (C₆D₅CD₃, *asymm.*): δ -63.48 (s). $^{13}\text{C}\{^1\text{H}\}$ NMR (CDCl₃, *symm.*): δ 132.22 (q, *m-ArCCF*₃, $^2J_{\text{C-F}} = 33.8$ Hz), 131.6 (q, *o-ArC*, $^3J_{\text{C-F}} = 2.9$ Hz), 124.17 (s, ArC), 122.57 (q,

CF_3 , $^1\text{J}_{\text{C-F}} = 273.1$ Hz), 89.18 ($-\text{C}\equiv\text{C}-$). GC/MS $[\text{M/Z}]^+$: 266 ($\text{C}_{12}\text{H}_8\text{F}_6$, Rt 3.6 min), 450 ($\text{C}_{16}\text{H}_6\text{F}_{12}$, Rt 6.5 min).

3,5-dimethylbenzotrile (Table 2.1, entry #6)

Following the general procedure: Complex **2.1** (5.3 mg, 0.0064 mmol), 3,5-dimethylbenzotrile (17.1 mg, 0.130 mmol), and 3-hexyne (7.5 μL , 0.066 mmol) were dissolved in toluene- d_8 (1.06 mL). After 6 h of heating, additional 3-hexyne (7.5 μL , 0.066 mmol) was added. The reaction was further heated for 18 h, at which point ^1H NMR spectroscopy indicated conversion to symmetric alkyne, 1,2-bis(3,5-dimethylphenyl)acetylene (37%), and asymmetric alkyne, 1-(but-1-ynyl)-3,5-dimethylbenzene (63%). The volatiles were then removed *in vacuo*. The resulting residue was dissolved in toluene- d_8 (1.06 mL) and heated for 3 h, at which point ^1H NMR spectroscopy indicated conversion to 1,2-bis(3,5-dimethylphenyl)acetylene ($\geq 95\%$). The resulting reaction mixture was washed through a plug of alumina with chloroform and concentrated *in vacuo*. ^1H NMR data were consistent with the literature values.³⁶ GC/MS $[\text{M/Z}]^+$: 131 ($\text{C}_8\text{H}_9\text{N}$, Rt 5.0 min), 234 ($\text{C}_{16}\text{H}_{18}$, Rt 13.7 min).

3-iodopropionitrile (Table 2.1, entry #7)

Following the general procedure: Complex **2.1** (3.6 mg, 0.0043 mmol), 3-iodopropionitrile (7.5 μL , 0.085 mmol), and 3-hexyne (5.0 μL , 0.044 mmol) were dissolved in toluene- d_8 (0.72 mL). After 4 h of heating, additional 3-hexyne (5.0 μL , 0.044 mmol) was added. Further heating for 3 h did not result in further conversion as indicated by ^1H NMR spectroscopy. Additional **2.1** (5.4 mg, 0.0065 mmol) and toluene-

d_8 (0.36 mL) were added. The reaction was further heated for 2 h, at which point ^1H NMR spectroscopy indicated conversion to symmetric alkyne, 1,6-diiodohex-3-yne (33%), and asymmetric alkyne, 1-iodohex-3-yne (40%). The resulting reaction mixture was washed through a plug of silica with chloroform and concentrated *in vacuo*, yielding solely 1,6-diiodohex-3-yne. The product's identity was further confirmed through independent synthesis according to a literature procedure.³⁷ ^1H NMR (300 MHz, CDCl_3): δ 3.22 (t, ICH_2 , $^3J_{\text{H-H}} = 7.5$ Hz), 2.74 (t, $-\text{CH}_2\equiv$, $^3J_{\text{H-H}} = 7.5$ Hz). $^{13}\text{C}\{^1\text{H}\}$ NMR (CDCl_3): δ 81.07, 24.15, 2.15. GC/MS $[\text{M/Z}]^+$: 334 ($\text{C}_6\text{H}_8\text{I}_2$, R_t 8.1 min).

t-butyl-4-cyanobenzoate (Table 2.1, entry #11)

Following the general procedure: Complex **2.1** (3.3 mg, 0.0040 mmol), *tert*-butyl-4-cyanobenzoate (16.2 mg, 0.080 mmol, 20.0 equiv), and 3-hexyne (4.5 μL , 0.040 mmol, 10.0 equiv) were dissolved in C_6D_6 (1.0 mL). After 4 h of heating, ^1H NMR spectroscopy indicated the presence of a molar quantity of propionitrile equal to the molar quantity of **2.1** used. The volatiles were vacuum transferred into a separate J. Young tube. Isobutene was identified as a component of the volatiles by analysis of the ^1H NMR spectrum.

4-acetylbenzotrile (Table 2.2, entry #2)

Following the general procedure: Complex **2.1** (5.0 mg, 0.0060 mmol), 4-acetylbenzotrile (17.9 mg, 0.123 mmol, 20.5 equiv), and 3-hexyne (7.0 μL , 0.062 mmol, 10.3 equiv) were dissolved in toluene- d_8 (1.0 mL). After 4 h of heating, no metathesis products were observed by ^1H NMR spectroscopy.

4-nitrobenzotrile (Table 2.2, entry #3)

Following the general procedure: Complex **2.1** (5.0 mg, 0.0060 mmol), 4-nitrobenzotrile (18.5 mg, 0.125 mmol, 20.8 equiv), and 3-hexyne (7.0 μ L, 0.062 mmol, 10.3 equiv) were dissolved in toluene- d_8 (1.0 mL). After 4 h of heating, ^1H NMR spectroscopy indicated the presence of a molar quantity of propionitrile equal to the molar quantity of **2.1** used.

p-toluenesulfonyl acetonitrile (Table 2.2, entry #5)

Following the general procedure: Complex **2.1** (5.0 mg, 0.0060 mmol), *p*-toluenesulfonylacetonitrile (24.2 mg, 0.124 mmol, 20.7 equiv), and 3-hexyne (7.0 μ L, 0.062 mmol, 10.3 equiv) were dissolved in toluene- d_8 (1.0 mL). After 6 h of heating, ^1H NMR spectroscopy indicated the presence of a molar quantity of propionitrile equal to the molar quantity of **2.1** used.

2-cyanopyridine (Table 2.2, entry #6)

Following the general procedure: Complex **2.1** (5.0 mg, 0.0060 mmol), 2-cyanopyridine (11.8 μ L, 0.123 mmol, 20.5 equiv), and 3-hexyne (7.0 μ L, 0.062 mmol, 10.3 equiv) were dissolved in toluene- d_8 (1.0 mL). After 4 h of heating, ^1H NMR spectroscopy indicated the presence of a molar quantity of propionitrile equal to the molar quantity of **2-DME** used.

4-hydroxybenzotrile (Table 2.2, entry #7)

Following the general procedure: Complex **2.1** (5.3 mg, 0.0064 mmol), 4-hydroxybenzotrile (15.8 mg, 0.133 mmol, 20.8 equiv), and 3-hexyne (7.25 μ L, 0.0638 mmol, 10.0 equiv) were dissolved in toluene- d_8 (1.06 mL). After 2 h of heating, no metathesis products were observed by ^1H NMR spectroscopy.

3-aminopropionitrile (Table 2.2, entry #10)

Following the general procedure: Complex **2.1** (5.0 mg, 0.0060 mmol), 3-aminopropionitrile (8.9 μ L, 0.122 mmol, 20.3 equiv), and 3-hexyne (6.8 μ L, 0.060 mmol, 10.0 equiv) were dissolved in toluene- d_8 (1.0 mL). After 4 h of heating, no metathesis products were observed by ^1H NMR spectroscopy.

N-methyl- β -alaninenitrile (Table 2.2, entry #11)

Following the general procedure: Complex **2.1** (5.0 mg, 0.0060 mmol), N-methyl- β -alaninenitrile (11.3 μ L, 0.120 mmol, 20.0 equiv), and 3-hexyne (6.8 μ L, 0.060 mmol, 10.0 equiv) were dissolved in toluene- d_8 (1.0 mL). After 4 h of heating, no metathesis products were observed by ^1H NMR spectroscopy.

3-(dimethylamino)propionitrile (Table 2.2, entry #12)

Following the general procedure: Complex **2.1** (5.0 mg, 0.0060 mmol), 3-(dimethylamino)propionitrile (13.6 μ L, 0.120 mmol), and 3-hexyne (6.8 μ L, 0.060 mmol) were dissolved in toluene- d_8 (1.0 mL). After 13 h of heating, only stoichiometric

conversion of the catalyst to produce propionitrile was observed by ^1H NMR spectroscopy. At this point, the catalyst had been destroyed.

trimethylacetoneitrile (Table 2.2, entry #14)

Following the general procedure: Complex **2.1** (4.3 mg, 0.0052 mmol), trimethylacetoneitrile (11.5 μL , 0.104 mmol, 20.0 equiv), and 3-hexyne (6.0 μL , 0.053 mmol, 10.2 equiv) were dissolved in toluene- d_8 (0.86 mL). After 70 h of heating, ^1H NMR spectroscopy indicated the presence of a molar quantity of propionitrile equal to the molar quantity of **2.1** used.

1,2-dicyanobenzene (**2.3**)

Following the general procedure: Complex **2.1** (3.7 mg, 0.0045 mmol), **2.3** (5.3 mg, 0.0414 mmol, 9.2 equiv), and 3-hexyne (4.7 μL , 0.0414 mmol, 9.2 equiv) were dissolved in bromobenzene- d_5 (0.74 mL). After 60 h of heating, ^1H NMR spectroscopy indicated 79 % remaining **2.3**.

1,2-dimethylphthalonitrile (**2.4**)

Following the general procedure: Complex **2.1** (2.4 mg, 0.0029 mmol), **2.4** (4.4 mg, 0.0282 mmol, 10.1 equiv), and 3-hexyne (6.8 μL , 0.0594 mmol, 20.6 equiv) were dissolved in toluene- d_8 (0.80 mL). After 37 h of heating, ^1H NMR spectroscopy indicated 67 % remaining **2.4**.

4,5-dimethoxyphthalonitrile (2.5)

Following the general procedure: Complex **2.1** (7.9 mg, 0.0042 mmol), **2.5** (7.9 mg, 0.0420 mmol, 10.0 equiv), and 3-hexyne (9.5 μ L, 0.0836 mmol, 19.9 equiv) were dissolved in bromobenzene-*d*₅ (1.0 mL). After 4 h of heating, no metathesis products were observed by ¹H NMR spectroscopy.

5-tert-butylisophthalonitrile (2.6)

Following the general procedure: Complex **2.1** (6.7 mg, 0.0081 mmol), **2.6** (14.4 mg, 0.0782 mmol, 9.7 equiv), and 3-hexyne (8.9 μ L, 0.0783 mmol, 9.7 equiv) were dissolved in C₆D₆ (1.3 mL). After 23 h of heating, a large number of *tert*-butyl containing products were observed by ¹H NMR spectroscopy. The volatiles were then removed *in vacuo*. The resulting residue was dissolved in C₆D₆ (1.3 mL) and heated for 19 h, at which point 1H NMR spectroscopy indicated the formation of at least 8 resonances corresponding to a *tert*-butyl group.

Substrate studies with the following nitriles and with **2.2** were completed by Andrea Geyer and are reported elsewhere:^{1, 2, 6} anisonitrile, *p*-bromobenzonitrile, 2-thiopheneacetonitrile, 4-cyanostyrene, 4-cyano-benzoic acid methyl ester, 4-(1-(ethylenedioxy)ethyl)benzonitrile, 4-(1,3-dioxolan-2-yl)benzonitrile, *p*-dimethylaminobenzonitrile, 4-cyanobenzaldehyde, *p*-aminobenzonitrile, *N*-(4-cyanophenyl)acetamide, *o*-tolunitrile, **2.10**.

2.10.5 Additional Protonolysis Reactions

With HOSiPh₂^tBu

NMo(NMe₂)₃: A solid mixture of NMo(NMe₂)₃ (11.6 mg, 0.0479 mmol, 1.0 equiv) and HOSiPh₂^tBu (39.3 mg, 0.153 mmol, 3.2 equiv) was dissolved in THF (1 mL) and the solution was transferred to a J. Young tube. The solution was placed in a 60 °C oil bath for 16 hours, then the volatiles were removed *in vacuo*. ¹H NMR analysis of the residue (C₆D₆) indicated a conversion to **2.16** (74 %) and **2.17** (26 %). The C₆D₆ solution was placed in a 90 °C oil bath and the reaction progress monitored by ¹H NMR. After 17 hours, the product makeup was 58 % **2.16** and 42 % **2.17**. After 17 hours, the product makeup was 41 % **2.16** and 59 % **2.17**. After 17 hours, the product makeup was 15 % **2.16** and 85 % **2.17**. Reaction progress was monitored with the following distinctive ¹H NMR resonances: δ 3.82 (s, **2.16**, 3H, NCH₃), 2.80 (s, **2.16**, 3H, NCH₃), 1.26 (s, **2.16**, 18H, C(CH₃)₃), 1.19 (s, **2.17**, 27H, C(CH₃)₃).

NMo[N(CMe₃)(3,5-Me₂C₆H₃)]₃: A solid mixture of NMo[N(CMe₃)(3,5-Me₂C₆H₃)]₃ (6.5 mg, 0.0102 mmol, 1.0 equiv) and HOSiPh₂^tBu (8.5 mg, 0.0332 mmol, 3.3 equiv) was dissolved in C₆D₆ (0.8 mL) and the solution was transferred to a J. Young tube. The solution was placed in a 95 °C oil bath and the reaction progress monitored by ¹H NMR. After 24 hours, a 35 % conversion to **2.25** was observed. After 8 days, a 50 % conversion to **2.25** was observed.

NMo[N(CHMe₂)(3,5-Me₂C₆H₃)]₃: A solid mixture of NMo[N(CHMe₂)(3,5-Me₂C₆H₃)]₃ (9.7 mg, 0.0163 mmol, 1.0 equiv) and HOSiPh₂^tBu (13.3 mg, 0.0519 mmol, 3.2 equiv) was dissolved in C₆D₆ (0.7 mL) and the solution was transferred to a J. Young

tube and the reaction progress monitored by ^1H NMR. After 10 minutes at room temperature, a 100 % conversion to **2.24** was observed. The reaction solution was placed in a 95 °C oil bath and the monitoring of the reaction progress by ^1H NMR was continued. After 3 hours, the product makeup was 21 % **2.24** and 79 % **2.25**. Compound **2.24** was identified through the following distinctive ^1H NMR resonances (C_6D_6 , 400 MHz): δ 6.55 (s, 1H, ArH), 6.42 (s, 2H, ArH), 4.53 (sep., 1H, CHMe₂, $^3J_{\text{H-H}} = 6.6$ Hz), 1.49 (d, 6H, CH(CH₃)₂, $^3J_{\text{H-H}} = 6.6$ Hz), 1.24 (s, 18H, C(CH₃)₃).

With 2,6-diisopropylphenol

NMo[N(CMe₃)(3,5-Me₂C₆H₃)]₃: Neat 2,6-diisopropylphenol (5.0 μL , 0.0270 mmol, 3.1 equiv) was added to a solution of *NMo[N(CMe₃)(3,5-Me₂C₆H₃)]₃* (5.5 mg, 0.00880 mmol, 1.0 equiv) in C_6D_6 (0.7 mL). The solution was transferred to a J. Young tube and heated in a 60 °C oil bath. After 20 hours, 2 major reaction products were observed in the ^1H NMR spectrum containing at least five CH(CH₃)₂ resonances. After heating for an additional 23 h, no significant change in the product composition had occurred.

NMo[N(CHMe₂)(3,5-Me₂C₆H₃)]₃: Neat 2,6-diisopropylphenol (15.0 μL , 0.0596 mmol, 3.2 equiv) was added to a solution of *NMo[N(CHMe₂)(3,5-Me₂C₆H₃)]₃* (11.0 mg, 0.0184 mmol, 1.0 equiv) in C_6D_6 (0.7 mL). The solution was transferred to a J. Young tube, heated in a 90 °C oil bath, and the reaction progress was monitored by ^1H NMR. After 3 hours, five major reaction products were observed by the CHMe₂ resonance. After heating overnight, no significant change in the product composition had occurred.

2.10.6 ACM Studies

General Procedure: [Mo] (5.0 mg) and an internal standard of 1,3,5-trimethoxybenzene were dissolved in C₆D₆ (0.50 mL) to give a catalyst concentration of 10 mg mL⁻¹. The solution was transferred to a J. Young tube and 1-phenyl-1-butyne (20 equiv) was added *via* syringe. The sample was frozen and the overlying atmosphere was removed *in vacuo*. The J. Young tube was heated at the desired temperature and the reaction was monitored by ¹H NMR spectroscopy.

NMo(OSiPh₃)₃(NHMe₂) (2.15): Following the general procedure at 75 °C: **2.15** (5.0 mg, 0.0051 mmol), 1-phenyl-1-butyne (14.5 μL, 0.102 mmol). After 1.5 hours, a 25 % conversion to diphenylacetylene was observed.

NMo(OCPh₂Me)₃ (2.19). Following the general procedure at 75 °C: **2.19** (5.1 mg, 0.00743 mmol), 1-phenyl-1-butyne (21.0 μL, 0.148 mmol). After 21 hours, no metathesis products were observed and **2.19** had completely decomposed.

NMo(O-2,6-ⁱPr₂C₆H₃)₃(NHMe₂) (2.21). Following the general procedure at 75 °C: **2.21** (5.0 mg, 0.0073 mmol), 1-phenyl-1-butyne (20.0 μL, 0.141 mmol). After 2.5 hours, a 25 % conversion to diphenylacetylene was observed.

NMo(OSiPh₃)₃ (2.23). Complex **2.23** (6.7 mg, 0.0072 mmol, 1.0 equiv) and an internal standard of 1,3,5-trimethoxybenzene were dissolved in C₆D₆ (0.7 mL), then the solution was transferred to a J. Young tube. Neat 1-phenyl-1-butyne (5.1 μL, 0.036 mmol, 5.0

equiv) was added and the reaction was monitored by ^1H NMR spectroscopy at room temperature. After 5 hours, a 25 % conversion to diphenylacetylene was observed.

NMo(OSiPh $_2$ ^tBu) $_3$ (2.25). Following the general procedure at 90 °C: **2.25** (20.0 μL of a 0.25 mg μL^{-1} stock solution in C_6D_6 , 0.0057 mmol), 1-phenyl-1-butyne (16.0 μL , 0.113 mmol). After 9 hours, no metathesis products were observed.

2.10.7 NACM Concentration Studies with 2.23

General Procedure: Complex **2.23**, anisonitrile (10 equiv) and an internal standard of 1,3,5-trimethoxybenzene were dissolved in bromobenzene- d_5 at the desired concentration of **2.23**, then the solution was transferred to a J. Young tube. Then 1-phenyl-1-butyne (10 equiv) was introduced *via* syringe and the overlying atmosphere was removed *in vacuo*. The reaction was heated at 180-185 °C and monitored by ^1H NMR spectroscopy. The results are reported in Table 2.4.

20 mg mL $^{-1}$ Following the general procedure: **2.23** (10.0 mg, 0.011 mmol), anisonitrile (14.6 mg, 0.11 mmol), 1-phenyl-1-butyne (15.2 μL , 0.11 mmol), bromobenzene- d_5 (5.0 mL).

30 mg mL $^{-1}$ Following the general procedure: **2.23** (15.0 mg, 0.016 mmol), anisonitrile (21.3 mg, 0.16 mmol), 1-phenyl-1-butyne (23.0 μL , 0.16 mmol), bromobenzene- d_5 (5.0 mL).

40 mg mL⁻¹ Following the general procedure: **2.23** (20.0 mg, 0.021 mmol), anisonitrile (28.0 mg, 0.21 mmol), 1-phenyl-1-butyne (30.4 μ L, 0.21 mmol), bromobenzene-*d*₅ (5.0 mL).

Table 2.4. NACM studies with **2.23**.

Concentration (mg mL ⁻¹)	Time (h)	ArCCPh ^a	+/-	ArCCEt ^a	+/-	Total	+/-
20	4	5.33	0.62	3.67	0.85	9.00	1.47
	8	7.33	0.62	5.33	0.62	12.66	1.24
	12	8.50	0.00	5.50	0.00	14.00	0.00
30	4	6.83	1.18	2.83	1.43	9.66	2.61
	8	8.83	0.94	6.50	0.71	15.33	1.65
	12	11.00	1.78	7.50	0.41	18.50	2.19
40	4	10.67	1.18	7.00	0.41	17.67	1.59
	8	15.50	1.47	7.83	0.47	23.33	1.94
	12	14.50		8.50		23.00	

^a Ar = 4-MeOC₆H₄.

2.10.8 Attempted NACM with [Mo] Complexes

General Procedure: [Mo] (20.0 mg), anisonitrile (10 equiv), and an internal standard of 1,3,5-trimethoxybenzene were dissolved in bromobenzene-*d*₅ (5.0 mL) at a concentration of 40 mg mL⁻¹, then the solution was transferred to a J. Young tube. Then 1-phenyl-1-butyne (10 equiv) was introduced *via* syringe and the overlying atmosphere was removed *in vacuo*. The reaction was heated at 180-185 °C and monitored by ¹H NMR spectroscopy. ACM products were observed in all cases, but are indicated only for those complexes that have not been previously been shown to catalyze ACM.

NMo(OSiPh₃)₃(NHMe₂) (2.15). Following the general procedure: **2.15** (20.3 mg, 0.021 mmol), anisonitrile (26.8 mg, 0.20 mmol), and 1-phenyl-1-butyne (29.0 μ L, 0.20 mmol). After 20 h, no NACM products were observed. The fate of **2.15** was unclear, and so additional 1-phenyl-1-butyne (87.0 μ L, 0.61 mmol) was added and the reaction heated at 90 °C. After 1 h, no additional ACM products were observed, indicating decomposition of **2.15**.

NMo(O-2,6-ⁱPr₂C₆H₃)₃(NHMe₂) (2.21). Following the general procedure: **2.19** (19.6 mg, 0.029 mmol), anisonitrile (39.3 mg, 0.30 mmol), and 1-phenyl-1-butyne (41.4 μ L, 0.29 mmol). After 20 h, no NACM products were observed with 2,6-diisopropylphenol being the only phenolic species present.

NMo(OSiPh₂^tBu)₃ (2.25). Following the general procedure: **2.25** (80.0 μ L of a 0.25 mg μ L⁻¹ stock solution in C₆D₆, 0.023 mmol), anisonitrile (30.1 mg, 0.26 mmol), and 1-phenyl-1-butyne (32.4 μ L, 0.23 mmol). After 8 h, no NACM products were observed.

NMo(O^tBu)₃ (2.26). Following the general procedure: **2.26** (20.5 mg, 0.062 mmol), anisonitrile (80.8 mg, 0.61 mmol), and 1-phenyl-1-butyne (86.0 μ L, 0.61 mmol). After 4 h, no NACM products were observed, but ACM had occurred to give a mixture of 1-phenyl-1-butyne (50 %), diphenylacetylene (25 %), and 3-hexyne (25 %). After 16 h, no NACM was observed and **2.26** had decomposed.

NMo(OCMe₂CF₃)₃ (2.27). Following the general procedure: **2.27** (20.6 mg, 0.042 mmol), anisonitrile (56.9 mg, 0.43 mmol), and 1-phenyl-1-butyne (58.0 μ L, 0.41 mmol). After 4 h, no NACM products were observed, but 82 % **2.27** remained and ACM had occurred to give a mixture of 1-phenyl-1-butyne (50 %), diphenylacetylene (25 %), and 3-hexyne (25 %). After 16 h, no NACM was observed and 51 % **2.27** remained.

NMo(OC(CF₃)₂Me)₃ (2.28). Following the general procedure: **2.28** (22.0 mg, 0.034 mmol), anisonitrile (40.7 mg, 0.41 mmol), and 1-phenyl-1-butyne (40.0 μ L, 0.28 mmol). After 4 h, no NACM was observed and **2.28** had largely decomposed.

NMo(OC(CF₃)₃)(NCMe) (2.29). Following the general procedure: **2.29** (20.7 mg, 0.024 mmol), anisonitrile (31.2 mg, 0.23 mmol), and 1-phenyl-1-butyne (33.0 μ L, 0.23 mmol). After 4 h, no NACM was observed and **2.29** had largely decomposed.

EtCMo(OAd) (Ad = 1-adamantyl) (2.30). Following the general procedure: **2.30** (20.4 mg, 0.035 mmol), anisonitrile (46.0 mg, 0.35 mmol), and 1-phenyl-1-butyne (48.0 μ L, 0.34 mmol). After 16 h, no NACM products were observed. The fate of **2.30** was unclear, and so additional 1-phenyl-1-butyne (144.0 μ L, 1.01 mmol) was added and the reaction heated at 90 °C. After 1 h, no additional ACM products were observed, indicating decomposition of **2.30**.

2.11 References

1. Geyer, A. M.; Gdula, R. L.; Wiedner, E. S.; Johnson, M. J. A., *J. Am. Chem. Soc.* **2007**, *129*, 3800-3801.
2. Geyer, A. M.; Wiedner, E. S.; Gary, J. B.; Gdula, R. L.; Kuhlmann, N. C.; Johnson, M. J. A.; Dunietz, B. D.; Kampf, J. W., *J. Am. Chem. Soc.* **2008**, *130*, 8984-8999.
3. Zhang, W.; Moore, J. S., *Advanced Synthesis & Catalysis* **2007**, *349*, 93-120.
4. Furstner, A.; Davies, P. W., *Chem. Commun.* **2005**, 2307-2320.
5. Zhang, W.; Moore, J. S., *J. Am. Chem. Soc.* **2004**, *126*, 12796-12796.
6. Geyer, A. M. Development and Investigation of NW(OR)₃, NMo(OR)₃, and Mo₂(OR)₆ Complexes for Triple-Bond Metathesis. University of Michigan, Ann Arbor, 2009.
7. Pschirer, N. G.; Fu, W.; Adams, R. D.; Bunz, U. H. F., *Chem. Commun.* **2000**, 87-88.
8. Zhu, J.; Jia, G.; Lin, Z., *Organometallics* **2006**, *25*, 1812-1819.
9. Nugent, W. A.; Mayer, J. M., *Metal-Ligand Multiple Bonds*. John Wiley & Sons: New York, 1988; p 26-26
10. Mayer, J. M., *Polyhedron* **1995**, *14*, 3273-3292.
11. Gdula, R. L.; Johnson, M. J. A., *J. Am. Chem. Soc.* **2006**, *128*, 9614-9615.
12. Schrock, R. R., *Polyhedron* **1995**, *14*, 3177-3195.
13. Bordwell, F. G.; McCallum, R. J.; Olmstead, W. N., *J. Org. Chem.* **1984**, *49*, 1424-1427.
14. Steward, O. W.; Fussaro, D. R., *J. Organomet. Chem.* **1977**, *129*, C28-C32.
15. Johnson, M. J. A.; Lee, P. M.; Odom, A. L.; Davis, W. M.; Cummins, C. C., *Angew. Chem., Int. Ed. Engl.* **1997**, *36*, 87-91.
16. Mullen, D. G.; Barany, G., *J. Org. Chem.* **1988**, *53*, 5240-5248.
17. An analysis of Cambridge Crystallographic Database (September 2009) revealed 60 structures with a Mo nitrido ligand (both terminal and oligomeric), with an average Mo-N triple bond length of 1.662(33) Å.
18. Laplaza, C. E.; Johnson, M. J. A.; Peters, J. C.; Odom, A. L.; Kim, E.; Cummins, C. C.; George, G. N.; Pickering, I. J., *J. Am. Chem. Soc.* **1996**, *118*, 8623-8638.
19. Tsai, Y. C.; Johnson, M. J. A.; Mindiola, D. J.; Cummins, C. C.; Klooster, W. T.; Koetzle, T. F., *J. Am. Chem. Soc.* **1999**, *121*, 10426-10427.
20. Tsai, Y. C.; Diaconescu, P. L.; Cummins, C. C., *Organometallics* **2000**, *19*, 5260-5262.
21. Shriver, D. G.; Sailor, M. J., *The Manipulations of Air-sensitive Compounds*. 2 ed.; Wiley-Interscience: New York, 1986.
22. Pangborn, A. B.; Giardello, M. A.; Grubbs, R. H.; Rosen, R. K.; Timmers, F. J., *Organometallics* **1996**, *15*, 1518-1520.
23. Zanon, J.; Klapars, A.; Buchwald, S. L., *J. Am. Chem. Soc.* **2003**, *125*, 2890-2891.
24. Cole, J. E.; Walker, J.; Robins, P. A.; Johnson, W. S., *J. Chem. Soc.* **1962**, 244-&.
25. Herre, S.; Steinle, W.; Ruck-Braun, K., *Synthesis-Stuttgart* **2005**, 3297-3300.
26. Stanton, M. G.; Gagne, M. R., *Journal of Organic Chemistry* **1997**, *62*, 8240-8242.
27. Yasui, K.; Fugami, K.; Tanaka, S.; Tamaru, Y., *J. Org. Chem.* **1995**, *60*, 1365-1380.
28. Bradley, D. C.; Thomas, I. M., *J. Chem. Soc.* **1960**, 3857 - 3861.
29. Kovshev, E. I.; Solov'eva, L. I.; Mikhalenko, S. A.; Luk'yanets, E. A., *Zhurnal Vsesoyuznogo Khimicheskogo Obshchestva im. D. I. Mendeleeva* **1976**, *21*, 465-6.
30. Metz, J.; Schneider, O.; Hanack, M., *Inorg. Chem.* **1984**, *23*, 1065-1071.

31. Chan, D. M. T.; Chisholm, M. H.; Folting, K.; Huffman, J. C.; Marchant, N. S., *Inorg. Chem.* **1986**, *25*, 4170-4174.
32. Gdula, R. L. Design and Synthesis of Highly Active Group 6 Metal Catalysts for use in Triple-Bond Metathesis. University of Michigan, Ann Arbor, 2006.
33. Gdula, R. L.; Johnson, M. J. A.; Ockwig, N. W., *Inorg. Chem.* **2005**, *44*, 9140-9142.
34. Zhang, W.; Kraft, S.; Moore, J. S., *J. Am. Chem. Soc.* **2004**, *126*, 329-335.
35. Jafarpour, L.; Heck, M. P.; Baylon, C.; Lee, H. M.; Mioskowski, C.; Nolan, S. P., *Organometallics* **2002**, *21*, 671-679.
36. Rudenko, A. P.; Vasilev, A. V., *Zh. Org. Khim.* **1995**, *31*.
37. Pohnert, G.; Boland, W., *Eur. J. Org. Chem.* **2000**, 1821.

Chapter 3:

Design and Synthesis of Trianionic (XXX) Pincer Ligands

3.1 Introduction

In Chapter 2, it was demonstrated that NACM is possible with Mo catalysts. However, the Mo catalysts are short-lived at the high temperatures required to overcome the activation barrier for the Mo alkylidyne-to-nitride conversion. The high operating temperatures and low substrate conversions make the Mo-based NACM impractical for widespread use in organic synthesis. A Mo complex possessing a lower energy barrier for azametallacyclobutadiene formation would likely operate at lower temperatures, and therefore would be appealing as a functional catalyst. In the azametallacyclobutadiene transition state for NACM, the alkoxide ligands adopt a meridional geometry as shown in Figure 3.1.¹ Substitution of the alkoxide ligands with a trianionic (XXX) pincer ligand would reduce the amount of ligand re-organization required to form an azametallacyclobutadiene, thereby reducing the activation barrier as desired.

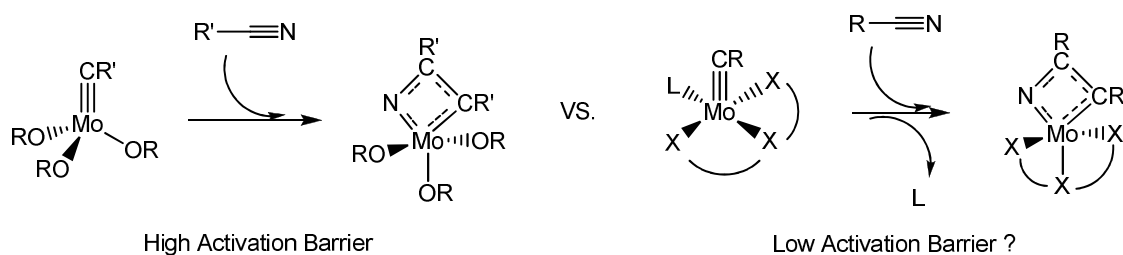


Figure 3.1. Monodentate vs. tridentate ligand coordination in NACM transition state.

A second application for an XXX pincer ligand would be to support high oxidation state ruthenium alkylidyne species previously synthesized in our lab.² Alkylidyne complexes of the form $\text{Ru}(\text{CAr})(\text{PCy}_3)_3\text{X}_3$ are not active for alkyne cross-metathesis (ACM),³ presumably due to the absence of an open coordination site for an incoming alkyne substrate. Replacement of the halide ligands by a bulky XXX ligand would likely prevent coordination of the large PCy_3 ligand, thereby allowing for isolation of a Ru species containing either a weakly bound ligand or an open coordination site *cis* to the $\text{Ru}\equiv\text{CR}$ bond (Figure 3.2). Approach of an alkyne to the Ru-C triple bond could be possible, making such a complex interesting as a potential Ru ACM catalyst.

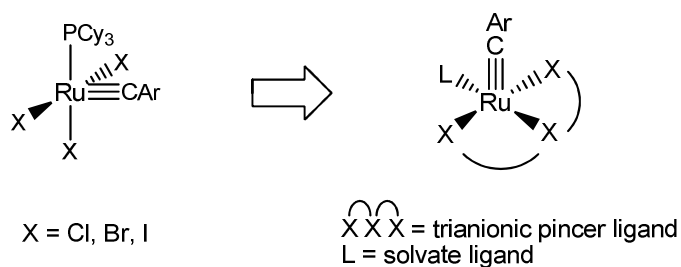


Figure 3.2. Comparison of known and proposed Ru alkylidyne complexes.

For these reasons, XXX pincer ligands are expected to facilitate the triple-bond metathesis reactions of interest to our lab. Given the dearth of reported bulky XXX pincer ligands at the time the current work was begun (see Chapter 1), the synthesis of new XXX pincer ligands was a primary research objective. The design, synthesis, and metallation of trianionic pincer ligands containing imidazoles will be discussed below.

3.2 Bis-Imidazole Ligand

Upon searching the literature, we found a report of a variety of 1,3-bis(4,5-diaryl-1*H*-imidazol-2-yl)benzene structures that we envisioned could serve as a precursor to a trianionic pincer ligand (Fig 3.3).⁴ Such a structure is attractive as an XXX ligand precursor for two reasons. First, the molecules are readily synthesized by condensing a benzil derivative with commercially available isophthalaldehyde. Secondly, the ligand steric profile can be adjusted through variation of the pendant aryl groups on the imidazole rings. In this chapter, C_A will denote the phenyl carbon atom that is *ortho* to both imidazole rings, N_B will denote the pyrrolic nitrogen atoms, and N_C will denote the pyridyl nitrogen atoms as shown in Figure 2.3.

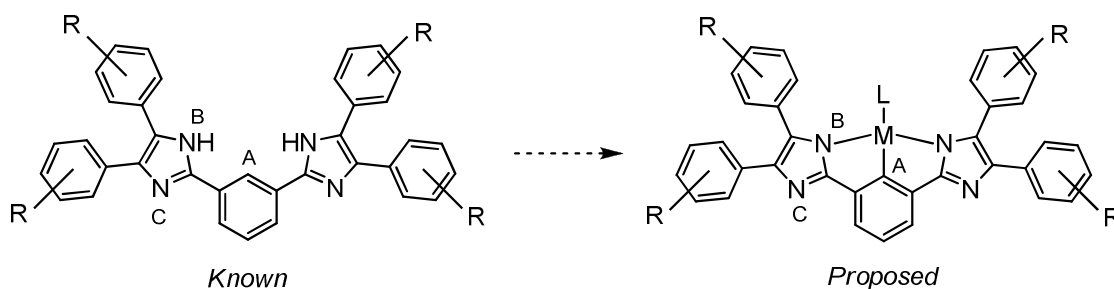
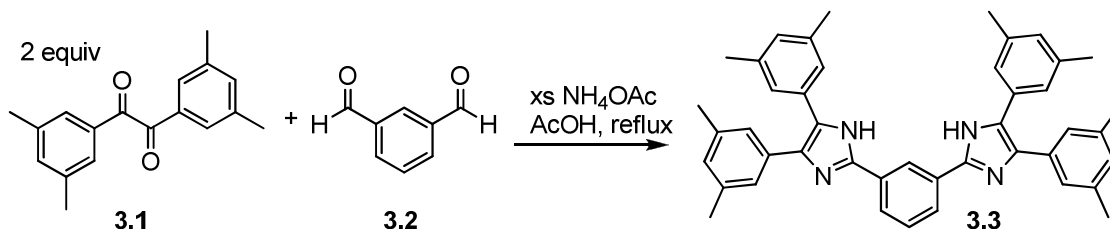


Figure 3.3. Proposed use of 1,3-bis(4,5-diaryl-1*H*-imidazol-2-yl)benzene molecules as XXX pincer ligands.

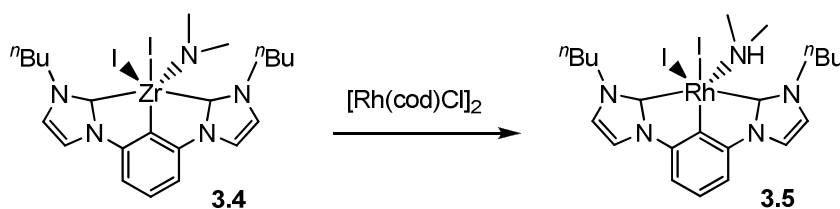
Upon condensing 3,3',5,5'-tetramethylbenzil (**3.1**)⁵ with isophthalaldehyde (**3.2**) and excess ammonium acetate in refluxing acetic acid, imidazole NCN-H₃ (**3.3**) could be obtained upon precipitation with water (Scheme 3.1). The *m*-xylyl group was chosen for its moderate steric protection and the simplicity of its ¹H NMR spectrum. Compound **3.3** displays low solubility in a variety of solvents. Therefore, it was purified readily by washing the crude product with excess ethanol, resulting in an 83 % yield of **3.3** upon

drying *in vacuo*. Ligand precursor **3.3** could now be tested for activation of C_A and N_B by Mo and Ru complexes.



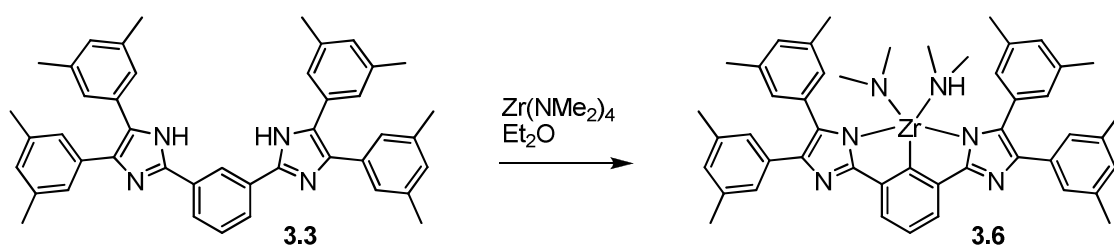
Scheme 3.1. Synthesis of imidazole **3.3**.

The activation of **3.3** to give an XXX complex was investigated using NMo(NMe₂)₃, NMo(O^tBu)₃, Mo(CO)₆, and Mo(CO)₃(NCEt)₃. It was anticipated that the C_A-H bond of **3.3** would be deprotonated by the basic ligands -NMe₂ and -O^tBu, or activated by Mo(0) precursors. However, the C_A-H remained intact under all conditions tested as judged by ¹H NMR spectroscopy. The activation of **3.3** with RuCl₂(PPh₃)₃ and [RuCl₂(*p*-cymene)]₂ was also investigated, but again CH activation was not observed. This was not unexpected, as examples of pincer ligand CH activation by Ru are rare.⁶ Furthermore, addition of KO^tBu to **3.3** did not facilitate C_A-H activation by Ru.



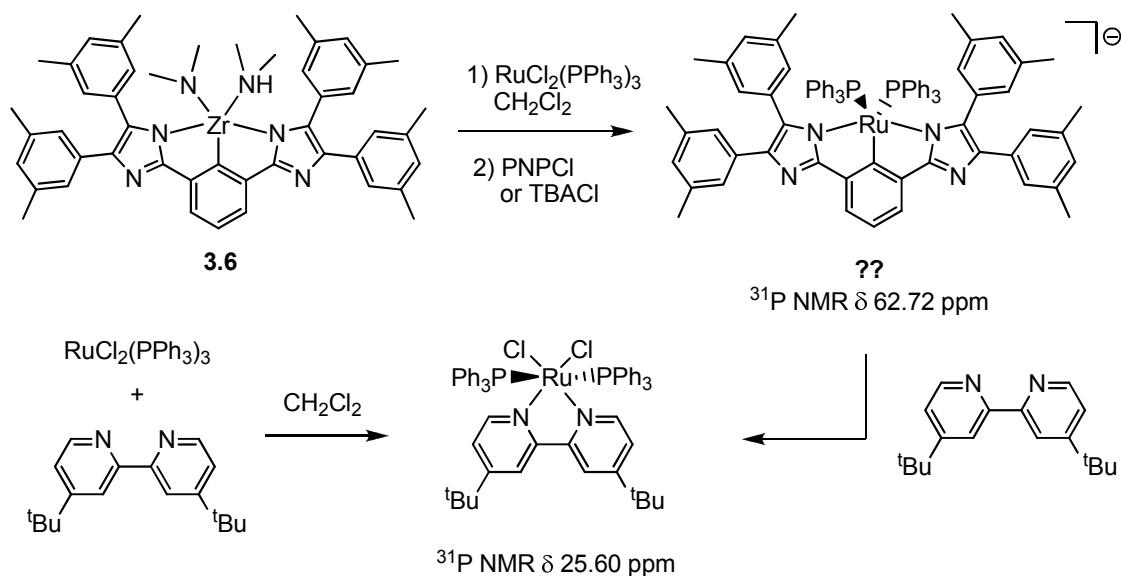
Scheme 3.2. Known pincer ligand transmetalation from Zr to Rh.

The literature Zr complex **3.4** (Scheme 3.2), which contains a pincer ligand that is structurally similar to **3.3**, has been shown to transmetallate its pincer ligand to Rh to afford **3.5**.⁷ Hoping to employ a similar strategy, **3.3** was found to react cleanly with $\text{Zr}(\text{NMe}_2)_4$ to yield $\text{Zr}(\text{NCN})(\text{NMe}_2)(\text{NHMe}_2)$ (**3.6**) in 93 % yield as shown in Scheme 3.3. Complex **3.6** is insoluble in nonpolar solvents and has a low solubility in CH_2Cl_2 and THF. The ^1H NMR spectrum of **3.6** in CD_2Cl_2 displays broadened peaks for the $-\text{NMe}_2$ and NHMe_2 resonances, indicating a ligand exchange process. Upon cooling the NMR sample to $0\text{ }^\circ\text{C}$, the broadened peaks sharpened significantly in the spectrum. The NHMe_2 resonance appears far downfield at δ 17.77 ppm, which suggests that the exchange process may involve hydrogen bonding. The tridentate nature of the imidazole ligand of **3.6** was confirmed by the deshielded ^{13}C NMR resonance of C_A at δ 184.05 ppm, which is indicative of metal coordination. However, X-ray quality crystals of **3.6** could not be grown due to its low solubility, and so its precise geometry remains unknown. Given the successful formation of **3.6**, activation of **3.3** was also attempted with the lighter congener $\text{Ti}(\text{NMe}_2)_4$. Reaction of $\text{Ti}(\text{NMe}_2)_4$ with **3.3** clearly resulted in deprotonation at N_B , but the $\text{C}_A\text{-H}$ remained intact as observed by ^1H NMR spectroscopy.



Scheme 3.3. Zr mediated activation of **3.3**.

Complex **3.6** was tested for pincer ligand transmetalation to a variety of substrates. In most cases, no discernible product was observed via ^1H or ^{31}P NMR spectroscopy. Reaction of **3.6** with $\text{RuCl}_2(\text{PPh}_3)_3$ initially seemed promising, as combination of the two complexes in CD_2Cl_2 led to generation of a new peak in the ^{31}P NMR spectrum at δ 62.67 ppm in a 2:1 ratio with free PPh_3 , which suggests a structure of the form $[\text{Ru}(\text{NCN})(\text{PPh}_3)_2]^-$ (Scheme 3.4). However, the ^1H NMR spectrum of the mixture was quite complex, and repeated attempts to isolate a clean product proved unsuccessful. Attempted cation exchange of the unknown product with TBACl or PNPCl did not result in a shift of the ^{31}P NMR signal. Introduction of 4,4'-di-*tert*-butyl-2,2'-bipyridyl led to the gradual formation of $\text{RuCl}_2(^t\text{Bu}_2\text{-bipy})(\text{PPh}_3)_2$, which was confirmed independently through reaction of 4,4'-di-*tert*-butyl-2,2'-bipyridyl directly with $\text{RuCl}_2(\text{PPh}_3)_3$ (Scheme 3.4). It is not likely that a bidentate ligand would displace a XXX pincer ligand. Therefore, the reaction of **3.6** with $\text{RuCl}_2(\text{PPh}_3)_3$ probably does not result in XXX transmetalation as originally believed. The ^{31}P NMR peak at δ 62.67 ppm may indicate the formation of a weak adduct, which is then broken up through addition of bipyridine.

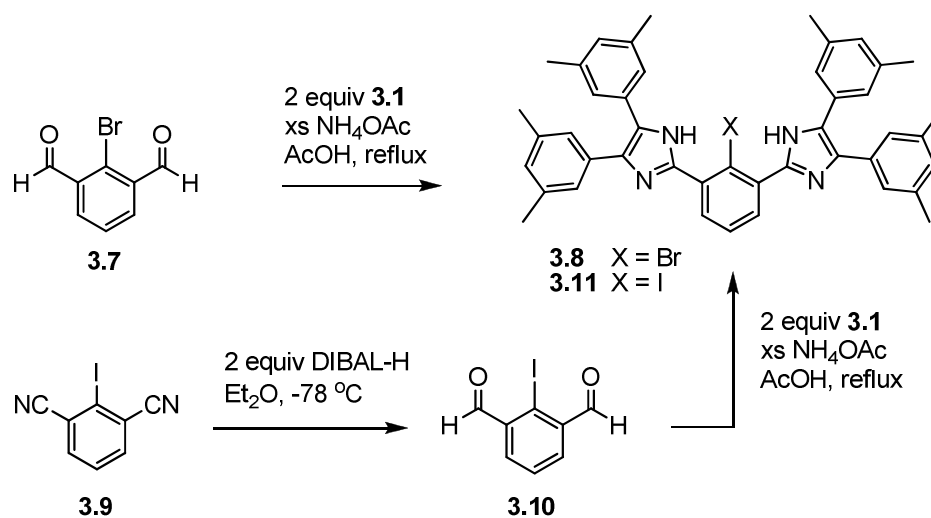


Scheme 3.4. Attempted XXX transmetalation from **3.6**.

3.3 Trianion Generation

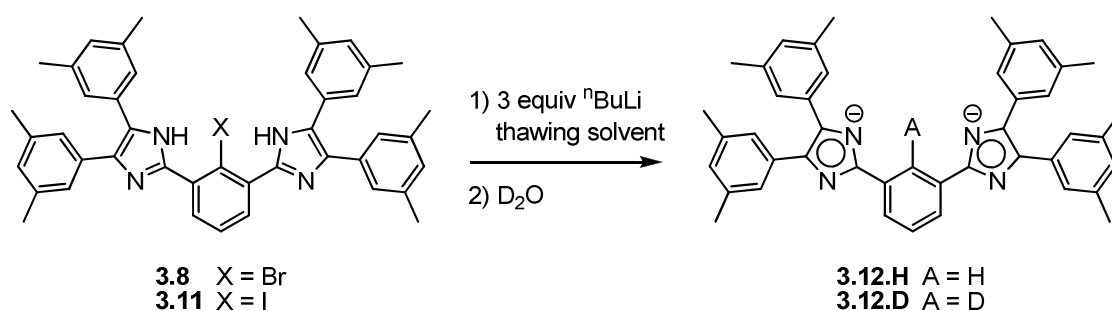
In Chapter 1 it was seen that formation of an NCN- Li_3 complex allowed for the formation of Hf(XXX) complexes through salt elimination.⁸ Therefore, we next investigated whether tri-lithium or tri-magnesium salts of **3.3** could be generated. As determined by D_2O quenching experiments, treatment of **3.3** with alkyl lithium reagents did not result in deprotonation of C_A . We sought to replace $\text{C}_A\text{-H}$ with $\text{C}_A\text{-X}$ (X = halogen) in order to generate an arylide species *via* lithium- or magnesium-halogen exchange. The imidazole compound NCN-Br- H_2 (**3.8**) was readily synthesized by condensation of 2-bromoisophthalaldehyde (**3.7**)⁹ with 2 equiv of **3.1** (Scheme 3.5), and upon purification was isolated in 68 % yield. In our hands, the published procedure for synthesizing **3.7** was not consistently reproducible and did not scale very readily. Therefore, readily obtained 2-iodoisophthalonitrile (**3.9**)¹⁰ was reduced with 2 equiv of DIBAL-H, leading the formation of 2-iodoisophthalaldehyde (**3.10**) after acidic workup

(Scheme 3.5). Unoptimized reaction conditions gave a crude mixture of **3.9** that was not purified. Subsequent condensation of impure **3.10** with 2 equiv of **3.1** generated NCN-I-H₂ (**3.11**), which could be readily isolated due to its low solubility. The synthesis of **3.11** could be performed on a multigram scale in 20 % yield from **3.9**.



Scheme 3.5. Synthesis of imidazoles NCN-X-H₂.

With ligand precursors **3.8** and **3.11** in hand, investigations into the generation of trilitium salts commenced. In the test reactions, **3.8** or **3.11** were treated with 3 equiv *n*-BuLi in thawing solvent and the resulting solution was quenched with D₂O (Scheme 3.6). In all cases, ¹H NMR analysis of the quenched reaction mixtures indicated a sole product having chemical shifts identical to NCN-H₃ (**3.3**), except that a single xylyl-group environment was observed on the NMR timescale. Therefore, dianionic species **3.12.H(D)** was assigned as the reaction product, suggesting that tri-lithiation was successful.



Scheme 3.6. Tri-lithiation followed by deuterium quenching.

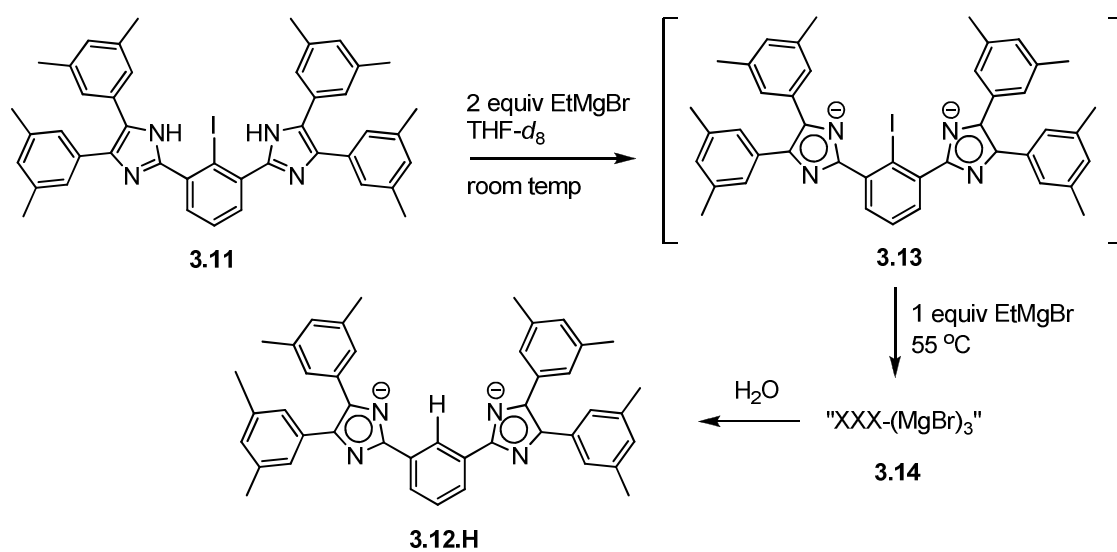
While tri-lithiation was successful, the subsequent deuteration at C_A was not complete and varying amounts of protonation were observed as shown in Table 3.1. Protonation of C_A suggests that the $XXX-Li_3$ complex is somewhat unstable with respect to proton abstraction from the solvent. The least amount of proton incorporation (24 %) was observed upon lithiation of **3.8** (X = Br) in thawing Et_2O followed by D_2O quenching after 15 minutes. Under identical reaction conditions, the iodo derivative **3.11** yielded a greater percentage of proton incorporation (68 %), likely due to a more rapid rate of Li–I exchange¹¹ followed by decomposition. Performing the reactions in thawing THF resulted in greater amounts of protonation for both **3.8** and **3.11**, despite the decreased reaction times prior to quenching. These data indicate that while tri-lithiation is facile, the resulting species are not very stable with respect to protonation at C_A , thus limiting their synthetic utility.

Table 3.1. Results of tri-lithiation reactions.

Compound	Solvent	Temperature	Time / min	% H ^a
3.8	Et_2O	thawing	15	24
3.11	Et_2O	thawing	15	68
3.8	THF	thawing	5	36
3.11	THF	thawing	5	97

^a Determined by integration of the C_AH signal in the 1H NMR spectrum.

We next investigated the reactivity of Grignard reagents in the hope of generating a more stable tri-anionic species that would persist in solution long enough to react with metal substrates. Treatment of **3.11** with 2 equiv of EtMgBr in THF-*d*₈ resulted in rapid deprotonation of the imidazole rings to give **3.13** as judged by ¹H NMR spectroscopy (Scheme 3.7). Addition of a third equivalent of EtMgBr followed by heating to 55 °C resulted in a complicated ¹H NMR spectrum containing large numbers of broad resonances. Upon quenching with H₂O, the ¹H NMR spectrum revealed the presence of **3.12.H**, suggesting the intermediate formation of an XXX-(MgBr)₃ (**3.14**) complex as desired.



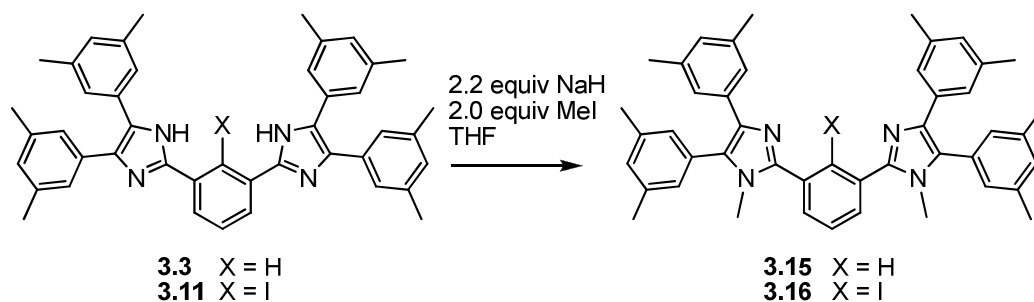
Scheme 3.7. Tri-anion formation using a Grignard reagent.

Complex **3.14** was generated *in situ* and then treated with a variety of metal compounds. The Mo complexes NMo(O^tBu)₃, NMo(OCMe₂CF₃)₃, and EtCMoCl₃(DME) did not give any identifiable reaction products with **3.14** in THF-*d*₈; the

corresponding ^1H NMR spectra matched the **3.14** spectrum in complexity. Reaction of **3.14** with $\text{RuCl}_2(\text{PPh}_3)_3$ in THF generated free PPh_3 as observed by ^{31}P NMR spectroscopy, as well as a very broad peak at $\delta \sim 60$ ppm. However, a ^1H NMR spectrum of the reaction mixture in CD_2Cl_2 showed a large number of NCN-containing products as judged by the xylyl group region of the spectrum. Dissolution of the reaction mixture in pyridine- d_5 resulted in the formation of multiple products in both the ^1H and ^{31}P NMR spectra. Therefore, it seems that **3.14** is not suitable for metalation of transition metal complexes. One possible explanation for the lack of reactivity is the formation of imidazole-Mg oligomers that prevent the required approach with a metal substrate.

3.4 Monoanion Generation

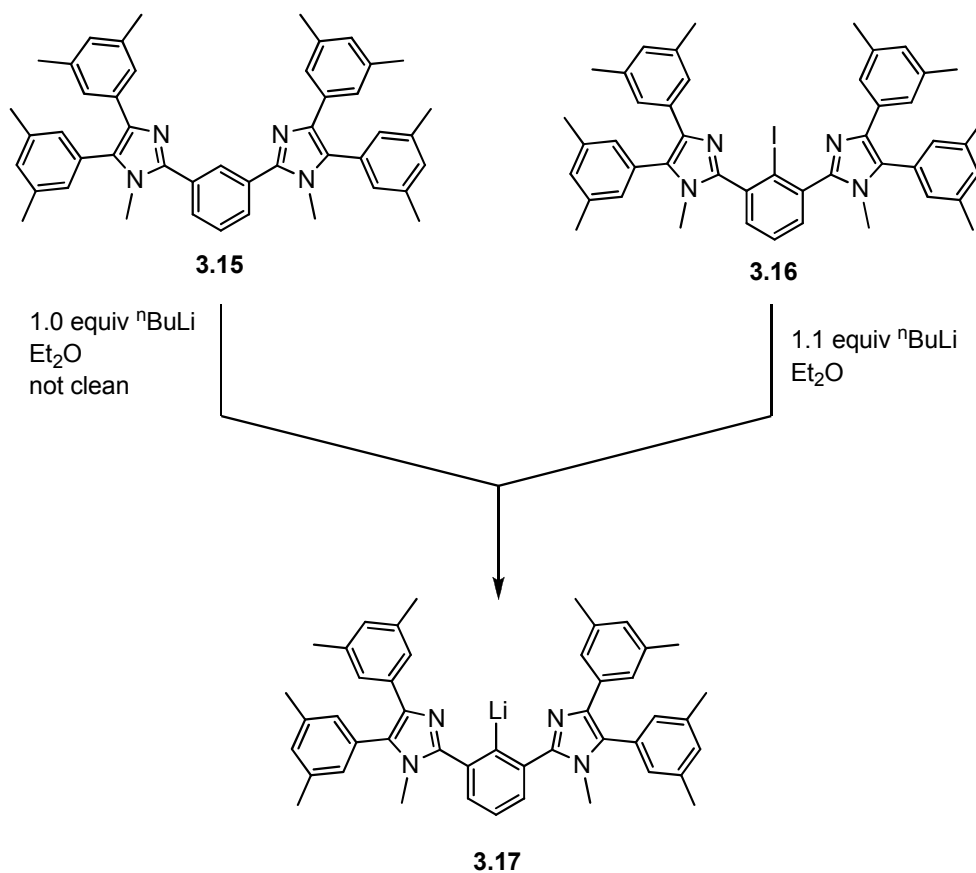
We thought it interesting to determine whether lack of acidic protons would affect the formation and stability of the C_A lithium arylide species. Therefore the dimethyl imidazoles NCN-H-Me₂ (**3.15**) and NCN-I-Me₂ (**3.16**) were also synthesized from the corresponding parent imidazoles **3.3** and **3.11** as shown in Scheme 3.8. Upon metalation, these compounds would be structurally similar to a variety of known monoanionic (LXL) NCN pincer ligands.⁶ Additionally, we anticipated that the corresponding LXL ligand would be a good ancillary ligand for Ru alkylidyne¹² and carbide¹³⁻¹⁶ complexes of interest to our group.



Scheme 3.8. Synthesis of potential LXL precursors NCN-X-Me₂.

Precursor **3.15** was found to be deprotonated by *n*-BuLi at C_A to give NCN-Li-Me₂ (**3.17**) as desired (Scheme 3.9). However, a large number of unidentifiable byproducts were also formed in the reaction. Cleaner conversion was achieved by Li-I exchange between **3.16** and *n*-BuLi and allowed for the isolation of **3.17** as an off-white powder in 70 % yield. Solid **3.17** was found to be rapidly protonated in THF solution even at low temperatures, and so reactions of **3.17** were typically performed in either Et₂O or C₆H₆.

Compound **3.17** was treated with the substrates RuCl₂(PPh₃)₃, [RuCl₂(*p*-cymene)]₂, Ru(C-*p*-C₆H₄Me)(PCy₃)₂Cl,¹² and Ru(CS)(PCy₃)₂Cl₂.¹⁴ Under all of the conditions tested, either no reaction was observed or the reaction was sluggish and yielded multiple products. The poor reactivity is possibly due to the large size of the NCN ligand, which could inhibit its approach towards Ru substrates. Because the use of **3.15** and **3.16** as LXL pincer ligand precursors was not expected to advance the primary research interest of triple-bond metathesis, investigations of these ligands were not pursued further.

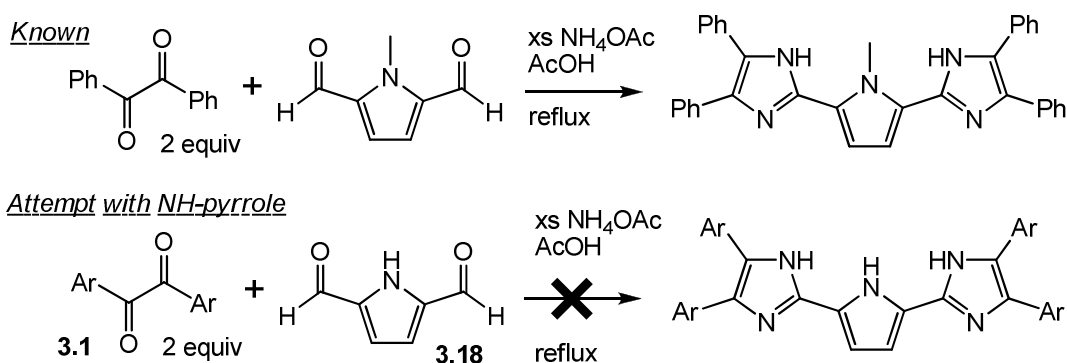


Scheme 3.9. Lithiation to give an LXL precursor **3.17**.

3.5 Synthesis of XXX Precursors Containing Three Acidic Protons

Given the difficulty encountered in activation of **3.3** and its derivatives, we reasoned that an XXX ligand precursor possessing three acidic protons would be easier to ligate via protonolysis or salt elimination pathways. To this end we targeted a 2,5-bisimidazole-pyrrole framework, in which the central phenyl ring of **3.3** has been replaced with a pyrrole ring. A closely related molecule was synthesized through the condensation of benzil with 1-methyl-1*H*-pyrrole-2,5-dicarbaldehyde.¹⁷ Therefore, we targeted a similar route to obtain the desired molecules (Scheme 3.10). Attempts to condense 3,3',5,5'-tetramethylbenzil (**3.1**), pyrrole-2,5-dicarbaldehyde (**3.18**),¹⁸ and

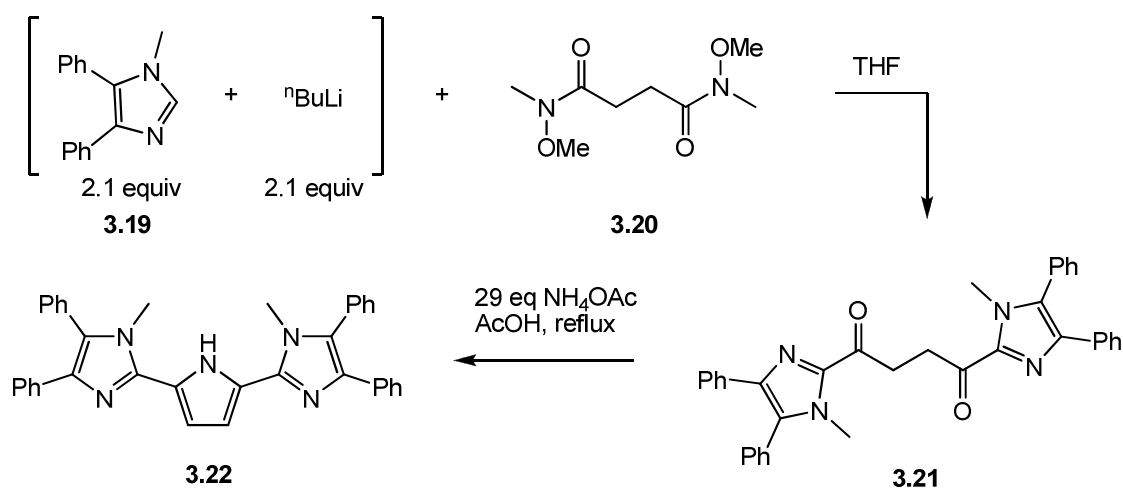
NH₄OAc in refluxing acetic acid resulted in the isolation of a black solid. The only identifiable compound observed in the ¹H NMR spectrum was **3.1**, indicating that the pyrrole component was unstable under the reaction conditions. The pyrrole **3.18** was observed to be thermally unstable, with significant decomposition of **3.18** being qualitatively observed even upon storing **3.18** at low temperatures in the solid-state. Therefore, the instability of **3.18** in refluxing acetic acid was not entirely surprising.



Scheme 3.10. Attempted synthesis of desired 2,5-bisimidazole-pyrrole.

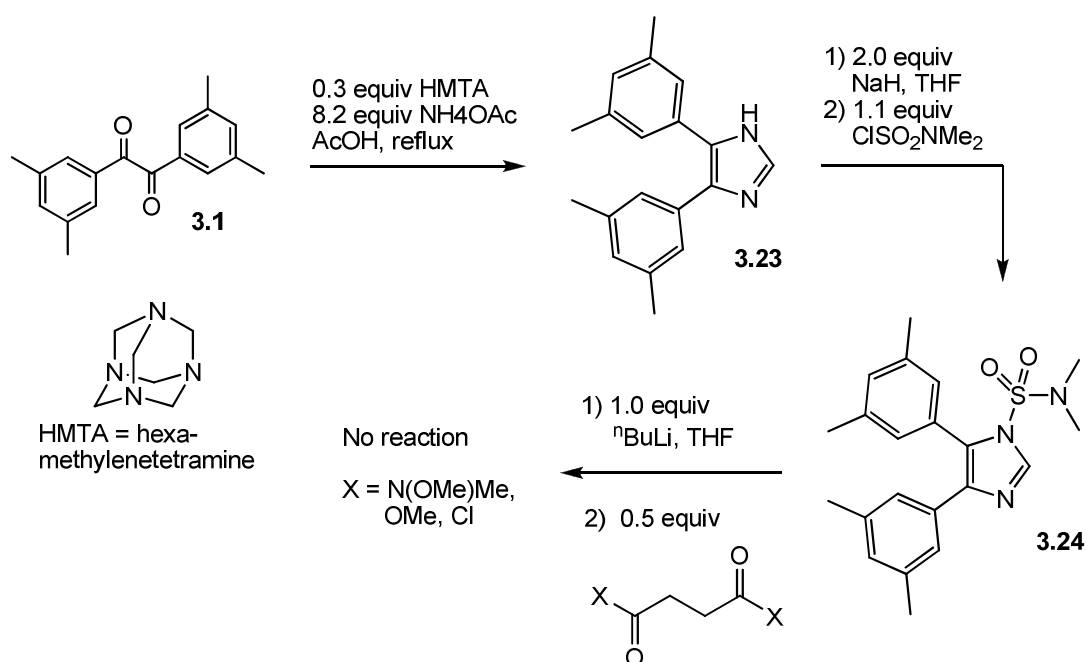
Seeking other synthetic routes, we turned our attention to the Paal-Knorr synthesis of pyrroles, in which a 1,4-diketone substrate is condensed with an amine to form a pyrrole ring. For example, use of 1,4-diphenylbutane-1,4-dione as the substrate leads to the formation of 2,5-diphenylpyrrole.¹⁹ Therefore, known 1-methyl-4,5-diphenylimidazole (**3.19**)²⁰ was used as a model substrate to test the feasibility of the synthetic route. Imidazole rings are known to be incompatible with Friedel-Crafts chemistry,²¹ and so **3.19** could not be acylated *via* electrophilic aromatic substitution. Consequently, the required 1,4-dione **3.21** was synthesized by lithiation at the 2-position

of **3.19** followed by nucleophilic addition into *N,N'*-dimethoxy-*N,N'*-dimethylsuccinamide (**3.20**),²² as shown in Scheme 3.11. Upon workup, dione (**3.21**) was isolated in 59 % yield. In a test reaction, **3.21** was condensed with excess NH_4OAc in refluxing acetic acid. The desired 2,5-bisimidazole-pyrrole species **3.22** was precipitated upon quenching the reaction with water. Compound **3.22** was identified through its ^1H NMR and MS spectra, indicating the applicability of the Paal-Knorr synthesis to the current systems.



Having determined that the Paal-Knorr synthesis was feasible for construction of the desired imidazole-pyrrole scaffolds, we turned to a system employing *N*-protecting groups on the parent imidazole. Synthesis of the parent 4,5-bis(3,5-dimethylphenyl)imidazole **3.23** was achieved by condensing **3.1** with hexamethylenetetramine (HMTA) in refluxing acetic acid, with **3.23** being isolated in 64 % yield. Deprotonation of **3.23** with NaH followed by treatment with dimethylsulfamoyl chloride gave imidazole **3.24** in 64 % yield after purification. Lithiation of **3.24** with *n*-

BuLi followed by treatment with $\text{XC(O)C}_2\text{H}_4\text{C(O)X}$ ($\text{X} = \text{N(OMe)Me, OMe, Cl}$) did not result in acylation of the imidazole ring. Starting imidazole **3.24** was the only imidazole-containing product observed in the ^1H NMR spectrum of the crude reaction mixtures. A deuterium quenching experiment under similar conditions revealed only partial deuteration at the imidazole ($\text{CH} = 60\%$), suggesting that H-atom abstraction from the solvent is relatively slow. Therefore, the low reactivity of the lithiated imidazole species with acyl substrates could be due either to favorable lithium chelation by the sulfamoyl group, or to steric hindrance associated with the sulfamoyl group.

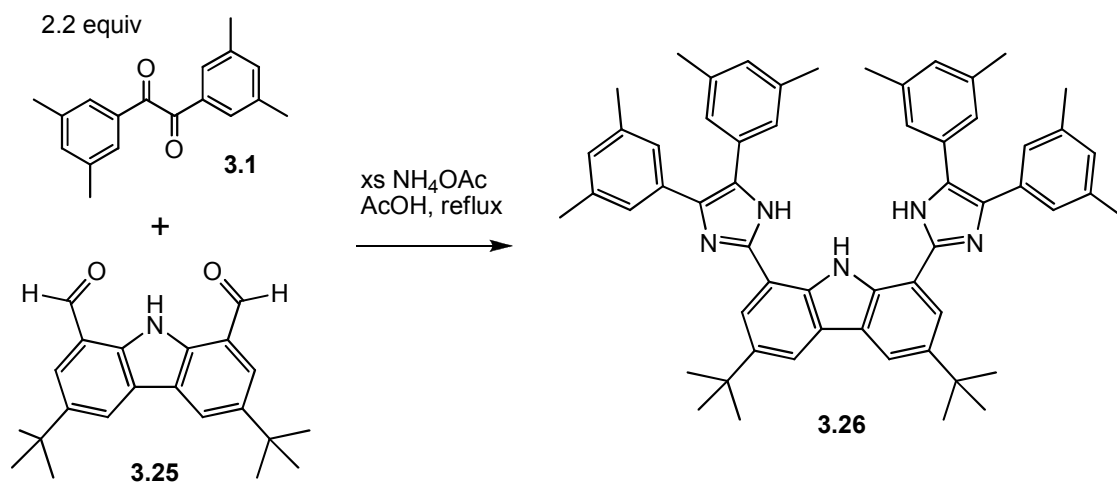


Scheme 3.12. Attempted dione formation with an N-protected imidazole.

Other protecting groups for the imidazole nitrogen were considered in the hope of increasing the reactivity of the lithiated imidazole. However, a judicious choice of protecting groups was necessary, as a variety of common imidazole N-protecting groups

are not compatible with organolithium reagents. For example, imidazole N-trimethylsilyl and N-benzyl groups are known to react with alkyllithium reagents.²¹ Facile lithiation of N-methoxymethyl (MOM) protected imidazoles is known; however, the N-MOM protecting group can be difficult to remove.²¹ Fortunately the dimethylaminomethyl group has been shown to be suitable for lithiation chemistry and can be removed easily.²³ However due to the hydrophobicity of **3.23**, attempts to install a dimethylaminomethyl group failed under the typical aqueous conditions for the Mannich reaction.

Due to the difficulty in finding an appropriate protecting group for the Paal-Knorr synthetic route, we returned to the previously attempted imidazole condensation pathway. Unlike the other heterocyclic substrates tested, the compound 3,6-di-*tert*-butyl-9*H*-carbazole-1,8-dicarbaldehyde (**3.25**)²⁴ was found to readily condense with **3.1** to give NNN-H₃ (**3.26**) as shown in Scheme 3.13. Upon purification of the reaction mixture, **3.26** was obtained in 55 % yield as a yellow powder. Unlike **3.3**, imidazole **3.26** is soluble in a wide range of solvents due to the presence of the *tert*-butyl groups on the carbazole ring. Future investigations into metallation of **3.26** will be discussed further in Chapter 5.



Scheme 3.13. Synthesis of an NNN-H₃ ligand precursor.

3.6 Conclusions

Two new rare XXX ligands have been developed and synthesized. The NCN ligand (**3.3**) was found to be activated by Zr(NMe₂)₄ to give a Zr(XXX) complex (**3.6**). The activation of **3.1** with other metal substrates was found to be challenging, which is not surprising given the limited scope of other XXX ligand precursors that contain only two acidic protons (see Chapter 1). Upon synthesis of the appropriate imidazole substrates, tri-lithiation of the NCN ligand could be achieved, though the species was unstable with respect to protonation at C_A. An XXX-(MgBr)₃ (**3.14**) species could also be generated *in situ* and was found to be more stable than the XXX-Li₃ species. However, **3.14** did not react cleanly with metal substrates, possibly due to the large size of the ligand. A monoanionic NCN-Li species (**3.17**) could be formed, but was found to have a low reactivity with metal substrates.

It was hypothesized that the difficulties encountered in metalation of the NCN ligand could be remedied by synthesizing a derivative containing three acidic protons.

Formation of a model 2,5-bis-imidazole-pyrrole compound (**3.22**) demonstrated the feasibility of the Paal-Knorr synthesis for making imidazole-pyrrole compounds. Difficulties were encountered in making the requisite dione intermediate when using protecting groups other than the N-methyl group. This obstacle was bypassed by designing a new target ligand containing a carbazole backbone *via* condensation of a benzil derivative (**3.1**) with a substituted carbazole-1,8-dicarbaldehyde (**3.24**) to give a new imidazole-carbazole compound (**3.26**). Imidazole **3.26** is a rare example of an XXX-pincer ligand precursor containing three acidic protons.

3.7 Experimental

3.7.1 Methods

All reactions were performed in an atmosphere of dinitrogen, either in a nitrogen-filled MBRAUN Labmaster 130 glove box or by using standard air-free techniques unless indicated otherwise.²⁵ ¹H NMR spectra were recorded at 499.909 MHz, 399.967 MHz, or or 300.075 MHz on a Varian Inova 500, Varian Inova 400, Varian MR400, or Varian Inova 300 spectrometer and referenced to the residual protons in pyridine-*d*₅ (8.79 ppm), CDCl₃ (7.26 ppm), C₆D₆ (7.16 ppm), CD₂Cl₂ (5.32 ppm), THF-*d*₈ (2.09 ppm), (CD₃)₂SO (2.05 ppm), or CD₃CN (1.94 ppm). ¹³C NMR spectra were recorded at 100.724 MHz on a Varian Inova 400 or Varian MR400 spectrometer and were referenced to naturally abundant ¹³C nuclei in CDCl₃ (77.16 ppm), CD₂Cl₂ (54.00 ppm), or (CD₃)₂SO (39.52 ppm). HRMS data were collected on a Micromass AutoSpec Ultima with electrospray ionization. LCT-MS data were collected on a Micromass LCT Time-

of-Flight mass spectrometer. Combustion analyses were performed on a Perkin-Elmer 200 Series II Analyzer.

3.7.2 Materials

All bulk solvents were obtained from VWR scientific. Benzene and CH_2Cl_2 were degassed and dried over 4 Å molecular sieves, and all other solvents used were dried and deoxygenated by the method of Grubbs. $\text{Zr}(\text{NMe}_2)_4$,²⁶ $\text{NMo}(\text{O}^t\text{Bu})_3$,²⁷ $\text{NMo}(\text{OCMe}_2\text{CF}_3)_3$,²⁸ $\text{EtCMoCl}_3(\text{DME})$,²⁹ $\text{Mo}(\text{CO})_3(\text{NCEt})_3$,³⁰ $\text{Ti}(\text{NMe}_2)_4$,²⁶ $\text{RuCl}_2(\text{PPh}_3)_3$,³¹ $[\text{RuCl}_2(p\text{-cymene})]_2$,³² $[\text{RuI}_2(\text{PPh}_3)_2]_n$,³³ $[\text{Ru}(\text{cod})\text{Cl}_2]_n$,³⁴ $\text{Ru}(\text{C-}p\text{-C}_6\text{H}_4\text{Me})(\text{PCy}_3)_2\text{Cl}$,¹² $\text{Ru}(\text{CS})(\text{PCy}_3)_2\text{Cl}_2$,¹⁴ 3,3',5,5'-tetramethylbenzil (**3.1**),⁵ 2-bromoisophthalaldehyde (**3.7**),⁹ iodoisophthalonitrile (**3.9**),¹⁰ pyrrole-2,5-dicarbaldehyde (**3.18**),¹⁸ N-methyl-4,5-diphenylimidazole (**3.19**),²⁰ N,N'-dimethoxy-N,N'-dimethylsuccinamide (**3.20**),²² and 3,6-di-*tert*-butyl-9*H*-carbazole-1,8-dicarbaldehyde (**3.29**)²⁴ were synthesized according to literature procedures. Ammonium acetate, methyl iodide, sodium hydride (60 % dispersion in mineral oil), hexamethylenetetramine, dimethylsulfamoyl chloride, dimethylamine hydrochloride, 1.0 M EtMgBr in hexanes, dimethyl succinate, succinyl chloride, and 4,4'-di-*t*-butyl-2,2'-bipyridyl were obtained from Acros. Acetic acid, acetone, methanol, 2-propanol, aqueous ammonia, HCl, and formaldehyde (37% w/w aqueous) were obtained from Fisher. $\text{Mo}(\text{CO})_6$, PNPCl, 1.6 M *n*-BuLi in hexanes, and 3.0 M EtMgBr in Et_2O were obtained from Strem. Isophthalaldehyde was obtained from TCI, and 1.0 M DIBAL-H in hexanes was obtained from Alfa Aesar. TBACl was obtained from Fluka. All reagents were used as received.

3.7.3 Synthetic Procedures

NCN-H₃ (3.3). In 250 mL round bottom flask equipped with a reflux condensor open to air, a suspension of isophthalaldehyde (**3.2**) (1.80 g, 13.4 mmol, 1.0 equiv), 3,3',5,5'-tetramethylbenzil (**3.1**) (7.29 g, 27.4 mmol, 2.0 equiv), and ammonium acetate (16.6 g, 215 mmol, 16 equiv) in acetic acid (150 mL) was brought to reflux for 4 hours. After cooling, the solution was poured into H₂O (250 mL), causing a light powder to precipitate. The solid was collected by filtration and washed with H₂O (2 x 250 mL). The solid was stirred in EtOH (300 mL) for 20 minutes, then filtered and washed with Et₂O (100 mL). Addition of H₂O (100 mL) to the EtOH / Et₂O filtrate yielded a second crop of product, which was collected by filtration. The crops were combined and heated at 145 °C for 24 hours to remove traces of acetic acid, yielding **3.3** (6.97 g, 11.1 mmol, 82.8 %) as a light cream powder. ¹H NMR ((CD₃)₂SO): δ 12.70 (s, 2H, NH), 8.77 (pseudo t, 1H, ArH), 8.07 (dd, ³J_{HH} = 7.9 Hz, ⁴J_{HH} = 1.8 Hz, 2H, ArH), 7.56 (t, ³J_{HH} = 7.9 Hz), 7.24 (s, 4H, ArH), 7.17 (s, 4H, ArH), 7.00 (s, 2H, ArH), 6.86 (s, 2H, ArH), 2.27 (s, 12H, ArCH₃), 2.21 (s, 12H, ArCH₃). ¹³C{¹H} NMR ((CD₃)₂SO): δ 145.05, 137.40, 137.24, 136.81, 135.04, 130.93, 130.89, 129.05, 128.91, 128.44, 127.96, 126.07, 125.04, 124.90, 122.29, 20.97, 20.88. Anal. Calcd for C₄₄H₄₂N₄: C, 84.31; H, 6.75; N, 8.94. Found C, 84.25; H, 6.41; N, 8.87.

Zr(NCN)(NMe₂)(NHMe₂) (3.6). Compound **3.3** (6.4611 g, 10.32 mmol, 1.0 equiv) and Zr(NMe₂)₄ (2.8990 g, 10.84 mmol, 1.05 equiv) were suspended in Et₂O (175 mL). The mixture was stirred vigorously for 5 hrs, then diluted with pentane (75 mL). The solid was collected by vacuum filtration, washed with pentane (3 x 40 mL), then

dried *in vacuo* to yield **3.6** (7.7428 g, 9.63 mmol, 93 %) as a cream colored powder. ^1H NMR (CD_2Cl_2 , 0 °C): δ 17.77 (s, 1H, NHMe_2), 7.80 (d, $^3J_{\text{HH}} = 7.6$ Hz, 2H, ArH), 6.97 (t, $^3J_{\text{HH}} = 7.6$ Hz, 2H, ArH), 6.95 (s, 2H, ArH), 6.92 (s, 4H, ArH), 6.90 (s, 4H, ArH), 6.62 (s, 2H, ArH), 2.68 (s, 6H, N- CH_3), 2.41 (s, 6H, N- CH_3), 2.28 (s, 12H, Ar CH_3), 1.92 (s, 12H, Ar CH_3). $^{13}\text{C}\{^1\text{H}\}$ NMR (CD_2Cl_2 , 0 °C): δ 184.05 (s, Zr- C_{ipso}), 158.38, 140.08, 137.66, 137.40, 135.31, 132.91, 130.14, 129.27, 127.56, 127.43, 125.40, 120.73, 38.58, 37.86, 21.56, 21.03. Anal. Calcd for $\text{C}_{48}\text{H}_{52}\text{N}_6\text{Zr}$: C, 71.69; H, 6.52; N, 10.45. Found C, 71.22; H, 6.37; N, 9.99.

NCN-Br- H_2 (3.8). In 500 mL round bottom flask equipped with a reflux condenser open to air, a suspension of 2-bromoisophthalaldehyde (**3.7**) (1.70 g, 7.98 mmol, 1.0 equiv), 3,3',5,5'-tetramethylbenzil (**3.1**) (4.27 g, 16.1 mmol, 2.0 equiv), and ammonium acetate (19.7 g, 256 mmol, 32 equiv) in acetic acid (150 mL) was brought to reflux for 3 hours 15 minutes. After cooling, the solution was poured into H_2O (300 mL) and the resulting mixture made alkaline with NH_4OH . The solid was collected by filtration and washed with H_2O (400 mL). The product was purified by multiple precipitations from THF / hexane at -10 °C, with the crops collected by filtration, washed with hexane, and dried *in vacuo* to yield **3.8** (3.84 g, 5.44 mmol, 68 %) as an off-white powder. ^1H NMR ($(\text{CD}_3)_2\text{SO}$, 300 MHz): δ 12.77 (s, 2H, NH), 7.72 (d, 2H, ArH, $^3J_{\text{HH}} = 7.6$ Hz), 7.59 (t, 1H, ArH, $^3J_{\text{HH}} = 7.3$ Hz), 7.23 (s, 4H, ArH), 7.16 (s, 4H, ArH), 6.99 (s, 2H, ArH), 6.86 (s, 2H, ArH), 2.26 (s, 12H, Ar CH_3), 2.21 (s, 12H, Ar CH_3). $^{13}\text{C}\{^1\text{H}\}$ NMR ($(\text{CD}_3)_2\text{SO}$): δ 144.86, 137.46, 136.78, 136.46, 135.12, 134.09, 131.99, 130.86,

128.95, 127.87, 127.64, 127.15, 125.72, 124.99, 122.56, 20.98, 20.89. MS [M+H]⁺ = 705; HRMS calcd for C₄₄H₄₂BrN₄ 705.2593, found 705.2604.

2-iodoisophthalaldehyde (3.10). In a glovebox, iodoisophthalonitrile (**3.9**) (6.44 g, 25.4 mmol, 1.0 equiv) and dry Et₂O (200 mL) were measured into a 500 mL 3-neck flask fitted with a gas adapter and rubber septum. An addition funnel containing DIBAL-H (1.0 M in hexane, 53 mL, 53 mmol, 2.1 equiv) was attached, then the flask was placed under N₂ on a Schlenk line and cooled to -78 °C. The DIBAL-H solution was added slowly over 10 minutes, then the mixture was allowed to gradually warm overnight with stirring. The mixture was then cooled to 0 °C and quenched with 25% v/v aqueous HCl (100 mL). The aqueous layer was extracted with CH₂Cl₂ (3 x 50 mL), then the combined organics were filtered to remove particulates and the volatiles removed *in vacuo*, yielding 4.87 g of solid. The crude material contained ~ 50 % **3.10** as judged by comparison to the reported ¹H NMR spectrum.³⁵ The remainder of the material consisted of mostly 2-iodoisophthalonitrile (**3.9**). The crude mixture proved suitable to carry on without purification.

NCN-I-H₂ (3.11). In 500 mL round bottom flask equipped with a reflux condenser open to air, a suspension of crude **3.10** (~50 %, 4.87 g, ~9.6 mmol, 1.0 equiv), 3,3',5,5'-tetramethylbenzil (**3.1**) (5.11 g, 19.2 mmol, 2.0 equiv), and ammonium acetate (12.6 g, 164 mmol, 17 equiv) in acetic acid (100 mL) was brought to reflux for 4 hours. After cooling, the solution was poured into H₂O (200 mL). The precipitate was collected by filtration, washed with H₂O (3 x 100 mL), then suspended in EtOH (300 mL) and

stirred vigorously for 20 minutes. The mixture was then filtered and the solid washed with Et₂O (3 x 100 mL), CH₂Cl₂ (100 mL), and Et₂O (100 mL). The white solid was then dried *in vacuo* at 100 °C to yield **3.11** (3.87 g, 5.14 mmol, 20 % from **3.9**) ¹H NMR ((CD₃)₂SO, 400 MHz): δ 12.58 (s, 2H, NH), 7.58–7.60 (m, 3H, ArH), 7.24 (s, 4H, ArH), 7.17 (s, 4H, ArH), 6.99 (s, 2H, ArH), 6.86 (s, 2H, ArH), 2.27 (s, 12H, ArCH₃), 2.21 (s, 12H, ArCH₃). ¹³C{¹H} NMR ((CD₃)₂SO): δ 147.45, 138.51, 137.44, 136.75, 136.14, 135.23, 131.02, 130.96, 128.88, 127.80, 127.61, 127.30, 125.68, 125.00, 102.29, 20.99, 20.89. MS [M+H]⁺ = 753; HRMS calcd for C₄₄H₄₂IN₄ 753.2454, found 753.2484.

NCN-H-Me₂ (3.15). THF (30 mL) was added via cannula to a solid mixture of NCN-H₃ (1.5184 g, 2.42 mmol, 1.0 equiv) and NaH (60 % in mineral oil, 0.2162 g, 5.37 mmol, 2.2 equiv) at –78 °C. The mixture was stirred 30 minutes at –78 °C, then 2 hours 15 minutes at room temperature. The solution was cooled to 0 °C, then a solution of MeI (0.30 mL, 4.82 mmol, 2.0 equiv) was added via cannula. The solution was stirred overnight, then quenched with H₂O (30 mL), causing a white powder to precipitate. The powder was collected by filtration, washed with excess H₂O, and dried *in vacuo* to yield **3.15** (1.4431 g, 2.21 mmol, 91.3 %) as a white powder. ¹H NMR (CDCl₃, 400 MHz): δ 8.07 (t, ⁴J_{HH} = 1.6 Hz, 1H, ArH), 7.82 (dd, ³J_{HH} = 7.8 Hz, ⁴J_{HH} = 1.6 Hz, 2H, ArH), 7.61 (t, ³J_{HH} = 7.8 Hz, 1H, ArH), 7.24 (s, 4H, ArH), 7.09 (s, 2H, ArH), 7.05 (s, 4H, ArH), 6.80 (s, 2H, ArH), 3.53 (s, 6H, NCH₃), 2.37 (s, 12H, ArCH₃), 2.20 (s, 12H, ArCH₃). ¹³C{¹H} NMR (CDCl₃): δ 146.94, 138.38, 137.52, 137.28, 134.51, 131.58, 131.11, 130.83, 130.19, 129.63, 129.34, 128.84, 128.55, 127.89, 124.53, 33.15, 21.32, 21.27. Anal. Calcd for C₄₆H₄₆N₄: C, 84.36; H, 7.08; N, 8.56. Found C, 84.10; H, 6.73; N, 8.12.

NCN-I-Me₂ (3.16). A mixture of THF (100 mL) and Et₂O (100 mL) was added via cannula to a solid mixture of NCN-I-H₂ (8.43 g, 11.2 mmol, 1.0 equiv) and NaH (0.6781 g, 28.3 mmol, 2.6 equiv) at 0 °C. The mixture was stirred for 3 hours at room temperature, then a solution of MeI (1.40 mL, 22.5 mmol, 2.0 equiv) in Et₂O (80 mL) was added *via* cannula. The suspension was stirred overnight, then quenched with H₂O (200 mL). The mixture was filtered, the solid was washed with excess H₂O, and dried *in vacuo* to yield **3.16** (7.40 g, 9.48 mmol, 85 %) as a white powder. ¹H NMR (CDCl₃, 400 MHz): δ 7.64–7.56 (m, 3H, ArH), 7.22 (s, 4H, ArH), 7.08 (s, 2H, ArH), 7.04 (s, 4H, ArH), 6.79 (s, 4H, ArH), 3.27 (s, 6H, NCH₃), 2.36 (s, 12H, ArCH₃), 2.19 (s, 12H, ArCH₃). ¹³C{¹H} NMR (CDCl₃): δ 148.39, 138.82, 138.55, 137.50, 136.95, 134.66, 132.86, 131.03, 130.37, 129.85, 128.72, 128.55, 128.01, 124.69, 106.51, 32.52, 21.45, 21.422. Anal. Calcd for C₄₆H₄₅IN₄: C, 70.76; H, 5.81; N, 7.18. Found C, 70.17; H, 5.41; N, 6.97.

NCN-Li-Me₂ (3.17). *Method A:* A 2.5 M hexane solution of *n*-BuLi (0.18 mL, 0.450 mmol, 1.1 equiv) was added to a stirring suspension of **3.9** (0.3188 g, 0.408 mmol, 1.0 equiv) in Et₂O (30 mL). The mixture was stirred for 35 minutes, then the solvent was removed *in vacuo*. The residue was dissolved in C₆H₆ (7.0 mL) and the solution was frozen and lyophilized *in vacuo*. The resulting powder was washed with pentane (3 x 10 mL) and dried *in vacuo* to yield **3.10** (0.1888 g, 0.286 mmol, 70 %) as an off-white powder. Small amounts of an unknown byproduct were observed in the ¹H NMR spectrum. ¹H NMR (C₆D₆, 300 MHz): δ 7.68 (d, ³J_{HH} = 7.0 Hz, 2H, ArH), 7.58 (t, ³J_{HH} =

7.0 Hz, 1H, ArH), 7.12 (s, 4H, ArH), 6.75 (s, 2H, ArH), 6.62 (s, 4H, ArH), 6.53 (s, 4H, ArH), 3.38 (s, 6H, NCH₃), 1.96 (s, 12H, ArCH₃), 1.93 (s, 12H, ArCH₃). *Method B*: A 2.5 M hexane solution of *n*-BuLi (6.4 μ L, 0.0160 mmol, 1.0 equiv) was added to a stirring suspension of **3.8** (10.5 mg, 0.0160 mmol, 1.0 equiv) in Et₂O (1.0 mL), resulting in an immediate color change to dark purple. The mixture was stirred for 30 minutes, then the solvent removed *in vacuo* and the residue was dissolved in C₆D₆ (0.7 mL). ¹H NMR analysis indicated the formation of **3.10** and a large number of impurity peaks in the spectrum baseline.

1,4-bis(1-methyl-4,5-diphenyl-1*H*-imidazol-2-yl)butane-1,4-dione (3.21).

Inside a glovebox, N-methyl-4,5-diphenylimidazole (**3.19**) (0.90 g, 3.84 mmol, 2.1 equiv) was measured into a 100 mL flask, dissolved in dry THF (25 mL), and cooled to near freezing. *n*-BuLi (1.6 M in hexanes, 2.4 mL, 3.84 mmol, 2.1 equiv) was then added *via* syringe and the solution stirred at ambient temperature for 20 minutes. N,N'-dimethoxy-N,N'-dimethylsuccinamide (**3.20**) (0.37 g, 1.83 mmol, 1.0 equiv) was added as a solid and the mixture stirred overnight. The reaction was then quenched with saturated aqueous NH₄Br solution, then the solution was extracted with CH₂Cl₂ and the organics were concentrated to dryness. The solid residue was slurried in acetone (15 mL), then cooled in the freezer. The solid precipitate was collected *via* suction filtration, washed with cold acetone (2 x 5 mL), and dried *in vacuo* to give **3.21** (0.59 g, 1.07 mmol, 59 %) as a yellow powder. ¹H NMR (CDCl₃, 400 MHz): δ 7.47–7.51 (m, 10H, ArH), 7.31–7.34 (m, 4H, ArH), 7.18–7.25 (m, 6H, ArH), 3.80 (s, 6H, NCH₃), 3.77 (s, 4H, C(O)CH₂). ¹³C{¹H} NMR (CDCl₃): δ 192.04, 142.35, 139.13, 134.94, 134.03, 130.84, 129.80,

129.41, 129.29, 128.36, 127.31, 127.13, 33.99, 33.86. MS $[M+Na]^+ = 573$; HRMS calcd for $C_{36}H_{30}N_4NaO_2$ 573.2266, found 573.2249.

2.5-bis(1-methyl-4,5-diphenyl-1*H*-imidazol-2-yl)-1*H*-pyrrole (3.22). In a 15 mL round bottom flask equipped with a reflux condensor open to air, a suspension of **3.25** (0.05 g, 0.09 mmol, 1.0 equiv) and NH_4OAc (0.20 g, 2.6 mmol, 29 equiv) in $AcOH$ (5 mL) was brought to reflux with stirring. After refluxing for 5 hours, the blue mixture was poured into H_2O (30 mL), causing a precipitate to form. The green solid was collected by suction filtration and washed with H_2O . The solid was then extracted through a sintered glass frit with CH_2Cl_2 , then the green filtrate was concentrated to dryness. 1H NMR and MS analysis of the crude mixture indicated the successful formation of **3.22** as the major product. 1H NMR (CD_2Cl_2 , 500 MHz, distinctive resonances): δ 10.60 (br s, 1H, pyrrole-NH), 6.67 (s, 2H, pyrrole-CH), 3.65 (s, 6H, imidazole NCH_3). LCT-MS: $m/z = 532.1$ ($C_{36}H_{29}N_5$).

4,5-bis(3,5-dimethylphenyl)-1*H*-imidazole (3.23). In a 250 mL round bottom flask equipped with a reflux condensor open to air, a suspension of hexamethylenetetramine (1.3 g, 9.3 mmol, 0.3 equiv), 3,3',5,5'-tetramethylbenzil (**3.1**) (7.64 g, 28.7 mmol, 1.0 equiv), and ammonium acetate (18.2 g, 236 mmol, 8.2 equiv) in acetic acid (170 mL) was brought to reflux. After 1 h, the solution was cooled and poured into H_2O (600 mL). The aqueous solution was cooled in an ice bath and slowly neutralized with NH_4OH , resulting in the precipitation of a powder. The powder was collected by suction filtration, washed with copious H_2O and Et_2O (1 x 50 mL, 1 x 30 mL). Upon drying *in*

vacuo, **3.23** (5.08 g, 18.4 mmol, 64 %) was obtained as a cream colored powder. ¹H NMR ((CD₃)₂SO, 500 MHz): δ 12.34 (s, 1H, NH), 7.69 (s, 1H, ArH), 7.14 (s, 2H, ArH), 7.04 (s, 2H, ArH), 6.95 (s, 1H, ArH), 6.82 (s, 1H, ArH), 2.23 (s, 6H, ArCH₃), 2.18 (s, 6H, ArCH₃). MS [M+H]⁺ = 277; HRMS calcd for C₁₉H₂₁N₂ 277.1705, found 277.1705.

4,5-bis(3,5-dimethylphenyl)-N,N-dimethyl-1H-imidazole-1-sulfonamide

(3.24). In a glovebox, **3.23** (1.00 g, 3.64 mmol, 1.0 equiv) and NaH (0.17 g, 7.25 mmol, 2.0 equiv) were measured into a 100 mL flask and suspended in dry THF (50 mL) with stirring. After 1 hour of reaction, the mixture appeared brown. Dimethylsulfamoylchloride (0.43 mL, 4.00 mmol, 1.1 equiv) was added via syringe, causing the solution to turn light red. After stirring overnight, the mixture was quenched with H₂O (25 mL). The organics were extracted with CH₂Cl₂ (20 mL), then the volatiles were removed *in vacuo*. The solid residue was dissolved in a mixture of MeOH (40 mL) and acetone (2 mL), then a solid was precipitated with the addition of H₂O (100 mL). The precipitate was collected *via* suction filtration, washed with H₂O, and dried *in vacuo* to yield **3.29** (0.89 g, 2.32 mmol, 64 %) as an off-white powder. ¹H NMR (CDCl₃, 500 MHz): δ 8.09 (s, 1H, ArH), 7.09 (s, 1H, ArH), 7.07 (s, 2H, ArH), 7.06 (s, 2H, ArH), 6.83 (s, 2H, ArH), 2.45 (s, 6H, N(CH₃)₂), 2.34 (s, 6H, ArCH₃), 2.18 (s, 6H, ArCH₃). ¹³C{¹H} NMR (CDCl₃): δ 140.18, 138.51, 138.20, 137.62, 132.99, 131.15, 129.58, 129.00, 128.91, 126.35, 124.88, 37.10, 21.40, 21.30. MS [M+Na]⁺ = 406; HRMS calcd for C₂₁H₂₅N₃NaO₂S 406.1565, found 406.1561.

NNN-H₃ (3.26). In 50 mL round bottom flask equipped with a reflux condensor open to air, a suspension of 3,6-di-*tert*-butyl-9*H*-carbazole-1,8-dicarbaldehyde (**3.29**) (0.54 g, 1.61 mmol, 1.0 equiv), 3,3',5,5'-tetramethylbenzil (**3.1**) (0.93 g, 3.50 mmol, 2.2 equiv), and NH₄OAc (2.4 g, 31.0 mmol, 19 equiv) in acetic acid (100 mL) was brought to reflux for 5 hours. Upon cooling, the solution was poured into H₂O (200 mL) causing a yellow powder to precipitate. The powder was collected by suction filtration, washed with H₂O (6 x 40 mL), and dried *in vacuo*. ¹H NMR analysis revealed the presence of small impurities. The solid was extracted through a sintered glass frit with Et₂O (30 mL), then the filtrate was concentrated to *ca.* 10 mL in volume, diluted with pentane (10 mL), and cooled to -5 °C. The resulting powder was collected by suction filtration, rinsed with cold pentane, and dried *in vacuo* to afford **3.30** (0.73 g, 0.88 mmol, 55 %) as a yellow powder. ¹H NMR (CDCl₃, 400 MHz): δ 11.87 (s, 1H, carbazole NH), 9.38 (s, 2H, imidazole NH), 8.17 (s, 2H, ArH), 7.70 (s, 2H, ArH), 7.40 (s, 4H, ArH), 7.22 (s, 4H, ArH), 7.00 (s, 2H, ArH), 6.63 (s, 2H, ArH), 2.32 (s, 12H, ArCH₃), 1.99 (s, 12H, ArCH₃), 1.19 (s, 18H, C(CH₃)₃). ¹³C{¹H} NMR (CDCl₃): δ 145.33, 142.02, 138.52, 138.21, 137.30, 136.37, 134.18, 131.72, 129.74, 128.28, 127.05, 126.23, 125.09, 124.27, 119.36, 117.13, 113.01, 35.00, 32.29, 21.39, 21.22. MS [M+Na]⁺ = 828; HRMS calcd for C₅₈H₆₃N₅Na 828.5005, found 828.5037.

3.7.4 Other Reactions

Attempts of **3.1** activation

*N*Mo(*N*Me₂)₃. Solid **3.3** (19.4 mg, 0.031 mmol, 1.0 equiv) was added to a solution of *N*Mo(*N*Me₂)₃ (7.5 mg, 0.031 mmol, 1.0 equiv) in C₆D₆ (1.0 mL) with stirring, causing

an immediate color change from yellow to orange-red. After 1.5 hours, ^1H NMR analysis revealed a large number of resonances that could not be identified. After 5 hours, the ^1H NMR spectrum was no cleaner.

$\text{NMo}(\text{O}^t\text{Bu})_3$. Method A: Solid **3.3** (10.8 mg, 0.017 mmol, 1.2 equiv) and $\text{NMo}(\text{O}^t\text{Bu})_3$ (4.8 mg, 0.015 mmol, 1.0 equiv) were rinsed into a J. young tube with C_6D_6 (1.0 mL). The overlying atmosphere was evacuated for 20 seconds, then the tube was heated in a 95 °C oil bath and the reaction progress monitored by ^1H NMR. 1 hour: a large number of unidentifiable peaks was observed. 6 hours: no improvement was observed. Method B: Solid **3.3** (49.8 mg, 0.080 mmol, 4.9 equiv) and $\text{NMo}(\text{O}^t\text{Bu})_3$ (5.3 mg, 0.016 mmol, 1.0 equiv) were rinsed into a J. young tube with C_6D_6 (1.5 mL). The overlying atmosphere was evacuated for 20 seconds, then the tube was heated in a 95 °C oil bath and the reaction progress monitored by ^1H NMR. 1 hour: $\text{NMo}(\text{O}^t\text{Bu})_3$ was observed, but not HO^tBu . 6 hours: no change was observed. Method C: A solid mixture of **3.3** (20.2 mg, 0.032 mmol, 1.0 equiv) and $\text{NMo}(\text{O}^t\text{Bu})_3$ (10.6 mg, 0.032 mmol, 1.0 equiv) were dissolved in THF (1.0 mL) with stirring. After stirring for 4 hours 30 minutes, no color change was noted. The solution was transferred to a J. Young tube and placed in a 65 °C oil bath. After heating 18 hours, the solution was cooled, the solvent was removed *in vacuo*, and the residue taken up in C_6D_6 (0.8 mL). ^1H NMR analysis indicated that no reaction had occurred.

$\text{Mo}(\text{CO})_6$ Solid **3.3** (9.3 mg, 0.015 mmol, 1.0 equiv) and $\text{Mo}(\text{CO})_6$ (4.1 mg, 0.016 mmol, 1.0 equiv) were measured into a J. Young tube and suspended in C_6D_6 (1.0 mL).

The tube was irradiated with a longwave UV lamp and the reaction progress monitored by ^1H NMR. 1 hour: 1 major NC(H)N environment was observed with a single ArCH₃ resonance, which suggests no coordination to Mo. 18 hours: no change had occurred. ^1H NMR (C₆D₆, 400 MHz): δ 10.1 (v br, 0.2H), 9.18 (v br, 0.2H), 7.83 (br s, 2H, ArH), 7.55 (br s, 4H, ArH), 7.22 (t, 1H, ArH), 7.01 (m, 4H, ArH), 6.70 (s, 4H, ArH), 2.05 (s, 24H, ArCH₃).

Mo(CO)₃(NCEt)₃. Method A: Solid **3.3** (14.8 mg, 0.024 mmol, 1.0 equiv) was added to a solution of Mo(CO)₃(NCEt)₃ (8.3 mg, 0.024 mmol, 1.0 equiv) in C₆D₆ (0.8 mL) with stirring. After stirring 1 hour 30 minutes, ^1H NMR analysis indicated one NC(H)N environment with a single ArCH₃ resonance. Method B: Solid **3.3** (14.0 mg, 0.022 mmol, 1.0 equiv) was added to a solution of Mo(CO)₃(NCEt)₃ (7.8 mg, 0.023 mmol, 1.0 equiv) in THF (1.0 mL) with stirring. After stirring 2 hours 30 minutes, the solvent was removed *in vacuo* and the residue was dissolved in C₆D₆ (0.8 mL). ^1H NMR analysis indicated one NC(H)N environment with a single ArCH₃ resonance.

Ti(NMe₂)₄. Method A: Solid **3.3** (10.2 mg, 0.016 mmol, 1.0 equiv) was added to a stirring solution of Ti(NMe₂)₄ (9.9 mg, 0.044 mmol, 2.7 equiv) in THF (0.8 mL). After stirring for 1 hour, the solvent was removed and the residue dissolved in C₆D₆ (0.7 mL). ^1H NMR analysis indicated a single NC(H)N environment with no imidazole NH signals visible. ^1H NMR (C₆D₆, 300 MHz): δ 8.84 (*pseudo-t*, 1H, C_AH), 8.06 (dd, $^3J_{\text{HH}} = 7.6$ Hz, $^4J_{\text{HH}} = 1.5$ Hz, 2H, ArH), 7.56 (br s, 8H, ArH), 7.38 (t, $^3J_{\text{HH}} = 7.6$ Hz, 1H, ArH), 6.79 (s, 4H, ArH), 3.12 (s, 79H, N(CH₃)₂), 2.80 (s, 30H, N(CH₃)₂), 2.20 (s, 24H, ArCH₃).

Method B: Solid **3.3** (15.7 mg, 0.025 mmol, 1.0 equiv) was added to a stirring solution of Ti(NMe₂)₄ (13.9 mg, 0.062 mmol, 2.5 equiv) in C₆H₆ (0.8 mL). After stirring for 1 hour, the solvent was removed and the residue dissolved in C₆D₆ (0.7 mL). The ¹H NMR spectrum was similar to Method A. Method C: A solution of Ti(NMe₂)₄ (12.3 mg, 0.055 mmol, 3.0 equiv) in C₆D₆ (0.8 mL) was added to a J. Young tube, followed by solid **3.3** (11.3 mg, 0.018 mmol, 1.0 equiv). The reaction was heated in a 70 °C oil bath for 2 hours. ¹H NMR analysis indicated a large number of unidentifiable products had formed.

RuCl₂(PPh₃)₃: Method A: A solid mixture of **3.3** (11.3 mg, 0.018 mmol, 1.0 equiv) and RuCl₂(PPh₃)₃ (17.4 mg, 0.018 mmol, 1.0 equiv) was dissolved in CD₃CN (1.0 mL), then the solution was transferred to a J. Young tube and placed in an 85 °C oil bath. After heating for 3 hours, 2 peaks were visible in the ³¹P NMR spectrum at δ 30.12 (s, 68 %) and -4.52 (s, 32 %, PPh₃). ¹H NMR spectroscopy indicated no activation of N_BH or C_AH with resonances at δ 12.67 (s, 2H, N_BH), 9.72 (s, 1H, C_AH), 2.24 (s, 12H, ArCH₃), 2.17 (s, 12H, ArCH₃). Method B: A solid mixture of **3.3** (7.0 mg, 0.011 mmol, 1.0 equiv), RuCl₂(PPh₃)₃ (10.3 mg, 0.011 mmol, 1.0 equiv), and KO^tBu (3.7 mg, 0.033 mmol, 3.0 equiv) was suspended in THF (1.0 mL), transferred to a J. Young tube, and heated at 70 °C in an oil bath. The reaction was monitored by ³¹P NMR spectroscopy. 11 hours: δ 40.7 (20 %), 35.7 (42 %), 24.83 (5 %), -4.6 (34 %). 21 hours: not much change. The volatiles were removed *in vacuo* and the residue dissolved in CD₂Cl₂. ¹H NMR analysis revealed a large number of very broad peaks. The volatiles were removed *in vacuo* and the residue dissolved in pyridine-*d*₅. ¹H NMR analysis revealed no improvement in the sample clarity. Method C: A solid mixture of **3.3** (6.2 mg, 0.0090

mmol, 1.0 equiv), $\text{RuCl}_2(\text{PPh}_3)_3$ (9.2 mg, 0.0096 mmol, 1.0 equiv), and KO^tBu (9.7 mg, 0.0864 mmol, 9.0 equiv) was suspended in THF (1.0 mL), transferred to a J. Young tube, and heated at 70 °C in an oil bath. The reaction was monitored by ^{31}P NMR spectroscopy. 11 hours: δ 63.0 (d, $^2J_{\text{PP}} = 49.0$ Hz, 31 %), 51.2 (d, $^2J_{\text{PP}} = 43.4$ Hz, 31 %), 24.76 (s, 8 %), -4.62 (s, 13 %), -16.3 (s, 17 %). 21 hours: no significant change was observed.

$[\text{RuCl}_2(p\text{-cymene})]_2$. A solid mixture of **3.3** (21.1 mg, 0.0337 mmol, 1.0 equiv) and $[\text{RuCl}_2(p\text{-cymene})]_2$ (10.2 mg, 0.0167 mmol, 0.5 equiv) was dissolved in CD_3CN (1.0 mL), then the solution was transferred to a J. Young tube and placed in an 85 °C oil bath. After heating for 3 hours, ^1H NMR spectroscopy revealed peaks for $\text{N}_\text{B}\text{H}$ (11.83 ppm) and $\text{C}_\text{A}\text{H}$ (9.18 ppm). No change was observed after 20 hours.

Transmetalation Reactions

$\text{NMo}(\text{O}^t\text{Bu})_3$. Solid **3.6** (8.3 mg, 0.010 mmol, 1.0 equiv) was added to a solution of $\text{NMo}(\text{O}^t\text{Bu})_3$ (3.4 mg, 0.010 mmol, 1.0 equiv) in CD_2Cl_2 (0.8 mL), causing the solution to turn yellow. After stirring 1 hour, ^1H NMR analysis revealed a large number of products. After reacting overnight, no improvement in the product composition was observed. The volatiles were removed *in vacuo* and the residue dissolved in pyridine- d_5 . ^1H NMR analysis indicated $\text{C}_\text{A}\text{H}$ protonation for the major NCN product.

$\text{RuCl}_2(\text{PPh}_3)_3$. Method A: A solid mixture of **3.6** (7.9 mg, 0.0098 mmol, 1.0 equiv) and $\text{RuCl}_2(\text{PPh}_3)_3$ (9.5 mg, 0.0099 mmol, 1.0 equiv) were dissolved in CD_2Cl_2 (0.7

mL). The solution underwent an immediate color change to green-yellow. After stirring 45 minutes, ^{31}P NMR indicated a new peak at δ 62.72 ppm and free PPh_3 in a 2:1 ratio, while ^1H NMR indicated a large number of products. **Method B:** Solid **3.6** (9.5 mg, 0.012 mmol, 1.0 equiv) was added to a solution of $\text{RuCl}_2(\text{PPh}_3)_3$ (11.0 mg, 0.012 mmol, 1.0 equiv) and TBACl (4.1 mg, 0.015 mmol, 1.3 equiv) in CH_2Cl_2 . The solution underwent an immediate color change to green-yellow. ^{31}P NMR spectroscopy revealed a new peak at δ 62.72 ppm and free PPh_3 in a 2:1 ratio. The solvent was removed and the residue taken up in C_6D_6 . ^1H NMR analysis indicated a large number of products. **Method C (861):** Solid **3.6** (28.7 mg, 0.036 mmol, 1.0 equiv), $\text{RuCl}_2(\text{PPh}_3)_3$ (34.1 mg, 0.036 mmol, 1.0 equiv), and PNPCl (21.1 mg, 0.037 mmol, 1.0 equiv) were dissolved in CH_2Cl_2 (2.0 mL) to give a green solution. The solution was stirred 1.5 hours, then 4,4'-di-*t*-butyl-2,2'-bipyridyl (9.6 mg, 0.036 mmol, 1.0 equiv) was added as a solid, causing the solution to turn red-brown. After 20 min, ^{31}P NMR analysis indicated the original product at δ 62.8 ppm (32 %) and a small new peak at δ 25.7 ppm (6 %). After 50 min, the peak at 62.8 ppm decreased intensity (22 %) and the peak at 25.7 ppm was larger in intensity (14 %). **Control reaction:** Solid 4,4'-di-*t*-butyl-2,2'-bipyridyl (3.5 mg, 0.013 mmol, 1.0 equiv) was added to a solution of $\text{RuCl}_2(\text{PPh}_3)_3$ (12.6 mg, 0.013 mmol, 1.0 equiv) in CH_2Cl_2 (0.8 mL), resulting in an immediate color change to dark red-orange. ^{31}P NMR spectroscopy revealed a peak at δ 25.6 ppm in a 2:1 ratio with free PPh_3 .

$[\text{RuI}_2(\text{PPh}_3)_2]_n$. Solid **3.6** (12.8 mg, 0.016 mmol, 1.0 equiv) was added to a suspension of $[\text{RuI}_2(\text{PPh}_3)_2]_n$ (14.2 mg, 0.016 mmol, 1.0 equiv) in THF (0.6 mL). The mixture was stirred for 50 minutes, then transferred to a J. Young Tube and placed in a

60 °C oil bath. After 25 minutes, ^{31}P NMR spectroscopy revealed peaks at δ 69.3 (s, 36 %), 58.1 (s, 54 %), and -4.6 (s, 10 %). The mixture was heated at 60 °C overnight, then ^{31}P NMR analysis revealed a broad peak at δ 58.23 ppm that accounted for 83 % of the total signal intensity in the spectrum. The solvent was removed and the residue taken up in CD_2Cl_2 (0.8 mL). The ^{31}P NMR spectrum was unchanged, while ^1H NMR analysis revealed $\text{NC}(\text{H})\text{N}$ as the major NCN product (δ 8.87, $\text{C}_\text{A}\text{H}$).

[Ru(cod)Cl₂]_n: Solid $[\text{Ru}(\text{cod})\text{Cl}_2]_n$ (3.1 mg, 0.011 mmol, 1.0 equiv) was added to a solution of **3.6** (9.3 mg, 0.012 mmol, 1.0 equiv) in CD_2Cl_2 (0.7 mL). The mixture was stirred and slowly changed color to a darker shade of brown. After 20 hours, a large number of broad resonances were observed in the ^1H NMR spectrum. The volatiles were removed *in vacuo* and the residue dissolved in pyridine-*d*₅. ^1H NMR analysis indicated the formation of multiple unidentifiable products.

Tri-lithiation reactions

General procedure. In a glovebox, solvent (1 mL) was added to solid NCN-X-H_2 (**3.8**, **3.11**) and the mixture was frozen in a cold well. Immediately upon thawing, *n*-BuLi (1.6M in hexane, 3.0 equiv) was added to the reaction mixture with vigorous stirring at ambient temperature. After 15 minutes (Et_2O) or 5 minutes (THF), the solution was quenched with D_2O outside of the glovebox. The solution was concentrated and the residue was analyzed by ^1H NMR spectroscopy. In all cases the clean formation of **3.12.H(D)** was observed, with the % H incorporation determined by integration of $\text{C}_\text{A}\text{H}$ relative to ArCH_3 . ^1H NMR ($(\text{CD}_3)_2\text{SO}$, 400 MHz, **3.12.H(D)**): δ 8.67 (s, $\text{C}_\text{A}\text{H}$), 7.86 (d,

$^3J_{\text{HH}} = 6.8$ Hz, 2H, ArH), 7.29 (t, $^3J_{\text{HH}} = 6.8$ Hz, 1H, ArH), 7.21 (s, 8H, ArH), 6.77 (s, 4H, ArH), 2.21 (s, 24H, ArCH₃).

3.8: *In Et₂O:* Following the general procedure with **3.8** (8.4 mg, 0.012 mmol, 1.0 equiv) and *n*-BuLi (23.0 μL , 0.037 mmol, 3.1 equiv). 24 % H incorporation was observed. *In THF:* Following the general procedure with **3.8** (7.7 mg, 0.011 mmol, 1.0 equiv) and *n*-BuLi (21.0 μL , 0.034 mmol, 3.1 equiv). 36 % H incorporation was observed.

3.11: *In Et₂O:* Following the general procedure with **3.11** (8.4 mg, 0.011 mmol, 1.0 equiv) and *n*-BuLi (22.0 μL , 0.035 mmol, 3.1 equiv). 68 % H incorporation was observed. *In THF:* Following the general procedure with **3.11** (11.2 mg, 0.015 mmol, 1.0 equiv) and *n*-BuLi (29.0 μL , 0.046 mmol, 3.1 equiv). 97 % H incorporation was observed.

Tri-magnesium reactions

Formation of 3.14: Solid **3.11** (13.4 mg, 0.018 mmol, 1.0 equiv) was measured into a J. Young tube and dissolved in THF-*d*₈ (0.6 mL). The sample was heated slightly to dissolve **3.11**, then an initial ¹H NMR spectrum was obtained. A 3.0 M solution of EtMgBr in Et₂O (11.8 μL , 0.035 mmol, 2.0 equiv) was added *via* syringe, causing the solution to turn yellow. ¹H NMR analysis indicated the clean formation of **3.13**. Additional EtMgBr (5.9 μL , 0.018 mmol, 1.0 equiv) was added to the THF-*d*₈ solution *via* syringe. ¹H NMR analysis indicated no reaction had occurred. The sample was

heated in a 55 °C oil bath for 30 minutes, then cooled. ^1H NMR analysis revealed a large number of unidentifiable peaks (presumably **3.14**). The solution was quenched with H_2O (2 drops), at which point ^1H NMR spectroscopy revealed the formation of **3.12.H**. ^1H NMR ($\text{THF-}d_8$, 300 MHz, **3.11**): δ 11.64 (s, 2H, NH), 7.61 (d, $^3J_{\text{HH}} = 6.8$ Hz, 2H, ArH), 7.51 (t, $^3J_{\text{HH}} = 6.8$ Hz, 1H, ArH), 7.39 (s, 4H, ArH), 7.21 (s, 4H, ArH), 6.95 (s, 2H, ArH), 2.29 (s, 12H, ArCH_3), 2.23 (s, 12H, ArCH_3). ^1H NMR ($\text{THF-}d_8$, 300 MHz, **3.13**): δ 7.57 (d, $^3J_{\text{HH}} = 7.3$ Hz, 2H, ArH), 7.42 (t, $^3J_{\text{HH}} = 7.3$ Hz, 1H, ArH), 7.32 (s, 4H, ArH), 7.27 (s, 4H, ArH), 6.87 (s, 2H, ArH), 6.62 (s, 2H, ArH), 2.33 (s, 12H, ArCH_3), 2.14 (s, 12H, ArCH_3). ^1H NMR ($\text{THF-}d_8$, 300 MHz, **3.12.H**): δ 8.79 (*pseudo*-t, 1H, ArH), 8.06 (dd, $^3J_{\text{HH}} = 7.7$ Hz, $^4J_{\text{HH}} = 1.6$ Hz, 2H, ArH), 7.48 (t, $^3J_{\text{HH}} = 7.7$ Hz, 1H, ArH), 7.28 (s, 8H, ArH), 6.88 (s, 4H, ArH), 2.25 (s, 12H, ArCH_3).

Reaction between 3.14 and $\text{RuCl}_2(\text{PPh}_3)_3$: Solid **3.11** (11.8 mg, 0.016 mmol, 1.0 equiv) was measured into a J. Young tube and dissolved in THF (0.7 mL). A 3.0 M solution of EtMgBr in Et_2O (11.8 μL , 0.035 mmol, 2.0 equiv) was added *via* syringe and the sample placed in a 60 °C oil bath for 30 minutes. Solid $\text{RuCl}_2(\text{PPh}_3)_3$ (14.2 mg, 0.015 mmol, 0.9 equiv) was rinsed into the J. Young tube with THF (0.3 mL), causing the solution to immediately turn red-purple in color. After 25 minutes, ^{31}P NMR spectroscopy revealed 2 broad peaks at δ 60 ppm and 40 ppm along with free PPh_3 . After reacting overnight, a brown precipitate had formed in the reaction tube. The solvent was removed *in vacuo* and the residue dissolved in CD_2Cl_2 (0.7 mL). ^{31}P NMR spectroscopy revealed peaks at δ 58.4 ppm and -5.1 ppm. ^1H NMR analysis indicated the formation of multiple unidentifiable products. The volatiles were removed *in vacuo* and the residue

dissolved in pyridine- d_5 . No improvement was noted in the ^1H NMR spectrum, and the ^{31}P NMR spectrum showed peaks at δ 55.2, 54.4, 49.3, 36.8, 30.1, and -5.1 ppm.

Reaction between 3.14 and $\text{NMo}(\text{O}^t\text{Bu})_3$: Solid **3.11** (10.9 mg, 0.015 mmol, 1.0 equiv) was measured into a J. Young tube and dissolved in THF- d_8 (0.6 mL). A 1.0 M solution of EtMgBr in THF (44.0 μL , 0.044 mmol, 3.0 equiv) was added *via* syringe, then the sample was heated in a 60 $^\circ\text{C}$ oil bath for 2 hours. ^1H NMR spectroscopy indicated a large number of peaks presumably corresponding to **3.14**. Solid $\text{NMo}(\text{O}^t\text{Bu})_3$ (5.1 mg, 0.016 mmol, 1.0 equiv) was rinsed into the J. Young tube with THF- d_8 (0.6 mL) and the reaction progress was monitored by ^1H NMR spectroscopy. 20 minutes (rt): no apparent reaction. 1 h 10 min (at 60 $^\circ\text{C}$): no apparent reaction. 10 d (rt): no apparent reaction.

Reaction between 3.14 and $\text{NMo}(\text{OCMe}_2\text{CF}_3)_3$: Solid **3.11** (14.2 mg, 0.019 mmol, 1.0 equiv) was measured into a J. Young tube and dissolved in THF- d_8 (0.6 mL). A 1.0 M solution of EtMgBr in THF (57.0 μL , 0.057 mmol, 3.0 equiv) was added *via* syringe, then the sample was heated in a 60 $^\circ\text{C}$ oil bath for 2 hours. ^1H NMR spectroscopy indicated a large number of peaks presumably corresponding to **3.14**. Solid $\text{NMo}(\text{OCMe}_2\text{CF}_3)_3$ (9.4 mg, 0.019 mmol, 1.0 equiv) was rinsed into the J. Young tube with THF- d_8 (0.6 mL) and the reaction progress was monitored by ^1H NMR spectroscopy. 20 minutes (rt): no apparent reaction. 1 h 10 min (at 60 $^\circ\text{C}$): no apparent reaction. 10 d (rt): no apparent reaction.

Reaction between 3.14 and EtCMoCl₃(DME): Solid **3.11** (12.3 mg, 0.016 mmol, 1.0 equiv) was measured into a J. Young tube and dissolved in THF-*d*₈ (0.6 mL). A 1.0 M solution of EtMgBr in THF (49.0 μL, 0.049 mmol, 3.0 equiv) was added *via* syringe, then the sample was heated in a 60 °C oil bath for 2 hours. ¹H NMR spectroscopy indicated a large number of peaks presumably corresponding to **3.14**. Solid EtCMoCl₃(DME) (5.3 mg, 0.016 mmol, 1.0 equiv) was rinsed into the J. Young tube with THF-*d*₈ (0.6 mL), causing the yellow solution to change color to purple. The reaction progress was monitored by ¹H NMR spectroscopy. 20 minutes (rt): no apparent reaction. 1 h 10 min (at 60 °C): no apparent reaction. 10 d (rt): no apparent reaction.

Reaction of 3.17 with Ru substrates

RuCl₂(PPh₃)₃: Method A: THF (1.0 mL) was frozen in a cold well, then immediately upon thawing was added to a solid mixture of **3.17** (5.4 mg, 0.0082 mmol, 1.0 equiv) and RuCl₂(PPh₃)₃ (7.8 mg, 0.0081 mmol, 1.0 equiv) with stirring. The solution was stirred inside a cold well for 30 minutes, then the volatiles were removed in vacuum and the residue dissolved in C₆D₆ (0.7 mL). A ³¹P NMR spectrum showed several signals δ 53.03 (s), 50.66 (s), 50.33 (s), 49.75 (s), 47.11 (s), -4.80 (s, PPh₃). Method B: A solid mixture of **3.17** (6.3 mg, 0.0095 mmol, 1.0 equiv) and RuCl₂(PPh₃)₃ (9.4 mg, 0.0098 mmol, 1.0 equiv) was suspended in Et₂O (1.0 mL) with vigorous stirring. The mixture was stirred overnight, then the volatiles were removed *in vacuo* and the residue was dissolved in C₆D₆ (0.7 mL). ¹H NMR analysis indicated **3.15** as the only NCN product. Method C: A solid mixture of **3.17** (7.9 mg, 0.012 mmol, 1.0 equiv) and RuCl₂(PPh₃)₃ (10.9 mg, 0.011 mmol, 1.0 equiv) was dissolved in C₆D₆ (1.0 mL) with

stirring. After stirring for 1 hour, ^1H NMR analysis indicated a 9.6 : 1 ratio of **3.17** : **3.15**. The solution was transferred to a J. Young tube and heated in a 70 °C oil bath. After heating for 3 hours, ^1H NMR analysis indicated a 2.8 : 1 ratio of **3.17** : **3.15**. Only $\text{RuCl}_2(\text{PPh}_3)_3$ (δ 41 ppm, br s) and PPh_3 (δ -4.80 ppm, s) were observed in the ^{31}P NMR spectrum.

[RuCl₂(p-cymene)]₂: A solid mixture of **3.17** (10.9 mg, 0.017 mmol, 2.0 equiv) and *[RuCl₂(p-cymene)]₂* (5.1 mg, 0.0083 mmol, 1.0 equiv) was dissolved in C_6D_6 (1.0 mL) with stirring. After stirring 2.5 hours, ^1H NMR analysis revealed mostly **3.17** with a variety of other products visible.

Ru(C-p-C₆H₄Me)(PCy₃)₂Cl: A solid mixture of **3.17** (4.7 mg, 0.0071 mmol, 1.1 equiv) and *Ru(C-p-C₆H₄Me)(PCy₃)₂Cl* (5.6 mg, 0.0067 mmol, 1.0 equiv) was dissolved in C_6D_6 (0.7 mL) and transferred to a J. Young tube. The solution was heated in a 65 °C oil bath and the reaction progress monitored by ^1H and ^{31}P NMR spectroscopy. 13 hours: ^1H NMR spectroscopy indicated no reaction of **3.17**, ^{31}P NMR spectroscopy showed peaks at δ 82.13 ppm (s, 4 %), 42.42 (s, SM, 44 %), 40.46 (s, 38 %), and 10.51 (s, PCy₃, 14 %). 24 hours: no significant change was observed.

Ru(CS)(PCy₃)₂Cl₂: A solid mixture of **3.17** (7.3 mg, 0.011 mmol, 1.0 equiv) and *Ru(CS)(PCy₃)₂Cl₂* (8.4 mg, 0.011 mmol, 1.0 equiv) was dissolved in C_6H_6 (1.0 mL) with stirring. The reaction progress was monitored by ^{31}P NMR spectroscopy. 24 hours: Peaks at δ 31.1 (s), 30.8 (s), 30.3 (s). 60 hours: No change was observed.

Attempted condensation of **3.1** with **3.18**

In a 100 mL round bottom flask equipped with a reflux condenser open to air, a suspension of **3.18** (0.10 g, 0.81 mmol, 1.0 equiv), **3.1** (0.46 g, 1.73 mmol, 2.1 equiv), and NH₄OAc (1.3 g, 17 mmol, 21 equiv) in AcOH (55 mL) was brought to reflux. The solution changed color to dark purple-red, then to black. After 4 h 30 min, the solution was cooled and poured into H₂O (150 mL), causing a dark precipitate to form. The solid was collected by suction filtration, washed with into H₂O (4 x 100 mL), and dried *in vacuo* to yield 0.46 g of a grey solid. Benzil **3.1** was the only compound observed in the ¹H NMR spectrum of the crude product.

Attempted acylation of **3.24**

General procedure: *n*-BuLi (1.6 M in hexanes, 2.0 equiv) was added *via* syringe to a -35 °C solution of **3.24** (2.0 equiv) in THF (1.0 mL) to give an orange solution. After stirring the solution for 20 minutes, XC(O)CH₂CH₂C(O)X (1.0 equiv) was added to the mixture, which was then stirred overnight. The reaction was quenched with H₂O, then the solution was concentrated to dryness and the residue analyzed by ¹H NMR spectroscopy.

X = N(OMe)Me: Following the general procedure with **3.24** (11.1 mg, 0.029 mmol), *n*-BuLi (18.1 μL, 0.029 mmol), and **3.20** (2.9 mg, 0.014 mmol). The only observed imidazole-containing product was **3.24**.

X = OMe: Following the general procedure with **3.24** (7.6 mg, 0.020 mmol), *n*-BuLi (12.4 μ L, 0.020 mmol), and MeOC(O)CH₂CH₂C(O)OMe (1.3 μ L, 0.001 mmol). The only observed imidazole-containing product was **3.24**.

X = Cl: Following the general procedure with **3.24** (35.6 mg, 0.093 mmol), *n*-BuLi (58.0 μ L, 0.093 mmol), and ClC(O)CH₂CH₂C(O)Cl (5.1 μ L, 0.046 mmol). The only observed imidazole-containing product was **3.24**.

Control reaction: *n*-BuLi (1.6 M in hexanes, 15.0 μ L 1.0 equiv) was added *via* syringe to a -35 °C solution of **3.24** (9.1 mg, 0.024 mmol, 1.0 equiv) in THF (1.0 mL) to give an orange solution. After stirring overnight, the orange solution was quenched with D₂O, resulting in a color change to yellow. ¹H NMR analysis indicated recovery of **3.24** with an integration of 0.6H for the imidazole CH resonance.

Attempted installation of a dimethylaminomethyl protecting group on 3.23

In a 100 mL round bottom flask open to the air, a solid mixture of **3.23** (1.50 g, 5.43 mmol, 1.0 equiv) and dimethylamine hydrochloride (0.45 g, 5.52 mmol, 1.0 equiv) was suspended in H₂O (20 mL) and concentrated HCl (15 mL). Compound **3.23** aggregated into clumps of solid on top of the aqueous solution. Isopropanol (20 mL) was added, resulting in the dissolution of **3.23**. Aqueous formaldehyde (37 % w/w, 0.46 g, 5.67 mmol) was added to the reaction solution. After stirring overnight, the solution was made strongly alkaline through the addition of 20 % KOH_(aq) solution, resulting in the precipitation of a solid. The mixture was extracted with CHCl₃ (2 x 100 mL) and the

organics were washed with H₂O (100 mL) and concentrated to dryness. ¹H NMR analysis of the residue indicated **3.23** as the only imidazole component.

3.8 References

1. Geyer, A. M.; Wiedner, E. S.; Gary, J. B.; Gdula, R. L.; Kuhlmann, N. C.; Johnson, M. J. A.; Dunietz, B. D.; Kampf, J. W., *J. Am. Chem. Soc.* **2008**, *130*, 8984-8999.
2. Caskey, S. R.; Stewart, M. H.; Ahn, Y. J.; Johnson, M. J. A.; Rowsell, J. L. C.; Kampf, J. W., *Organometallics* **2007**, *26*, 1912-1923.
3. Caskey, S. R. Exploration of Ruthenium Carbon Multiple Bond Complexes: Carbenes, Carbynes, and Carbides. Ph.D., University of Michigan, Ann Arbor, 2007.
4. Krieg, B.; Manecke, G., *Makromol. Chem.* **1967**, *108*, 210-217.
5. Lee, D.; Sarshar, S.; Corey, E., *Tetrahedron: Asymmetry* **1995**, *6*, 3-6.
6. Albrecht, M.; van Koten, G., *Angew. Chem., Int. Ed.* **2001**, *40*, 3750-3781.
7. Rubio, R. J.; Andavan, G. T. S.; Bauer, E. B.; Hollis, T. K.; Cho, J.; Tham, F. S.; Donnadieu, B., *J. Organomet. Chem.* **2005**, *690*, 5353-5364.
8. Koller, J.; Sarkar, S.; Abboud, K. A.; Veige, A. S., *Organometallics* **2007**, *26*, 5438-5441.
9. Harvey, R. G.; Dai, Q.; Ran, C.; Penning, T. M., *J. Org. Chem.* **2004**, *69*, 2024-2032.
10. Krizan, T. D.; Martin, J. C., *J. Org. Chem.* **1982**, *47*, 2681-2682.
11. Bailey, W. F.; Patricia, J. J., *J. Organomet. Chem.* **1988**, *352*, 1-46.
12. Caskey, S. R.; Stewart, M. H.; Ahn, Y. J.; Johnson, M. J. A.; Kampf, J. W., *Organometallics* **2005**, *24*, 6074-6076.
13. Caskey, S. R.; Stewart, M. H.; Johnson, M. J. A.; Kampf, J. W., *Angew. Chem. Int. Ed.* **2006**, *45*, 7422-7424.
14. Caskey, S. R.; Stewart, M. H.; Kivela, J. E.; Sootsman, J. R.; Johnson, M. J. A.; Kampf, J. W., *J. Am. Chem. Soc.* **2005**, *127*, 16750-16751.
15. Gary, J. B.; Buda, C.; Johnson, M. J. A.; Dunietz, B. D., *Organometallics* **2008**, *27*, 814-826.
16. Stewart, M. H.; Johnson, M. J. A.; Kampf, J. W., *Organometallics* **2007**, *26*, 5102-5110.
17. Kozaki, M.; Isoyama, A.; Akita, K.; Okada, K., *Org. Lett.* **2004**, *7*, 115-118.
18. Miller, R.; Olsson, K., *Acta Chem. Scand. B* **1981**, *35*, 303-310.
19. Amarnath, V.; Anthony, D. C.; Amarnath, K.; Valentine, W. M.; Wetterau, L. A.; Graham, D. G., *J. Org. Chem.* **1991**, *56*, 6924-6931.
20. LaRonde, F. J.; Brook, M. A., *Inorg. Chim. Acta* **1999**, *296*, 208-221.
21. Grimmet, M. R., *Imidazole and Benzimidazole Synthesis*. Academic Press: London, 1997; p 265.
22. Harding, M.; Hodgson, R.; Nelson, A., *J. Chem. Soc., Perkin Trans. 1* **2002**, 2403-2413.
23. Katritzky, A. R.; Rewcastle, G. W.; Fan, W. Q., *J. Org. Chem.* **1988**, *53*, 5685-5689.
24. Gibson, V. C.; Spitzmesser, S. K.; White, A. J. P.; Williams, A. F., *Dalton Trans.* **2003**, 2718-2727.
25. Pangborn, A. B.; Giardello, M. A.; Grubbs, R. H.; Rosen, R. K.; Timmers, F. J., *Organometallics* **1996**, *15*, 1518-1520.
26. Bradley, D. C.; Thomas, I. M., *J. Chem. Soc.* **1960**, 3857 - 3861.
27. Chan, D. M. T.; Chisholm, M. H.; Folting, K.; Huffman, J. C.; Marchant, N. S., *Inorg. Chem.* **1986**, *25*, 4170-4174.

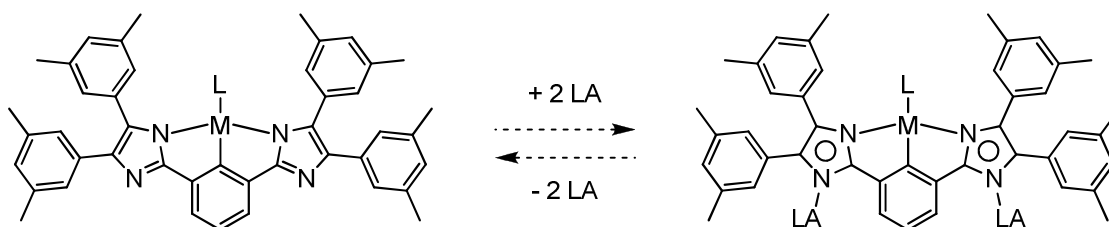
28. Gdula, R. L. Design and Synthesis of Highly Active Group 6 Metal Catalysts for use in Triple-Bond Metathesis. University of Michigan, Ann Arbor, 2006.
29. Geyer, A. M. Development and Investigation of $\text{NW}(\text{OR})_3$, $\text{NMo}(\text{OR})_3$, and $\text{Mo}_2(\text{OR})_6$ Complexes for Triple-Bond Metathesis. University of Michigan, Ann Arbor, 2009.
30. Kubas, G. J.; Van der Sluys, L. S., *Inorg. Synth.* **1990**, 28, 29-33.
31. Cenini, S.; Fusi, A.; Capparella, G., *J. Inorg. Nucl. Chem.* **1971**, 33, 3576-3579.
32. Hodson, E.; Simpson, S. J., *Polyhedron* **2004**, 23, 2695-2707.
33. Stewart, M. H. Synthesis and Reactivity of Terminal Carbide Complexes Prepared by Chalcogen Atom Transfer. Ph.D., University of Michigan, Ann Arbor, 2007.
34. Doi, T.; Nagamiya, H.; Kokubo, M.; Hirabayashi, K.; Takahashi, T., *Tetrahedron* **2002**, 58, 2957-2963.
35. Hoogervorst, W. J.; Goubitz, K.; Fraanje, J.; Lutz, M.; Spek, A. L.; Ernsting, J. M.; Elsevier, C. J., *Organometallics* **2004**, 23, 4550-4563.

Chapter 4:

Synthesis and Theoretical Investigations of Zr Complexes Containing a Charge-Versatile XXX Pincer Ligand

4.1 Introduction

In Chapter 3, the synthesis of new XXX pincer ligands was demonstrated. These formally XXX ligands possess nonbonding peripheral nitrogen atoms that are available for interaction with Lewis acids as depicted in Scheme 4.1. This mode of interaction is rare and opens up the possibility for charge and electron donor strength tuning as previously seen in Chapter 1.



Scheme 4.1. Interaction of XXX ligand with Lewis acids (LA).

When Lewis acid-base adducts of *N*-methylimidazole are formed (acid = BH_3 , BF_3 , CH_3^+), the ^1H and $^{13}\text{C}\{^1\text{H}\}$ NMR resonances for the *N*-methyl group are shifted downfield from the parent *N*-methylimidazole.¹ The degree of *N*-methyl group deshielding correlates with the group electronegativity² of the free Lewis acid, which suggests that stronger LA's result in a weaker N-C bond. A similar interaction with the

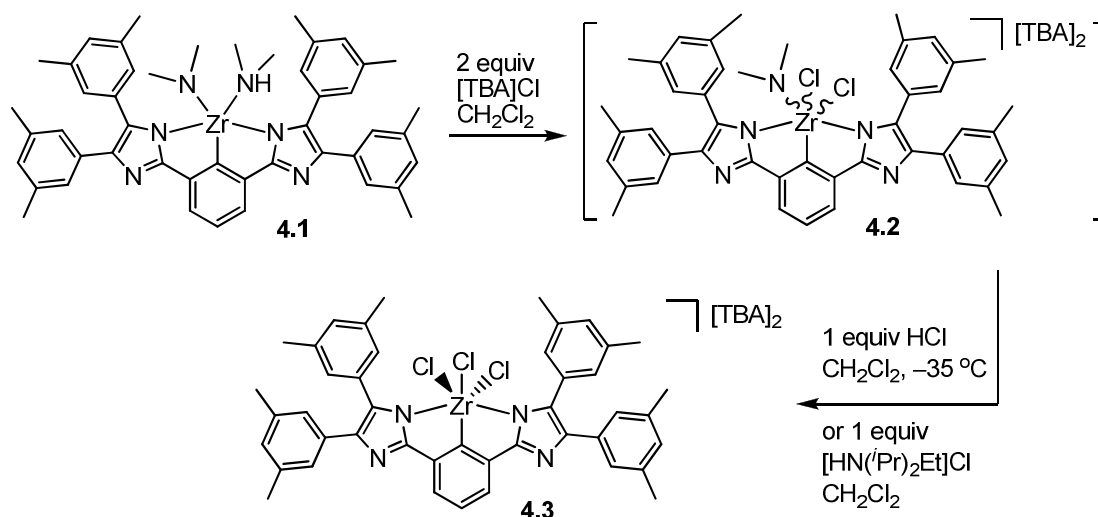
current XXX pincer ligands could allow for tuning of the electron donor strength (Scheme 4.1), with more electronegative LA's leading to a decrease in pincer electron donor strength.

The goal of Chapter 4 is to explore the scope of Lewis acids that can react in a manner similar to that shown in Scheme 4.1. Of particular interest are Lewis acids that can be selectively introduced to and removed from the remote N atom sites under mild conditions. Such reversibility could eventually serve as an “on/off” switch for catalytic systems. Finally, the effect of the Lewis acid identity on the donor strength will be investigated, as a greater range of accessible electron donor strengths could lead to a wider range of molecular reactivity.

4.2 Ancillary Ligand Substitution

Zr(XXX)(NMe₂)(NHMe₂) (**4.1**) proved a useful entry point into a study of Lewis acid interaction with the XXX pincer ligand (Scheme 4.2). The monodentate ancillary ligands first needed to be replaced, as the NHMe₂ and –NMe₂ ligands could also react with incoming Lewis acids. Addition of tetra-*n*-butylammonium chloride ([TBA]Cl) to a suspension of **4.1** in CH₂Cl₂ led to rapid dissolution, presumably forming [TBA]₂[Zr(XXX)(NMe₂)Cl₂] (**4.2**) (Scheme 4.2). The ¹H NMR spectrum of **4.2** was not clear, likely due to the existence of multiple isomers. Treatment of *in situ* generated **4.2** with either HCl or [HN(ⁱPr)₂Et]Cl yielded [TBA]₂[Zr(XXX)Cl₃] (**4.3**) as a bright orange solid which could be isolated in 86 % yield via crystallization from CH₂Cl₂ / Et₂O. The pincer ligand in **4.3** remains bound in an XXX fashion, as indicated by the arylide *ipso*-C ¹³C{¹H} NMR chemical shift of δ 190.49 ppm in CD₂Cl₂. Other chloride sources such as

[PNP]Cl, [TMA]Cl, and [PPh₄]Cl displayed the same reactivity as [TBA]Cl, but the corresponding analogues of **4.3** did not crystallize readily, thus making purification difficult. Therefore, **4.3** was the only complex isolated for further investigation.



Scheme 4.2. Ancillary ligand substitution of **4.1**.

X-ray quality crystals of **4.3** were grown from a CH₂Cl₂ solution at -35 °C. Single-crystal X-ray diffraction analysis revealed that **4.3** crystallizes in the monoclinic space group C2/c and confirmed the tridentate nature of the pincer ligand. As indicated in Figure 4.1, dianionic **4.3** is monomeric in the solid state and possesses a *pseudo*-octahedral geometry with a N-Zr-C bond angle of 71.38(9)°. The two halves of the molecule are related by a crystallographic two-fold rotation axis coincident with the Zr1-Cl2 bond. The solid-state structure displays Zr-C and Zr-N distances of 2.229(6) and 2.280(3) Å, respectively.

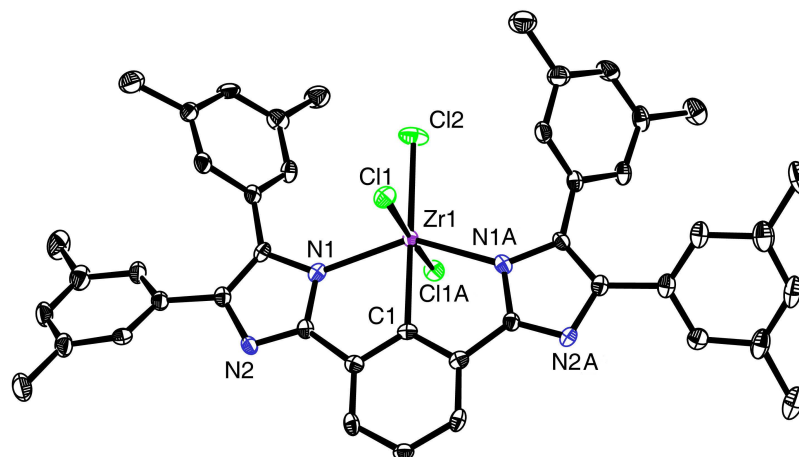
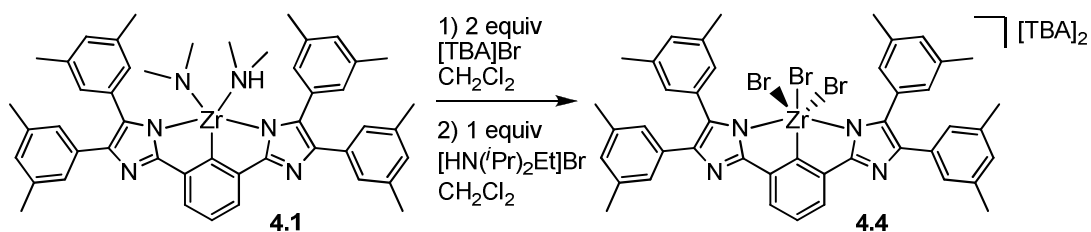


Figure 4.1. 50 % thermal ellipsoid plot of the molecular anion of **4.3**. The hydrogen atoms are omitted for clarity. Selected bond lengths (Å) and angles (deg): Zr1-C1, 2.229(6); Zr1-N1, 2.280(3); Zr1-Cl1, 2.4530(11); Zr1-Cl2, 2.5139(18); C1-Zr1-N1, 71.38(9); C1-Zr1-Cl1, 91.78(3); N1-Zr1-Cl2, 108.62(9); N1-Zr1-Cl1, 91.14(9); Cl1-Zr1-Cl2, 88.22(3). Full XRD data can be found in Appendix 3.

The NHMe_2 ligand of **4.1** could also be displaced through the addition of 2 equiv of tetra-*n*-butylammonium bromide; subsequent treatment with 1 equiv of $[\text{HN}(\text{}^i\text{Pr})_2\text{Et}]\text{Br}$ led to the formation of $[\text{TBA}]_2[\text{Zr}(\text{XXX})\text{Br}_3]$ (**4.4**) (Scheme 4.3). Two crystallizations of the crude reaction mixture allowed for the isolation of **4.4** as a deep red solid in 32 % yield. The ^1H NMR spectrum of **4.4** is similar to **4.3**, but reveals the presence of a small byproduct that is not removed upon crystallization. As the $[\text{ZrBr}_3]^+$ fragment is more acidic than $[\text{ZrCl}_3]^+$, the XXX pincer of **4.4** is expected to be a stronger electron donor than in **4.3**. Accordingly, the arylide *ipso*-C of **4.4** is observed at δ 191.68 ppm in the $^{13}\text{C}\{^1\text{H}\}$ NMR spectrum, which is slightly downfield from that observed for **4.3**.



Scheme 4.3. Synthesis of **4.4**.

X-ray quality crystals of **4.4** were grown from a CH_2Cl_2 solution at $-35\text{ }^\circ\text{C}$. Single-crystal X-ray diffraction analysis revealed that **4.4** crystallizes in the monoclinic space group $C2/c$ with a crystallographic two-fold rotation axis coincident along the Zr-Br2 axis (Figure 4.2). The Zr-C and Zr-N distances of 2.239(4) and 2.278(3) Å are not statistically different from the corresponding distances in the solid state structure of **4.3**.

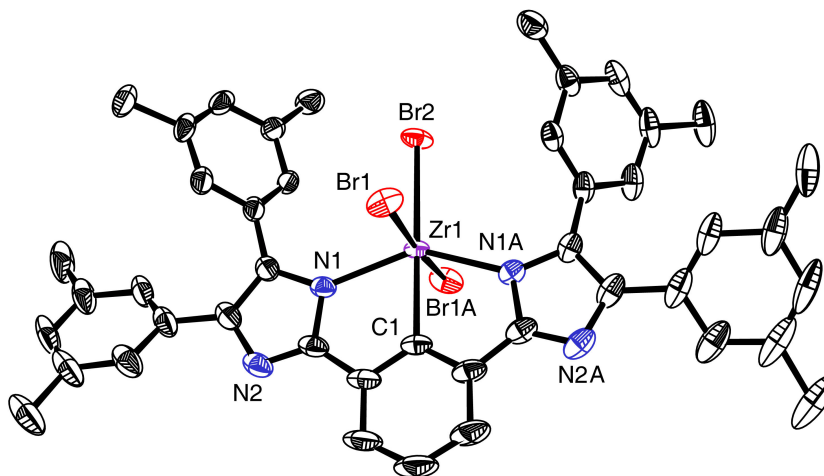
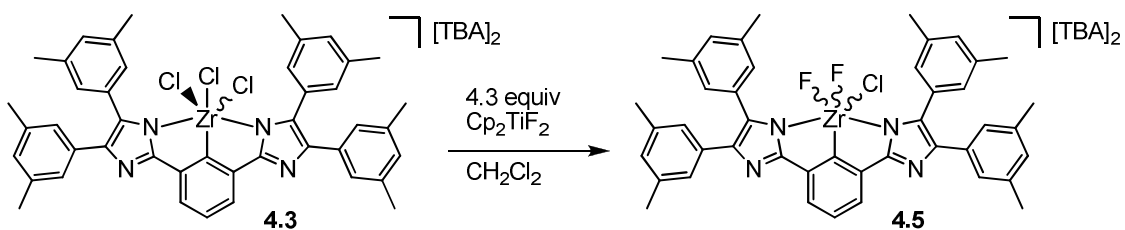


Figure 4.2. 50 % thermal ellipsoid plot of the molecular anion of **4.4**. The hydrogen atoms are omitted for clarity. Selected bond lengths (Å) and angles (deg): Zr1-C1, 2.239(4); Zr1-N1, 2.278(3); Zr1-Br1, 2.6007(4); Zr1-Br2, 2.6789(6); C1-Zr1-N1, 71.59(7); C1-Zr1-Br1, 93.341(12); N1-Zr1-Br2, 108.41(7); N1-Zr1-Br1, 89.46(7); Br1-Zr1-Br2, 86.569(12). Full XRD data can be found in Appendix 4.

Unlike chloride and bromide, iodide ion was unable to displace the NHMe_2 ligand from **4.1**, and so a triiodide complex could not be formed using $[\text{TBA}]\text{I}$ and $[\text{HN}(\text{iPr})_2\text{Et}]\text{I}$. No attempts were made at direct fluoride substitution with **4.1**, as the fluoride ion is notoriously hygroscopic. Therefore, a trifluoride complex was targeted via halide metathesis reactions with **4.3**. The reagents AgPF_6 , AgBF_4 , $[\text{TBA}][\text{PF}_6]$, and Ph_3SnF were all screened against **4.3** for halide metathesis, but led to either no reaction or decomposition of the reaction mixture. Ultimately treatment of **4.3** with 4.3 equiv of Cp_2TiF_2 resulted in the formation of $[\text{TBA}]_2[\text{Zr}(\text{XXX})\text{F}_2\text{Cl}]$ (**4.5**) as shown in Scheme 4.4. In order to isolate pure **4.5**, the crude product must first be washed with THF to remove a majority of the more soluble Ti-containing byproducts. Subsequent addition of THF to a CH_2Cl_2 solution of the remaining product precipitates **4.5** as a white powder in 48 % yield. Interestingly, use of an excess of Cp_2TiF_2 does not lead to formation of a trifluoride species.



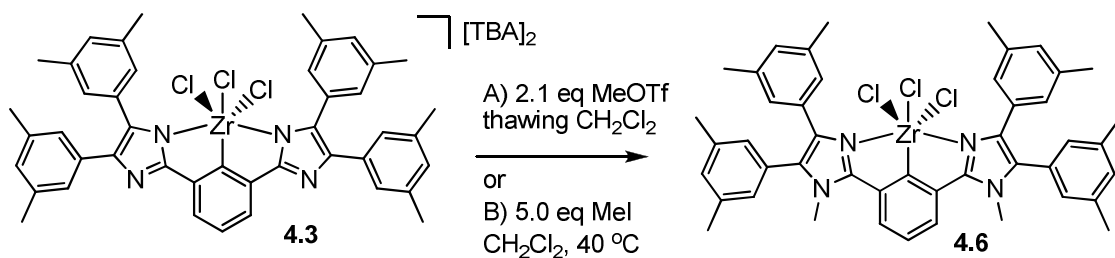
Scheme 4.4. Halide metathesis to give **4.5**.

The ^{19}F NMR spectrum of **4.5** displays a single resonance at $\delta +35.2$ ppm. This could indicate a discrete isomer in which the fluorides are mutually *trans*, or it could indicate that the halogens are rapidly interconverting. If the former were true, then the $^{13}\text{C}\{^1\text{H}\}$ NMR spectrum would be expected to contain a triplet for the arylide *ipso*-C.

However, no resonance for the arylide *ipso*-C is observed, which suggests that the signal is severely broadened by the exchanging fluorides. Unlike with **4.3** and **4.4**, attempts to crystallize **4.5** were unsuccessful.

4.3 Peripheral *N*-atom Alkylation

Due to its ease of synthesis and purification, **4.3** was chosen to investigate the peripheral *N*-atom interactions with Lewis acids. Accordingly, it was found that **4.3** reacted cleanly with 2.1 equiv of MeOTf in thawing CH₂Cl₂ or with 5.0 equiv of MeI in CH₂Cl₂ at 40 °C to give Zr(LXL-Me₂)Cl₃ (**4.6**) as shown in Scheme 4.5. As MeOTf and MeI both serve as CH₃⁺ synthons, the pincer ligand of **4.6** is formally monoanionic (LXL) and the overall complex is neutral. Depending on the alkylating agent, **4.6** could be isolated in 65 % (MeOTf) or 85 % (MeI) yield as a white powder after inducing precipitation from CH₂Cl₂ *via* the addition of pentane. The imidazole *N*-CH₃ groups of **4.6** display a ¹H NMR chemical shift of δ 3.86 ppm and a ¹³C{¹H} NMR chemical shift of δ 34.35 ppm, which are comparable to related *N,N'*-dimethylimidazolium ions.³



Scheme 4.5. *N*-atom methylation to give **4.6**.

X-ray quality crystals of **4.6** were grown from a CH₂Cl₂ solution at -35 °C. Single-crystal X-ray diffraction analysis revealed that **4.6** crystallizes in the triclinic space group $P\bar{1}$ and confirmed the LXL nature of the pincer framework as shown in Figure 4.3. The solid state structure of **4.6** displays a distorted octahedral geometry, with a C-Zr-Cl bond angle of 163.10(5)° for the chloride *trans* to the arylide, and a Cl-Zr-Cl bond angle of 169.607(18)° for the mutually *trans* chlorides. The chloride distortion is not attributed to an electronic effect from the LXL pincer, but rather to steric interaction of the five CH₂Cl₂ solvate molecules with the pendant xylyl groups and the chlorides. The N-Zr-C bond angles are observed to be 70.83(6)° and 70.11(6)° with Zr-N distances of 2.2698(16) and 2.2732(15) Å and a Zr-C distance of 2.2776(18) Å.

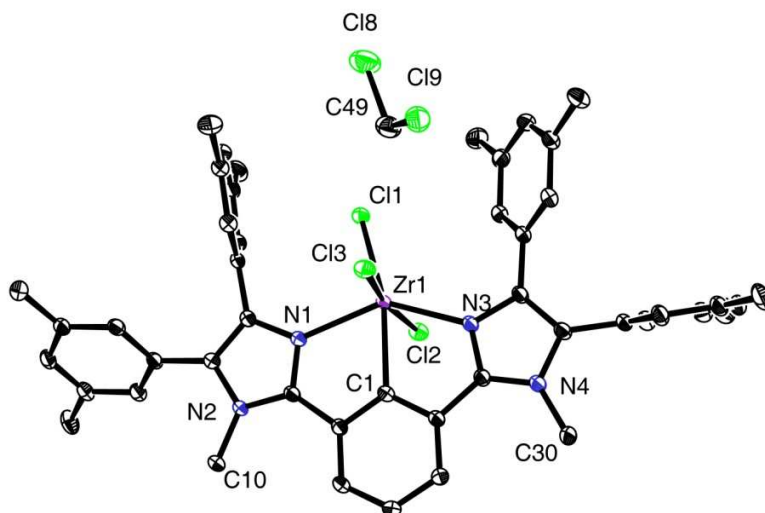
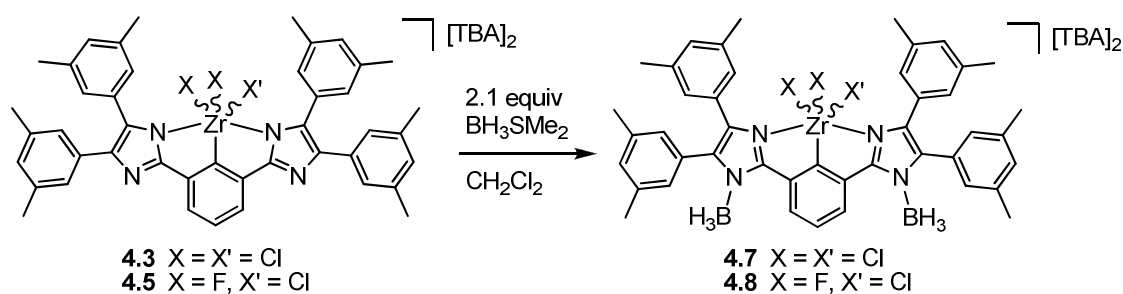


Figure 4.3. 50 % thermal ellipsoid plot of **4.6**. The hydrogen atoms and 4 of 5 CH₂Cl₂ solvate molecules are omitted for clarity. Selected bond lengths (Å) and angles (deg): Zr1-C1, 2.2776(18); Zr1-N1, 2.2732(15); Zr1-N3, 2.2698(16); Zr1-Cl1, 2.4371(5); Zr1-Cl2, 2.4550(5); Zr1-Cl3, 2.4415(5); N2-C10, 1.463(2), N4-C30, 1.461(2); C1-Zr1-N1, 70.11(6); C1-Zr1-N3, 70.83(6); C1-Zr1-Cl2, 84.86(5); C1-Zr1-Cl3, 94.61(5); N1-Zr1-Cl1, 95.57(4); N3-Zr1-Cl1, 123.78(4); N1-Zr1-Cl2, 97.57(4); N1-Zr1-Cl3, 91.98(4); N3-Zr1-Cl2, 83.64(4); Cl1-Zr1-Cl2, 88.35(1); Cl1-Zr1-Cl3, 94.816(18). Full XRD data can be found in Appendix 5.

Fluoride complex **4.5** was treated with the weaker methylating agent MeI at room temperature. At short reaction times, ^1H and ^{19}F NMR spectroscopy indicated the partial formation of a mono-methylated product. However, over extended reaction periods extensive decomposition occurred. Alternatively, halide metathesis was attempted by treating **4.6** with Cp_2TiF_2 . However, this approach again led to decomposition of the reaction mixtures. Therefore, it appears that a fluoride analogue of **4.6** is unstable.

4.4 Peripheral *N*-atom Borylation

Given the successful alkylation of **4.3**, we decided to investigate whether other Lewis acids would display similar chemistry. The B-N bond is generally quite strong,⁴ and so Lewis acids of the type BR_3 were next explored. Treatment of **4.3** with 2.1 equiv of $\text{BH}_3\cdot\text{SMe}_2$ in CH_2Cl_2 led to the formation of $[\text{TBA}]_2[\text{Zr}(\text{LXL}-(\text{BH}_3)_2)\text{Cl}_3]$ (**4.7**) as shown in Scheme 4.6. Removal of the volatiles and drying of the residue allowed for isolation of **4.7** as a bright yellow solid in 91 % yield. Resonances for NBH_3 are not visible in the ^1H NMR spectrum, as is common for pyridyl-borane adducts.⁵ Both the ^{11}B and $^{11}\text{B}\{^1\text{H}\}$ NMR spectra of **4.7** display a broad resonance at -19.5 ppm with $\Delta\nu_{1/2} \approx 700$ Hz, which is similar to the spectrum of *N*-methylimidazole-*N'*-borane.¹ Despite repeated attempts, X-ray quality crystals of **4.7** could not be grown.

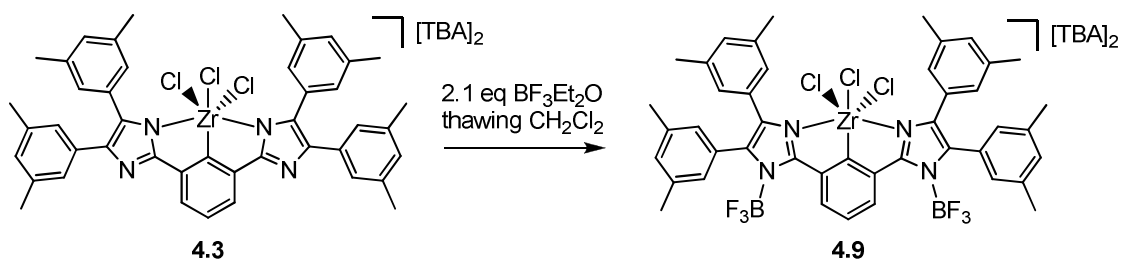


Scheme 4.6. N-atom borylation with $\text{BH}_3\cdot\text{SMe}_2$ to give **4.7**.

The difluoride complex **4.5** reacted similarly with $\text{BH}_3\cdot\text{SMe}_2$ to give $[\text{TBA}]_2[\text{Zr}(\text{LXL}-(\text{BH}_3)_2)\text{ClF}_2]$ (**4.8**) (Scheme 4.6). Complex **4.8** displays ^1H and ^{11}B NMR spectra that are nearly identical to **4.7**. A single resonance at $\delta +41.8$ ppm is observed in the ^{19}F NMR spectrum of **4.8**, which is 6.6 ppm downfield from that observed in the spectrum of **4.5**. Such a downfield shift is suggestive of weaker donation of $\text{NCN}-(\text{BH}_3)_2$ to Zr, resulting in the observed fluoride donation. However, other factors may also influence the fluoride chemical shift, such as changes in the xylyl group orientation, halide site occupation, or proximity of the TBA cation to the Zr fragment.

Treatment of **4.3** with 2.1 equiv of $\text{BF}_3\cdot\text{Et}_2\text{O}$ in CD_2Cl_2 resulted in rapid formation of a new product (**4.9**, Scheme 4.7) in which the two halves of the pincer ligand were equivalent on the NMR time scale, as judged by ^1H NMR. A variety of byproducts were also formed in the reaction, possibly stemming from halide exchange due to the strong Zr-F bond. Performing the reaction in thawing CH_2Cl_2 for 5 minutes followed by removal of the volatile components led to only a slight decrease in the amount of byproduct formation, which was insufficient to allow for isolation of **4.9**. The ^{19}F NMR spectrum of the crude mixture displayed a 1:1:1:1 quartet at $\delta -137.16$ ppm with $^1J_{\text{F-B}} = 17.3$ Hz. This quartet accounted for 77 % of the total ^{19}F NMR signal intensity and was

assigned to the major product **4.9**. Upon obtaining the $^{19}\text{F}\{^{11}\text{B}\}$ spectrum, the quartet collapsed into a broad singlet located at $\delta -137.16$ ppm and was accompanied by the observation of surrounding resonances derived from coupling to the naturally abundant ^{10}B nucleus. The ^{11}B NMR spectrum of crude **4.9** displayed a *pseudo*-quartet located at $\delta 0.16$ ppm with $^1J_{11\text{B}-19\text{F}} = 15.9$ Hz; a minor peak at $\delta -1.02$ ppm was also observed. The discrepancy in the value of the one-bond $^{11}\text{B}-^{19}\text{F}$ coupling constant likely arises from error in accurately assigning the chemical shift for the broadened ^{11}B NMR peak. Attempts to obtain a $^{11}\text{B}\{^{19}\text{F}\}$ NMR spectrum were unsuccessful. Given the above spectral analysis, it is reasonable to assign **4.9** as $[\text{TBA}]_2[\text{Zr}(\text{LXL}-(\text{BF}_3)_2)\text{Cl}_3]$, depicted in Scheme 4.7.



Scheme 4.7. *N*-atom borylation with $\text{BF}_3\cdot\text{Et}_2\text{O}$ to give **4.9**.

When **4.3** was treated with 2 equiv of BCl_3 in CD_2Cl_2 , the reaction mixture rapidly decomposed, possibly due to halide abstraction to generate BCl_4^- salts. Interestingly, **4.3** displayed no reactivity when treated with 2 equiv of either BEt_3 or $\text{B}(\text{OMe})_3$, suggesting that there is a size constraint for the Lewis acids that can be employed. Addition of the stronger Lewis acid AlEt_3 to **4.3** led to prompt decomposition.

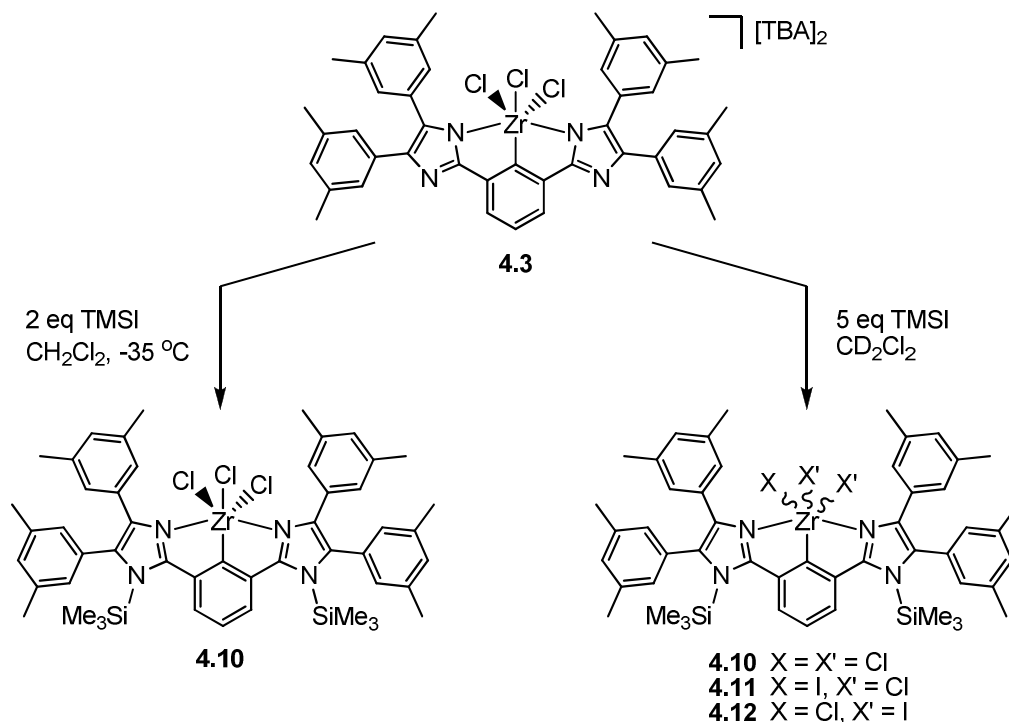
4.5 Peripheral *N*-atom Silylation

We next investigated the feasibility of *N*-silylation of **4.3** and **4.5** using a variety of trimethylsilyl halides (TMSX). It quickly became apparent that halide metathesis was kinetically competitive with *N*-silylation, leading to the formation of TMSCl and TMSF. However, the ¹H NMR spectra of the reaction mixtures were quite clear, and so reaction progress could be monitored readily. Distinctive spectral features included the arylyde *m*- and *p*-protons, the xylyl methyl groups, and the TMS region.

When a -35 °C CD₂Cl₂ solution of **4.3** was treated with 2.1 equiv of TMSI, ¹H NMR spectroscopy indicated the formation of Zr(LXL-TMS₂)Cl₃ (**4.10**) as the major product (Scheme 4.8, left pathway). A variety of unidentified byproducts were also formed in the reaction. Attempts to scale the reaction up led to a larger percentage of byproducts, even when the reaction was performed at lower temperatures.

By employing 5 equiv of TMSI, **4.3** could be transformed into a mixture of **4.10** and its mixed halide congeners containing either 2 chlorides and 1 iodide (**4.11**) or 1 chloride and 2 iodides (**4.12**) as shown in Scheme 4.8 (right pathway). After 25 minutes of reaction time, the product distribution was observed to consist of 13 % **4.10**, 43 % **4.11**, and 43 % **4.12** in the ¹H NMR spectrum. Also observed were the 1.3 equiv TMSCl required for the assigned product distribution. After 3 hours 45 minutes of reaction time, the product mixture contained 17 % **4.11**, 83 % **4.12**, and only trace amounts of **4.10**. As before, the 1.8 eq TMSCl required for the assigned product distribution were observed. No change in the product distribution was noted at longer reaction times, and no evidence of a triiodide analogue was observed, despite the presence of remaining TMSI in the

reaction mixture. Treatment of **4.3** with 10 equiv of TMSI in C₆D₆ at 95 °C again resulted in the formation of **4.12** as the major product.



Scheme 4.8. N-atom silylation of **4.3** with TMSI.

Attempts to isolate pure **4.12** proved unsuccessful due to the similar solubilities of the reaction byproducts. After separating **4.12** from a majority of the salt byproducts, a solution of impure **4.12** in toluene containing a trace of benzene at -35 °C yielded a small quantity of X-ray quality crystals of **4.12**. Single-crystal X-ray diffraction analysis revealed that **4.12** crystallizes in the monoclinic space group P2₁/c. The peripheral imidazole nitrogens are shown to be silylated, and the halides are site-substitution disordered with contributions from both chloride and iodide. Refinement of the X-ray data revealed the halide composition to be Cl_{0.43}I_{2.57} instead of the expected composition

of Cl_1I_2 . Because the halides are unequally distributed over the three sites, the molecular distances and angles cannot be discussed with a sufficient degree of accuracy. However, given the solid state iodide content of 2.57, it can reasonably be assumed that **4.12** undergoes intermolecular halogen exchange in solution. This makes the inability to fully replace the chlorides with iodides even more surprising.

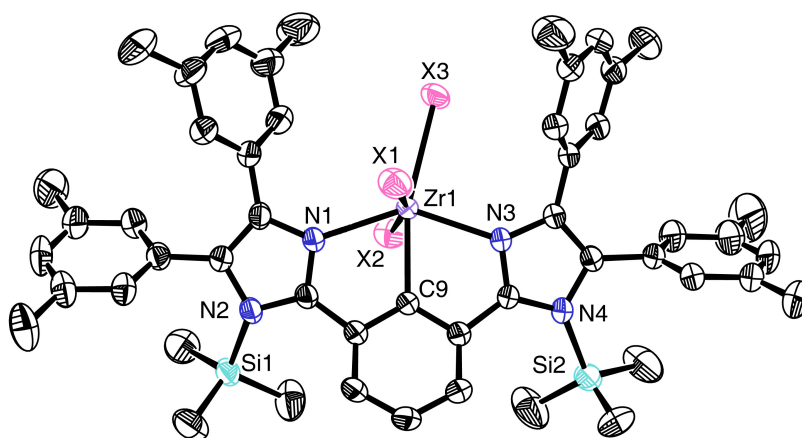


Figure 4.4. 50 % thermal ellipsoid plot of **4.12**. The hydrogen atoms and solvate molecules are omitted for clarity. Bond lengths and angles are not listed due to uncertainty resulting from halide site substitution disorder. Full XRD data are reported in Appendix 6.

Closer inspection of the solid state structure for **4.12** reveals that the pincer backbone is significantly distorted from planarity, while **4.3**, **4.4**, and **4.6** all display nearly planar pincer backbones in the solid state (Figure 4.5). Additionally, the $-\text{SiMe}_3$ groups of **4.12** are significantly bent away from the imidazole rings. The backbone distortions likely result from unfavorable steric interactions between the bulky $-\text{SiMe}_3$ groups and the rest of the pincer ligand. Furthermore, the observed steric impact of

introducing $-\text{SiMe}_3$ groups explains the lack of observed reaction between **4.3** and BEt_3 or B(OMe)_3 .

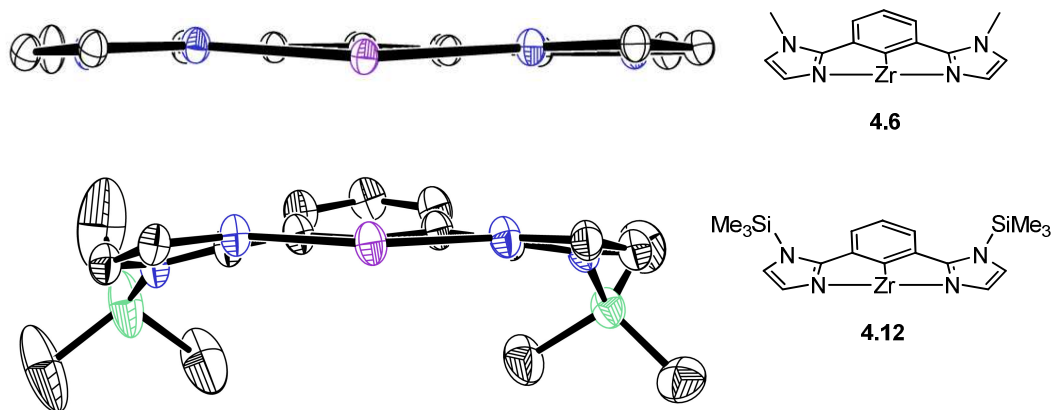
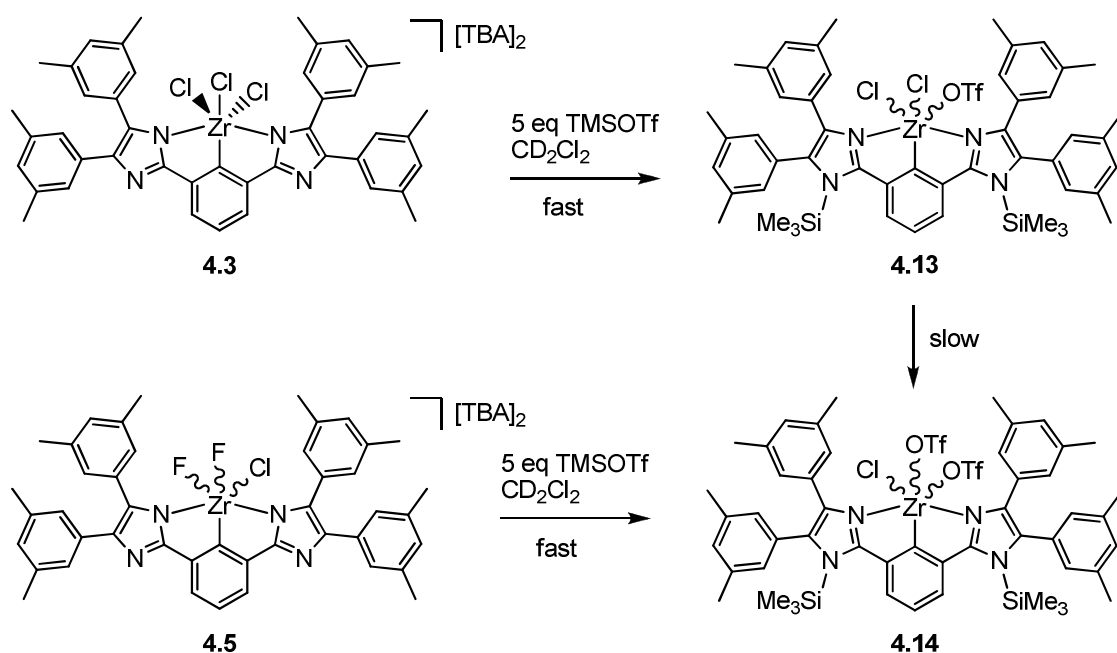


Figure 4.5. 50 % thermal ellipsoid plots of the front views showing the planarity of **4.6** and the non-planarity of **4.12**. Hydrogen atoms, halide atoms, pendant aryl rings, and solvate molecules are emitted for clarity.

When **4.3** was treated with 5 equiv of TMSOTf, ^1H NMR spectroscopy indicated the formation of two products in a 1:1 ratio at 20 minutes of reaction time, along with 1 equiv of TMSCl. Both products are presumed to be isomers of $\text{Zr(LXL-TMS}_2\text{)Cl}_2\text{OTf}$ (**4.13**) as shown in Scheme 4.9; after 3 hours 40 minutes, only a single isomer of **4.13** was observed. At longer reaction times, **4.13** continued to react with the remaining TMSOTf to generate $\text{Zr(LXL-TMS}_2\text{)ClOTf}_2$ (**4.14**). For example, 11 % **4.14** was observed after 6 hours, while 38 % **4.14** was observed after 2 days of reaction. By treating **4.5** with 5 equiv of TMSOTf, **4.14** could be generated as the sole Zr-containing product in 20 minutes, along with the formation of 2 equiv of TMSF. Upon concentrating the solution and redissolving in CD_2Cl_2 , significant decomposition occurred, possibly through a bimolecular pathway.

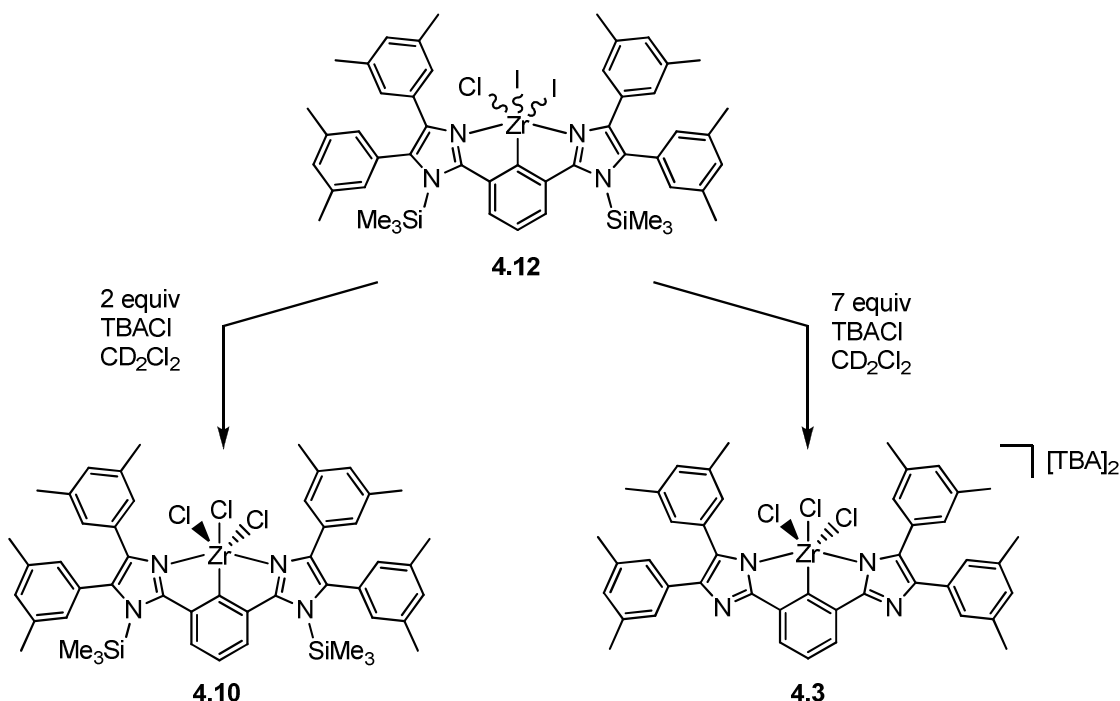


Scheme 4.9. N-atom Silylation with TMSOTf.

Reactions employing TMSBr were more difficult to interpret; treating **4.3** with 5 equiv of TMSBr led to the formation of at least 2 products in a nearly 1:1 ratio, as well as TMSCl resulting from halogen exchange. Inspection of the xylyl methyl region suggested one product was mono-silylated (4 equal intensity singlets) and the other product was di-silylated (2 equal intensity singlets). While the trimethylsilyl region agreed with this assessment, only a single arylide *m*-proton resonance was observed which integrated to only 66 % of the expected intensity relative to the ArCH₃ resonances. Therefore, the product identities cannot be confirmed. The reaction was complete within 20 minutes, as no additional change was noted in the ¹H NMR spectrum at longer reaction times. Treatment of **4.5** with 5 equiv of TMSBr yielded similar results.

It was reasoned that the TMS groups could be removed by introducing a strong enough nucleophile to cleave the N-Si bond. Because the Si-Cl bond is very strong,⁴ it

was anticipated that addition of chloride ion would lead to the desired bond scission. When a solution of **4.12** in CD_2Cl_2 was treated with 2 equiv of $[\text{TBA}]\text{Cl}$, ^1H NMR analysis revealed the formation of multiple products. The major product was **4.10**, which was formed *via* halide metathesis with free chloride ion. When an excess of $[\text{TBA}]\text{Cl}$ was added to **4.12**, halide metathesis and the desired silyl group cleavage occurred to give **4.3**, with TMSCl being observed as a byproduct (Scheme 4.10).

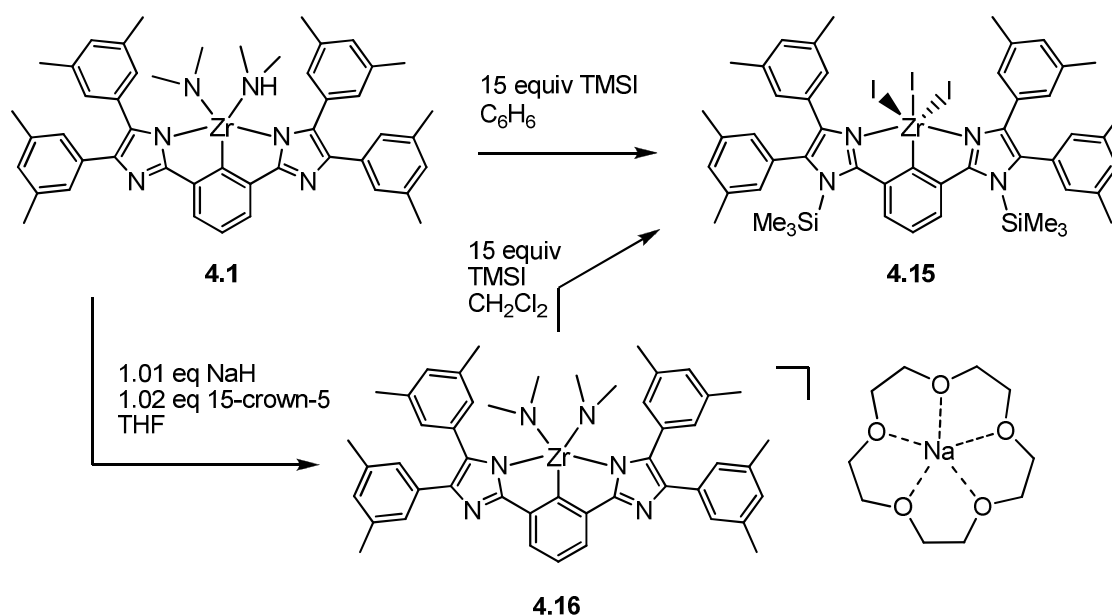


Scheme 4.10. Silyl group cleavage with $[\text{TBA}]\text{Cl}$.

4.6 Other Silylation Pathways

Given that a bis-*N*-silylated complex could not be isolated in pure form from **4.3**, other routes of synthesis were investigated. Treatment of **4.1** with an excess of TMSI in C_6H_6 initially appeared to cleanly produce $\text{Zr}(\text{NCN-SiMe}_3)_3$ (**4.15**) after lyophilization to

remove excess TMSX species (Scheme 4.11). However, large quantities of an insoluble byproduct were formed during the course of the reaction, and complex **4.15** could only be recovered impurely in very small yields by this route. In a separate NMR-scale reaction, $[\text{Me}_3\text{SiN}(\text{H})\text{Me}_2]\text{I}$ was observed as a byproduct of the reaction between **4.1** and TMSI, presumably through direct silylation of NHMe_2 . Therefore, it is possible that decomposition of **4.15** during attempted purification is due to the presence of an acidic proton in the crude reaction mixture.



Scheme 4.11. Alternative silylation pathway.

In order to obtain **4.15** cleanly, the removal of the acidic proton in **4.1** was investigated. The NHMe_2 proton was found to be deprotonated with 1.01 equiv of NaH and 1.02 equiv of 15-crown-5 to afford $[\text{Na}(\text{15-crown-5})][\text{Zr}(\text{XXX})(\text{NMe}_2)_2]$ (**4.16**), which was isolated in 68 % yield (Scheme 4.12). The $-\text{NMe}_2$ ligands of **4.16** were equivalent on the ^1H NMR timescale, suggesting net trigonal bipyramidal geometry in

solution. Satisfyingly, **4.16** did react cleanly with 15 equiv of TMSI to form **4.15** as desired; however, **4.15** could not be separated from the crown ether products. Attempts to deprotonate **4.1** by NaH without using a crown ether were unsuccessful, indicating that the crown ether facilitates the deprotonation step.

4.7 Computational Investigations

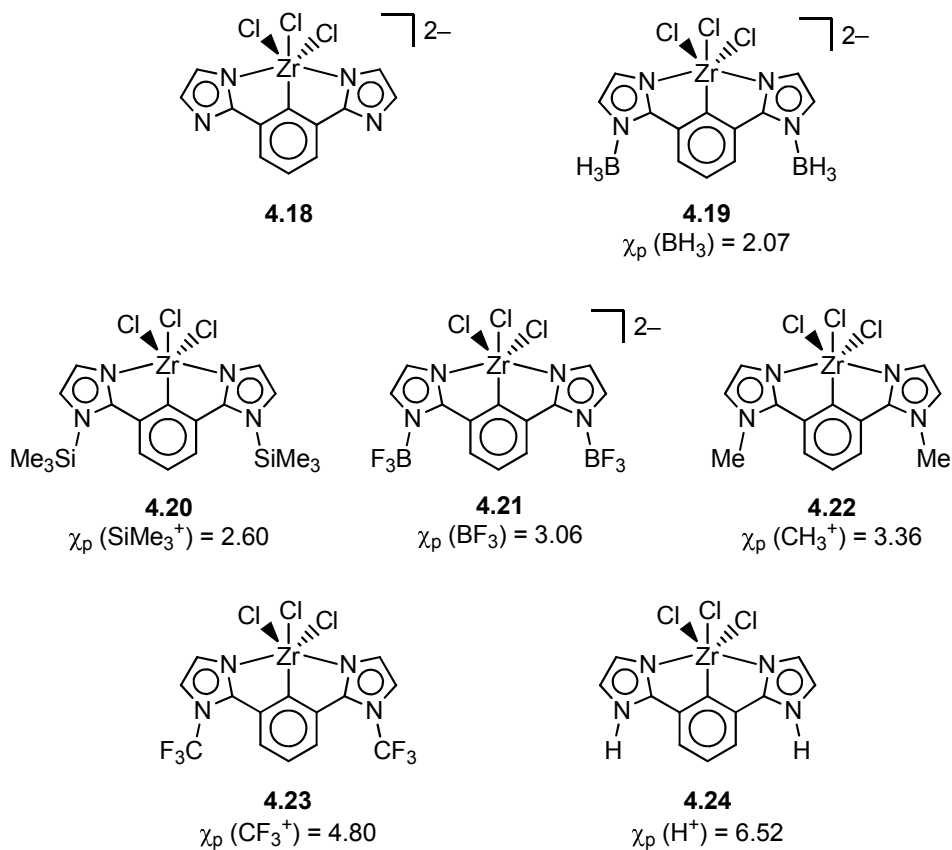


Figure 4.6. Structures modeled by computation. Full atomic coordinates can be found in Appendix 7.

Given the successful interaction of **4.3** with a variety of Lewis acids, we sought to gain a better understanding of the changes in NCN electron donor strength as a function

of Lewis acid identity. As the Zr complexes lacked a suitable spectroscopic handle, we turned to computational investigation to better understand the electronic structure of these molecules. Figure 4.6 displays the model structures employed in these studies; complexes **4.18** – **4.22** were modeled after complexes discussed previously, while the hypothetical complexes **4.23** and **4.24** were modeled for additional insight. Also listed in Figure 4.6 are the group electronegativities (χ_p) for each NR group, which were determined on the Mulliken scale and converted into the entry in Pauling values.² For ease of comparison, compounds **4.19-4.24** have been ordered with increasing χ_p .

Table 4.1. Calculated Gibbs energy of C_1 and C_{2v} structures.

Structure	G (C_1) / kcal mol ⁻¹	G (C_{2v}) / kcal mol ⁻¹	ΔG^a / kcal mol ⁻¹
4.18	-1322885.94	-1322888.17	-2.23
4.19	-1356348.67	-1356348.67	0.00
4.20	-1836434.59	-1836435.47	-0.88
4.21	-1730426.64	-1730426.29	0.34
4.22	-1372884.96	-1372884.73	0.23
4.23	-1746682.62	-1746678.63	3.99
4.24	-1323574.94	-1323574.64	0.30

^a $\Delta G = G(C_{2v}) - G(C_1)$.

Using the Jaguar 7.0 program,⁶ the geometries of **4.18-4.24** were optimized with no symmetry constraints (C_1 symmetry) using the LACV3P*+ basis set⁷ and the B3LYP density functional.⁸⁻¹⁰ All structures minimized to a ground state with the exception of **4.21**, which was found to have a single imaginary frequency. Some of the optimized geometries were found to deviate significantly from an octahedral geometry as a result of halide distortions. Anticipating that large geometry variations might influence the calculated electronic properties, each of the structures was also optimized within C_{2v}

symmetry constraints, giving structures **4.18.S-4.24.S**, which all minimized to a ground state. The calculated Gibbs energy was found to differ only slightly between the C_1 and C_{2v} structures (Table 4.1). Two compounds, **4.18** and **4.20**, were found to minimize to a lower energy within C_{2v} symmetry constraints, while the other C_{2v} structures were found to be 0–4 kcal mol⁻¹ less stable than their C_1 counterparts.

Table 4.2. Natural charges q of the inner coordination sphere calculated by NPA.

Compound	Zr	C	N ¹	N ²	Cl _{Eq}	Cl _{Ax} ¹	Cl _{Ax} ²
4.18	1.638	-0.366	-0.669	-0.671	-0.579	-0.508	-0.504
4.18.S	1.639	-0.367	-0.671	-0.671	-0.581	-0.504	-0.504
4.19	1.604	-0.360	-0.638	-0.638	-0.555	-0.480	-0.480
4.19.S	1.598	-0.377	-0.638	-0.638	-0.547	-0.480	-0.480
4.20	1.507	-0.252	-0.590	-0.599	-0.453	-0.430	-0.428
4.20.S	1.507	-0.253	-0.596	-0.596	-0.439	-0.428	-0.428
4.21	1.575	-0.357	-0.622	-0.634	-0.543	-0.470	-0.469
4.21.S	1.583	-0.374	-0.633	-0.633	-0.537	-0.470	-0.470
4.22	1.502	-0.315	-0.585	-0.586	-0.429	-0.420	-0.421
4.23.S	1.502	-0.335	-0.587	-0.587	-0.429	-0.421	-0.421
4.23	1.478	-0.246	-0.571	-0.559	-0.433	-0.406	-0.402
4.23.S	1.480	-0.319	-0.579	-0.579	-0.416	-0.408	-0.408
4.24	1.500	-0.300	-0.581	-0.582	-0.422	-0.415	-0.415
4.24.S	1.501	-0.300	-0.582	-0.582	-0.422	-0.415	-0.415
4.3 ^a	1.547	-0.355	-0.655	-0.655	-0.520	-0.466	-0.466
4.6 ^a	1.469	-0.343	-0.589	-0.587	-0.438	-0.421	-0.413

^a NPA was performed on the XRD coordinates.

The natural atomic charges (q) were determined through Natural Population Analysis (NPA)¹¹ of the model structures. Table 4.2 lists the charges of Zr and each atom within the inner coordination sphere. Differences in structural symmetry (C_1 vs. C_{2v}) were found to have little effect on all values of q . The natural atomic charge on Zr, $q(\text{Zr})$, can be used to describe the amount of electron density on the Zr nucleus, with a smaller

$q(\text{Zr})$ corresponding to a more electron-rich Zr atom. Examination of the data reveals that introduction of a Lewis acid to give an LXL ligand leads to a *decrease* in $q(\text{Zr})$ such that $\Delta q(\text{Zr}) = q(\text{Zr}_{\text{XXX}}) - q(\text{Zr}_{\text{LXL}}) > 0$. This observation is opposite that which is expected, and can be rationalized by noting the increased chloride donation for the LXL complexes (**4.19-4.24**) relative to the XXX complex **4.18** (Table 4.2). As seen in Figure 4.7, $\Delta q(\text{Zr})$ has only a very weak correlation with χ_{p} (group), and so no definitive relationship can be established between the two parameters. Natural Population Analysis was also performed for molecular **4.3** (the molecular dianion only) and **4.6** in their solid-state structures (Table 4.2). The $q(\text{Zr})$ values for **4.3** and **4.6** are slightly lower than for the corresponding model compounds **4.18** and **4.22**. As in the model system, $q(\text{Zr})$ of **4.6** (LXL ligand) is less than $q(\text{Zr})$ of **4.3** (XXX ligand).

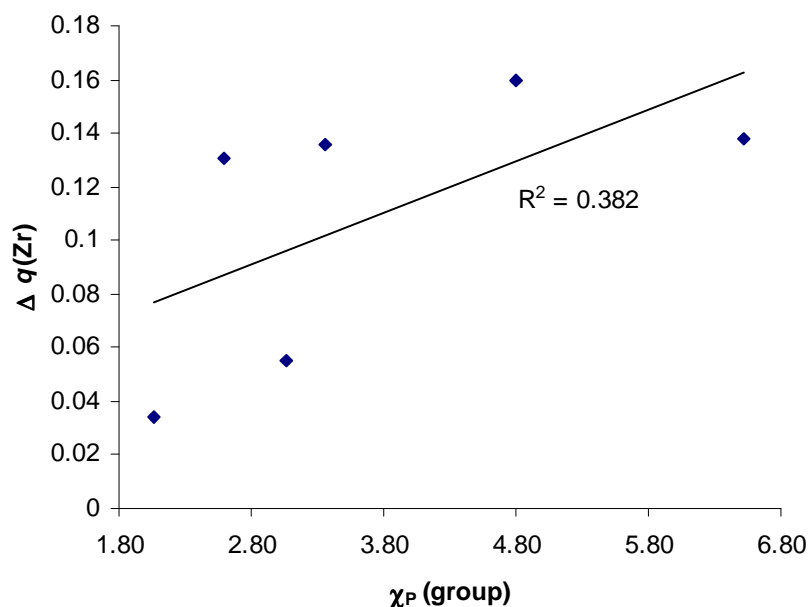


Figure 4.7. Effect of χ_{p} on $\Delta q(\text{Zr})$.

Some question existed as to the significance of the calculated q_{Zr} differences, especially with respect to potential Mo-based triple-bond metathesis catalysts. In a recent study by Chisholm, a series of Group 6 $NM(OR)_3$ complexes was investigated both spectroscopically and computationally.¹² Mulliken charges were calculated for $NMo(OCMe_3)_3$ and $NMo(OCMe_2CF_3)_3$, with the charge at Mo differing by 0.08 between the two structures. As seen in Chapter 1, Group 6 complexes containing $-OCMe_3$ differ substantially in triple-bond metathesis reactions than analogous complexes containing $-OCMe_2CF_3$ as a ligand. Therefore, the current variations in q_{Zr} (Δ 0.03 – 0.16) are considered to be significant with respect to potential Mo-based triple-bond metathesis catalysts.

Natural Bond Orbital (NBO) analysis^{13, 14} was next performed in order to gain a better understanding of the electronic differences arising from R-group identity. Due to the high ionic character of the Zr-ligand bonds, the NBO program describes each Zr-ligand bond as a ligand-centered lone-pair (lp) of electrons and a Zr-centered non-Lewis lone-pair (lp*) of electrons. From this bonding description, the Donor-Acceptor (D-A) stabilization energy ($\Delta E_{i \rightarrow j^*}^{(2)}$) is calculated by the NBO program and gives a measure of the energetic stabilization arising from ligand-to-metal lp \rightarrow lp* donation as seen in Figure 4.8.¹⁵

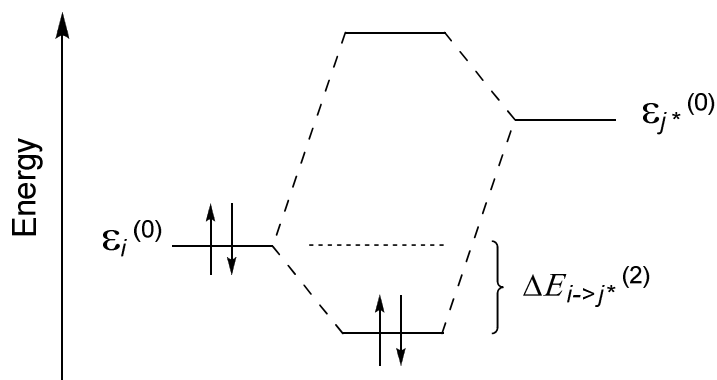


Figure 4.8. Pictorial description of the D-A stabilization energy ($\Delta E_{i \rightarrow j^*}^{(2)}$).

In order to have a common frame of reference from which to compare the calculated D-A energies, all compounds were first defined as having the Lewis structure depicted in Figure 4.9. While this structure may not be the “best” structure to describe the bonding, it is one of many valid resonance forms for these highly delocalized compounds. The calculated D-A energies therefore will not correspond to an absolute bond strength, but will give an indication of the inherent ability of each ligand to stabilize the Zr center. In addition to providing a common frame of reference for **4.18-4.24**, the chosen Lewis structure allows for easy determination of both $N(\sigma)$ and $N(\pi)$ effects on the D-A energies due to the presence of both σ and π lp's on the N-ligand.

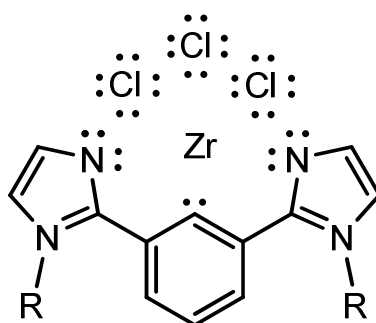


Figure 4.9. Assigned Lewis structure for NBO calculations.

The calculated D-A stabilization energies are tabulated below in Table 4.3 for each N- σ , N- π , and C- σ interaction. Upon examination of the data, it is seen that the C_1 models display large amounts of scatter relative to the C_{2v} models, especially amongst the energies of the N σ -lp's. Therefore, the analysis was completed using the C_{2v} dataset. The change in D-A stabilization energy, $\Delta D-A = D-A_{LXL} - D-A_{XXX}$, was plotted as a function of the group χ_P for the total N-stabilization (N_T), the C σ -lp stabilization, and the total NCN stabilization (NCN_T) as shown in Figure 4.9. As expected, the D-A stabilization energy for both N_T and NCN_T was found to decrease with increasing χ_P . There is a significant amount of scatter to the data ($R^2 = 0.6-0.7$), and so determination of χ_P for a particular group is not sufficient to make accurate predictions about changes the D-A stabilization energy upon coordination of a specific Lewis acid. The scatter for the C σ -lp is very large ($R^2 = 0.06$), indicating that electronic changes in the imidazole rings have little effect on the Zr-C bonding interaction.

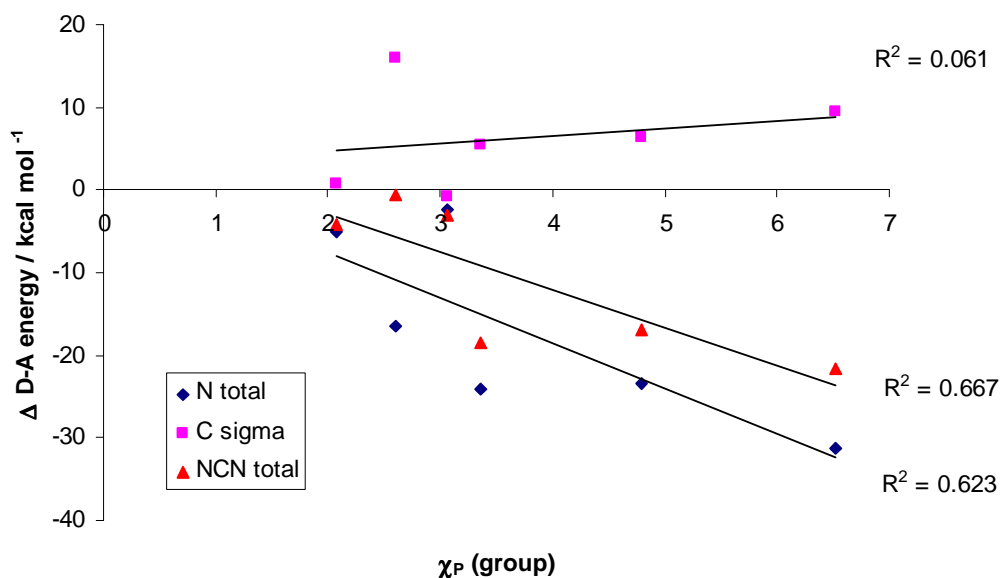


Figure 4.10. Effect of χ_P on $\Delta D-A$ stabilization energy.

Table 4.3. D-A stabilization energies in units of kcal mol⁻¹.

Compound	N ¹ σ	N ² σ	N ¹ π	N ² π	N _T ^a	Cσ	NCN _T ^b
4.18	117.31	109.32	30.24	13.46	270.33	255.29	525.62
4.19	92.22	92.57	20.48	20.63	225.90	244.88	470.78
4.20	106.83	105.28	16.92	19.07	248.10	lp* ^c	--
4.21	106.23	113.75	17.06	20.75	257.79	235.18	492.97
4.22	88.72	86.23	16.49	16.43	207.87	230.42	438.29
4.23	100.14	98.47	16.95	13.32	228.88	73.42	302.30
4.24	89.09	81.70	15.64	15.56	201.99	228.45	430.44
4.18.S	92.85	92.85	22.66	22.66	231.02	237.79	468.81
4.19.S	92.34	92.34	20.67	20.67	226.02	238.52	464.54
4.20.S	88.97	88.97	18.26	18.26	214.46	253.78	468.24
4.21.S	94.16	94.16	20.18	20.18	228.68	237.04	465.72
4.22.S	87.02	87.02	16.47	16.47	206.98	243.33	450.31
4.23.S	87.38	87.38	16.41	16.41	207.58	244.22	451.80
4.24.S	84.27	84.27	15.62	15.62	199.78	247.28	447.06

^a N_T = N¹σ + N²σ + N¹π + N²π. ^b NCN_T = N_T + Cσ. ^c This lp was described as a non-Lewis lp* orbital by the NBO program and did not result in stabilization of the Zr lp* orbitals.

4.8 Conclusions

The complex [TBA]₂[Zr(XXX)Cl₃] (**4.3**) was found to react with a variety of Lewis acids, resulting in formation of complexes [TBA]_n[Zr(LXL)Cl₃]ⁿ⁻ (n = 0, 2). Methyl cation synthons (MeI, MeOTf) readily formed the neutral complex (**4.6**). Trimethylsilylation of **4.3** could also be achieved to afford silyl analogues of **4.6**. Halide metathesis was found to be kinetically competitive with silylation, and so mixed halide complexes of the form Zr(LXL-(SiMe₃)₂)X'X''₂ were obtained. X-ray diffraction analysis of Zr(LXL-(SiMe₃)₂)ClI₂ (**4.12**) revealed that substitution by the large trimethylsilyl group causes the pincer ligand to distort from planarity. The silyl groups of **4.12** were readily removed under mild conditions through addition of chloride ion.

Use of the neutral Lewis acids BH_3 and BF_3 led to the formation of zwitterionic complexes $[\text{TBA}]_2[\text{Zr}(\text{LXL}-(\text{BR}_3)_2)\text{Cl}_3]$ (**4.7**, **4.9**). When $[\text{TBA}]_2[\text{Zr}(\text{XXX})\text{ClF}_2]$ (**4.5**) was treated with a BH_3 source, the complex $[\text{TBA}]_2[\text{Zr}(\text{LXL}-(\text{BH}_3)_2)\text{ClF}_2]$ (**4.8**) was formed. The ^{19}F NMR resonance for Zr-F was found to shift downfield by 6.6 ppm upon formation of **4.8**. This chemical shift suggests that the $\text{LXL}-(\text{BH}_3)_2$ is a weaker electron donor than the parent XXX ligand, though at this point steric factors cannot be ruled out.

DFT calculations support the hypothesis that coordination of a Lewis acid decreases the electron donor strength of the NCN ligand. The highly ionic Zr-ligand bonds were best described as a ligand-centered lone pair and a Zr-centered non-Lewis lone pair. Subsequent determination of the donor-acceptor stabilization energy ($\text{lp} \rightarrow \text{lp}^*$) revealed a gradual decrease in the D-A energy that loosely correlated with an increase in the Lewis acid electronegativity.

4.9 Experimental

4.9.1 Methods

All reactions were performed in a nitrogen-filled MBRAUN Labmaster 130 glove box. ^1H NMR spectra were recorded at 499.909 MHz, 399.967 MHz, or 300.075 MHz on a Varian Inova 500, Varian Inova 400, Varian MR400, or Varian Inova 300 spectrometer and referenced to the residual protons in pyridine- d_5 (8.79 ppm), C_6D_6 (7.16 ppm), or CD_2Cl_2 (5.32 ppm). ^{13}C NMR spectra were recorded at 100.724 MHz on a Varian Inova 400 or Varian MR400 spectrometer and were referenced to naturally abundant ^{13}C nuclei in CD_2Cl_2 (54.00 ppm). Combustion analyses were performed by Midwest Microlabs or on a Perkin-Elmer 200 Series II Analyzer.

4.9.2 Materials

All bulk solvents were obtained from VWR scientific. Benzene and CH₂Cl₂ were degassed and dried over 4 Å molecular sieves, and all other solvents used were dried and deoxygenated by the method of Grubbs.¹⁶ CpTiF₂ was prepared according to the literature procedure,¹⁷ which was found to require the use of “wet” acetone. [HN(ⁱPr)₂Et]X were prepared in analogy to a literature procedure for the preparation of lutidinium iodide.¹⁸ Zr(XXX)(NMe₂)(NHMe₂) (**4.1**) was prepared according to Section 3.9.3. NMR solvents were obtained from Cambridge Isotope Laboratories and were dried over 4Å molecular sieves for at least 24 hours. Methyl triflate (MeOTf), methyl iodide (MeI), 94 % BH₃·SMe₂, iodotrimethylsilane (TMSI), trimethylsilyl triflate (TMSOTf), chlorotrimethylsilane (TMSCl), NaH (60% in mineral oil), tetra-*n*-butylammonium bromide (TBABr) and BF₃·Et₂O were purchased from Acros. Tetra-*n*-butylammonium chloride was purchased from Fluka. Bromotrimethylsilane (TMSBr), tetra-*n*-butylammonium iodide (TBAI), BCl₃ (1.0 M in heptane), BEt₃ (1.0 M in hexane), and AlEt₃ (1.0 M in hexane) were purchased from Aldrich. AgPF₆, AgBF₄, tetra-*n*-butylammonium hexafluorophosphate (TBAPF₆), triphenyltin fluoride (Ph₃SnF), and B(OMe)₃ were purchased from Strem. All TBA-halides were dried by heating to > 100 °C under vacuum for at least 12 hours. All other reagents were used as received.

4.9.3 Synthetic Procedures

[Zr(NCN)Cl₃]TBA₂ (**4.3**). Solid TBACl (1.4186 g, 5.104 mmol, 2.05 equiv) was added to a suspension of **4.1** (2.0033 g, 2.491 mmol, 1.0 equiv) in CH₂Cl₂ (50 mL) with

stirring. The mixture was stirred for 10 minutes, at which point the solution was clear yellow in appearance. Solid $[\text{HN}(\text{}^i\text{Pr})_2\text{Et}]\text{Cl}$ (0.4133 g, 2.494 mmol, 1.0 equiv) was added and the solution stirred for 3.5 hours. The solution was concentrated *in vacuo* to *ca.* 20 mL in volume, then the orange solid was immediately collected by vacuum filtration and washed with cold CH_2Cl_2 (2 x 8 mL) and pentane (1 x 10 mL). ^1H NMR analysis indicated that the solid contained approximately 13 % TBACl. The solid was dissolved in CH_2Cl_2 (90 mL), then Et_2O (40 mL) was added and the solution cooled to -35 °C. The orange solid that formed was collected by vacuum filtration, washed with Et_2O (40 mL), and dried *in vacuo* to yield **4.3** (2.0973 g, 1.606 mmol, 65 %) as a bright orange powder. ^1H NMR (CD_2Cl_2 , 400 MHz): δ 7.35 (d, $^3J_{\text{HH}} = 7.4$ Hz, 2H, ArH), 7.32 (s, 4H, ArH), 7.18 (s, 4H, ArH), 7.05 (t, $^3J_{\text{HH}} = 7.4$ Hz, 1H, ArH), 6.86 (s, 2H, ArH), 6.69 (s, 2H, ArH), 2.72 (m, 16H, TBA), 2.27 (s, 12H, ArCH₃), 2.19 (s, 12H, ArCH₃), 1.31 (m, 16H, TBA), 1.18 (m, 16H, TBA), 0.84 (t, $^3J_{\text{HH}} = 7.2$ Hz, 24H, TBA). $^{13}\text{C}\{^1\text{H}\}$ NMR (CD_2Cl_2): δ 190.49 (s, Zr-C_{ipso}), 162.57, 142.98, 138.24, 137.31, 136.99, 136.79, 136.42, 135.93, 129.03, 128.14, 128.04, 126.13, 125.37, 117.77, 58.46, 24.21, 21.49, 21.43, 19.87, 13.79. Anal. Calcd. for $\text{C}_{76}\text{H}_{111}\text{Cl}_3\text{N}_6\text{Zr}$: C, 69.88; H, 8.56; N, 6.43. Found C, 68.93; H, 8.55; N, 6.14.

[Zr(NCN)Br₃]TBA₂ (4.4). Solid TBABr (0.4127g, 1.280 mmol, 2.0 equiv) was added to a suspension of **4.1** (0.5113 g, 0.636 mmol, 1.0 equiv) in CH_2Cl_2 (20 mL) with stirring. The mixture was stirred for 15 minutes, at which point the solution was clear yellow in appearance. Solid $[\text{HN}(\text{}^i\text{Pr})_2\text{Et}]\text{Br}$ (0.1337 g, 0.636 mmol, 1.0 equiv) was added and the solution stirred for 5 hours. The orange residue was dissolved in CH_2Cl_2

(5 mL), then Et₂O (3 mL) was added and the solution cooled to –35 °C. The red crystals were collected by vacuum filtration, washed with Et₂O (3 x 4 mL), and dried *in vacuo*. The solid was then recrystallized from CH₂Cl₂ (8 mL) at –35 °C. Collection by vacuum filtration and drying *in vacuo* yielded **4.4** (0.2922 g, 0.203 mmol, 32 %) as a deep red solid. ¹H NMR analysis indicated that the solid contained approximately 13 % of an NCN-containing impurity. ¹H NMR (CD₂Cl₂, 400 MHz): δ 7.34 (d, ³J_{HH} = 7.4 Hz, 2H, ArH), 7.34 (s, 4H, ArH), 7.18 (s, 4H, ArH), 7.07 ppm (t, ³J_{HH} = 7.4 Hz, 1H, ArH), 6.86 (s, 2H, ArH), 6.68 (s, 2H, ArH), 2.77 (m, 16H, TBA), 2.27 (s, 12H, ArCH₃), 2.18 (s, 12H, ArCH₃), 1.33 (m, 16H, TBA), 1.20 (m, 16H, TBA), 0.86 t, ³J_{HH} = 7.2 Hz, 24H, TBA). ¹H NMR, impurity (CD₂Cl₂, 400 MHz): δ 8.15 (dd, J_{HH} = 7.8 Hz, 1.7 Hz, 0.1H), 7.40–7.60 (m, 0.5H), 6.91 (s, 0.3H), 2.30 (s, 1.7H). ¹³C{¹H} NMR (CD₂Cl₂, 53.80): δ 191.68 (s, Zr-C_{ipso}), 162.41, 142.51, 138.06, 137.52, 136.93, 136.81, 136.32, 135.48, 129.61, 128.31, 126.14, 125.26, 117.84, 58.69, 24.28, 21.50, 19.96, 13.80. Anal. Calcd. for C₇₆H₁₁₁Br₃N₆Zr: C, 63.40; H, 7.77; N, 5.84. Found C, 64.03; H, 7.95; N, 5.74.

[Zr(NCN)ClF₂]TBA₂ (4.5). Solid CpTiF₂ (0.1127 g, 0.579 mmol, 4.3 equiv) was added to a solution of **4.3** (0.1768 g, 0.135 mmol, 1.0 equiv) in CH₂Cl₂ (10 mL) with stirring. The orange solution was stirred for 2 hours, then concentrated to dryness. The residue was slurried in THF (10 mL) and stirred vigorously for 20 minutes. The resulting precipitate was collected by vacuum filtration, rinsed with THF (2 x 2 mL), and dried *in vacuo*. ¹H NMR analysis indicated that the solid contained approximately 0.15 equiv Cp₂TiX₂. The crude solid was dissolved in CH₂Cl₂ (2 mL), diluted with THF (11 mL), and cooled to –35 °C. The resulting powder was collected by vacuum filtration,

rinsed with Et₂O (4 mL), and dried *in vacuo* to yield **4.5** (0.0821 g, 0.0645 mmol, 48 %) as a white powder. ¹H NMR (CD₂Cl₂, 400 MHz): δ 7.36 (d, ³J_{HH} = 7.4 Hz, 2H, ArH), 7.28 (s, 4H, ArH), 7.20 (s, 4H, ArH), 7.04 (t, ³J_{HH} = 7.4 Hz, 1H, ArH), 6.82 (s, 2H, ArH), 6.70 (s, 2H, ArH), 2.70 (m, 16H, TBA), 2.27 (s, 12H, ArCH₃), 2.21 (s, 12H, ArCH₃), 1.24 (m, 16H, TBA), 1.12 (m, 16H, TBA), 0.81 (t, ³J_{HH} = 7.2 Hz, 24H, TBA). ¹³C{¹H} NMR (CD₂Cl₂, 53.80): δ 162.92, 144.74, 138.92, 137.36, 137.25, 137.08, 137.02, 136.79, 127.95, 127.43, 127.38, 126.01, 125.60, 117.43, 58.28, 24.06, 21.47, 21.40, 19.68, 13.83. ¹⁹F{¹H} NMR: δ 35.19 (s). Anal. Calcd. for C₇₆H₁₁₁Cl₂FN₆Zr: C, 71.68; H, 8.79; N, 6.60. Found C, 71.66; H, 8.61; N, 6.45.

Zr(NCN-Me₂)Cl₃ (4.6). Method A: A solution of **4.3** (604.5 mg, 0.463 mmol, 1.0 equiv) in CH₂Cl₂ (15 mL) was frozen. Immediately upon thawing, MeOTf (107.4 μL, 0.949 mmol, 2.1 eq) was added via syringe. After stirring at ambient temperature for 1.5 hours, the solution was pipetted into cold Et₂O (30mL). The precipitate was collected by vacuum filtration, rinsed with Et₂O (2 x 5 mL), then dried *in vacuo* to yield **4.6** (256.8 mg, 0.302 mmol, 65 %) as a white powder. Method B: A solution of **4.3** (211.5 mg, 0.162 mmol, 1.0 equiv) in CH₂Cl₂ (10 mL) was transferred to a bomb flask (with equal solution volume and head space volume). MeI (50.0 μL, 0.803 mmol, 5.0 equiv) was added in the dark, then the bomb flask was sealed and the overlying atmosphere briefly evacuated. The solution was heated for 18 hours in a 45 °C oil bath. The solution was then cooled, returned into the glovebox, and concentrated to dryness. The remaining solid was then re-dissolved in CH₂Cl₂ (4.5 mL), and the solution was slowly diluted with Et₂O (6.5 mL) with stirring. The precipitate was collected by vacuum filtration, rinsed

with Et₂O (2 x 2 mL), then dried *in vacuo* to yield **4.6** (116.4 mg, 0.137 mmol, 85 %) as a white powder. ¹H NMR (CD₂Cl₂, 400 MHz): δ 7.75 (d, ³J_{HH} = 7.8 Hz, 2H, ArH), 7.43 (t, ³J_{HH} = 7.8 Hz, 1H, ArH), 7.20 (s, 4H, ArH), 7.09 (s, 2H, ArH), 6.99 (s, 4H, ArH), 6.92 (s, 2H, ArH), 3.86 (s, 6H, NCH₃), 2.33 (s, 12H, ArCH₃), 2.22 (s, 12H, ArCH₃). ¹³C{¹H} NMR (CD₂Cl₂): δ 192.99 (s, Zr-C_{ipso}), 154.45, 138.87, 138.32, 138.16, 135.76, 131.98, 131.43, 131.34, 130.41, 129.49, 128.83, 128.43, 127.72, 123.37, 34.35, 21.35, 21.31. Anal. Calcd for C₄₆H₄₅Cl₃N₄Zr: C, 64.89; H, 5.33; N, 6.58. Found C, 64.08; H, 5.31; N, 6.45.

[Zr(NCN-(BH₃)₂)Cl₃]TBA₂ (**4.7**). Complex **4.3** (0.2287 g, 0.175 mmol, 1.0 equiv) was dissolved in CH₂Cl₂ (10 mL), then 94 % BH₃·SMe₂ (38.0 μL, 0.372 mmol, 2.1 equiv) was added *via* syringe with stirring. After 4 hours of stirring, the volatiles were removed *in vacuo* to yield **4.7** (0.2116 g, 0.159 mmol, 91 %) as a bright yellow solid. ¹H NMR (CD₂Cl₂, 400 MHz): δ 8.74 (d, ³J_{HH} = 7.8 Hz, 2H, ArH), 7.22 (t, ³J_{HH} = 7.8 Hz, 1H, ArH), 7.15 (s, 4H, ArH), 6.92 (s, 4H, ArH), 6.89 (s, 4H, ArH), 6.81 (s, 4H, ArH), 2.73 (m, 16H, TBA), 2.27 (s, 12H, ArCH₃), 2.20 (s, 12H, ArCH₃), 1.40 (m, 16H, TBA), 1.25 (m, 16H, TBA), 0.93 (t, ³J_{HH} = 7.3 Hz, 24H, TBA). ¹³C{¹H} NMR (CD₂Cl₂): δ 192.57 (s, Zr-C_{ipso}), 158.34, 139.98, 137.38, 137.19, 136.57, 136.19, 134.13, 133.78, 130.39, 129.47, 129.04, 128.70, 127.35, 125.56, 58.82, 24.36, 21.60, 21.55, 21.47, 20.07, 14.01. ¹¹B NMR (CD₂Cl₂): -19.46 (br s, Δν_{1/2} ≈ 700 Hz). Anal. Calcd for C₇₆H₁₁₇B₂Cl₃N₆Zr: C, 68.43; H, 8.84; N, 6.30. Found C, 68.20; H, 8.69; N, 6.01.

Zr(NCN-(SiMe₃)₂)I₂Cl (4.12). Trimethylsilyl iodide (0.11 mL, 0.77 mmol, 5.0 equiv) was added to a stirring solution of **4.3** (201.3 mg, 0.154 mmol, 1.0 equiv) in CH₂Cl₂ (10 mL). The solution stirred for 4 hours, the the volatiles were removed *in vacuo*. The residue was extracted through Celite with toluene until the filtrate ran colorless. The filtrate was concentrated to dryness, then the residue was slurried in pentane (8 mL) and stirred vigorously for 10 minutes. The suspension was filtered, then the solid was rinsed with pentane (3 x 4 mL) and dried *in vacuo* to give crude **4.11** (117.9 mg, *ca.* 0.1 mmol, *ca.* 66 %) as a bright yellow solid. NMR analysis indicated that the solid contained approximately 9 % of an NCN-containing impurity. ¹H NMR (CD₂Cl₂, 500 MHz): δ 7.62 (d, ³J_{HH} = 7.6 Hz, 2H, ArH), 7.45 (t, ³J_{HH} = 7.6 Hz, 1H, ArH), 7.30 (s, 4H, ArH), 7.08 (s, 4H, ArH), 7.02 (s, 2H, ArH), 6.90 (s, 2H, ArH), 2.30 (s, 12H, ArCH₃), 2.25 (s, 12H, ArCH₃), 0.39 (s, 18H, Si(CH₃)₃). ¹H NMR, impurities (CD₂Cl₂, 500 MHz): δ 7.34 (s, 0.2H), 7.14–7.26 (m, 1.2H), 3.17 (m, 0.3H, TBA), 2.34 (s, 1.2H), 1.63 (m, 0.4H, TBA), 1.43 (m, 0.4H, TBA), 1.02 (t, 0.5H, TBA). ¹³C{¹H} NMR (CD₂Cl₂): δ 193.95 (s, Zr-C_{ipso}), 163.00, 140.16, 138.54, 137.98, 136.52, 135.75, 131.76, 131.24, 131.00, 130.97, 130.82, 129.28, 126.85, 125.93, 21.60, 21.49, 3.31.

[Zr(NCN)(NMe₂)₂]Na(15-crown-5) (4.17). A solid mixture of **4.1** (1.5105 g, 1.878 mmol, 1.0 equiv) and NaH (45.4 mg, 1.892 mmol, 1.0 equiv) was suspended in THF (45 mL) with stirring. After 3 hours, 15-crown-5 (0.38 mL, 1.913 mmol, 1.0 equiv) was added, causing the cloudy mixture to clear. After stirring an additional 25 minutes, the solution was concentrated to dryness under vacuum. The residue was dissolved in CH₂Cl₂ (30 mL), then pentane (40 mL) was added, resulting in precipitation of a white

powder. The powder was collected by vacuum filtration, rinsed with excess pentane, and then dried *in vacuo* to yield [Zr(NCN)(NMe₂)₂]Na(15-crown-5) (1.3354 g, 1.276 mmol, 67.9 %) as a white powder. ¹H NMR (CD₂Cl₂, 400 MHz): δ 7.40 (d, ³J_{HH} = 7.5 Hz, 2H, ArH), 7.16 (t, ³J_{HH} = 7.5 Hz, 1H, ArH), 7.15 (s, 4H, ArH), 6.89 (s, 6H, overlapping ArH), 6.68 (s, 2H, ArH), 3.32 (s, 20H, 15-crown-5), 2.46 (s, 12H, -NMe₂), 2.29 (s, 12H, ArCH₃), 2.17 (s, 12H, ArCH₃). ¹³C{¹H} NMR (CD₂Cl₂, 53.80): δ 183.53 (s, Zr-C_{ipso}), 161.98, 143.51, 138.16, 137.99, 137.63, 137.34, 137.20, 136.82, 128.72, 128.40, 127.74, 126.30, 124.87, 117.97, 68.47, 38.43, 21.68, 21.47. Anal. Calcd. for C₅₈H₇₁N₆NaO₅Zr: C, 66.57; H, 6.84; N, 8.03. Found C, 65.51; H, 6.51; N, 7.29.

In-situ complexes

[Zr(NCN-(BH₃)₂)ClF₂]TBA₂ (**4.8**). Solid **4.5** (8.3 mg, 0.0065 mmol, 1.0 equiv) was dissolved in CH₂Cl₂ (1.0 mL) at -35 °C, then 94 % BH₃·SMe₂ (1.4 μL, 0.014 mmol, 2.2 equiv) was added *via* syringe to the stirring solution. After stirring for 20 minutes, the volatiles were removed and the residue was dissolved in CD₂Cl₂ (0.7 mL). NMR analysis indicated the formation of **4.8** as the major product. ¹H NMR (CD₂Cl₂, 500 MHz): δ 8.66 (d, ³J_{HH} = 7.8 Hz, 2H, ArH), 7.21 (t, ³J_{HH} = 7.8 Hz, 1H, ArH), 7.05 (s, 4H, ArH), 6.92 (s, 6H, ArH), 6.79 (s, 2H, ArH), 2.70 (m, 19H, TBA), 2.28 (s, 12H, ArCH₃), 2.18 (s, 12H, ArCH₃), 1.33 (m, 19H, TBA), 1.17 (s, 19H, TBA), 0.89 (t, ³J_{HH} = 7.3 Hz). ¹¹B NMR (CD₂Cl₂): -19.97 (br s, Δv_{1/2} ≈ 700 Hz) ¹⁹F{¹H} NMR: δ 44.77 (s).

[Zr(NCN-(BF₃)₂)Cl₃]TBA₂ (**4.9**). A solution of **4.3** (14.2 mg, 0.011 mmol, 1.0 equiv) in CH₂Cl₂ (2 mL) was frozen. Immediately upon thawing, BF₃·Et₂O (2.9 μL,

0.023 mmol, 2.1 equiv) was added via syringe to the stirring solution. The yellow color of the solution faded to colorless in *ca.* 2 minutes. After 5 minutes of stirring, the volatiles were removed *in vacuo*. NMR analysis of the resulting residue indicated that [Zr(NCN-(BF₃)₂)Cl₃]TBA₂ (**4.8**) was the major product, with a variety of other peaks being observed that corresponded to various NCN byproducts. ¹H NMR (CD₂Cl₂, 400 MHz): δ 8.23 (d, ³J_{HH} = 7.6 Hz, 2H, ArH), 7.18 (t, ³J_{HH} = 7.6 Hz, 1H, ArH), 7.11 (s, 4H, CH₃), 6.92 (s, 4H), 6.89 (s, 2H, ArH), 6.83 (s, 2H, ArH), 2.78 (m, TBA), 2.25 (s, 12H, ArCH₃), 2.19 (s, 12H, ArCH₃), 1.42 (m, TBA), 1.27 (m, TBA), 0.95 (t, ³J_{HH} = 7.3 Hz, TBA). ¹⁹F NMR (CD₂Cl₂): δ -137.16 (q, ¹J_{F-B} = 17.3 Hz, 77 % of total ¹⁹F signal). ¹⁹F{¹¹B} NMR (CD₂Cl₂): δ -137.16 (s). ¹¹B NMR (CD₂Cl₂): δ 0.16 (*pseudo*-q, ¹J_{B-F} = 15.9 Hz).

4.9.4 Silylation Reactions

Silylation reactions of 4.3:

2 equiv TMSI.

Method A: Neat TMSI (3.4 μL, 0.024 mmol, 2.2 equiv) was added to a stirring – 35 °C solution of **4.3** (14.9 mg, 0.011 mmol, 1.0 equiv). After stirring for 1 h at ambient temperature, ¹H NMR analysis indicated the formation of Zr(NCN-(SiMe₃)₂)Cl₃ (**4.10**) as the major product with other impurities observed. ¹H NMR (CD₂Cl₂, 300 MHz): δ 7.62 (d, ³J_{HH} = 7.7 Hz, 2H, ArH), 7.37 (t, ³J_{HH} = 7.7 Hz, 1H, ArH), 7.19 (s, 2H, ArH), 7.04 (s, 6H, ArH), 6.91 (s, 6H, ArH), 2.30 (s, 12H, ArCH₃), 2.23 (s, 12H, ArCH₃), 0.40 (s, 18H, Si(CH₃)₃).

Method B: Neat TMSI (29.0 μL , 0.204 mmol, 2.0 equiv) was added to a stirring just-thawed solution of **4.3** (0.1334 g, 0.102 mmol, 1.0 equiv) in CH_2Cl_2 (10 mL) inside of a 20 mL glass vial. The solution was stirred at ambient temperature for 2 minutes, then moved to a $-35\text{ }^\circ\text{C}$ freezer. The reaction vial was periodically removed and stirred for *ca.* 20 seconds, at which point the vial was returned to the freezer. After 1 hour, the solvent was removed *in vacuo*, then the orange-yellow residue was extracted with Et_2O (5 x 10 mL) and filtered through a sintered glass frit. The filtrate was concentrated to dryness and was determined contain several NCN products and TBA cation as judged by ^1H NMR spectroscopy. The Et_2O -insoluble filter cake was dissolved in CH_2Cl_2 (3 mL) to give an orange solution, which was then diluted with Et_2O (10 mL) and cooled to $-35\text{ }^\circ\text{C}$, resulting in the formation of a white precipitate. The mixture was filtered through a sintered glass frit and the filtrate was concentrated to dryness. ^1H NMR analysis of the residue revealed the presence of 2-3 unidentified products as judged by the ArCH_3 resonances.

5 equiv TMSI.

Method A: Neat TMSI (4.4 μL , 0.031 mmol, 5.1 equiv) was added *via* syringe to a solution of **4.3** (8.0 mg, 0.0061 mmol, 1.0 equiv) inside of a J. Young tube. The solution was mixed well and the reaction progress was monitored by ^1H NMR spectroscopy. 25 minutes: 13 % **4.10**, 43 % **4.11**, 43 % **4.12**, and 1.38 equiv TMSCl relative to the total $\text{Si}(\text{CH}_3)_3$ integrations of **4.10-4.12**. 3 hours 45 minutes: trace **4.10**, 17 % **4.11**, 83 % **4.12**, and 1.71 equiv TMSCl. 6 hours: no change in the reaction composition was observed. ^1H NMR (CD_2Cl_2 , 500 MHz, **4.11**): δ 7.63 (d, $^3J_{\text{HH}} = 7.6\text{ Hz}$,

2H, ArH), 7.42 (t, $^3J_{\text{HH}} = 7.6$ Hz, 1H, ArH), 7.25 (s, 2H, ArH), 7.06 (s, 4H, ArH), 7.03 (s, 2H, ArH) 6.92 (s, 2H, ArH), 2.30 (s, 12H, ArCH₃), 2.24 (s, 12H, ArCH₃), 0.39 (s, 18H, Si(CH₃)₃).

Method B: Solid **4.3** (8.9 mg, 0.0068 mmol, 1.0 equiv) was measured into a J. Young tube and suspended in C₆D₆ (0.8 mL). Neat TMSI (9.7 μ L, 0.068 mmol, 10.0 equiv) was added to the suspension *via* syringe. The reaction was placed in a 60 °C oil bath for 15 hours. ¹H NMR spectroscopy indicated the clean formation of **4.12** and 2 equiv TMSCl. The solution was frozen and the overlying atmosphere was removed *in vacuo*, then the reaction was placed in a 95 °C oil bath for 6 hours. ¹H NMR spectroscopy revealed no change in the product composition. ¹H NMR (C₆D₆, 500 MHz): δ 7.75 (s, 4H, ArH), 7.61 (d, $^3J_{\text{HH}} = 7.8$ Hz, 2H, ArH), 7.32 (t, $^3J_{\text{HH}} = 7.8$ Hz, 1H, ArH), 6.84 (s, 4H, ArH), 6.78 (s, 2H, ArH), 6.58 (s, 2H, ArH), 2.20 (s, 12H, ArCH₃), 1.99 (s, 12H, ArCH₃), 0.16 (s, 18H, Si(CH₃)₃).

5 equiv TMSOTf.

Neat TMSOTf (7.9 μ L, 0.044 mmol, 5.1 equiv) was added *via* syringe to a solution of **4.3** (11.4 mg, 0.0087 mmol, 1.0 equiv) in CD₂Cl₂ (0.7 mL) inside of a J. Young tube. The solution was mixed well and the reaction progress was monitored by ¹H NMR spectroscopy. 20 minutes: 2 products in a 1:1 ratio, 1.0 equiv TMSCl. Distinctive features of ¹H NMR (CD₂Cl₂, 500 MHz): δ 7.65 (d, $^3J_{\text{HH}} = 7.8$ Hz, 2H, ArH), 7.65 (d, $^3J_{\text{HH}} = 7.8$ Hz, 2H, ArH), 7.45 (t, $^3J_{\text{HH}} = 7.8$ Hz, 1H, ArH), 7.41 (t, $^3J_{\text{HH}} = 7.8$ Hz, 1H, ArH), 0.38 (s, 18H, Si(CH₃)₃), 0.37 (s, 18H, Si(CH₃)₃). 3 hours 40 minutes: **4.13** and 1

equiv TMSCl. 6 hours: 89 % **4.13**, 11 % **4.14**, 1.3 equiv TMSCl. 2 days: 62 % **4.13**, 38 % **4.14**, 1.5 equiv TMSCl. ^1H NMR (CD_2Cl_2 , 500 MHz, **4.13**): δ 7.65 (d, $^3J_{\text{HH}} = 7.8$ Hz, 2H, ArH), 7.45 (t, $^3J_{\text{HH}} = 7.8$ Hz, 1H, ArH), 7.20 (s, 4H, ArH), 7.09 (br s, 4H, ArH), 7.01 (s, 2H, ArH), 6.86 (s, 2H, ArH), 2.30 (s, 12H, ArCH₃), 2.21 (s, 12H, ArCH₃), 0.37 (s, 18H, Si(CH₃)₃). ^1H NMR (CD_2Cl_2 , 500 MHz, **4.14**): δ 7.65 (d, $^3J_{\text{HH}} = 7.8$ Hz, 2H, ArH), 7.49 (t, $^3J_{\text{HH}} = 7.8$ Hz, 1H, ArH), 7.07 (s, 4H, ArH), 7.06 (br s, 4H, ArH), 7.02 (s, 2H, ArH), 6.86 (s, 2H, ArH), 2.30 (s, 12H, ArCH₃), 2.20 (s, 12H, ArCH₃), 0.38 (s, 18H, Si(CH₃)₃).

5 equiv TMSBr.

Neat TMSBr (5.2 μL , 0.039 mol, 5.0 equiv) was added *via* syringe to a solution of **4.3** (10.2 mg, 0.0078 mmol, 1.0 equiv) in CD_2Cl_2 (0.7 mL) inside of a J. Young tube, and the reaction progress was monitored by ^1H NMR spectroscopy. 30 min: at least 2 products seen with distinctive ^1H NMR resonances at δ 7.3(d, $^3J_{\text{HH}} = 7.8$ Hz, 2.2H, ArH), 2.30 (s, 11.3H, ArCH₃), 2.29 (s, 6.4H, ArCH₃), 2.26 (s, 4.9H, ArCH₃), 2.24 (s, 4.8H, ArCH₃), 2.23 (s, 12.0H, ArCH₃), 2.21 (s, 5.2H, ArCH₃), 0.58 (s, 24.7H, TMSBr) 0.43 (s, 26.6H, TMSCl), 0.40 (s, 18.2H, Si(CH₃)₃), 0.37 (s, 7.3H, Si(CH₃)₃). 2 h 40 min: a slight change in the product ratios was observed. 9 h 30 min: no change was observed.

Silylation of 4.5:

TMSOTf

Neat TMSOTf (6.2 μL , 0.034 mmol, 5.1 equiv) was added *via* syringe to a solution of **4.5** (8.5 mg, 0.0067 mmol, 1.0 equiv) in CD_2Cl_2 (0.7 mL) inside of a J. Young

tube, causing an immediate color change from colorless to bright yellow. After 20 minutes, ^1H NMR analysis indicated clean conversion to **4.14** and 2 equiv TMSF. The volatiles were removed *in vacuo*, then the residue was dissolved in CD_2Cl_2 (0.7 mL). ^1H NMR analysis revealed partial decomposition to unknown products.

TMSBr

Neat TMSBr (3.4 μL , 0.026 mmol, 5.0 equiv) was added *via* syringe to a solution of **4.5** (6.6 mg, 0.0052 mmol, 1.0 equiv) in CD_2Cl_2 (0.7 mL) inside of a J. Young tube, causing an immediate color change from colorless to bright yellow. After 30 min, ^1H NMR spectroscopy indicated a similar spectrum to that observed for **4.3** + TMSBr, with a product ratio near 1:1. 4 h: no change was observed.

Silylation of 4.1:

Method A: Neat TMSI (23.1 μL , 0.16 mmol, 14.8 equiv) was added to a stirring solution of **4.1** in CH_2Cl_2 (1.0 mL). After stirring overnight, the clear yellow solution was concentrated to dryness and the residue dried *in vacuo*. ^1H NMR analysis of the residue indicated the clean formation of $\text{Zr}(\text{NCN}-(\text{SiMe}_3)_2)\text{Cl}_3$ (**4.15**) and $[\text{Me}_3\text{SiN}(\text{H})\text{Me}_2]\text{I}$ in a 1:1 ratio. ^1H NMR (CD_2Cl_2 , 500 MHz, **4.15**): δ 7.62 (d, $^3J_{\text{HH}} = 7.5$ Hz, 2H, ArH), 7.45 (t, $^3J_{\text{HH}} = 7.7$ Hz, 1H, ArH), 7.31 (s, 4H, ArH), 7.08 (s, 4H, ArH), 7.02 (s, 2H, ArH), 6.90 (s, 2H, ArH), 2.30 (s, 12H, ArCH₃), 2.25 (s, 12H, ArCH₃), 0.39 (s, 18H, Si(CH₃)₃). ^1H NMR (CD_2Cl_2 , 500 MHz, $[\text{Me}_3\text{SiN}(\text{H})\text{Me}_2]\text{I}$): δ 9.41 (br s, 1H, NH), 2.57 (br s, 6H, N(CH₃)₂), 0.54 (br s, 9H, Si(CH₃)₃).

Method B: Neat TMSI (0.68 mL, 4.79 mmol, 15.0 equiv) was added *via* syringe to a suspension of **4.1** (0.2572 g, 0.320 mmol, 1.0 equiv) in C₆H₆ (5 mL). After stirring for 22 hours, the solution was lyophilized and dried *in vacuo*. The resulting bright yellow solid was extracted through sintered glass frit with CH₂Cl₂ and the filtrate was concentrated to dryness. ¹H NMR analysis of the residue indicated significant decomposition.

Silylation of 4.16:

Neat TMSI (0.40 mL, 2.81 mmol, 14.9 equiv) was added *via* syringe to a stirring solution of **4.16** (0.1979 g, 0.189 mmol, 1.0 equiv) in CH₂Cl₂ (10 mL). The solution was stirred overnight, then the volatiles were removed *in vacuo*. The residue was washed with excess Et₂O and dried *in vacuo*. ¹H NMR spectroscopy identified the yellow solid as **4.15** containing a large signal for a 15-crown-5 product at δ 3.73 ppm. Analysis of the filtrate revealed the presence of both **4.15** and 15-crown-5.

4.9.5 Other Reactions

Reaction of 4.12 with TBACl

Method A: Solid TBACl (7.0 mg, 0.025 mmol, 1.9 equiv) was added to a solution of **4.12** (15.0 mg, 0.013 mmol, 1.0 equiv) in CD₂Cl₂ (0.7 mL) with stirring. After 35 minutes, ¹H NMR analysis indicated the formation of **4.10** in a 2:1 ratio with a second unidentified product. Only trace amounts of TMSCl were observed at δ 0.43 ppm.

Method B: A solid mixture of **4.1** (7.0 mg, 0.0061 mmol, 1.0 equiv) and TBACl (12.2 mg, 0.044 mmol, 7.2 equiv) was dissolved in CD₂Cl₂ (0.7 mL) with stirring. After 15 minutes, ¹H NMR analysis indicated the clean formation of **4.3** with TMSCl as the only observable TMS-containing product.

Reaction between 4.1, TBAI, and [HNⁱPr₂Et]I

Solid TBAI (8.2 mg, 0.022 mmol, 2.0 equiv) was added to a stirring solution of **4.1** (8.7 mg, 0.011 mmol, 1.0 equiv) in CH₂Cl₂ (1.0 mL). After five minutes the solution color had changed from near colorless to yellow. Solid [HNⁱPr₂Et]I (2.8 mg, 0.011 mmol, 1.0 equiv) was added to the solution, causing a color change to orange. After stirring 4 h 30 m, the volatiles were removed *in vacuo*. ¹H NMR analysis of the residue indicated 5 broad overlapping peaks in the xylyl region of δ 1.90 – 2.30 ppm.

Attempts at fluorine exchange of 4.3.

AgPF₆: In the dark, a solid mixture of **4.3** (17.6 mg, 0.014 mmol, 1.0 equiv) and AgPF₆ (3.3 mg, 0.013 mmol, 1.0 equiv) was dissolved in CD₂Cl₂ (1.0 mL) with stirring. After 3 hours, ¹H NMR analysis indicated extensive decomposition to unknown products.

3 equiv AgPF₆: In the dark, a solid mixture of **4.3** (16.3 mg, 0.013 mmol, 1.0 equiv) and AgPF₆ (10.0 mg, 0.040 mmol, 3.2 equiv) was dissolved in CD₂Cl₂ (1.0 mL) with stirring. After 30 minutes, ¹H NMR analysis indicated extensive decomposition to unknown products. Only PF₆⁻ was observed in the ³¹P{¹H} and ¹⁹F NMR spectra.

AgBF₄: In the dark, a solid mixture of **4.3** (20.5 mg, 0.016 mmol, 1.0 equiv) and AgBF₄ (3.4 mg, 0.018 mmol, 1.1 equiv) was dissolved in CD₂Cl₂ (1.0 mL) with stirring. After 3 hours, ¹H NMR analysis indicated extensive decomposition to unknown products.

3 equiv [TBA][PF₆]: A solid mixture of **4.3** (10.9 mg, 0.0083 mmol, 1.0 equiv) and [TBA][PF₆] (9.7 mg, 0.025 mmol, 3.0 equiv) was dissolved in CD₂Cl₂ (0.8 mL) with stirring. After 30 minutes, ¹H NMR analysis indicated no reaction had occurred. The solution was transferred to a J. Young tube and heated in a 40 °C oil bath overnight. ¹H NMR analysis again indicated no reaction had occurred.

3 equiv Ph₃SnF: In CD₂Cl₂: Solid Ph₃SnF (11.9 mg, 0.032 mmol, 3.2 equiv) was added to a solution of **4.3** (13.2 mg, 0.010 mmol, 1.0 equiv) in CD₂Cl₂ (0.8 mL) with stirring. Polymeric Ph₃SnF was gradually dispersed during the course of the reaction. After 2.5 hours, ¹H and ¹⁹F NMR analysis indicated the formation of multiple unknown products. No improvement was observed after 6 hours. In CH₂Cl₂ / THF: A solution of **4.3** (9.7 mg, 0.0074 mmol, 1.0 equiv) in CH₂Cl₂ (1.0 mL) was added to a suspension of Ph₃SnF (8.9 mg, 0.024 mmol, 3.2 equiv) in THF (1.0 mL). The mixture was mixed well by pipet and stirred. After 2.5 hours, no signal was observed in the ¹⁹F NMR spectrum. The mixture was stirred overnight, then the volatiles were removed *in vacuo*. ¹H NMR analysis of the residue displayed a single ArCH₃ at δ 1.83 ppm, suggesting that the NCN ligand was no longer coordinated to Zr.

Attempts to synthesize Zr(NCN-Me₂)F₂Cl

Method A: Neat MeI (1.6 μ L, 0.026 mmol, 5.0 equiv) was added to a solution of **4.5** (6.5 mg, 0.0051 mmol, 1.0 equiv) in CH₂Cl₂ (0.7 mL). After stirring for 45 minutes, the volatiles were removed *in vacuo*. ¹H and ¹⁹F NMR analysis indicated the presence of **4.5** and a monomethylated product in a 1:2.5 ratio. Identifying peaks of new product: ¹H NMR (CD₂Cl₂): δ 7.63 (d, 1H, ArH), 7.43 (d, 1H ArH), 3.78 (s, 3H, NCH₃). ¹⁹F NMR (CD₂Cl₂): 44.70. Additional MeI (2.0 μ L, 0.0321 mmol, 6.3 equiv) was added to the solution. After stirring 3 hours, ¹H NMR analysis indicated extensive decomposition.

Method B: Solid Cp₂TiF₂ (4.8 mg, 0.025 mmol, 2.7 equiv) was added to a solution of **4.6** (7.9 mg, 0.0093 mmol, 1.0 equiv) in CD₂Cl₂ (0.7 mL). After 45 minutes of stirring, ¹H and ¹⁹F NMR indicated extensive decomposition.

Attempted reactions between 4.3 and BX₃ / AlEt₃

BCl₃: A solution of BCl₃ (1.0 M in heptane, 20.0 μ L, 0.020 mmol, 2.0 equiv) was added to a solution of **4.3** (13.1 mg, 0.010 mmol, 1.0 equiv) in CD₂Cl₂ (1.0 mL). After 15 minutes, ¹H NMR analysis indicated extensive decomposition.

BEt₃: A solution of BEt₃ (1.0 M in hexane, 14.7 μ L, 0.015 mmol, 2.0 equiv) was added to a solution of **4.3** (9.6 mg, 0.0074 mmol, 1.0 equiv) in CD₂Cl₂ (0.8 mL). After 30 minutes, ¹H NMR analysis indicated that no reaction had occurred.

B(OMe)₃: Neat B(OMe)₃ (1.4 μL, 0.012 mmol, 2.0 equiv) was added to a solution of **4.3** (7.8 mg, 0.0060 mmol, 1.0 equiv) in CD₂Cl₂ (0.8 mL). After 30 minutes, ¹H NMR analysis indicated that no reaction had occurred.

AlEt₃: A solution of AlEt₃ (1.0 M in hexane, 15.3 μL, 0.015 mmol, 2.0 equiv) was added to a solution of **4.3** (10.0 mg, 0.0077 mmol, 1.0 equiv) in CD₂Cl₂ (0.8 mL). After 30 minutes, ¹H NMR analysis indicated extensive decomposition.

4.9.6 Computational Details

Calculations were carried out at the DFT level, employing the commonly used B3LYP functional⁸⁻¹⁰ and the LACV3P*+ basis set.⁷ The Jaguar 7.0 package⁶ was used to implement the calculations. Coordinates for all atoms in the optimized structures are detailed in the Appendix 7. All geometry optimizations ground state structures were confirmed by calculation of the vibrational frequencies. All structures were found to be at a ground state with the sole exception of **4.21**, which possessed 1 imaginary frequency at -8.25 cm⁻¹. All Δ*G* values were corrected for zero-point energies. The NBO 5.0 program,¹⁴ included with Jaguar 7.0, was used for the NPA analysis and the determination of the donor-acceptor stabilization energies. The listed D-A energies were tabulated by the summation of all lp donations into Zr lp* and Ry* orbitals.

4.10 References

1. Itzia Irene Padilla-Martínez; Armando Ariza-Castolo; Rosalinda Contreras, *Magn. Reson. Chem.* **1993**, *31*, 189-193.
2. Huheey, J. E., *J. Phys. Chem.* **1965**, *69*, 3284-3291.
3. Nifant'ev, E. E.; Gratchev, M. K.; Burmistrov, S. Y.; Vasyanina, L. K.; Antipin, M. Y.; Struchkov, Y. T., *Tetrahedron* **1991**, *47*, 9839-9860.
4. Cottrell, T. L., *The Strengths of Chemical Bonds*. 2nd ed.; Butterworths: London, 1958.
5. Schaefer, T.; Sebastian, R.; Salman, S. R., *Can. J. Chem.* **1981**, *59*, 3026-3029.
6. Jaguar, v. *Jaguar 7.0*, Schrodinger, LLC: New York, NY, 2007.
7. Hay, P. J.; Wadt, W. R., *Journal of Chemical Physics* **1985**, *82*, 299-310.
8. Becke, A. D., *Journal of Chemical Physics* **1993**, *98*, 5648-5652.
9. Vosko, S. H.; Wilk, L.; Nusair, M., *Canadian Journal of Physics* **1980**, *58*, 1200-1211.
10. Lee, C. T.; Yang, W. T.; Parr, R. G., *Physical Review B* **1988**, *37*, 785-789.
11. Reed, A. E.; Weinstock, R. B.; Weinhold, F., *J. Chem. Phys.* **1985**, *83*, 735-746.
12. Chen, S.; Chisholm, M. H.; Davidson, E. R.; English, J. B.; Lichtenberger, D. L., *Inorg. Chem.* **2008**, *48*, 828-837.
13. Foster, J. P.; Weinhold, F., *J. Am. Chem. Soc.* **1980**, *102*, 7211-7218.
14. Glendening, E. D.; Badenhoop, J. K.; Reed, A. E.; Carpenter, J. E.; Bohmann, J. A.; Morales, C. M.; Weinhold, F. *NBO 5.0*, Theoretical Chemistry Institute, University of Wisconsin: Madison, WI, 2001.
15. Weinhold, F.; Landis, C. R., *Valency and Bonding. A Natural Bond Orbital Donor-Acceptor Perspective*. Cambridge University Press: Cambridge, 2005.
16. Pangborn, A. B.; Giardello, M. A.; Grubbs, R. H.; Rosen, R. K.; Timmers, F. J., *Organometallics* **1996**, *15*, 1518-1520.
17. Seyam, A.; Hussein, S.; Hodali, H., *Gazz. Chim. Ital.* **1990**, *120*, 527-530.
18. Odom, A. L.; Cummins, C. C., *Organometallics* **1996**, *15*, 898-900.

Chapter 5

Conclusions and Future Directions

5.1 Conclusions

This work has focused on the development of nitrile-alkyne cross-metathesis (NACM) as a methodology for the construction of organic molecules. The utility of NACM was demonstrated in the synthesis of arylene ethynylene macrocycles, but the limited functional group tolerance of the W-based catalyst limited its practical application. These limitations led to the synthesis of a variety of new Mo nitride complexes and the discovery of the first Mo-based NACM catalyst. A new XXX pincer ligand was developed in order to lower the activation barrier for NACM, but full activation of the ligand proved challenging. Zirconium complexes containing an XXX ligand were found to undergo an unusual and rare charge-switching reaction when treated with Lewis acid synthons. Such charge-switching could ultimately allow for tuning of triple-bond metathesis catalyst reactivity. In an effort to extend XXX pincer ligation to Mo, a new XXX ligand precursor was developed and is anticipated to be more facily bound to Mo complexes.

5.2 Nitrile-Alkyne Cross Metathesis

Previous work detailed investigations of the mechanism of NACM catalyzed by $\text{N}\equiv\text{W}(\text{OC}(\text{CF}_3)_2\text{CH}_3)_3(\text{DME})$ (**5.1**) and $\text{N}\equiv\text{W}(\text{OCMe}_2\text{CF}_3)_3$ (**5.2**).^{1, 2} A substrate survey was undertaken in order to ascertain the tolerance of **5.1** and **5.2** for various functional groups. Catalyst sensitivity to protic and very polar groups was discovered, though thiophene substrates were surprisingly tolerated by the catalysts. Different modes of catalyst deactivation were observed for different substrates, with deactivation of either the nitride or alkylidyne complex occurring. Sterically hindered dinitrile substrates reacted very sluggishly with **5.1**, but the use of unhindered dinitrile substrates led to the formation of arylene ethynylene macrocycles. A carbazole-derived tetramer could be synthesized in three fewer steps than the best alternative route, which employs alkyne cross-metathesis (ACM).³

Molybdenum-based catalysts were proposed as a means of expanding the range of functional groups tolerated in NACM. In order to overcome the higher activation barrier to metalacycle formation that is associated with Mo,⁴ thermally robust ancillary ligands were chosen for investigation. Amido complexes of the form $\text{N}\equiv\text{Mo}(\text{NR}'\text{R}'')_3$ were found to undergo protonolysis with bulky alcohols (HOR ; $\text{R} = \text{SiPh}_3, \text{SiPh}_2^t\text{Bu}, 2,6\text{-}^i\text{Pr}_2\text{C}_6\text{H}_3$) to afford a variety of tris-alkoxide complexes $\text{N}\equiv\text{Mo}(\text{OR})_3(\text{L})$ ($\text{L} = \text{NHMe}_2$, vacant coordination site). Steric constraints were found to play a role in the protonolysis reactions, as subtle changes in size affected whether the desired complexes were formed.

Upon investigating the NACM activity of the new nitride complexes, $\text{N}\equiv\text{Mo}(\text{OSiPh}_3)_3$ (**5.3**) was found to mediate NACM at 180 °C. Two observations indicated the importance of catalyst concentration. First, the conversions to NACM

products increased at higher catalyst concentrations. Second, NACM activity was observed to cease prior to complete catalyst decomposition. Even when performing NACM at a catalyst concentration of 40 mg mL^{-1} , only slightly more than two catalyst turnovers were achieved. Most importantly, other nitride and alkylidyne complexes were not active for NACM under similar conditions, which indicates that the triphenylsiloxide ligand has both a proper electron donor strength and thermal stability to allow NACM to occur.

5.3 XXX Pincer Ligand Development

A means to drastically lower the operating temperature of Mo-catalyzed NACM was desired in order to make NACM more practical. It was anticipated that a trianionic (XXX) pincer ligand would lower the energy barrier for metalacycle formation by tethering the ancillary ligands into the geometry required for azametallacyclobutadiene formation.² To this end, an NCN-H₃ (**5.4**) ligand precursor was designed and prepared. Activation of **5.4** by Mo complexes proved challenging and was not achieved. A variety of ligand derivatives were prepared, allowing for the *in-situ* formation of an XXX-Mg₃ (**5.5**) species. Unexpectedly, the reactivity of **5.5** with metal substrates was found to be very low. One hypothesis is that oligomeric (XXX-Mg-)_n species form which are too sterically hindered to allow the approach of metal substrates. A second possibility is that the hard-hard N-Mg coordination of **5.5** is relatively favorable, thus limiting the desired metal substitution.

Zr(NMe₂)₄ was discovered to successfully activate **5.4**. Upon proper ancillary ligand transformation, [TBA]₂[Zr(XXX)Cl₃] (**5.6**) could be obtained. X-ray diffraction

analysis confirmed the tridentate coordination of the NCN ligand. An interesting reactivity of **5.6** was observed, in which the XXX ligand could be directly transformed into an LXL ligand through interaction of the peripheral imidazole N-atom with a Lewis acid. A formal charge-switching transformation could be effected using synthons of CH_3^+ , BH_3 , BF_3 , and SiMe_3^+ . The trimethylsilyl group was found to be removed under mild conditions through the addition of chloride ion, returning an XXX ligand from an LXL ligand.

An investigation of the change in pincer ligand electron donor strength as a function of LXL identity was undertaken. ^{19}F NMR spectroscopy was anticipated to be a useful spectroscopic means of investigation. Therefore $[\text{TBA}]_2[\text{Zr}(\text{XXX})\text{ClF}_2]$ (**5.7**) was synthesized through halide metathesis of **5.6**. The presence of the fluoride ligands greatly limited the scope of the charge-switching transformation. However, the complex $[\text{TBA}]_2[\text{Zr}(\text{LXL}-(\text{BH}_3)_2)\text{ClF}_2]$ (**5.8**) was successfully formed through reaction of **5.7** with $\text{BH}_3\cdot\text{SMe}_2$. The ^{19}F NMR spectrum of **5.8** displayed a fluoride resonance that was deshielded by $\Delta(\delta)$ 6.6 ppm relative to **5.7**, which suggests less electron donation from the $\text{LXL}-(\text{BH}_3)_2$ ligand as compared to the XXX ligand. This trend was corroborated by DFT analysis of model complexes, though the exact effects of the Lewis acid identity on the electron donor strength could not be ascertained. Therefore, though some degree of electron donor strength fine-tuning may be possible, at present any variations would need to be examined on an individual basis.

At this point, research efforts were returned to the primary goal of using an XXX-pincer ligand to facilitate the NACM reaction. As the challenges encountered in activation of **5.4** often related to the necessary CH activation, it was expected that an

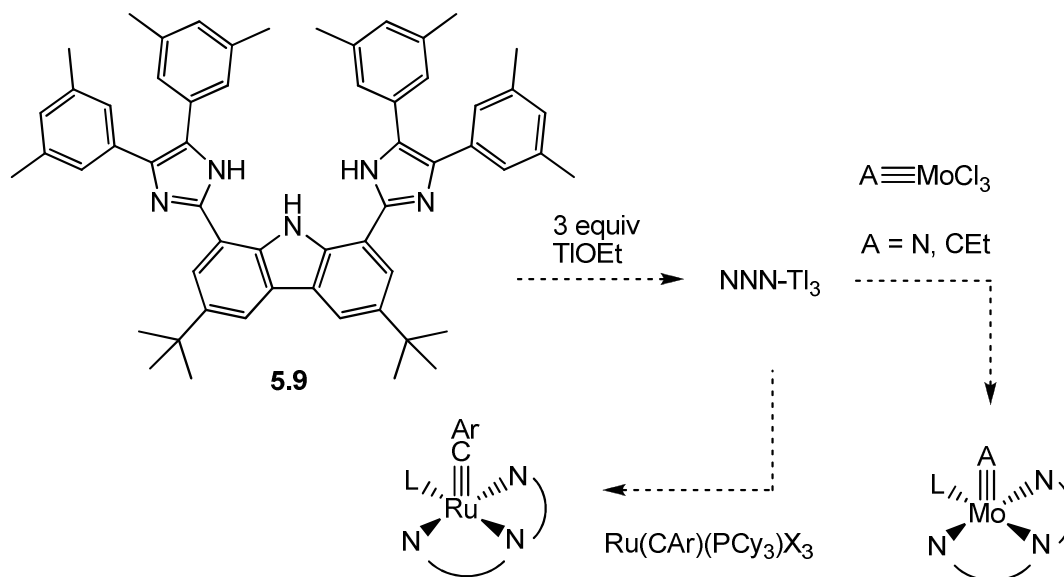
XXX-H₃ precursor with three acidic protons would facilitate XXX ligation with a variety of metals. Two separate synthetic routes to a bis-imidazole-pyrrole ligand were devised, but problems with reactivity and stability of key synthetic intermediates prevented the formation of the desired ligand precursor. An NNN-H₃ (**5.9**) ligand precursor was successfully obtained, with the backbone consisting of an imidazole-carbazole-imidazole linkage. Time constraints precluded investigations into the ligation of **5.9**, which remains for future work.

5.4 Future Directions

With the XXX-precursor **5.9** in-hand, immediate future studies should focus on the installation of **5.9** onto metal complexes. Both protonolysis and salt elimination pathways can be investigated. For a protonolysis pathway, **5.9** could be treated with N≡Mo(NMe₂)₃, N≡Mo(N^{*i*}Pr)Ar₃, or N≡Mo(N^{*t*}Bu)Ar₃ (Ar = 3,5-Me₂C₆H₃). Difficulties that may be encountered through this method include dimethylamine coordination or steric inhibition of the protonation, both of which were observed in Chapter 2 for monodentate ligands.

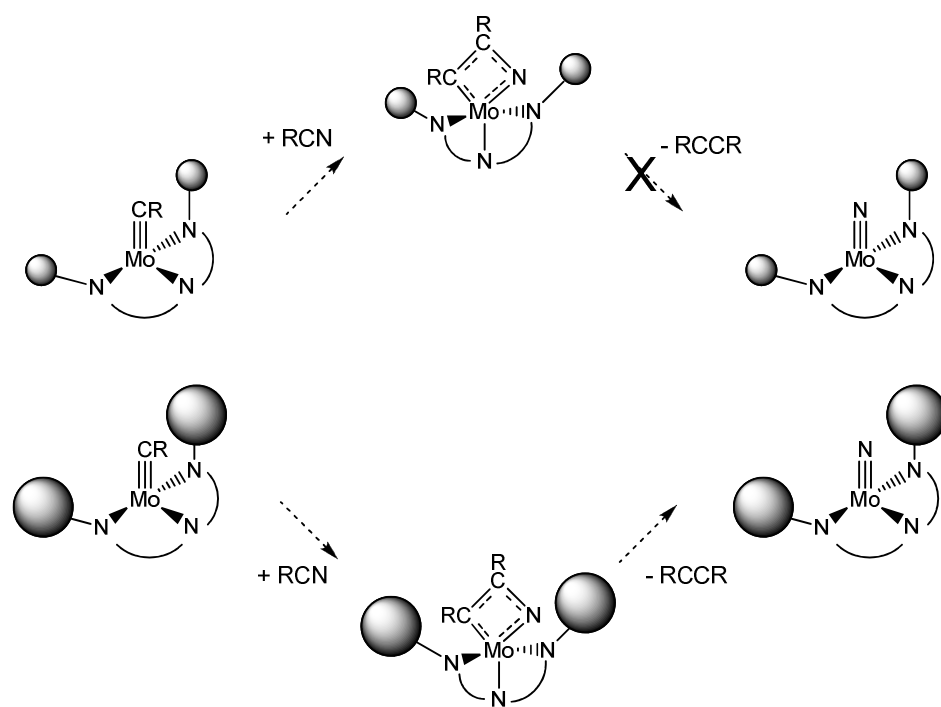
Salt elimination is perhaps a better method for the installation of **5.9** as an XXX ligand. Because of the three acidic N–H bonds, an NNN-Tl₃ complex should be readily formed from reaction of **5.9** with 3 equiv of TlOEt (Scheme 5.1). Metalation reactions of NNN-Tl₃ are expected to proceed readily due to the unfavorable hard-soft combination of N-Tl and to the precipitation of insoluble TlX products. Both EtC≡MoCl₃(DME) and [N≡MoCl₃]_n generated *in situ* are good candidates for ligation of a NNN-Tl₃ species. Additionally, this route could be extended to Ru alkylidyne species of the form

$\text{Ru}(\equiv\text{CAr})(\text{PCy}_3)\text{X}_3$ ($\text{X} = \text{Cl}, \text{Br}, \text{I}$) to afford new Ru alkylidyne complexes for ACM investigations.



Scheme 5.1. Use of NNN-Tl_3 as a pincer ligand transfer reagent.

Utilization of an XXX ligand in triple-bond metathesis may lead to an isolable metalacycle with a high energy barrier for cycloreversion. This situation would be unfavorable as it could lead to slower rates of NACM or no NACM at all. A potential remedy would be to increase the size of the pincer ligand, which would destabilize the metalacycle through steric pressure and make cycloreversion more favorable (Scheme 5.2). Given the route of synthesis for **5.9** (Chapter 3), it would be relatively simple to employ a larger benzil derivative to make a larger version of NNN-H_3 .



Scheme 5.2. Possible effect of NNN size on metathesis reactivity.

5.5 References

1. Geyer, A. M.; Gdula, R. L.; Wiedner, E. S.; Johnson, M. J. A., *J. Am. Chem. Soc.* **2007**, *129*, 3800-3801.
2. Geyer, A. M.; Wiedner, E. S.; Gary, J. B.; Gdula, R. L.; Kuhlmann, N. C.; Johnson, M. J. A.; Dunitz, B. D.; Kampf, J. W., *J. Am. Chem. Soc.* **2008**, *130*, 8984-8999.
3. Zhang, W.; Moore, J. S., *J. Am. Chem. Soc.* **2004**, *126*, 12796-12796.
4. Zhu, J.; Jia, G.; Lin, Z., *Organometallics* **2006**, *25*, 1812-1819.

Appendices

Appendix 1

Crystallographic Data for $\text{N}\equiv\text{Mo}(\text{OCPh}_2\text{Me})_3(\text{NHMe}_2)$

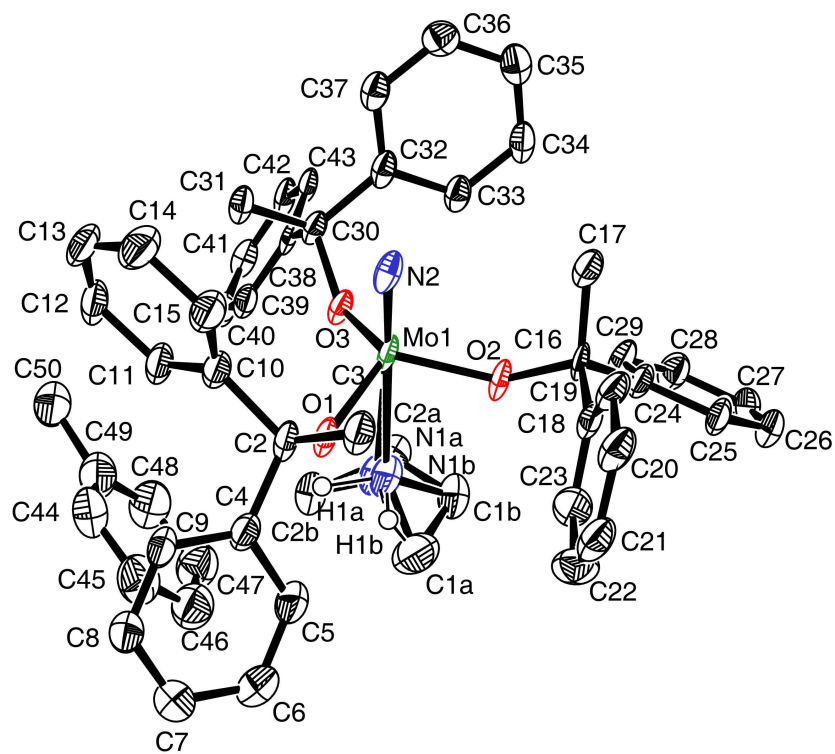


Figure A.1. 50 % thermal ellipsoid plot of $\text{N}\equiv\text{Mo}(\text{OCPh}_2\text{Me})_3(\text{NHMe}_2)$.

Structure Determination.

Colorless plates of **ew1352** were grown from a toluene/pentane solution at -35 °C. A crystal of dimensions $0.26 \times 0.14 \times 0.12$ mm was mounted on a Bruker SMART APEX CCD-based X-ray diffractometer equipped with a low temperature device and fine focus Mo-target X-ray tube ($\lambda = 0.71073$ Å) operated at 1500 W power (50 kV, 30 mA). The X-ray intensities were measured at 85(1) K; the detector was placed at a distance 5.055 cm from the crystal. A total of 3690 frames were collected with a scan width of 0.5° in ω and 0.45° in ϕ with an exposure time of 30 s/frame. The integration of the data yielded a total of 40336 reflections to a maximum 2θ value of 53.08° of which 8251 were independent and 6223 were greater than $2\sigma(I)$. The final cell constants (Table 1) were based on the xyz centroids of 9312 reflections above $10\sigma(I)$. Analysis of the data showed negligible decay during data collection; the data were processed with SADABS and corrected for absorption. The structure was solved and refined with the Bruker SHELXTL (version 2008/3) software package, using the space group $P1bar$ with $Z = 2$ for the formula $C_{44}H_{46}N_2O_3Mo \cdot (C_6H_8)_{0.5}$. All non-hydrogen atoms were refined anisotropically with the hydrogen atoms placed in idealized positions. The dimethylamine group is rotationally disordered over two equally occupied positions. The toluene solvate is located at an inversion center and is also disordered. Full matrix least-squares refinement based on F^2 converged at $R1 = 0.0673$ and $wR2 = 0.1519$ [based on $I > 2\sigma(I)$], $R1 = 0.0948$ and $wR2 = 0.1651$ for all data.

Sheldrick, G.M. SHELXTL, v. 2008/3; Bruker Analytical X-ray, Madison, WI, 2008.

Sheldrick, G.M. SADABS, v. 2008/1. Program for Empirical Absorption Correction of Area Detector Data, University of Gottingen: Gottingen, Germany, 2008.

Saint Plus, v. 7.53a, Bruker Analytical X-ray, Madison, WI, 2008.

Table 1. Crystal data and structure refinement for ew1352.

Identification code	ew1352
Empirical formula	C _{47.50} H ₅₀ Mo N ₂ O ₃
Formula weight	792.84
Temperature	85(2) K
Wavelength	0.71073 Å
Crystal system, space group	Triclinic, P-1
Unit cell dimensions	a = 10.9987(16) Å alpha = 87.778(2) deg. b = 12.6721(18) Å beta = 85.186(2) deg. c = 14.715(2) Å gamma = 78.835(2) deg.
Volume	2004.5(5) Å ³
Z, Calculated density	2, 1.314 Mg/m ³
Absorption coefficient	0.371 mm ⁻¹
F(000)	830
Crystal size	0.26 x 0.14 x 0.12 mm
Theta range for data collection	2.12 to 26.54 deg.
Limiting indices	-13<=h<=13, -15<=k<=15, -18<=l<=18
Reflections collected / unique	40336 / 8251 [R(int) = 0.0863]
Completeness to theta	= 26.54 99.1 %
Absorption correction	Semi-empirical from equivalents
Max. and min. transmission	0.9569 and 0.9098
Refinement method	Full-matrix least-squares on F ²

Data / restraints / parameters	8251 / 167 / 547
Goodness-of-fit on F ²	1.057
Final R indices [I > 2σ(I)]	R1 = 0.0673, wR2 = 0.1519
R indices (all data)	R1 = 0.0948, wR2 = 0.1651
Largest diff. peak and hole	1.082 and -1.319 e.Å ⁻³

Table 2. Atomic coordinates (× 10⁴) and equivalent isotropic displacement parameters (Å² × 10³) for ew1352. U(eq) is defined as one third of the trace of the orthogonalized U_{ij} tensor.

	x	y	z	U(eq)
Mo(1)	6190(1)	3143(1)	7226(1)	27(1)
N(1A)	6351(7)	3207(6)	8980(4)	52(2)
C(1A)	5628(10)	4151(8)	9501(7)	61(2)
C(2A)	7608(7)	2962(9)	9321(7)	57(2)
N(1B)	6329(9)	3352(6)	8953(4)	52(2)
C(1B)	7096(9)	4053(7)	9323(7)	54(2)
C(2B)	6314(12)	2385(7)	9543(7)	61(2)
O(1)	4594(3)	3082(2)	7773(2)	32(1)
O(2)	6635(3)	4497(2)	7304(2)	31(1)
O(3)	7482(3)	1973(2)	7445(2)	28(1)
N(2)	6000(3)	3039(3)	6101(3)	30(1)
C(2)	3443(4)	3011(3)	7385(3)	29(1)
C(3)	3077(4)	4018(3)	6777(3)	37(1)
C(4)	2459(4)	3041(3)	8183(3)	32(1)
C(5)	2425(4)	3757(4)	8881(3)	44(1)
C(6)	1525(5)	3822(4)	9605(4)	52(1)
C(7)	663(5)	3153(4)	9641(4)	50(1)
C(8)	684(4)	2453(4)	8955(3)	45(1)
C(9)	1581(4)	2391(3)	8236(3)	37(1)
C(10)	3625(4)	1962(3)	6870(3)	32(1)
C(11)	4155(4)	1007(3)	7312(4)	38(1)
C(12)	4289(4)	31(4)	6877(4)	45(1)
C(13)	3917(5)	-9(4)	6022(4)	52(2)
C(14)	3396(5)	930(4)	5575(4)	54(2)
C(15)	3252(4)	1916(4)	6001(4)	41(1)

C(16)	6647(4)	5452(3)	6733(3)	28(1)
C(17)	7147(4)	5157(3)	5765(3)	33(1)
C(18)	5303(4)	6082(3)	6792(3)	30(1)
C(19)	4673(4)	6436(3)	6037(3)	33(1)
C(20)	3427(4)	6950(3)	6118(4)	38(1)
C(21)	2823(4)	7106(4)	6973(4)	41(1)
C(22)	3453(4)	6781(4)	7740(4)	45(1)
C(23)	4686(4)	6270(4)	7651(4)	40(1)
C(24)	7545(4)	6034(3)	7149(3)	28(1)
C(25)	7348(4)	7153(3)	7189(3)	32(1)
C(26)	8214(5)	7653(4)	7530(3)	42(1)
C(27)	9301(4)	7063(4)	7834(3)	36(1)
C(28)	9519(4)	5951(4)	7792(3)	39(1)
C(29)	8645(4)	5455(3)	7461(4)	37(1)
C(30)	8279(4)	1171(3)	6873(3)	27(1)
C(31)	7447(4)	466(3)	6509(3)	29(1)
C(32)	8961(4)	1734(3)	6116(3)	28(1)
C(33)	9471(4)	2606(3)	6338(3)	30(1)
C(34)	10093(4)	3140(3)	5662(4)	35(1)
C(35)	10247(4)	2815(4)	4766(4)	37(1)
C(36)	9765(4)	1926(4)	4558(3)	36(1)
C(37)	9124(4)	1398(3)	5223(3)	32(1)
C(38)	9170(4)	503(3)	7519(3)	27(1)
C(39)	8692(4)	196(3)	8372(3)	30(1)
C(40)	9473(4)	-417(3)	8974(3)	33(1)
C(41)	10718(4)	-708(3)	8739(3)	36(1)
C(42)	11200(4)	-416(3)	7892(4)	36(1)
C(43)	10423(4)	185(3)	7280(3)	29(1)
C(44)	4265(7)	246(6)	9705(5)	55(2)
C(45)	3758(8)	1218(6)	10116(5)	58(2)
C(46)	4454(8)	1703(7)	10661(6)	59(2)
C(47)	5666(8)	1207(7)	10785(7)	59(2)
C(48)	6147(8)	240(7)	10402(7)	62(2)
C(49)	5476(8)	-242(7)	9849(7)	59(2)
C(50)	6134(14)	-1275(11)	9419(11)	82(4)

Table 3. Bond lengths [Å] and angles [deg] for ew1352.

Mo(1)-N(2)	1.700(4)
Mo(1)-O(1)	1.883(3)
Mo(1)-O(3)	1.883(3)

Mo(1)-O(2)	1.884(3)
Mo(1)-N(1B)	2.584(6)
Mo(1)-N(1A)	2.606(6)
N(1A)-C(2A)	1.482(7)
N(1A)-C(1A)	1.501(7)
N(1B)-C(2B)	1.475(7)
N(1B)-C(1B)	1.485(7)
O(1)-C(2)	1.451(5)
O(2)-C(16)	1.448(5)
O(3)-C(30)	1.451(5)
C(2)-C(4)	1.525(6)
C(2)-C(10)	1.526(6)
C(2)-C(3)	1.538(6)
C(4)-C(9)	1.382(6)
C(4)-C(5)	1.389(6)
C(5)-C(6)	1.386(7)
C(6)-C(7)	1.385(7)
C(7)-C(8)	1.366(6)
C(8)-C(9)	1.378(6)
C(10)-C(15)	1.383(7)
C(10)-C(11)	1.398(6)
C(11)-C(12)	1.390(6)
C(12)-C(13)	1.362(8)
C(13)-C(14)	1.384(8)
C(14)-C(15)	1.395(7)
C(16)-C(17)	1.517(6)
C(16)-C(24)	1.520(6)
C(16)-C(18)	1.535(6)
C(18)-C(19)	1.373(6)
C(18)-C(23)	1.389(7)
C(19)-C(20)	1.396(6)
C(20)-C(21)	1.375(7)
C(21)-C(22)	1.380(7)
C(22)-C(23)	1.383(7)
C(24)-C(29)	1.391(6)
C(24)-C(25)	1.395(5)
C(25)-C(26)	1.378(7)
C(26)-C(27)	1.380(7)
C(27)-C(28)	1.385(6)
C(28)-C(29)	1.376(6)
C(30)-C(32)	1.522(6)
C(30)-C(38)	1.534(6)
C(30)-C(31)	1.536(5)
C(32)-C(37)	1.384(6)
C(32)-C(33)	1.394(6)
C(33)-C(34)	1.389(6)

C(34)-C(35)	1.383(7)
C(35)-C(36)	1.389(7)
C(36)-C(37)	1.385(6)
C(38)-C(43)	1.378(6)
C(38)-C(39)	1.392(6)
C(39)-C(40)	1.394(6)
C(40)-C(41)	1.366(6)
C(41)-C(42)	1.377(7)
C(42)-C(43)	1.395(6)
C(44)-C(49)	1.385(8)
C(44)-C(45)	1.389(8)
C(45)-C(46)	1.390(9)
C(46)-C(47)	1.383(8)
C(47)-C(48)	1.360(8)
C(48)-C(49)	1.377(8)
C(49)-C(50)	1.502(15)
N(2)-Mo(1)-O(1)	102.18(15)
N(2)-Mo(1)-O(3)	103.01(15)
O(1)-Mo(1)-O(3)	117.53(12)
N(2)-Mo(1)-O(2)	104.09(15)
O(1)-Mo(1)-O(2)	113.64(12)
O(3)-Mo(1)-O(2)	113.91(12)
N(2)-Mo(1)-N(1B)	176.3(2)
O(1)-Mo(1)-N(1B)	74.5(2)
O(3)-Mo(1)-N(1B)	80.1(2)
O(2)-Mo(1)-N(1B)	76.07(19)
N(2)-Mo(1)-N(1A)	175.5(2)
O(1)-Mo(1)-N(1A)	74.0(2)
O(3)-Mo(1)-N(1A)	77.07(18)
O(2)-Mo(1)-N(1A)	79.8(2)
N(1B)-Mo(1)-N(1A)	4.0(3)
C(2A)-N(1A)-C(1A)	106.9(7)
C(2A)-N(1A)-Mo(1)	117.8(6)
C(1A)-N(1A)-Mo(1)	119.5(6)
C(2B)-N(1B)-C(1B)	110.5(7)
C(2B)-N(1B)-Mo(1)	117.1(5)
C(1B)-N(1B)-Mo(1)	123.2(6)
C(2)-O(1)-Mo(1)	131.7(3)
C(16)-O(2)-Mo(1)	137.9(3)
C(30)-O(3)-Mo(1)	134.3(3)
O(1)-C(2)-C(4)	106.5(4)
O(1)-C(2)-C(10)	109.1(3)
C(4)-C(2)-C(10)	111.5(3)
O(1)-C(2)-C(3)	108.0(3)
C(4)-C(2)-C(3)	108.3(3)

C(10)-C(2)-C(3)	113.3(4)
C(9)-C(4)-C(5)	118.3(4)
C(9)-C(4)-C(2)	122.4(4)
C(5)-C(4)-C(2)	119.3(4)
C(6)-C(5)-C(4)	120.7(4)
C(7)-C(6)-C(5)	119.6(4)
C(8)-C(7)-C(6)	120.1(5)
C(7)-C(8)-C(9)	120.1(4)
C(8)-C(9)-C(4)	121.2(4)
C(15)-C(10)-C(11)	119.0(4)
C(15)-C(10)-C(2)	122.7(4)
C(11)-C(10)-C(2)	118.3(4)
C(12)-C(11)-C(10)	119.9(5)
C(13)-C(12)-C(11)	120.8(5)
C(12)-C(13)-C(14)	119.9(5)
C(13)-C(14)-C(15)	120.0(5)
C(10)-C(15)-C(14)	120.3(5)
O(2)-C(16)-C(17)	110.9(3)
O(2)-C(16)-C(24)	104.8(3)
C(17)-C(16)-C(24)	108.6(3)
O(2)-C(16)-C(18)	105.9(3)
C(17)-C(16)-C(18)	112.9(4)
C(24)-C(16)-C(18)	113.3(3)
C(19)-C(18)-C(23)	118.7(4)

C(19)-C(18)-C(16)	123.1(4)
C(23)-C(18)-C(16)	118.2(4)
C(18)-C(19)-C(20)	121.4(5)
C(21)-C(20)-C(19)	119.1(5)
C(20)-C(21)-C(22)	120.2(4)
C(21)-C(22)-C(23)	120.1(5)
C(22)-C(23)-C(18)	120.5(5)
C(29)-C(24)-C(25)	117.3(4)
C(29)-C(24)-C(16)	120.1(3)
C(25)-C(24)-C(16)	122.4(4)
C(26)-C(25)-C(24)	120.7(4)
C(25)-C(26)-C(27)	121.0(4)
C(26)-C(27)-C(28)	119.2(4)
C(29)-C(28)-C(27)	119.6(4)
C(28)-C(29)-C(24)	122.1(4)
O(3)-C(30)-C(32)	109.3(3)
O(3)-C(30)-C(38)	104.9(3)
C(32)-C(30)-C(38)	112.2(3)
O(3)-C(30)-C(31)	107.3(3)
C(32)-C(30)-C(31)	112.9(4)

C(38)-C(30)-C(31)	109.9(3)
C(37)-C(32)-C(33)	118.7(4)
C(37)-C(32)-C(30)	122.8(4)
C(33)-C(32)-C(30)	118.5(4)
C(34)-C(33)-C(32)	119.9(4)
C(35)-C(34)-C(33)	121.6(4)
C(34)-C(35)-C(36)	118.0(4)
C(37)-C(36)-C(35)	120.9(5)
C(32)-C(37)-C(36)	120.8(4)
C(43)-C(38)-C(39)	118.8(4)
C(43)-C(38)-C(30)	122.5(4)
C(39)-C(38)-C(30)	118.7(4)
C(38)-C(39)-C(40)	120.2(4)
C(41)-C(40)-C(39)	120.4(4)
C(40)-C(41)-C(42)	119.8(4)
C(41)-C(42)-C(43)	120.2(4)
C(38)-C(43)-C(42)	120.4(4)
C(49)-C(44)-C(45)	119.2(7)
C(44)-C(45)-C(46)	120.7(7)
C(47)-C(46)-C(45)	119.0(7)
C(48)-C(47)-C(46)	120.1(7)
C(47)-C(48)-C(49)	121.5(7)
C(48)-C(49)-C(44)	119.4(7)
C(48)-C(49)-C(50)	116.6(9)
C(44)-C(49)-C(50)	123.9(9)

Symmetry transformations used to generate equivalent atoms:

Table 4. Anisotropic displacement parameters ($\text{\AA}^2 \times 10^3$) for ew1352.
The anisotropic displacement factor exponent takes the form:
 $-2 \pi^2 [h^2 a^{*2} U_{11} + \dots + 2 h k a^* b^* U_{12}]$

	U11	U22	U33	U23	U13	U12
Mo(1)	28(1)	10(1)	46(1)	-4(1)	-4(1)	-6(1)
N(1A)	63(3)	38(3)	60(3)	-16(2)	1(3)	-23(2)
C(1A)	72(4)	50(4)	59(4)	-14(4)	1(4)	-3(3)
C(2A)	63(3)	41(4)	67(4)	-8(4)	0(4)	-12(3)
N(1B)	62(3)	37(3)	62(3)	-15(2)	4(3)	-25(2)
C(1B)	62(4)	38(3)	66(4)	-4(3)	-1(4)	-24(3)

C(2B)	81(5)	39(4)	68(5)	-10(3)	14(5)	-30(4)
O(1)	34(2)	13(1)	49(2)	-4(1)	-4(1)	-8(1)
O(2)	31(2)	10(1)	52(2)	-2(1)	-8(1)	-6(1)
O(3)	28(1)	13(1)	43(2)	-6(1)	-4(1)	-3(1)
N(2)	31(2)	20(2)	44(2)	-3(2)	-17(2)	-8(1)
C(2)	28(2)	14(2)	48(3)	-2(2)	-5(2)	-7(2)
C(3)	38(2)	22(2)	51(3)	-1(2)	-4(2)	-8(2)
C(4)	33(2)	20(2)	43(3)	-6(2)	-1(2)	-6(2)
C(5)	47(3)	33(2)	55(3)	-11(2)	1(2)	-18(2)
C(6)	65(3)	40(3)	51(3)	-15(2)	3(3)	-12(3)
C(7)	53(3)	45(3)	52(3)	-3(2)	11(3)	-14(3)
C(8)	45(3)	30(2)	61(3)	-6(2)	11(3)	-12(2)
C(9)	41(2)	22(2)	51(3)	-7(2)	2(2)	-12(2)
C(10)	27(2)	20(2)	50(3)	-8(2)	4(2)	-7(2)
C(11)	34(2)	20(2)	60(3)	-6(2)	3(2)	-10(2)
C(12)	34(2)	20(2)	82(4)	-9(2)	11(3)	-10(2)
C(13)	45(3)	34(3)	82(4)	-33(3)	17(3)	-20(2)
C(14)	54(3)	47(3)	64(4)	-26(3)	5(3)	-20(3)
C(15)	40(3)	32(2)	54(3)	-11(2)	1(2)	-11(2)
C(16)	29(2)	6(2)	48(3)	0(2)	-2(2)	-4(2)
C(17)	29(2)	20(2)	50(3)	-7(2)	-1(2)	-4(2)
C(18)	29(2)	15(2)	46(3)	-6(2)	-3(2)	-8(2)
C(19)	32(2)	18(2)	49(3)	-8(2)	-2(2)	1(2)
C(20)	32(2)	22(2)	57(3)	-7(2)	-8(2)	1(2)
C(21)	30(2)	24(2)	67(3)	-12(2)	-2(2)	-1(2)
C(22)	33(2)	53(3)	49(3)	-12(2)	8(2)	-6(2)
C(23)	33(2)	39(3)	48(3)	-3(2)	0(2)	-7(2)
C(24)	30(2)	13(2)	42(3)	-5(2)	0(2)	-3(2)
C(25)	36(2)	14(2)	48(3)	-5(2)	0(2)	-7(2)
C(26)	61(3)	22(2)	46(3)	-7(2)	3(2)	-15(2)
C(27)	41(2)	31(2)	43(3)	-6(2)	3(2)	-22(2)
C(28)	37(2)	30(2)	52(3)	-9(2)	-3(2)	-11(2)
C(29)	31(2)	18(2)	63(3)	-11(2)	-5(2)	-5(2)
C(30)	26(2)	14(2)	40(2)	-5(2)	-4(2)	-3(2)
C(31)	24(2)	18(2)	48(3)	-3(2)	-4(2)	-8(2)
C(32)	21(2)	16(2)	49(3)	-2(2)	-5(2)	-3(2)
C(33)	26(2)	18(2)	46(3)	0(2)	-4(2)	-3(2)
C(34)	27(2)	20(2)	60(3)	3(2)	0(2)	-7(2)
C(35)	26(2)	28(2)	55(3)	6(2)	2(2)	-3(2)
C(36)	29(2)	37(2)	39(3)	-3(2)	-1(2)	-2(2)
C(37)	29(2)	21(2)	46(3)	0(2)	-6(2)	-4(2)
C(38)	27(2)	11(2)	45(3)	-7(2)	-5(2)	-8(2)
C(39)	30(2)	20(2)	44(3)	-6(2)	-2(2)	-10(2)
C(40)	41(2)	22(2)	40(3)	-2(2)	-4(2)	-14(2)
C(41)	40(2)	21(2)	51(3)	-4(2)	-13(2)	-8(2)
C(42)	31(2)	13(2)	64(3)	-2(2)	-4(2)	-6(2)

C(43)	29(2)	12(2)	48(3)	-4(2)	-2(2)	-7(2)
C(44)	53(4)	46(4)	70(4)	10(4)	-7(4)	-21(3)
C(45)	52(4)	49(4)	70(5)	13(4)	-8(4)	-7(4)
C(46)	57(4)	50(4)	71(5)	-3(4)	-3(4)	-10(4)
C(47)	56(4)	55(4)	69(5)	-6(4)	-10(4)	-14(4)
C(48)	59(4)	53(4)	75(5)	-2(4)	-10(4)	-12(4)
C(49)	55(4)	44(4)	78(5)	-1(4)	3(4)	-15(3)
C(50)	83(7)	54(6)	110(9)	-25(6)	36(7)	-32(5)

Table 5. Hydrogen coordinates ($\times 10^4$) and isotropic displacement parameters ($\text{\AA}^2 \times 10^3$) for ew1352.

	x	y	z	U(eq)
H(1A)	5990	2637	9210	62
H(1A1)	5682	4004	10157	92
H(1A2)	4756	4273	9361	92
H(1A3)	5974	4794	9327	92
H(2A1)	8180	3300	8913	85
H(2A2)	7904	2181	9339	85
H(2A3)	7571	3242	9936	85
H(1B)	5537	3742	9110	62
H(1B1)	7137	3913	9980	80
H(1B2)	6721	4809	9213	80
H(1B3)	7938	3901	9020	80
H(2B1)	6728	2454	10096	92
H(2B2)	6752	1747	9214	92
H(2B3)	5452	2314	9710	92
H(3A)	3704	4016	6262	55
H(3B)	3026	4664	7134	55
H(3C)	2267	4017	6546	55
H(5A)	3025	4208	8861	53
H(6A)	1500	4321	10075	62
H(7A)	57	3182	10143	60
H(8A)	80	2007	8973	55
H(9A)	1595	1892	7768	44
H(11A)	4424	1025	7907	45
H(12A)	4645	-616	7182	54
H(13A)	4015	-681	5732	63

H(14A)	3136	903	4978	65
H(15A)	2895	2559	5692	50
H(17A)	8006	4761	5768	50
H(17B)	7126	5814	5388	50
H(17C)	6633	4705	5515	50
H(19A)	5093	6328	5448	40
H(20A)	3002	7189	5590	45
H(21A)	1970	7439	7037	49
H(22A)	3038	6908	8329	55
H(23A)	5115	6047	8180	48
H(25A)	6609	7574	6980	39
H(26A)	8061	8415	7556	51
H(27A)	9892	7414	8068	44
H(28A)	10267	5534	7991	47
H(29A)	8797	4692	7444	45
H(31A)	6881	897	6096	44
H(31B)	6963	187	7021	44
H(31C)	7966	-137	6178	44
H(33A)	9393	2835	6951	36
H(34A)	10421	3744	5819	42
H(35A)	10669	3188	4308	44
H(36A)	9876	1677	3950	43
H(37A)	8792	798	5064	38
H(39A)	7829	404	8545	36
H(40A)	9138	-634	9552	40
H(41A)	11251	-1110	9157	44
H(42A)	12064	-625	7725	43
H(43A)	10760	376	6695	35
H(44)	3788	-80	9329	66
H(45)	2926	1554	10024	69
H(46)	4103	2366	10944	71
H(47)	6163	1541	11138	71
H(48)	6965	-111	10520	74
H(50A)	7022	-1263	9309	122
H(50B)	5787	-1353	8838	122
H(50C)	6020	-1882	9829	122

Appendix 2

Crystallographic Data for $\text{N}\equiv\text{Mo}(\text{OAr})_3(\text{NHMe}_2)$ ($\text{Ar} = 2,6\text{-}^i\text{Pr}_2\text{C}_6\text{H}_3$)

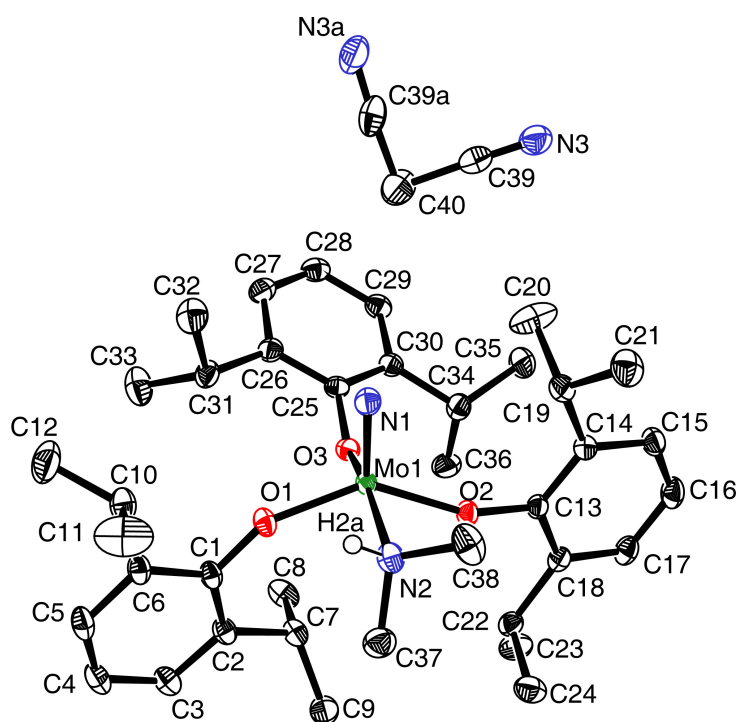


Figure A.2. 50 % thermal ellipsoid plot of $\text{N}\equiv\text{Mo}(\text{OAr})_3(\text{NHMe}_2)$ ($\text{Ar} = 2,6\text{-}^i\text{Pr}_2\text{C}_6\text{H}_3$).

Structure Determination.

Purple blocks of **ew1743** were grown from an acetonitrile solution at $-35\text{ }^{\circ}\text{C}$. A crystal of dimensions $0.38 \times 0.32 \times 0.23\text{ mm}$ was mounted on a Bruker SMART APEX CCD-based X-ray diffractometer equipped with a low temperature device and fine focus Mo-target X-ray tube ($\lambda = 0.71073\text{ \AA}$) operated at 1500 W power (50 kV, 30 mA). The X-ray intensities were measured at 85(1) K; the detector was placed at a distance 5.055 cm from the crystal. A total of 5190 frames were collected with a scan width of 0.5° in ω and 0.45° in ϕ with an exposure time of 15 s/frame. The integration of the data yielded a total of 190801 reflections to a maximum 2θ value of 60.22° of which 11005 were independent and 10231 were greater than $2\sigma(I)$. The final cell constants (Table 1) were based on the xyz centroids of 9793 reflections above $10\sigma(I)$. Analysis of the data showed negligible decay during data collection; the data were processed with SADABS and corrected for absorption. The structure was solved and refined with the Bruker SHELXTL (version 2008/4) software package, using the space group $P2(1)/n$ with $Z = 4$ for the formula $\text{C}_{38}\text{H}_{58}\text{N}_2\text{O}_3\text{Mo}\cdot\text{CH}_3\text{CN}$. All non-hydrogen atoms were refined anisotropically with the hydrogen atoms placed in idealized positions except for the dimethylamino hydrogen which was allowed to refine isotropically. Full matrix least-squares refinement based on F^2 converged at $R1 = 0.0261$ and $wR2 = 0.0721$ [based on $I > 2\sigma(I)$], $R1 = 0.0286$ and $wR2 = 0.0747$ for all data.

Sheldrick, G.M. SHELXTL, v. 2008/4; Bruker Analytical X-ray, Madison, WI, 2008.

Sheldrick, G.M. SADABS, v. 2008/4. Program for Empirical Absorption Correction of Area Detector Data, University of Gottingen: Gottingen, Germany, 2008.

Saint Plus, v. 7.53a, Bruker Analytical X-ray, Madison, WI, 2008.

Table 1. Crystal data and structure refinement for ew1743.

Identification code	ew1743
Empirical formula	C ₄₀ H ₆₁ Mo N ₃ O ₃
Formula weight	727.86
Temperature	85(2) K
Wavelength	0.71073 Å
Crystal system, space group	Monoclinic, P2(1)/n
Unit cell dimensions	a = 17.0283(9) Å alpha = 90 deg. b = 13.2624(7) Å beta = 114.780(1) deg. c = 19.0848(10) Å gamma = 90 deg.
Volume	3913.2(4) Å ³
Z, Calculated density	4, 1.235 Mg/m ³
Absorption coefficient	0.374 mm ⁻¹
F(000)	1552
Crystal size	0.38 x 0.32 x 0.23 mm
Theta range for data collection	1.35 to 29.61 deg.
Limiting indices	-23 ≤ h ≤ 23, -18 ≤ k ≤ 18, -26 ≤ l ≤ 26
Reflections collected / unique	190801 / 11005 [R(int) = 0.0538]
Completeness to theta = 29.61	100.0 %
Absorption correction	Semi-empirical from equivalents
Max. and min. transmission	0.9190 and 0.8711
Refinement method	Full-matrix least-squares on F ²
Data / restraints / parameters	11005 / 0 / 461
Goodness-of-fit on F ²	1.072

Final R indices [$I > 2\sigma(I)$]	R1 = 0.0261, wR2 = 0.0721
R indices (all data)	R1 = 0.0286, wR2 = 0.0747
Largest diff. peak and hole	0.794 and -0.560 e. \AA^{-3}

Table 2. Atomic coordinates ($\times 10^4$) and equivalent isotropic displacement parameters ($\text{\AA}^2 \times 10^3$) for ew1743. $U(\text{eq})$ is defined as one third of the trace of the orthogonalized U_{ij} tensor.

	x	y	z	$U(\text{eq})$
Mo(1)	7187(1)	1179(1)	4185(1)	16(1)
N(1)	7020(1)	1582(1)	3315(1)	23(1)
N(2)	8525(1)	1907(1)	4742(1)	23(1)
N(3)	5680(1)	-1089(1)	572(1)	36(1)
N(3A)	4150(3)	964(4)	-116(4)	41(1)
O(1)	6898(1)	2325(1)	4653(1)	21(1)
O(2)	7874(1)	-27(1)	4420(1)	20(1)
O(3)	6133(1)	447(1)	3989(1)	19(1)
C(1)	6792(1)	2746(1)	5256(1)	19(1)
C(2)	6867(1)	2175(1)	5905(1)	20(1)
C(3)	6745(1)	2669(1)	6498(1)	25(1)
C(4)	6556(1)	3692(1)	6455(1)	29(1)
C(5)	6480(1)	4239(1)	5812(1)	27(1)
C(6)	6589(1)	3784(1)	5199(1)	22(1)
C(7)	7015(1)	1045(1)	5946(1)	21(1)
C(8)	6149(1)	490(1)	5689(1)	28(1)
C(9)	7654(1)	680(1)	6743(1)	29(1)
C(10)	6500(1)	4383(1)	4494(1)	27(1)
C(11)	7292(1)	5036(2)	4666(1)	56(1)
C(12)	5671(1)	5017(1)	4168(1)	45(1)
C(13)	8121(1)	-969(1)	4318(1)	18(1)
C(14)	8207(1)	-1229(1)	3639(1)	21(1)
C(15)	8403(1)	-2234(1)	3548(1)	25(1)
C(16)	8533(1)	-2943(1)	4119(1)	28(1)
C(17)	8482(1)	-2662(1)	4800(1)	24(1)
C(18)	8277(1)	-1677(1)	4914(1)	20(1)
C(19)	8056(1)	-460(1)	3009(1)	25(1)
C(20)	7164(1)	-562(2)	2367(1)	48(1)

C(21)	8743(1)	-495(1)	2694(1)	36(1)
C(22)	8260(1)	-1351(1)	5672(1)	22(1)
C(23)	7942(1)	-2166(1)	6058(1)	31(1)
C(24)	9167(1)	-1002(1)	6224(1)	31(1)
C(25)	5368(1)	203(1)	3391(1)	19(1)
C(26)	4713(1)	930(1)	3062(1)	21(1)
C(27)	3925(1)	622(1)	2475(1)	25(1)
C(28)	3780(1)	-369(1)	2225(1)	25(1)
C(29)	4429(1)	-1080(1)	2562(1)	23(1)
C(30)	5230(1)	-814(1)	3144(1)	20(1)
C(31)	4833(1)	2020(1)	3331(1)	24(1)
C(32)	4851(1)	2700(1)	2693(1)	33(1)
C(33)	4121(1)	2358(1)	3574(1)	37(1)
C(34)	5920(1)	-1599(1)	3534(1)	24(1)
C(35)	5914(1)	-2476(1)	3009(1)	31(1)
C(36)	5836(1)	-2003(1)	4251(1)	33(1)
C(37)	8894(1)	1914(1)	5596(1)	31(1)
C(38)	9174(1)	1517(1)	4481(1)	36(1)
C(39)	5365(1)	-544(2)	837(1)	29(1)
C(40)	4988(1)	178(2)	1197(1)	45(1)
C(39A)	4545(3)	652(4)	489(4)	36(1)
C(40A)	4988(1)	178(2)	1197(1)	45(1)

Table 3. Bond lengths [Å] and angles [deg] for ew1743.

Mo(1)-N(1)	1.6509(10)
Mo(1)-O(2)	1.9206(8)
Mo(1)-O(1)	1.9292(8)
Mo(1)-O(3)	1.9333(8)
Mo(1)-N(2)	2.2859(11)
N(2)-C(37)	1.4809(17)
N(2)-C(38)	1.4819(17)
N(3)-C(39)	1.137(3)
N(3A)-C(39A)	1.142(8)
O(1)-C(1)	1.3572(13)
O(2)-C(13)	1.3573(13)
O(3)-C(25)	1.3634(13)
C(1)-C(2)	1.4120(16)
C(1)-C(6)	1.4127(15)
C(2)-C(3)	1.3960(16)
C(2)-C(7)	1.5165(16)
C(3)-C(4)	1.3892(18)

C(4)-C(5)	1.384(2)
C(5)-C(6)	1.3971(17)
C(6)-C(10)	1.5140(18)
C(7)-C(9)	1.5313(18)
C(7)-C(8)	1.5329(17)
C(10)-C(11)	1.519(2)
C(10)-C(12)	1.533(2)
C(13)-C(14)	1.4066(16)
C(13)-C(18)	1.4128(16)
C(14)-C(15)	1.4029(16)
C(14)-C(19)	1.5142(17)
C(15)-C(16)	1.3853(19)
C(16)-C(17)	1.3898(19)
C(17)-C(18)	1.3922(16)
C(18)-C(22)	1.5199(17)
C(19)-C(20)	1.506(2)
C(19)-C(21)	1.5231(18)
C(22)-C(23)	1.5288(18)
C(22)-C(24)	1.5320(18)
C(25)-C(26)	1.4071(16)
C(25)-C(30)	1.4155(16)
C(26)-C(27)	1.4008(17)
C(26)-C(31)	1.5186(17)
C(27)-C(28)	1.3855(19)
C(28)-C(29)	1.3883(18)
C(29)-C(30)	1.3958(16)
C(30)-C(34)	1.5117(17)
C(31)-C(32)	1.5251(18)
C(31)-C(33)	1.5349(18)
C(34)-C(36)	1.5297(19)
C(34)-C(35)	1.5321(17)
C(39)-C(40)	1.474(3)
N(1)-Mo(1)-O(2)	109.65(4)
N(1)-Mo(1)-O(1)	103.93(4)
O(2)-Mo(1)-O(1)	142.79(4)
N(1)-Mo(1)-O(3)	102.35(5)
O(2)-Mo(1)-O(3)	92.97(3)
O(1)-Mo(1)-O(3)	95.12(4)
N(1)-Mo(1)-N(2)	92.79(5)
O(2)-Mo(1)-N(2)	81.49(4)
O(1)-Mo(1)-N(2)	81.34(4)
O(3)-Mo(1)-N(2)	164.85(4)
C(37)-N(2)-C(38)	109.89(11)
C(37)-N(2)-Mo(1)	113.31(8)
C(38)-N(2)-Mo(1)	115.75(8)

C(1)-O(1)-Mo(1)	150.14(8)
C(13)-O(2)-Mo(1)	158.04(8)
C(25)-O(3)-Mo(1)	139.91(7)
O(1)-C(1)-C(2)	121.89(10)
O(1)-C(1)-C(6)	116.79(11)
C(2)-C(1)-C(6)	121.32(11)
C(3)-C(2)-C(1)	118.02(11)
C(3)-C(2)-C(7)	120.06(11)
C(1)-C(2)-C(7)	121.79(10)
C(4)-C(3)-C(2)	121.38(12)
C(5)-C(4)-C(3)	119.82(12)
C(4)-C(5)-C(6)	121.40(12)
C(5)-C(6)-C(1)	118.06(12)
C(5)-C(6)-C(10)	121.29(11)
C(1)-C(6)-C(10)	120.65(11)
C(2)-C(7)-C(9)	113.34(10)
C(2)-C(7)-C(8)	109.92(10)
C(9)-C(7)-C(8)	110.71(10)
C(6)-C(10)-C(11)	110.99(12)
C(6)-C(10)-C(12)	112.41(11)
C(11)-C(10)-C(12)	110.97(14)
O(2)-C(13)-C(14)	121.10(10)
O(2)-C(13)-C(18)	117.44(10)
C(14)-C(13)-C(18)	121.46(10)
C(15)-C(14)-C(13)	118.01(11)
C(15)-C(14)-C(19)	120.76(11)
C(13)-C(14)-C(19)	121.19(10)
C(16)-C(15)-C(14)	121.03(12)
C(15)-C(16)-C(17)	120.09(11)
C(16)-C(17)-C(18)	121.12(12)
C(17)-C(18)-C(13)	118.19(11)
C(17)-C(18)-C(22)	121.46(11)
C(13)-C(18)-C(22)	120.30(10)
C(20)-C(19)-C(14)	111.25(12)
C(20)-C(19)-C(21)	110.84(12)
C(14)-C(19)-C(21)	112.99(11)
C(18)-C(22)-C(23)	114.12(11)
C(18)-C(22)-C(24)	109.00(10)
C(23)-C(22)-C(24)	109.91(11)
O(3)-C(25)-C(26)	120.76(10)
O(3)-C(25)-C(30)	118.16(10)
C(26)-C(25)-C(30)	120.96(11)
C(27)-C(26)-C(25)	118.15(11)
C(27)-C(26)-C(31)	119.67(11)
C(25)-C(26)-C(31)	122.17(11)
C(28)-C(27)-C(26)	121.61(12)

C(27)-C(28)-C(29)	119.54(11)
C(28)-C(29)-C(30)	121.29(12)
C(29)-C(30)-C(25)	118.44(11)
C(29)-C(30)-C(34)	121.09(11)
C(25)-C(30)-C(34)	120.39(10)
C(26)-C(31)-C(32)	109.82(11)
C(26)-C(31)-C(33)	111.62(11)
C(32)-C(31)-C(33)	110.53(11)
C(30)-C(34)-C(36)	109.73(10)
C(30)-C(34)-C(35)	114.15(11)
C(36)-C(34)-C(35)	110.00(11)
N(3)-C(39)-C(40)	177.9(2)

Symmetry transformations used to generate equivalent atoms:

Table 4. Anisotropic displacement parameters ($\text{Å}^2 \times 10^3$) for ew1743. The anisotropic displacement factor exponent takes the form: $-2 \pi^2 [h^2 a^{*2} U_{11} + \dots + 2 h k a^* b^* U_{12}]$

	U11	U22	U33	U23	U13	U12
Mo(1)	21(1)	12(1)	16(1)	1(1)	9(1)	1(1)
N(1)	29(1)	22(1)	23(1)	6(1)	14(1)	5(1)
N(2)	26(1)	19(1)	28(1)	-1(1)	14(1)	-2(1)
N(3)	38(1)	32(1)	30(1)	-2(1)	5(1)	3(1)
N(3A)	35(2)	33(2)	48(3)	0(2)	9(2)	10(2)
O(1)	27(1)	15(1)	24(1)	-1(1)	14(1)	1(1)
O(2)	24(1)	15(1)	21(1)	1(1)	11(1)	4(1)
O(3)	22(1)	16(1)	17(1)	0(1)	7(1)	-1(1)
C(1)	20(1)	15(1)	25(1)	-4(1)	12(1)	-2(1)
C(2)	21(1)	18(1)	24(1)	-4(1)	12(1)	-4(1)
C(3)	29(1)	26(1)	26(1)	-5(1)	15(1)	-3(1)
C(4)	32(1)	27(1)	31(1)	-11(1)	18(1)	-1(1)
C(5)	30(1)	18(1)	36(1)	-7(1)	16(1)	1(1)
C(6)	23(1)	15(1)	29(1)	-3(1)	13(1)	-1(1)
C(7)	28(1)	18(1)	23(1)	-1(1)	15(1)	-2(1)
C(8)	37(1)	23(1)	28(1)	-5(1)	18(1)	-10(1)
C(9)	34(1)	28(1)	27(1)	3(1)	15(1)	3(1)

C(10)	32(1)	16(1)	35(1)	0(1)	17(1)	0(1)
C(11)	57(1)	63(1)	46(1)	6(1)	19(1)	-32(1)
C(12)	57(1)	35(1)	52(1)	16(1)	31(1)	23(1)
C(13)	17(1)	16(1)	20(1)	-1(1)	7(1)	2(1)
C(14)	20(1)	22(1)	20(1)	-1(1)	8(1)	2(1)
C(15)	24(1)	24(1)	28(1)	-7(1)	10(1)	2(1)
C(16)	26(1)	18(1)	37(1)	-5(1)	12(1)	2(1)
C(17)	23(1)	17(1)	31(1)	3(1)	10(1)	3(1)
C(18)	18(1)	18(1)	22(1)	1(1)	7(1)	1(1)
C(19)	28(1)	28(1)	22(1)	1(1)	14(1)	5(1)
C(20)	31(1)	67(1)	35(1)	20(1)	3(1)	-5(1)
C(21)	36(1)	39(1)	41(1)	3(1)	24(1)	1(1)
C(22)	22(1)	22(1)	20(1)	4(1)	8(1)	3(1)
C(23)	33(1)	33(1)	25(1)	9(1)	10(1)	-2(1)
C(24)	28(1)	37(1)	25(1)	-5(1)	10(1)	-5(1)
C(25)	20(1)	21(1)	16(1)	1(1)	8(1)	-1(1)
C(26)	24(1)	22(1)	19(1)	4(1)	10(1)	2(1)
C(27)	22(1)	30(1)	22(1)	5(1)	9(1)	3(1)
C(28)	21(1)	33(1)	21(1)	1(1)	7(1)	-3(1)
C(29)	23(1)	26(1)	22(1)	-3(1)	9(1)	-4(1)
C(30)	21(1)	20(1)	19(1)	0(1)	9(1)	-1(1)
C(31)	27(1)	20(1)	26(1)	5(1)	12(1)	5(1)
C(32)	42(1)	25(1)	40(1)	8(1)	24(1)	1(1)
C(33)	50(1)	26(1)	50(1)	2(1)	35(1)	3(1)
C(34)	22(1)	18(1)	28(1)	-4(1)	7(1)	-1(1)
C(35)	37(1)	21(1)	35(1)	-5(1)	14(1)	1(1)
C(36)	41(1)	28(1)	23(1)	3(1)	6(1)	6(1)
C(37)	25(1)	37(1)	28(1)	-1(1)	9(1)	0(1)
C(38)	32(1)	37(1)	49(1)	-12(1)	27(1)	-10(1)
C(39)	27(1)	31(1)	26(1)	6(1)	6(1)	-2(1)
C(40)	43(1)	61(1)	43(1)	19(1)	28(1)	16(1)
C(39A)	28(2)	30(3)	56(4)	5(2)	23(2)	5(2)
C(40A)	43(1)	61(1)	43(1)	19(1)	28(1)	16(1)

Table 5. Hydrogen coordinates ($\times 10^4$) and isotropic displacement parameters ($\text{\AA}^2 \times 10^3$) for ew1743.

	x	y	z	U(eq)
H(2A)	8416(11)	2537(14)	4600(10)	31(4)
H(3A)	6793	2298	6940	31
H(4A)	6479	4015	6866	35
H(5A)	6351	4938	5788	33
H(7A)	7264	872	5570	26
H(8A)	5900	623	6059	41
H(8B)	6243	-236	5668	41
H(8C)	5752	729	5177	41
H(9A)	8209	1027	6889	43
H(9B)	7740	-48	6727	43
H(9C)	7423	829	7123	43
H(10A)	6465	3889	4086	32
H(11A)	7344	5532	5064	85
H(11B)	7233	5388	4195	85
H(11C)	7810	4611	4850	85
H(12A)	5171	4584	4077	68
H(12B)	5606	5326	3680	68
H(12C)	5706	5547	4537	68
H(15A)	8446	-2432	3087	30
H(16A)	8659	-3623	4045	33
H(17A)	8587	-3150	5193	29
H(19A)	8090	222	3244	30
H(20A)	7116	-1209	2104	72
H(20B)	7061	-10	1997	72
H(20C)	6733	-533	2582	72
H(21A)	8690	-1128	2412	54
H(21B)	9318	-456	3122	54
H(21C)	8662	76	2344	54
H(22A)	7862	-760	5562	26
H(23A)	7355	-2371	5707	46
H(23B)	7939	-1898	6535	46
H(23C)	8329	-2750	6178	46
H(24A)	9566	-1575	6358	46
H(24B)	9149	-727	6694	46
H(24C)	9366	-479	5974	46
H(27A)	3479	1106	2242	30
H(28A)	3240	-562	1827	31
H(29A)	4326	-1761	2392	28

H(31A)	5403	2079	3788	29
H(32A)	5327	2495	2563	50
H(32B)	4938	3401	2872	50
H(32C)	4302	2642	2235	50
H(33A)	3558	2318	3129	56
H(33B)	4230	3055	3761	56
H(33C)	4122	1917	3986	56
H(34A)	6494	-1257	3711	28
H(35A)	5405	-2900	2903	47
H(35B)	6440	-2879	3266	47
H(35C)	5893	-2209	2523	47
H(36A)	5892	-1445	4605	50
H(36B)	6293	-2500	4509	50
H(36C)	5269	-2323	4097	50
H(37A)	8953	1220	5787	46
H(37B)	8511	2291	5766	46
H(37C)	9465	2236	5800	46
H(38A)	9715	1893	4737	54
H(38B)	8956	1601	3920	54
H(38C)	9278	801	4612	54
H(40A)	5397	296	1734	68
H(40B)	4449	-97	1185	68
H(40C)	4868	817	913	68
H(40D)	4573	-73	1388	68
H(40E)	5380	662	1568	68
H(40F)	5324	-387	1135	68

Table 6. Hydrogen bonds for ew1743 [Å and deg.].

D-H...A	d(D-H)	d(H...A)	d(D...A)	<(DHA)
N(2)-H(2A)...N(3A)#1	0.875(18)	2.289(19)	2.990(5)	137.1(15)
N(2)-H(2A)...N(3)#2	0.875(18)	2.494(18)	3.153(2)	132.6(15)

Symmetry transformations used to generate equivalent atoms:

#1 $x+1/2, -y+1/2, z+1/2$ #2 $-x+3/2, y+1/2, -z+1/2$

Appendix 3

Crystallographic Data for [TBA₂][Zr(XXX)Cl₃]

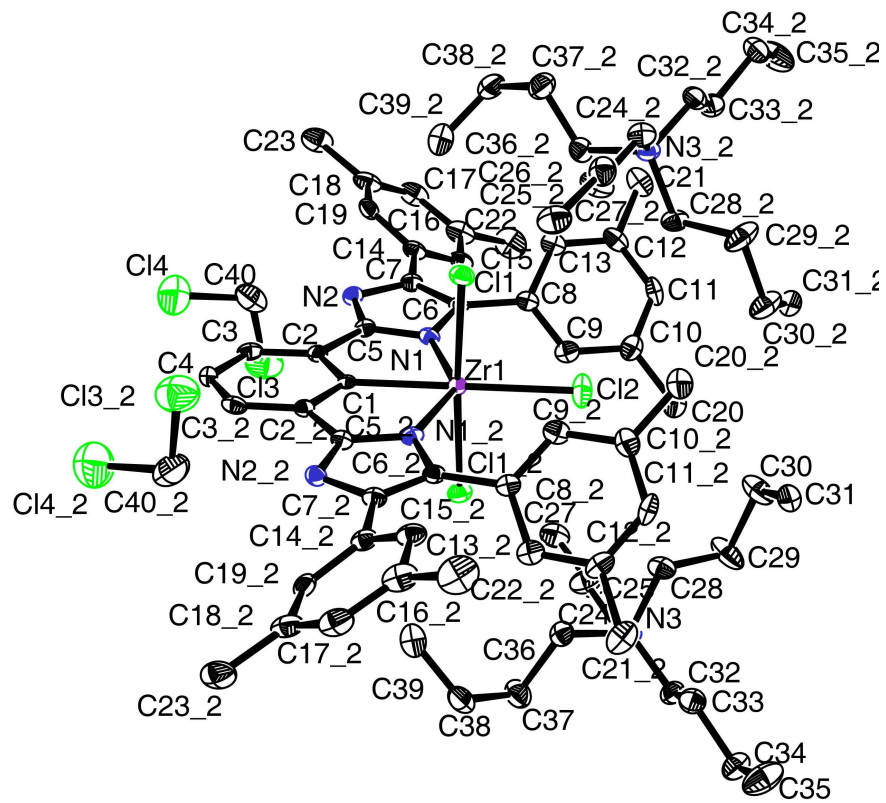


Figure A.3. 50 % thermal ellipsoid plot of [TBA₂][Zr(XXX)Cl₃].

Structure Determination

Orange block-like crystals of **ew1061** were crystallized from a dichloromethane solution at $-35\text{ }^{\circ}\text{C}$. A crystal of dimensions $0.17 \times 0.11 \times 0.10\text{ mm}$ was mounted on a standard Bruker SMART APEX CCD-based X-ray diffractometer equipped with a low-temperature device and fine-focus Mo-target X-ray tube ($\lambda = 0.71073\text{ \AA}$) operated at 2000 W power (50 kV, 30 mA). The X-ray intensities were measured at 85(2) K; the detector was placed at a distance 5.055 cm from the crystal. A total of 2610 frames were collected with a scan width of 0.5° in ω and 0.45° in ϕ with an exposure time of 30 s/frame. Indexing was performed by use of the CELL_NOW program which indicated that the crystal was a three-component, non-merohedral twin. The frames were integrated with the Bruker SAINT software package with a narrow frame algorithm. The integration of the data yielded a total of 129400 reflections to a maximum 2θ value of 46.74° of which 5790 were independent and 4507 were greater than $2\sigma(I)$. The final cell constants (Table 1) were based on the xyz centroids of 4877 reflections above $10\sigma(I)$. Analysis of the data showed negligible decay during data collection; the data were processed with TWINABS and corrected for absorption. The second twin domain is related by a rotation of 179.4 degrees about the direct and reciprocal $[0\ 1\ 0]$ axis while a third domain is related by a rotation of 176.3 degrees about the same axis. For this refinement, single reflections from component one as well as composite reflections containing a contribution from this component were used. Merging of the data was performed in TWINABS and an HKLF 4 format file used for refinement. The structure was solved and refined with the Bruker SHELXTL (version 2008/3) software package, using the space group $C2/c$ with $Z = 4$ for the formula $2(\text{C}_{16}\text{H}_{36}\text{N})$,

$C_{44}H_{39}N_4Cl_3Zr \cdot 2(CH_2Cl_2)$. The Zr-complex lies on a two-fold rotation axis of the crystal lattice. All non-hydrogen atoms were refined anisotropically with the hydrogen atoms placed in idealized positions. Full-matrix least-squares refinement based on F^2 converged at $R1 = 0.0673$ and $wR2 = 0.1299$ [based on $I > 2\sigma(I)$], $R1 = 0.0943$ and $wR2 = 0.1393$ for all data.

Sheldrick, G.M. SHELXTL, v. 2008/3; Bruker Analytical X-ray, Madison, WI, 2008.

Saint Plus, v. 7.34, Bruker Analytical X-ray, Madison, WI, 2006.

Sheldrick, G.M. CELL_NOW, v. 2008/2, Program for Indexing Twins and Other Problem Crystals, University of Gottingen: Gottingen, Germany, 2008.

Sheldrick, G.M. TWINABS, v. 2008/1. Program for Empirical Absorption Correction of Area Detector Data, University of Gottingen: Gottingen, Germany, 2008.

Table 1. Crystal data and structure refinement for ew1061.

Identification code	ew1061
Empirical formula	$C_{78}H_{115}Cl_{17}N_6Zr$
Formula weight	1476.13
Temperature	85(2) K
Wavelength	0.71073 Å
Crystal system, space group	Monoclinic, $C2/c$
Unit cell dimensions	$a = 17.758(2)$ Å $\alpha = 90$ deg. $b = 14.530(2)$ Å $\beta = 98.206(2)$ deg. $c = 31.237(4)$ Å $\gamma = 90$ deg.
Volume	$7977.3(18)$ Å ³

Z, Calculated density	4, 1.229 Mg/m ³
Absorption coefficient	0.416 mm ⁻¹
F(000)	3136
Crystal size	0.17 x 0.11 x 0.10 mm
Theta range for data collection	1.82 to 23.37 deg.
Limiting indices	-19<=h<=19, -16<=k<=16, -34<=l<=34
Reflections collected / unique	129400 / 5790 [R(int) = 0.0742]
Completeness to theta = 23.37	99.6 %
Absorption correction	Semi-empirical from equivalents
Max. and min. transmission	0.9596 and 0.9326
Refinement method	Full-matrix least-squares on F ²
Data / restraints / parameters	5790 / 0 / 425
Goodness-of-fit on F ²	1.109
Final R indices [I>2sigma(I)]	R1 = 0.0673, wR2 = 0.1299
R indices (all data)	R1 = 0.0943, wR2 = 0.1393
Largest diff. peak and hole	0.629 and -0.522 e.A ⁻³

Table 2. Atomic coordinates (x 10⁴) and equivalent isotropic displacement parameters (A² x 10³) for ew1061. U(eq) is defined as one third of the trace of the orthogonalized U_{ij} tensor.

	x	y	z	U(eq)
Zr(1)	0	3764(1)	7500	14(1)
Cl(1)	1355(1)	3816(1)	7422(1)	22(1)
Cl(2)	0	5494(1)	7500	31(1)

Cl(3)	9335(1)	537(1)	9487(1)	55(1)
Cl(4)	10352(1)	-698(1)	9101(1)	74(1)
N(1)	306(2)	3263(2)	8195(1)	16(1)
N(2)	594(2)	2073(2)	8664(1)	17(1)
N(3)	7280(2)	6280(3)	7015(1)	21(1)
C(1)	0	2229(4)	7500	13(1)
C(2)	168(2)	1732(3)	7886(1)	16(1)
C(3)	160(2)	773(3)	7890(1)	19(1)
C(4)	0	301(4)	7500	18(2)
C(5)	356(2)	2329(3)	8259(1)	15(1)
C(6)	547(2)	3625(3)	8609(1)	16(1)
C(7)	708(2)	2889(3)	8887(1)	18(1)
C(8)	595(2)	4613(3)	8706(1)	16(1)
C(9)	33(3)	5220(3)	8546(1)	21(1)
C(10)	70(3)	6151(3)	8656(1)	26(1)
C(11)	689(3)	6455(3)	8946(1)	26(1)
C(12)	1263(3)	5859(3)	9122(1)	23(1)
C(13)	1225(3)	4951(3)	8984(1)	21(1)
C(14)	952(2)	2852(3)	9360(1)	19(1)
C(15)	725(3)	3501(3)	9642(1)	23(1)
C(16)	956(3)	3441(4)	10088(1)	31(1)
C(17)	1390(3)	2689(4)	10245(2)	31(1)
C(18)	1617(3)	2018(4)	9975(1)	28(1)
C(19)	1406(2)	2129(3)	9533(1)	21(1)
C(20)	-549(3)	6807(3)	8473(2)	35(1)
C(21)	1898(3)	6179(4)	9463(2)	33(1)
C(22)	735(3)	4189(4)	10382(2)	40(1)
C(23)	2089(3)	1204(4)	10156(2)	36(1)
C(24)	6978(2)	6186(3)	7450(1)	23(1)
C(25)	7460(3)	5619(4)	7787(1)	31(1)
C(26)	7182(3)	5699(3)	8221(1)	28(1)
C(27)	7625(3)	5115(4)	8570(2)	34(1)
C(28)	8075(2)	6689(3)	7074(1)	24(1)
C(29)	8162(3)	7597(4)	7306(2)	41(1)
C(30)	8964(3)	7975(4)	7303(2)	36(1)
C(31)	9095(3)	8358(3)	6871(2)	33(1)
C(32)	6718(3)	6898(3)	6741(1)	24(1)
C(33)	6910(3)	7155(3)	6297(1)	26(1)
C(34)	6284(3)	7765(3)	6064(2)	29(1)
C(35)	6453(3)	8083(4)	5624(2)	45(2)
C(36)	7359(2)	5349(3)	6804(1)	22(1)
C(37)	6645(3)	4774(3)	6708(2)	32(1)
C(38)	6755(3)	4033(3)	6373(2)	35(1)
C(39)	7375(3)	3350(3)	6513(2)	32(1)
C(40)	10255(3)	386(4)	9343(2)	45(2)

Table 3. Bond lengths [Å] and angles [deg] for ew1061.

Zr(1)-C(1)	2.229(6)
Zr(1)-N(1)#1	2.280(3)
Zr(1)-N(1)	2.280(3)
Zr(1)-Cl(1)	2.4530(11)
Zr(1)-Cl(1)#1	2.4530(11)
Zr(1)-Cl(2)	2.5139(18)
Cl(3)-C(40)	1.770(6)
Cl(4)-C(40)	1.765(6)
N(1)-C(5)	1.372(6)
N(1)-C(6)	1.407(5)
N(2)-C(5)	1.327(5)
N(2)-C(7)	1.376(5)
N(3)-C(32)	1.514(5)
N(3)-C(28)	1.518(6)
N(3)-C(36)	1.519(6)
N(3)-C(24)	1.536(5)
C(1)-C(2)#1	1.401(5)
C(1)-C(2)	1.401(5)
C(2)-C(3)	1.394(6)
C(2)-C(5)	1.454(6)
C(3)-C(4)	1.392(5)
C(4)-C(3)#1	1.392(5)
C(6)-C(7)	1.380(6)
C(6)-C(8)	1.468(6)
C(7)-C(14)	1.480(6)
C(8)-C(9)	1.372(6)
C(8)-C(13)	1.405(6)
C(9)-C(10)	1.395(7)
C(10)-C(11)	1.392(6)
C(10)-C(20)	1.505(7)
C(11)-C(12)	1.389(7)
C(12)-C(13)	1.386(6)
C(12)-C(21)	1.511(6)
C(14)-C(19)	1.387(6)
C(14)-C(15)	1.388(6)
C(15)-C(16)	1.398(6)
C(16)-C(17)	1.386(7)
C(16)-C(22)	1.512(7)
C(17)-C(18)	1.387(7)
C(18)-C(19)	1.387(6)
C(18)-C(23)	1.511(7)
C(24)-C(25)	1.504(6)

C(25)-C(26)	1.514(6)
C(26)-C(27)	1.510(6)
C(28)-C(29)	1.502(7)
C(29)-C(30)	1.528(7)
C(30)-C(31)	1.508(7)
C(32)-C(33)	1.520(6)
C(33)-C(34)	1.522(6)
C(34)-C(35)	1.519(6)
C(36)-C(37)	1.513(6)
C(37)-C(38)	1.531(7)
C(38)-C(39)	1.500(7)
C(1)-Zr(1)-N(1)#1	71.38(9)
C(1)-Zr(1)-N(1)	71.38(9)
N(1)#1-Zr(1)-N(1)	142.75(18)
C(1)-Zr(1)-Cl(1)	91.78(3)
N(1)#1-Zr(1)-Cl(1)	91.14(9)
N(1)-Zr(1)-Cl(1)	90.00(9)
C(1)-Zr(1)-Cl(1)#1	91.78(3)
N(1)#1-Zr(1)-Cl(1)#1	90.00(9)
N(1)-Zr(1)-Cl(1)#1	91.14(9)
Cl(1)-Zr(1)-Cl(1)#1	176.45(6)
C(1)-Zr(1)-Cl(2)	180.000(1)
N(1)#1-Zr(1)-Cl(2)	108.62(9)
N(1)-Zr(1)-Cl(2)	108.62(9)
Cl(1)-Zr(1)-Cl(2)	88.22(3)
Cl(1)#1-Zr(1)-Cl(2)	88.22(3)
C(5)-N(1)-C(6)	103.3(3)
C(5)-N(1)-Zr(1)	117.2(2)
C(6)-N(1)-Zr(1)	139.2(3)
C(5)-N(2)-C(7)	104.2(3)
C(32)-N(3)-C(28)	111.4(3)
C(32)-N(3)-C(36)	112.2(3)
C(28)-N(3)-C(36)	105.0(3)
C(32)-N(3)-C(24)	105.5(3)
C(28)-N(3)-C(24)	111.2(3)
C(36)-N(3)-C(24)	111.6(3)
C(2)#1-C(1)-C(2)	117.8(6)
C(2)#1-C(1)-Zr(1)	121.1(3)
C(2)-C(1)-Zr(1)	121.1(3)
C(3)-C(2)-C(1)	121.6(4)
C(3)-C(2)-C(5)	126.2(4)
C(1)-C(2)-C(5)	112.2(4)
C(4)-C(3)-C(2)	118.9(4)
C(3)-C(4)-C(3)#1	121.1(6)
N(2)-C(5)-N(1)	114.9(4)

N(2)-C(5)-C(2)	127.0(4)
N(1)-C(5)-C(2)	118.0(3)
C(7)-C(6)-N(1)	107.3(4)
C(7)-C(6)-C(8)	128.9(4)
N(1)-C(6)-C(8)	123.8(4)
N(2)-C(7)-C(6)	110.3(3)
N(2)-C(7)-C(14)	118.4(4)
C(6)-C(7)-C(14)	131.3(4)
C(9)-C(8)-C(13)	118.3(4)
C(9)-C(8)-C(6)	122.5(4)
C(13)-C(8)-C(6)	119.1(4)
C(8)-C(9)-C(10)	121.8(4)
C(11)-C(10)-C(9)	118.2(4)
C(11)-C(10)-C(20)	120.9(4)
C(9)-C(10)-C(20)	120.9(4)
C(12)-C(11)-C(10)	121.8(4)
C(13)-C(12)-C(11)	118.0(4)
C(13)-C(12)-C(21)	120.6(4)
C(11)-C(12)-C(21)	121.3(4)
C(12)-C(13)-C(8)	121.6(4)
C(19)-C(14)-C(15)	118.3(4)
C(19)-C(14)-C(7)	119.1(4)
C(15)-C(14)-C(7)	122.6(4)
C(14)-C(15)-C(16)	121.2(4)
C(17)-C(16)-C(15)	118.2(4)
C(17)-C(16)-C(22)	122.0(4)
C(15)-C(16)-C(22)	119.8(5)
C(16)-C(17)-C(18)	122.3(4)
C(17)-C(18)-C(19)	117.6(4)
C(17)-C(18)-C(23)	121.1(4)
C(19)-C(18)-C(23)	121.3(4)
C(14)-C(19)-C(18)	122.3(4)
C(25)-C(24)-N(3)	115.7(4)
C(24)-C(25)-C(26)	111.1(4)
C(27)-C(26)-C(25)	113.6(4)
C(29)-C(28)-N(3)	115.6(4)
C(28)-C(29)-C(30)	110.1(4)
C(31)-C(30)-C(29)	113.6(4)
N(3)-C(32)-C(33)	116.4(4)
C(32)-C(33)-C(34)	109.6(4)
C(35)-C(34)-C(33)	112.7(4)
C(37)-C(36)-N(3)	116.9(4)
C(36)-C(37)-C(38)	109.8(4)
C(39)-C(38)-C(37)	115.2(4)
Cl(4)-C(40)-Cl(3)	111.7(3)

Symmetry transformations used to generate equivalent atoms:

#1 -x,y,-z+3/2

Table 4. Anisotropic displacement parameters ($\text{Å}^2 \times 10^3$) for ew1061.

The anisotropic displacement factor exponent takes the form:

$-2 \pi^2 [h^2 a^{*2} U_{11} + \dots + 2 h k a^* b^* U_{12}]$

	U11	U22	U33	U23	U13	U12
Zr(1)	14(1)	15(1)	12(1)	0	2(1)	0
Cl(1)	15(1)	25(1)	25(1)	-2(1)	3(1)	-2(1)
Cl(2)	42(1)	16(1)	40(1)	0	21(1)	0
Cl(3)	46(1)	70(1)	49(1)	10(1)	7(1)	-6(1)
Cl(4)	79(1)	54(1)	89(1)	-11(1)	4(1)	6(1)
N(1)	12(2)	20(2)	16(2)	-4(2)	4(1)	-1(2)
N(2)	16(2)	18(2)	15(2)	4(2)	1(1)	1(2)
N(3)	16(2)	24(2)	23(2)	-3(2)	4(2)	-1(2)
C(1)	5(3)	14(3)	21(3)	0	5(2)	0
C(2)	11(2)	17(3)	20(2)	2(2)	3(2)	0(2)
C(3)	14(2)	27(3)	15(2)	4(2)	-1(2)	2(2)
C(4)	17(3)	13(3)	24(3)	0	0(3)	0
C(5)	14(2)	19(3)	13(2)	-1(2)	3(2)	2(2)
C(6)	13(2)	19(3)	16(2)	-6(2)	1(2)	1(2)
C(7)	15(2)	22(3)	15(2)	1(2)	2(2)	0(2)
C(8)	16(2)	23(3)	11(2)	1(2)	6(2)	-2(2)
C(9)	22(3)	27(3)	14(2)	-2(2)	1(2)	2(2)
C(10)	29(3)	23(3)	26(2)	1(2)	7(2)	4(2)
C(11)	37(3)	14(3)	28(3)	-3(2)	6(2)	-8(2)
C(12)	26(3)	29(3)	14(2)	1(2)	4(2)	-11(2)
C(13)	22(3)	28(3)	13(2)	3(2)	4(2)	-3(2)
C(14)	17(2)	25(3)	16(2)	4(2)	2(2)	-6(2)
C(15)	20(3)	32(3)	17(2)	3(2)	-1(2)	-5(2)
C(16)	27(3)	43(3)	22(3)	1(2)	4(2)	-8(2)
C(17)	31(3)	43(3)	16(2)	9(2)	-3(2)	-11(3)
C(18)	21(3)	39(3)	21(3)	8(2)	-4(2)	-10(2)
C(19)	21(3)	18(3)	23(2)	2(2)	1(2)	-7(2)
C(20)	35(3)	25(3)	44(3)	-3(2)	1(2)	2(2)
C(21)	38(3)	33(3)	30(3)	-4(2)	8(2)	-11(3)
C(22)	50(3)	54(4)	18(3)	-8(2)	8(2)	-5(3)
C(23)	32(3)	48(3)	26(3)	14(2)	-6(2)	-7(3)
C(24)	21(2)	31(3)	19(2)	0(2)	8(2)	-1(2)

C(25)	27(3)	44(3)	21(2)	-1(2)	2(2)	9(2)
C(26)	30(3)	26(3)	29(3)	2(2)	9(2)	-1(2)
C(27)	29(3)	42(3)	29(3)	-1(2)	1(2)	-4(3)
C(28)	16(2)	32(3)	24(2)	-7(2)	8(2)	-1(2)
C(29)	30(3)	45(3)	53(3)	-27(3)	22(2)	-19(3)
C(30)	28(3)	41(3)	42(3)	-19(2)	15(2)	-14(3)
C(31)	28(3)	22(3)	49(3)	-3(2)	2(2)	-2(2)
C(32)	20(3)	23(3)	30(3)	4(2)	4(2)	4(2)
C(33)	21(3)	28(3)	30(3)	1(2)	7(2)	-1(2)
C(34)	26(3)	29(3)	33(3)	7(2)	7(2)	7(2)
C(35)	39(3)	61(4)	36(3)	23(3)	12(2)	18(3)
C(36)	25(3)	23(3)	21(2)	-4(2)	5(2)	3(2)
C(37)	27(3)	29(3)	42(3)	-7(2)	10(2)	-5(2)
C(38)	27(3)	30(3)	47(3)	-9(2)	1(2)	-7(2)
C(39)	42(3)	27(3)	29(3)	-2(2)	12(2)	-4(3)
C(40)	40(3)	48(4)	44(3)	2(3)	0(3)	-15(3)

Table 5. Hydrogen coordinates ($\times 10^4$) and isotropic displacement parameters ($\text{\AA}^2 \times 10^3$) for ew1061.

	x	y	z	U(eq)
H(3A)	263	446	8156	23
H(4)	0	-353	7500	22
H(9A)	-393	5001	8354	26
H(11A)	720	7086	9025	32
H(13A)	1635	4548	9081	25
H(15A)	405	3995	9529	28
H(17A)	1538	2631	10548	37
H(19A)	1579	1694	9342	25
H(20A)	-454	7413	8607	53
H(20B)	-1042	6575	8531	53
H(20C)	-555	6861	8160	53
H(21A)	1762	6056	9751	50
H(21B)	1978	6842	9430	50
H(21C)	2367	5848	9429	50
H(22A)	187	4156	10394	60
H(22B)	860	4791	10271	60
H(22C)	1014	4103	10674	60
H(23A)	2282	876	9920	54

H(23B)	1773	788	10301	54
H(23C)	2518	1421	10364	54
H(24A)	6924	6810	7569	28
H(24B)	6464	5909	7396	28
H(25A)	7995	5830	7813	37
H(25B)	7443	4966	7695	37
H(26A)	7216	6351	8314	33
H(26B)	6640	5516	8188	33
H(27A)	7560	4463	8492	51
H(27B)	7436	5225	8845	51
H(27C)	8165	5277	8599	51
H(28A)	8428	6242	7237	29
H(28B)	8235	6767	6785	29
H(29A)	8067	7516	7608	49
H(29B)	7784	8040	7162	49
H(30A)	9060	8467	7523	43
H(30B)	9336	7476	7386	43
H(31A)	9009	7874	6651	50
H(31B)	9619	8582	6890	50
H(31C)	8741	8868	6790	50
H(32A)	6665	7472	6904	29
H(32B)	6216	6588	6701	29
H(33A)	6959	6591	6126	31
H(33B)	7402	7487	6329	31
H(34A)	5799	7420	6026	35
H(34B)	6221	8310	6245	35
H(35A)	6933	8428	5660	67
H(35B)	6040	8481	5490	67
H(35C)	6496	7547	5439	67
H(36A)	7563	5451	6529	27
H(36B)	7742	4987	6995	27
H(37A)	6210	5172	6595	39
H(37B)	6531	4479	6977	39
H(38A)	6270	3695	6300	42
H(38B)	6866	4341	6107	42
H(39A)	7863	3672	6574	48
H(39B)	7398	2901	6281	48
H(39C)	7268	3032	6774	48
H(40A)	10354	877	9139	54
H(40B)	10639	442	9605	54

Appendix 4

Crystallographic Data for [TBA]₂[Zr(XXX)Br₃]

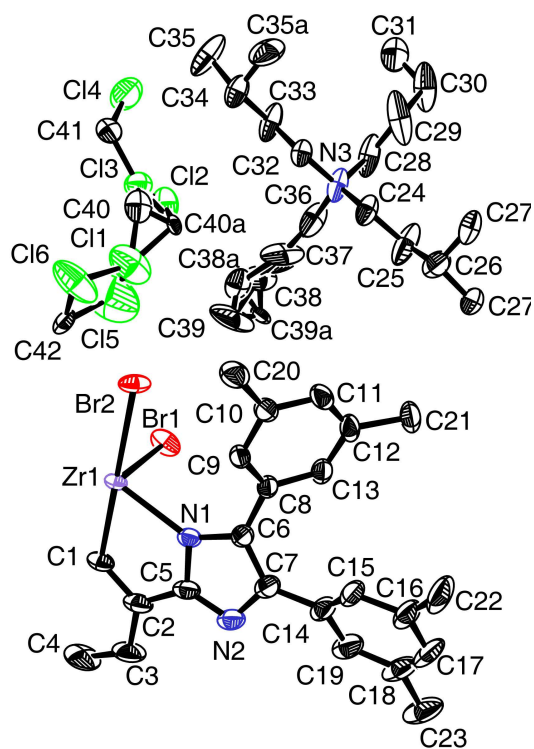


Figure A.4. 50% thermal ellipsoid plot of [TBA]₂[Zr(XXX)Br₃].

Structure Determination.

Orange plates of **ew1170** were grown from a dichloromethane solution at $-35\text{ }^{\circ}\text{C}$. A crystal of dimensions $0.20 \times 0.16 \times 0.13\text{ mm}$ was mounted on a Bruker SMART APEX CCD-based X-ray diffractometer equipped with a low temperature device and fine focus Mo-target X-ray tube ($\lambda = 0.71073\text{ \AA}$) operated at 1500 W power (50 kV, 30 mA). The X-ray intensities were measured at 85(1) K; the detector was placed at a distance 5.055 cm from the crystal. A total of 3855 frames were collected with a scan width of 0.5° in ω and 0.45° in ϕ with an exposure time of 25 s/frame. The integration of the data yielded a total of 137132 reflections to a maximum 2θ value of 56.76° of which 10356 were independent and 8599 were greater than $2\sigma(I)$. The final cell constants (Table 1) were based on the xyz centroids of 9278 reflections above $10\sigma(I)$. Analysis of the data showed negligible decay during data collection; the data were processed with SADABS and corrected for absorption. The structure was solved and refined with the Bruker SHELXTL (version 2008/3) software package, using the space group C2/c with $Z = 4$ for the formula $2(\text{C}_{16}\text{H}_{36}\text{N})(\text{C}_{44}\text{H}_{39}\text{N}_4\text{Br}_3\text{Zr})\cdot(\text{CH}_2\text{Cl}_2)_{1.5}$. The Zr-complex lies on a two-fold axis in the crystal lattice. The tetrabutylammomium cations are disordered as well as the dichloromethane solvates. All non-hydrogen atoms were refined anisotropically with the hydrogen atoms placed in idealized positions. Full matrix least-squares refinement based on F^2 converged at $R1 = 0.0588$ and $wR2 = 0.1595$ [based on $I > 2\sigma(I)$], $R1 = 0.0712$ and $wR2 = 0.1692$ for all data.

Sheldrick, G.M. SHELXTL, v. 2008/3; Bruker Analytical X-ray, Madison, WI, 2008.

Sheldrick, G.M. SADABS, v. 2008/1. Program for Empirical Absorption Correction of Area Detector Data, University of Gottingen: Gottingen, Germany, 2008.

Saint Plus, v. 7.53a, Bruker Analytical X-ray, Madison, WI, 2008.

Table 1. Crystal data and structure refinement for ew1170.

Identification code	ew1170
Empirical formula	C _{86.50} H ₁₁₃ Br ₃ Cl _{13.50} N ₆ Zr
Formula weight	1691.85
Temperature	85(2) K
Wavelength	0.71073 Å
Crystal system, space group	Monoclinic, C2/c
Unit cell dimensions	a = 17.6952(18) Å alpha = 90 deg. b = 15.2772(15) Å beta = 99.520(2) deg. c = 31.048(3) Å gamma = 90 deg.
Volume	8277.7(14) Å ³
Z, Calculated density	4, 1.358 Mg/m ³
Absorption coefficient	1.741 mm ⁻¹
F(000)	3514
Crystal size	0.20 x 0.16 x 0.13 mm
Theta range for data collection	1.77 to 28.38 deg.
Limiting indices	-23 ≤ h ≤ 23, -20 ≤ k ≤ 20, -41 ≤ l ≤ 41
Reflections collected / unique	137172 / 10356 [R(int) = 0.0455]
Completeness to theta = 28.38	99.7 %
Absorption correction	Semi-empirical from equivalents
Max. and min. transmission	0.8053 and 0.7222
Refinement method	Full-matrix least-squares on F ²

Data / restraints / parameters	10356 / 53 / 543
Goodness-of-fit on F ²	1.052
Final R indices [I > 2σ(I)]	R1 = 0.0588, wR2 = 0.1595
R indices (all data)	R1 = 0.0712, wR2 = 0.1692
Largest diff. peak and hole	1.014 and -1.022 e.Å ⁻³

Table 2. Atomic coordinates (x 10⁴) and equivalent isotropic displacement parameters (Å² x 10³) for ew1170.

U(eq) is defined as one third of the trace of the orthogonalized U_{ij} tensor.

	x	y	z	U(eq)
Zr(1)	0	3789(1)	7500	22(1)
Br(1)	1452(1)	3888(1)	7456(1)	42(1)
Br(2)	0	5542(1)	7500	39(1)
N(1)	304(2)	3318(2)	8203(1)	30(1)
N(2)	545(2)	2178(2)	8679(1)	42(1)
N(3)	7335(2)	6498(3)	6994(1)	54(1)
C(1)	0	2323(3)	7500	33(1)
C(2)	155(2)	1862(2)	7890(1)	41(1)
C(3)	155(3)	946(3)	7895(2)	58(1)
C(4)	0	508(4)	7500	71(2)
C(5)	326(2)	2418(2)	8271(1)	36(1)
C(6)	544(2)	3653(2)	8620(1)	33(1)
C(7)	682(2)	2951(3)	8907(1)	41(1)
C(8)	645(2)	4591(2)	8724(1)	33(1)
C(9)	89(2)	5205(2)	8571(1)	32(1)
C(10)	189(2)	6081(2)	8688(1)	38(1)
C(11)	846(2)	6321(3)	8978(1)	45(1)
C(12)	1396(2)	5722(3)	9144(1)	45(1)
C(13)	1307(2)	4862(3)	9005(1)	41(1)
C(14)	915(2)	2924(3)	9387(1)	48(1)
C(15)	711(2)	3570(3)	9657(1)	49(1)
C(16)	944(2)	3547(4)	10111(1)	59(1)

C(17)	1365(2)	2830(4)	10286(2)	72(2)
C(18)	1570(2)	2164(4)	10027(2)	73(2)
C(19)	1349(2)	2219(3)	9578(2)	59(1)
C(20)	-408(3)	6744(3)	8512(1)	47(1)
C(21)	2077(3)	5968(4)	9487(1)	60(1)
C(22)	739(3)	4274(4)	10392(1)	74(2)
C(23)	2021(3)	1363(4)	10221(2)	90(2)
C(24)	7039(3)	6431(3)	7431(1)	52(1)
C(25)	7533(4)	5895(4)	7782(2)	95(2)
C(26)	7231(4)	5935(4)	8207(2)	67(1)
C(27)	7591(5)	5387(5)	8564(2)	56(2)
C(27A)	7321(6)	6810(9)	8430(3)	55(3)
C(28)	8125(2)	6916(4)	7050(2)	73(2)
C(29)	8201(3)	7804(6)	7259(2)	107(3)
C(30)	9001(3)	8215(6)	7252(2)	94(2)
C(31)	9138(3)	8518(4)	6824(2)	76(2)
C(32)	6755(2)	7062(3)	6701(1)	39(1)
C(33)	6934(2)	7285(4)	6257(1)	64(1)
C(34)	6312(2)	7859(4)	6010(1)	55(1)
C(35)	6486(5)	8201(7)	5569(2)	92(3)
C(35A)	6523(15)	8690(12)	6184(7)	85(7)
C(36)	7419(4)	5619(3)	6793(2)	76(2)
C(37)	6691(7)	5099(5)	6740(3)	99(3)
C(38)	6977(7)	4298(5)	6471(3)	80(3)
C(39)	6349(8)	3654(6)	6439(3)	143(5)
C(37A)	6776(13)	4937(11)	6745(7)	91(6)
C(38A)	6525(9)	4248(11)	6375(5)	60(4)
C(39A)	7127(8)	3526(7)	6523(4)	42(3)
Cl(1)	4332(3)	4885(3)	5840(1)	116(1)
Cl(2)	5799(2)	5459(2)	5626(1)	71(1)
C(40)	4849(5)	5712(7)	5643(4)	58(3)
Cl(1A)	4332(3)	4885(3)	5840(1)	116(1)
Cl(2A)	5799(2)	5459(2)	5626(1)	71(1)
C(40A)	5158(10)	5524(17)	5971(8)	28(7)
Cl(4)	6235(2)	6951(3)	4820(1)	115(1)
Cl(3)	5593(2)	5706(2)	5356(1)	60(1)
C(41)	5376(4)	6561(5)	4990(3)	48(2)
Cl(6)	2970(4)	4895(5)	5738(3)	115(2)
Cl(5)	4374(5)	4091(11)	5693(6)	190(6)
C(42)	3334(4)	3851(5)	5571(2)	46(2)

Table 3. Bond lengths [Å] and angles [deg] for ew1170.

Zr(1)-C(1)	2.239(4)
Zr(1)-N(1)#1	2.278(3)
Zr(1)-N(1)	2.278(3)
Zr(1)-Br(1)	2.6007(4)
Zr(1)-Br(1)#1	2.6007(4)
Zr(1)-Br(2)	2.6789(6)
N(1)-C(5)	1.389(4)
N(1)-C(6)	1.392(4)
N(2)-C(5)	1.316(5)
N(2)-C(7)	1.378(5)
N(3)-C(36)	1.498(6)
N(3)-C(28)	1.521(7)
N(3)-C(32)	1.522(5)
N(3)-C(24)	1.536(5)
C(1)-C(2)#1	1.389(4)
C(1)-C(2)	1.389(4)
C(2)-C(3)	1.400(5)
C(2)-C(5)	1.446(6)
C(3)-C(4)	1.384(6)
C(4)-C(3)#1	1.384(6)
C(6)-C(7)	1.389(5)
C(6)-C(8)	1.472(5)
C(7)-C(14)	1.480(5)
C(8)-C(9)	1.385(5)
C(8)-C(13)	1.404(4)
C(9)-C(10)	1.390(5)
C(10)-C(11)	1.397(5)
C(10)-C(20)	1.499(6)
C(11)-C(12)	1.373(6)
C(12)-C(13)	1.384(6)
C(12)-C(21)	1.517(5)
C(14)-C(15)	1.382(7)
C(14)-C(19)	1.396(6)
C(15)-C(16)	1.401(5)
C(16)-C(17)	1.383(7)
C(16)-C(22)	1.494(8)
C(17)-C(18)	1.381(9)
C(18)-C(19)	1.388(7)
C(18)-C(23)	1.530(7)
C(24)-C(25)	1.520(6)
C(25)-C(26)	1.504(8)
C(26)-C(27)	1.449(8)

C(26)-C(27A)	1.501(14)
C(28)-C(29)	1.501(9)
C(29)-C(30)	1.552(8)
C(30)-C(31)	1.466(8)
C(32)-C(33)	1.503(6)
C(33)-C(34)	1.515(6)
C(34)-C(35A)	1.41(2)
C(34)-C(35)	1.543(8)
C(36)-C(37)	1.499(11)
C(36)-C(37A)	1.531(17)
C(37)-C(38)	1.609(11)
C(38)-C(39)	1.475(12)
C(37A)-C(38A)	1.567(17)
C(38A)-C(39A)	1.551(16)
Cl(1)-C(40)	1.729(11)
Cl(2)-C(40)	1.734(9)
Cl(4)-C(41)	1.791(9)
Cl(3)-C(41)	1.733(8)
Cl(6)-C(42)	1.827(10)
Cl(5)-C(42)	1.853(11)
C(1)-Zr(1)-N(1)#1	71.59(7)
C(1)-Zr(1)-N(1)	71.59(7)
N(1)#1-Zr(1)-N(1)	143.18(14)
C(1)-Zr(1)-Br(1)	93.341(12)
N(1)#1-Zr(1)-Br(1)	92.65(7)
N(1)-Zr(1)-Br(1)	89.46(7)
C(1)-Zr(1)-Br(1)#1	93.341(12)
N(1)#1-Zr(1)-Br(1)#1	89.46(7)
N(1)-Zr(1)-Br(1)#1	92.65(7)
Br(1)-Zr(1)-Br(1)#1	173.32(2)
C(1)-Zr(1)-Br(2)	180.000(1)
N(1)#1-Zr(1)-Br(2)	108.41(7)
N(1)-Zr(1)-Br(2)	108.41(7)
Br(1)-Zr(1)-Br(2)	86.659(12)
Br(1)#1-Zr(1)-Br(2)	86.659(12)
C(5)-N(1)-C(6)	103.2(3)
C(5)-N(1)-Zr(1)	116.9(2)
C(6)-N(1)-Zr(1)	139.7(2)
C(5)-N(2)-C(7)	104.7(3)
C(36)-N(3)-C(28)	105.7(4)
C(36)-N(3)-C(32)	111.2(3)
C(28)-N(3)-C(32)	110.3(4)
C(36)-N(3)-C(24)	112.3(4)
C(28)-N(3)-C(24)	111.7(3)
C(32)-N(3)-C(24)	105.7(3)

C(2)#1-C(1)-C(2)	119.1(4)
C(2)#1-C(1)-Zr(1)	120.5(2)
C(2)-C(1)-Zr(1)	120.5(2)
C(1)-C(2)-C(3)	121.0(4)
C(1)-C(2)-C(5)	113.5(3)
C(3)-C(2)-C(5)	125.4(4)
C(4)-C(3)-C(2)	118.3(5)
C(3)-C(4)-C(3)#1	122.2(5)
N(2)-C(5)-N(1)	114.7(3)
N(2)-C(5)-C(2)	127.7(3)
N(1)-C(5)-C(2)	117.5(3)
C(7)-C(6)-N(1)	107.9(3)
C(7)-C(6)-C(8)	127.5(3)
N(1)-C(6)-C(8)	124.6(3)
N(2)-C(7)-C(6)	109.6(3)
N(2)-C(7)-C(14)	119.3(3)
C(6)-C(7)-C(14)	131.1(4)
C(9)-C(8)-C(13)	119.0(3)
C(9)-C(8)-C(6)	122.1(3)
C(13)-C(8)-C(6)	118.8(3)
C(8)-C(9)-C(10)	120.8(3)
C(9)-C(10)-C(11)	118.5(4)
C(9)-C(10)-C(20)	120.3(3)
C(11)-C(10)-C(20)	121.2(3)
C(12)-C(11)-C(10)	122.0(4)
C(11)-C(12)-C(13)	118.6(3)
C(11)-C(12)-C(21)	122.0(4)
C(13)-C(12)-C(21)	119.4(4)
C(12)-C(13)-C(8)	120.9(4)
C(15)-C(14)-C(19)	118.4(4)
C(15)-C(14)-C(7)	122.3(4)
C(19)-C(14)-C(7)	119.3(4)
C(14)-C(15)-C(16)	121.9(4)
C(17)-C(16)-C(15)	117.7(5)
C(17)-C(16)-C(22)	121.8(4)
C(15)-C(16)-C(22)	120.5(5)
C(18)-C(17)-C(16)	122.0(4)
C(17)-C(18)-C(19)	118.9(4)
C(17)-C(18)-C(23)	122.1(5)
C(19)-C(18)-C(23)	119.0(6)
C(18)-C(19)-C(14)	121.1(5)
C(25)-C(24)-N(3)	115.5(4)
C(26)-C(25)-C(24)	111.2(4)
C(27)-C(26)-C(27A)	99.3(6)

C(27)-C(26)-C(25)	118.1(6)
C(27A)-C(26)-C(25)	114.4(7)
C(29)-C(28)-N(3)	116.3(4)
C(28)-C(29)-C(30)	112.1(5)
C(31)-C(30)-C(29)	115.3(5)
C(33)-C(32)-N(3)	116.9(3)
C(32)-C(33)-C(34)	110.5(3)
C(35A)-C(34)-C(33)	101.7(9)
C(35A)-C(34)-C(35)	87.6(10)
C(33)-C(34)-C(35)	114.3(4)
N(3)-C(36)-C(37)	112.2(5)
N(3)-C(36)-C(37A)	121.8(10)
C(37)-C(36)-C(37A)	10.9(10)
C(36)-C(37)-C(38)	97.0(7)
C(39)-C(38)-C(37)	104.2(8)
C(36)-C(37A)-C(38A)	130.1(18)
C(39A)-C(38A)-C(37A)	99.4(13)
Cl(1)-C(40)-Cl(2)	114.9(6)
Cl(3)-C(41)-Cl(4)	109.7(4)
Cl(6)-C(42)-Cl(5)	98.9(7)

Symmetry transformations used to generate equivalent atoms:
 #1 -x,y,-z+3/2

Table 4. Anisotropic displacement parameters ($\text{\AA}^2 \times 10^3$) for ew1170.
 The anisotropic displacement factor exponent takes the form:
 $-2 \pi^2 [h^2 a^{*2} U_{11} + \dots + 2 h k a^* b^* U_{12}]$

	U11	U22	U33	U23	U13	U12
Zr(1)	20(1)	16(1)	32(1)	0	10(1)	0
Br(1)	26(1)	41(1)	63(1)	-12(1)	19(1)	-4(1)
Br(2)	63(1)	18(1)	41(1)	0	28(1)	0
N(1)	26(1)	26(1)	37(1)	5(1)	6(1)	-4(1)
N(2)	29(1)	40(2)	55(2)	20(1)	2(1)	-4(1)
N(3)	55(2)	74(2)	30(2)	-11(2)	-2(1)	38(2)
C(1)	29(2)	19(2)	51(3)	0	11(2)	0
C(2)	37(2)	22(2)	64(2)	7(2)	8(2)	-3(1)

C(3)	63(3)	22(2)	87(3)	14(2)	5(2)	-5(2)
C(4)	80(5)	18(2)	110(6)	0	4(4)	0
C(5)	28(2)	28(2)	52(2)	12(1)	7(1)	-4(1)
C(6)	24(1)	40(2)	34(2)	9(1)	1(1)	-6(1)
C(7)	25(2)	51(2)	44(2)	20(2)	-1(1)	-6(1)
C(8)	31(2)	44(2)	24(1)	5(1)	2(1)	-12(1)
C(9)	35(2)	38(2)	24(1)	-1(1)	3(1)	-12(1)
C(10)	49(2)	39(2)	26(2)	-3(1)	10(1)	-15(2)
C(11)	62(2)	49(2)	25(2)	-8(1)	12(2)	-29(2)
C(12)	44(2)	69(2)	20(1)	0(2)	4(1)	-30(2)
C(13)	35(2)	59(2)	26(2)	8(2)	2(1)	-19(2)
C(14)	29(2)	65(2)	44(2)	28(2)	-6(2)	-11(2)
C(15)	34(2)	74(3)	35(2)	26(2)	-5(1)	-15(2)
C(16)	40(2)	98(3)	37(2)	32(2)	-1(2)	-21(2)
C(17)	38(2)	121(4)	50(2)	58(3)	-8(2)	-22(2)
C(18)	29(2)	100(4)	82(3)	67(3)	-10(2)	-14(2)
C(19)	32(2)	73(3)	68(3)	39(2)	-6(2)	-10(2)
C(20)	64(3)	36(2)	44(2)	-8(2)	12(2)	-8(2)
C(21)	59(2)	92(3)	27(2)	-1(2)	0(2)	-46(2)
C(22)	72(3)	124(5)	24(2)	19(2)	4(2)	-17(3)
C(23)	39(2)	114(4)	109(4)	83(4)	-13(2)	-11(3)
C(24)	67(3)	57(2)	30(2)	-8(2)	2(2)	30(2)
C(25)	147(5)	99(4)	34(2)	-8(2)	-5(3)	86(4)
C(26)	83(4)	61(3)	53(3)	15(2)	4(2)	7(3)
C(27)	55(4)	59(4)	47(4)	11(3)	-11(3)	3(3)
C(27A)	42(5)	89(9)	33(5)	2(5)	2(4)	19(5)
C(28)	33(2)	143(5)	40(2)	-12(3)	-2(2)	41(3)
C(29)	32(2)	211(7)	81(3)	-88(4)	16(2)	-10(3)
C(30)	25(2)	200(8)	58(3)	-43(4)	8(2)	-6(3)
C(31)	77(3)	75(3)	71(3)	-18(3)	-1(3)	30(3)
C(32)	30(2)	50(2)	36(2)	-4(2)	3(1)	16(2)
C(33)	44(2)	114(4)	33(2)	-2(2)	2(2)	43(2)
C(34)	42(2)	81(3)	42(2)	4(2)	3(2)	25(2)
C(35)	84(5)	146(8)	50(4)	38(4)	21(3)	73(5)
C(35A)	123(18)	50(9)	80(13)	16(9)	16(12)	34(11)
C(36)	123(4)	67(3)	36(2)	-10(2)	4(2)	57(3)
C(37)	222(9)	21(3)	76(5)	-14(3)	86(6)	7(4)
C(38)	145(8)	48(4)	57(4)	-12(3)	46(5)	-11(4)
C(39)	288(14)	74(5)	90(6)	-54(4)	96(8)	-101(7)
C(37A)	177(14)	27(7)	70(11)	21(6)	22(13)	45(7)
C(38A)	46(8)	94(11)	43(8)	8(7)	18(6)	-2(6)
C(39A)	66(8)	32(5)	28(5)	-8(4)	10(5)	-31(5)
Cl(1)	137(3)	115(3)	110(3)	-46(2)	62(2)	-41(3)
Cl(2)	52(1)	86(2)	71(2)	-16(1)	3(1)	16(1)
C(40)	58(5)	61(6)	55(6)	-23(5)	12(5)	21(5)
Cl(1A)	137(3)	115(3)	110(3)	-46(2)	62(2)	-41(3)

Cl(2A)	52(1)	86(2)	71(2)	-16(1)	3(1)	16(1)
C(40A)	28(9)	18(9)	32(9)	-9(6)	-11(6)	4(6)
Cl(4)	89(2)	136(3)	109(3)	57(2)	-18(2)	-31(2)
Cl(3)	59(1)	57(1)	64(1)	7(1)	10(1)	-4(1)
C(41)	39(4)	33(4)	69(5)	-8(3)	2(3)	14(3)
Cl(6)	98(4)	118(4)	147(6)	-70(4)	73(4)	-54(3)
Cl(5)	74(4)	205(12)	303(18)	-8(13)	64(7)	-30(5)
C(42)	33(3)	69(4)	34(3)	26(3)	2(3)	-1(3)

Table 5. Hydrogen coordinates ($\times 10^4$) and isotropic displacement parameters ($\text{\AA}^2 \times 10^3$) for ew1170.

	x	y	z	U(eq)
H(3A)	259	633	8163	70
H(4)	0	-114	7500	85
H(9A)	-365	5026	8385	39
H(11A)	915	6918	9062	54
H(13A)	1700	4449	9102	49
H(15A)	403	4045	9532	59
H(17A)	1519	2795	10593	86
H(19A)	1495	1770	9397	71
H(20A)	-301	7296	8672	71
H(20B)	-914	6528	8550	71
H(20C)	-397	6842	8202	71
H(21A)	1995	5753	9773	90
H(21B)	2132	6607	9497	90
H(21C)	2543	5704	9412	90
H(22A)	203	4213	10430	111
H(22B)	809	4837	10252	111
H(22C)	1071	4250	10678	111
H(23A)	2288	1101	10000	135
H(23B)	1667	933	10312	135
H(23C)	2395	1541	10474	135
H(24A)	6991	7030	7544	62
H(24B)	6520	6171	7375	62

H(25A)	7543	5278	7685	115
H(25B)	8065	6121	7827	115
H(26A)	7267	6550	8309	80
H(26B)	6679	5783	8146	80
H(26C)	6681	5776	8151	80
H(26D)	7502	5491	8407	80
H(27A)	7426	4780	8509	83
H(27B)	7443	5590	8837	83
H(27C)	8149	5423	8586	83
H(27D)	7192	6758	8724	83
H(27E)	6978	7235	8260	83
H(27F)	7853	7008	8450	83
H(28A)	8493	6517	7227	88
H(28B)	8279	6962	6758	88
H(29A)	8115	7755	7565	128
H(29B)	7801	8196	7102	128
H(30A)	9067	8718	7456	113
H(30B)	9397	7776	7363	113
H(31A)	9034	8040	6612	114
H(31B)	9672	8705	6845	114
H(31C)	8798	9012	6728	114
H(32A)	6255	6756	6660	47
H(32B)	6693	7616	6856	47
H(33A)	6977	6740	6090	77
H(33B)	7432	7594	6289	77
H(34A)	6232	8367	6195	66
H(34B)	5827	7522	5956	66
H(34C)	6320	7839	5692	66
H(34D)	5799	7676	6064	66
H(35A)	6970	8526	5617	138
H(35B)	6071	8588	5435	138
H(35C)	6528	7705	5374	138
H(35D)	6259	8805	6432	127
H(35E)	6378	9138	5959	127
H(35F)	7078	8708	6283	127
H(36A)	7830	5288	6980	91
H(36B)	7574	5699	6504	91
H(36C)	7486	5717	6486	91
H(36D)	7901	5356	6946	91
H(37A)	6254	5417	6569	119
H(37B)	6559	4911	7023	119
H(38A)	7058	4491	6178	96
H(38B)	7461	4049	6629	96
H(39A)	6225	3544	6730	215
H(39B)	6510	3106	6317	215
H(39C)	5896	3884	6248	215

H(37C)	6306	5277	6763	109
H(37D)	6879	4589	7018	109
H(38C)	5995	4038	6375	72
H(38D)	6569	4482	6083	72
H(39D)	7643	3765	6530	62
H(39E)	7046	3034	6318	62
H(39F)	7073	3322	6816	62
H(40A)	4833	6236	5829	69
H(40B)	4593	5865	5345	69
H(40C)	5000	6144	5987	34
H(40D)	5419	5354	6266	34
H(41A)	5131	7042	5130	57
H(41B)	5012	6359	4733	57
H(42A)	3160	3731	5257	55
H(42B)	3191	3357	5748	55

Appendix 5

Crystallographic Data for $\text{Zr}(\text{LXL-Me}_2)\text{Cl}_3$

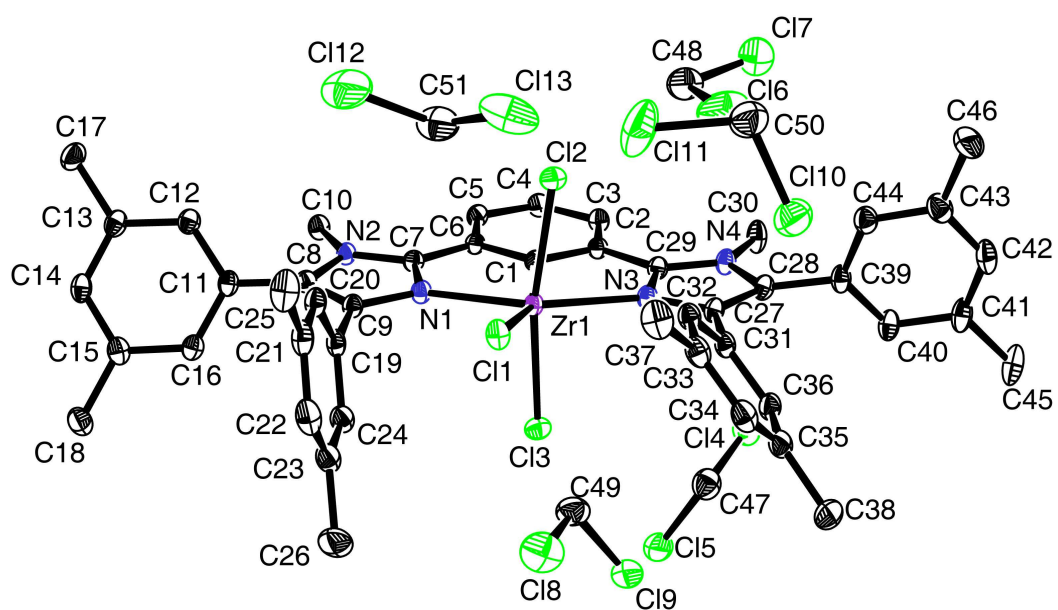


Figure A.5. 50% thermal ellipsoid plot of $\text{Zr}(\text{LXL-Me}_2)\text{Cl}_3$

Structure Determination

Yellow blocks of **ew1194** were grown from a dichloromethane solution at $-35\text{ }^{\circ}\text{C}$. A crystal of dimensions $0.29 \times 0.23 \times 0.17\text{ mm}$ was mounted on a Bruker SMART APEX CCD-based X-ray diffractometer equipped with a low temperature device and fine focus Mo-target X-ray tube ($\lambda = 0.71073\text{ \AA}$) operated at 1500 W power (50 kV, 30 mA). The X-ray intensities were measured at 85(1) K; the detector was placed at a distance 5.055 cm from the crystal. A total of 3830 frames were collected with a scan width of 0.5° in ω and 0.45° in phi with an exposure time of 20 s/frame. The integration of the data yielded a total of 93521 reflections to a maximum 2θ value of 56.72° of which 14215 were independent and 12308 were greater than $2\sigma(I)$. The final cell constants (Table 1) were based on the xyz centroids of 9643 reflections above $10\sigma(I)$. Analysis of the data showed negligible decay during data collection; the data were processed with SADABS and corrected for absorption. The structure was solved and refined with the Bruker SHELXTL (version 2008/3) software package, using the space group P1bar with $Z = 2$ for the formula $\text{C}_{46}\text{H}_{45}\text{N}_4\text{Cl}_3\text{Zr}\cdot(\text{CHCl})_5$. All non-hydrogen atoms were refined anisotropically with the hydrogen atoms placed in idealized positions. Full matrix least-squares refinement based on F^2 converged at $R1 = 0.0366$ and $wR2 = 0.0915$ [based on $I > 2\sigma(I)$], $R1 = 0.0450$ and $wR2 = 0.0993$ for all data.

Sheldrick, G.M. SHELXTL, v. 2008/3; Bruker Analytical X-ray, Madison, WI, 2008.

Sheldrick, G.M. SADABS, v. 2008/1. Program for Empirical Absorption Correction of Area Detector Data, University of Gottingen: Gottingen, Germany, 2008.

Saint Plus, v. 7.53a, Bruker Analytical X-ray, Madison, WI, 2008.

Identification code	ew1194
Empirical formula	C ₅₁ H ₅₅ Cl ₁₃ N ₄ Zr
Formula weight	1276.06
Temperature	85(2) K
Wavelength	0.71073 Å
Crystal system, space group	Triclinic, P-1
Unit cell dimensions	a = 13.7969(12) Å alpha = 69.925(1) deg. b = 13.8694(12) Å beta = 89.886(1) deg. c = 15.9048(14) Å gamma = 85.1320(1) deg.
Volume	2847.0(4) Å ³
Z, Calculated density	2, 1.489 Mg/m ³
Absorption coefficient	0.842 mm ⁻¹
F(000)	1300
Crystal size	0.29 x 0.23 x 0.17 mm
Theta range for data collection	1.69 to 28.36 deg.
Limiting indices	-18 ≤ h ≤ 18, -18 ≤ k ≤ 18, -21 ≤ l ≤ 21
Reflections collected / unique	93521 / 14215 [R(int) = 0.0276]
Completeness to theta = 28.36	99.8 %
Absorption correction	Semi-empirical from equivalents
Max. and min. transmission	0.8701 and 0.7923
Refinement method	Full-matrix least-squares on F ²
Data / restraints / parameters	14215 / 0 / 632
Goodness-of-fit on F ²	1.049
Final R indices [I > 2σ(I)]	R1 = 0.0366, wR2 = 0.0915

R indices (all data)

R1 = 0.0450, wR2 = 0.0993

Largest diff. peak and hole

1.572 and -1.062 e.A⁻³

Table 2. Atomic coordinates (x 10⁴) and equivalent isotropic displacement parameters (A² x 10³) for ew1194.

U(eq) is defined as one third of the trace of the orthogonalized Uij tensor.

	x	y	z	U(eq)
Zr(1)	2592(1)	4164(1)	3830(1)	15(1)
Cl(1)	3550(1)	2575(1)	3909(1)	21(1)
Cl(2)	4038(1)	4707(1)	4381(1)	21(1)
Cl(3)	1211(1)	3863(1)	3024(1)	22(1)
Cl(4)	528(1)	7153(1)	729(1)	36(1)
Cl(5)	-546(1)	5375(1)	943(1)	43(1)
Cl(6)	7240(1)	4618(1)	2889(1)	62(1)
Cl(7)	6388(1)	6582(1)	2950(1)	58(1)
Cl(8)	3062(1)	1059(1)	2102(1)	48(1)
Cl(9)	1727(1)	2855(1)	1123(1)	38(1)
Cl(10)	8336(1)	3046(1)	1546(1)	42(1)
Cl(11)	8764(1)	1915(1)	3431(1)	60(1)
Cl(12)	5769(1)	1725(1)	6791(1)	84(1)
Cl(13)	6431(1)	2772(1)	4980(1)	62(1)
N(1)	1881(1)	3490(1)	5172(1)	17(1)
N(2)	1114(1)	3605(1)	6358(1)	16(1)
N(3)	2639(1)	5678(1)	2678(1)	17(1)
N(4)	2434(1)	7367(1)	2072(1)	19(1)
C(1)	1766(1)	5448(1)	4202(1)	16(1)
C(2)	1740(1)	6468(1)	3614(1)	16(1)
C(3)	1270(1)	7274(1)	3842(1)	18(1)
C(4)	836(1)	7045(2)	4671(1)	20(1)
C(5)	855(1)	6043(2)	5270(1)	18(1)
C(6)	1324(1)	5247(1)	5026(1)	16(1)
C(7)	1422(1)	4140(1)	5541(1)	16(1)
C(8)	1365(1)	2563(1)	6522(1)	17(1)
C(9)	1832(1)	2499(1)	5784(1)	17(1)
C(10)	548(1)	4027(2)	6951(1)	20(1)

C(11)	1136(1)	1739(2)	7350(1)	18(1)
C(12)	1435(1)	1743(2)	8190(1)	20(1)
C(13)	1222(1)	960(2)	8967(1)	21(1)
C(14)	698(1)	176(2)	8899(1)	21(1)
C(15)	391(1)	150(2)	8076(1)	20(1)
C(16)	625(1)	935(2)	7301(1)	19(1)
C(17)	1587(2)	935(2)	9869(1)	29(1)
C(18)	-187(2)	-701(2)	8018(2)	27(1)
C(19)	2235(1)	1560(1)	5622(1)	19(1)
C(20)	3140(2)	1082(2)	5992(1)	21(1)
C(21)	3552(2)	230(2)	5799(1)	26(1)
C(22)	3021(2)	-150(2)	5265(2)	29(1)
C(23)	2108(2)	299(2)	4900(1)	27(1)
C(24)	1719(2)	1168(2)	5079(1)	23(1)
C(25)	4567(2)	-231(2)	6140(2)	33(1)
C(26)	1555(2)	-125(2)	4305(2)	38(1)
C(27)	3093(1)	5965(2)	1862(1)	18(1)
C(28)	2977(1)	7015(2)	1478(1)	18(1)
C(29)	2246(1)	6546(1)	2784(1)	17(1)
C(30)	2107(2)	8447(2)	1906(1)	26(1)
C(31)	3600(1)	5208(2)	1517(1)	19(1)
C(32)	4302(1)	4469(2)	2048(1)	20(1)
C(33)	4772(2)	3731(2)	1737(2)	24(1)
C(34)	4524(2)	3751(2)	884(2)	26(1)
C(35)	3828(2)	4475(2)	340(1)	25(1)
C(36)	3372(2)	5209(2)	662(1)	22(1)
C(37)	5535(2)	2938(2)	2309(2)	32(1)
C(38)	3555(2)	4462(2)	-572(2)	33(1)
C(39)	3451(1)	7700(2)	691(1)	20(1)
C(40)	2976(2)	8177(2)	-139(1)	23(1)
C(41)	3471(2)	8800(2)	-864(1)	26(1)
C(42)	4435(2)	8938(2)	-732(2)	28(1)
C(43)	4923(2)	8472(2)	92(2)	28(1)
C(44)	4422(2)	7849(2)	803(1)	24(1)
C(45)	2973(2)	9309(2)	-1771(2)	34(1)
C(46)	5975(2)	8624(2)	212(2)	39(1)
C(47)	611(2)	5843(2)	823(2)	34(1)
C(48)	6477(2)	5235(2)	3475(2)	41(1)
C(49)	2531(2)	2280(2)	2059(2)	34(1)
C(50)	9098(2)	2908(2)	2480(2)	39(1)
C(51)	5469(2)	2671(2)	5730(2)	47(1)

Table 3. Bond lengths [Å] and angles [deg] for ew1194.

Zr(1)-N(3)	2.2698(16)
Zr(1)-N(1)	2.2732(15)
Zr(1)-C(1)	2.2776(18)
Zr(1)-Cl(1)	2.4371(5)
Zr(1)-Cl(3)	2.4415(5)
Zr(1)-Cl(2)	2.4550(5)
Cl(4)-C(47)	1.765(3)
Cl(5)-C(47)	1.760(3)
Cl(6)-C(48)	1.760(3)
Cl(7)-C(48)	1.759(3)
Cl(8)-C(49)	1.767(3)
Cl(9)-C(49)	1.768(3)
Cl(10)-C(50)	1.768(3)
Cl(11)-C(50)	1.752(3)
Cl(12)-C(51)	1.769(3)
Cl(13)-C(51)	1.764(4)
N(1)-C(7)	1.351(2)
N(1)-C(9)	1.392(2)
N(2)-C(7)	1.345(2)
N(2)-C(8)	1.389(2)
N(2)-C(10)	1.463(2)
N(3)-C(29)	1.342(2)
N(3)-C(27)	1.386(2)
N(4)-C(29)	1.345(2)
N(4)-C(28)	1.394(2)
N(4)-C(30)	1.461(2)
C(1)-C(6)	1.394(2)
C(1)-C(2)	1.400(3)
C(2)-C(3)	1.399(3)
C(2)-C(29)	1.466(2)
C(3)-C(4)	1.393(3)
C(4)-C(5)	1.387(3)
C(5)-C(6)	1.400(3)
C(6)-C(7)	1.465(3)
C(8)-C(9)	1.364(2)
C(8)-C(11)	1.472(3)
C(9)-C(19)	1.477(3)
C(11)-C(16)	1.393(3)
C(11)-C(12)	1.401(3)
C(12)-C(13)	1.388(3)
C(13)-C(14)	1.389(3)
C(13)-C(17)	1.510(3)
C(14)-C(15)	1.391(3)

C(15)-C(16)	1.395(3)
C(15)-C(18)	1.507(3)
C(19)-C(24)	1.392(3)
C(19)-C(20)	1.392(3)
C(20)-C(21)	1.395(3)
C(21)-C(22)	1.383(3)
C(21)-C(25)	1.509(3)
C(22)-C(23)	1.391(3)
C(23)-C(24)	1.396(3)
C(23)-C(26)	1.511(3)
C(27)-C(28)	1.367(3)
C(27)-C(31)	1.470(3)
C(28)-C(39)	1.478(3)
C(31)-C(32)	1.393(3)
C(31)-C(36)	1.397(3)
C(32)-C(33)	1.395(3)
C(33)-C(34)	1.389(3)
C(33)-C(37)	1.505(3)
C(34)-C(35)	1.388(3)
C(35)-C(36)	1.394(3)
C(35)-C(38)	1.507(3)
C(39)-C(40)	1.393(3)
C(39)-C(44)	1.393(3)
C(40)-C(41)	1.399(3)
C(41)-C(42)	1.386(3)
C(41)-C(45)	1.507(3)
C(42)-C(43)	1.391(3)
C(43)-C(44)	1.390(3)
C(43)-C(46)	1.505(3)
N(3)-Zr(1)-N(1)	140.63(6)
N(3)-Zr(1)-C(1)	70.83(6)
N(1)-Zr(1)-C(1)	70.11(6)
N(3)-Zr(1)-Cl(1)	123.78(4)
N(1)-Zr(1)-Cl(1)	95.57(4)
C(1)-Zr(1)-Cl(1)	163.10(5)
N(3)-Zr(1)-Cl(3)	86.38(4)
N(1)-Zr(1)-Cl(3)	91.98(4)
C(1)-Zr(1)-Cl(3)	94.61(5)
Cl(1)-Zr(1)-Cl(3)	94.816(18)
N(3)-Zr(1)-Cl(2)	83.64(4)
N(1)-Zr(1)-Cl(2)	97.57(4)
C(1)-Zr(1)-Cl(2)	84.86(5)
Cl(1)-Zr(1)-Cl(2)	88.351(18)
Cl(3)-Zr(1)-Cl(2)	169.607(18)
C(7)-N(1)-C(9)	106.50(15)

C(7)-N(1)-Zr(1)	118.66(12)
C(9)-N(1)-Zr(1)	134.74(12)
C(7)-N(2)-C(8)	108.24(15)
C(7)-N(2)-C(10)	126.42(16)
C(8)-N(2)-C(10)	125.19(15)
C(29)-N(3)-C(27)	107.07(15)
C(29)-N(3)-Zr(1)	118.62(12)
C(27)-N(3)-Zr(1)	133.91(12)
C(29)-N(4)-C(28)	108.32(16)
C(29)-N(4)-C(30)	127.32(16)
C(28)-N(4)-C(30)	124.31(16)
C(6)-C(1)-C(2)	118.88(17)
C(6)-C(1)-Zr(1)	121.27(13)
C(2)-C(1)-Zr(1)	119.76(13)
C(3)-C(2)-C(1)	120.83(17)
C(3)-C(2)-C(29)	127.19(17)
C(1)-C(2)-C(29)	111.99(16)
C(4)-C(3)-C(2)	118.69(17)
C(5)-C(4)-C(3)	121.82(17)
C(4)-C(5)-C(6)	118.55(17)
C(1)-C(6)-C(5)	121.23(17)
C(1)-C(6)-C(7)	110.83(16)
C(5)-C(6)-C(7)	127.94(17)
N(2)-C(7)-N(1)	109.93(16)
N(2)-C(7)-C(6)	131.29(16)
N(1)-C(7)-C(6)	118.77(16)
C(9)-C(8)-N(2)	106.49(16)
C(9)-C(8)-C(11)	129.78(17)
N(2)-C(8)-C(11)	123.73(16)
C(8)-C(9)-N(1)	108.81(16)
C(8)-C(9)-C(19)	127.77(17)
N(1)-C(9)-C(19)	123.41(16)
C(16)-C(11)-C(12)	119.29(17)
C(16)-C(11)-C(8)	119.75(17)
C(12)-C(11)-C(8)	120.95(17)
C(13)-C(12)-C(11)	120.58(18)
C(12)-C(13)-C(14)	118.90(18)
C(12)-C(13)-C(17)	120.62(19)
C(14)-C(13)-C(17)	120.44(18)
C(13)-C(14)-C(15)	121.91(18)
C(14)-C(15)-C(16)	118.40(18)
C(14)-C(15)-C(18)	121.05(18)
C(16)-C(15)-C(18)	120.55(18)
C(11)-C(16)-C(15)	120.89(18)
C(24)-C(19)-C(20)	120.09(18)
C(24)-C(19)-C(9)	119.76(18)

C(20)-C(19)-C(9)	120.13(18)
C(19)-C(20)-C(21)	120.5(2)
C(22)-C(21)-C(20)	118.3(2)
C(22)-C(21)-C(25)	121.4(2)
C(20)-C(21)-C(25)	120.3(2)
C(21)-C(22)-C(23)	122.4(2)
C(22)-C(23)-C(24)	118.5(2)
C(22)-C(23)-C(26)	121.1(2)
C(24)-C(23)-C(26)	120.4(2)
C(19)-C(24)-C(23)	120.2(2)
C(28)-C(27)-N(3)	108.81(16)
C(28)-C(27)-C(31)	128.87(17)
N(3)-C(27)-C(31)	122.33(16)
C(27)-C(28)-N(4)	106.01(16)
C(27)-C(28)-C(39)	129.45(17)
N(4)-C(28)-C(39)	123.67(17)
N(3)-C(29)-N(4)	109.79(16)
N(3)-C(29)-C(2)	118.58(16)
N(4)-C(29)-C(2)	131.60(17)
C(32)-C(31)-C(36)	119.32(18)
C(32)-C(31)-C(27)	120.29(17)
C(36)-C(31)-C(27)	120.38(18)
C(31)-C(32)-C(33)	120.80(19)
C(34)-C(33)-C(32)	118.5(2)
C(34)-C(33)-C(37)	120.82(19)
C(32)-C(33)-C(37)	120.7(2)
C(35)-C(34)-C(33)	122.12(19)
C(34)-C(35)-C(36)	118.50(19)
C(34)-C(35)-C(38)	121.0(2)
C(36)-C(35)-C(38)	120.5(2)
C(35)-C(36)-C(31)	120.80(19)
C(40)-C(39)-C(44)	120.01(18)
C(40)-C(39)-C(28)	123.00(18)
C(44)-C(39)-C(28)	116.99(18)
C(39)-C(40)-C(41)	120.3(2)
C(42)-C(41)-C(40)	118.4(2)
C(42)-C(41)-C(45)	120.58(19)
C(40)-C(41)-C(45)	121.0(2)
C(41)-C(42)-C(43)	122.25(19)
C(44)-C(43)-C(42)	118.5(2)
C(44)-C(43)-C(46)	120.5(2)
C(42)-C(43)-C(46)	121.0(2)
C(43)-C(44)-C(39)	120.5(2)
Cl(5)-C(47)-Cl(4)	111.02(14)
Cl(7)-C(48)-Cl(6)	111.36(15)
Cl(8)-C(49)-Cl(9)	112.06(13)

Cl(11)-C(50)-Cl(10)	111.02(15)
Cl(13)-C(51)-Cl(12)	112.00(16)

Symmetry transformations used to generate equivalent atoms:

Table 4. Anisotropic displacement parameters ($\text{Å}^2 \times 10^3$) for ew1194.
The anisotropic displacement factor exponent takes the form:
 $-2 \pi^2 [h^2 a^{*2} U_{11} + \dots + 2 h k a^* b^* U_{12}]$

	U11	U22	U33	U23	U13	U12
Zr(1)	16(1)	15(1)	13(1)	-5(1)	3(1)	0(1)
Cl(1)	24(1)	17(1)	22(1)	-6(1)	6(1)	2(1)
Cl(2)	19(1)	24(1)	22(1)	-11(1)	0(1)	-1(1)
Cl(3)	21(1)	25(1)	22(1)	-12(1)	0(1)	-1(1)
Cl(4)	33(1)	39(1)	35(1)	-12(1)	9(1)	-6(1)
Cl(5)	46(1)	60(1)	31(1)	-21(1)	11(1)	-24(1)
Cl(6)	37(1)	121(1)	56(1)	-64(1)	15(1)	-15(1)
Cl(7)	57(1)	69(1)	43(1)	-9(1)	-1(1)	-22(1)
Cl(8)	43(1)	53(1)	58(1)	-33(1)	12(1)	1(1)
Cl(9)	47(1)	42(1)	32(1)	-17(1)	4(1)	-16(1)
Cl(10)	36(1)	57(1)	34(1)	-14(1)	0(1)	-7(1)
Cl(11)	97(1)	53(1)	28(1)	-11(1)	15(1)	4(1)
Cl(12)	107(1)	40(1)	87(1)	1(1)	-65(1)	-1(1)
Cl(13)	40(1)	44(1)	116(1)	-49(1)	-7(1)	7(1)
N(1)	20(1)	16(1)	15(1)	-6(1)	4(1)	-1(1)
N(2)	18(1)	17(1)	14(1)	-6(1)	4(1)	-2(1)
N(3)	17(1)	18(1)	15(1)	-6(1)	4(1)	0(1)
N(4)	21(1)	18(1)	16(1)	-5(1)	5(1)	1(1)
C(1)	15(1)	18(1)	15(1)	-7(1)	2(1)	-1(1)
C(2)	15(1)	18(1)	16(1)	-6(1)	3(1)	-1(1)
C(3)	20(1)	16(1)	19(1)	-5(1)	3(1)	0(1)
C(4)	21(1)	18(1)	21(1)	-9(1)	4(1)	0(1)
C(5)	20(1)	21(1)	16(1)	-8(1)	5(1)	-2(1)
C(6)	16(1)	18(1)	15(1)	-6(1)	2(1)	-2(1)
C(7)	16(1)	18(1)	16(1)	-7(1)	3(1)	-1(1)

C(8)	19(1)	17(1)	16(1)	-7(1)	3(1)	-2(1)
C(9)	19(1)	17(1)	15(1)	-5(1)	3(1)	-2(1)
C(10)	22(1)	20(1)	19(1)	-8(1)	7(1)	-1(1)
C(11)	18(1)	18(1)	16(1)	-4(1)	4(1)	1(1)
C(12)	20(1)	22(1)	18(1)	-6(1)	4(1)	-2(1)
C(13)	20(1)	26(1)	16(1)	-6(1)	4(1)	0(1)
C(14)	21(1)	22(1)	18(1)	-2(1)	6(1)	-1(1)
C(15)	20(1)	19(1)	21(1)	-6(1)	7(1)	0(1)
C(16)	20(1)	19(1)	16(1)	-6(1)	3(1)	1(1)
C(17)	29(1)	40(1)	16(1)	-6(1)	3(1)	-9(1)
C(18)	33(1)	23(1)	27(1)	-9(1)	9(1)	-8(1)
C(19)	26(1)	15(1)	16(1)	-4(1)	8(1)	-2(1)
C(20)	27(1)	18(1)	17(1)	-4(1)	6(1)	-1(1)
C(21)	32(1)	19(1)	21(1)	-2(1)	11(1)	2(1)
C(22)	41(1)	18(1)	28(1)	-9(1)	16(1)	-2(1)
C(23)	38(1)	23(1)	24(1)	-11(1)	12(1)	-10(1)
C(24)	28(1)	21(1)	21(1)	-9(1)	7(1)	-5(1)
C(25)	36(1)	28(1)	29(1)	-4(1)	10(1)	9(1)
C(26)	52(2)	35(1)	38(1)	-24(1)	10(1)	-14(1)
C(27)	18(1)	19(1)	14(1)	-5(1)	4(1)	-1(1)
C(28)	18(1)	20(1)	16(1)	-6(1)	3(1)	2(1)
C(29)	17(1)	18(1)	16(1)	-5(1)	2(1)	-1(1)
C(30)	35(1)	16(1)	22(1)	-1(1)	10(1)	3(1)
C(31)	20(1)	18(1)	18(1)	-6(1)	7(1)	-3(1)
C(32)	20(1)	20(1)	20(1)	-7(1)	6(1)	-3(1)
C(33)	23(1)	19(1)	29(1)	-7(1)	9(1)	-2(1)
C(34)	30(1)	22(1)	30(1)	-13(1)	15(1)	-6(1)
C(35)	31(1)	26(1)	23(1)	-12(1)	12(1)	-10(1)
C(36)	24(1)	22(1)	18(1)	-6(1)	6(1)	-4(1)
C(37)	31(1)	24(1)	39(1)	-9(1)	7(1)	5(1)
C(38)	45(1)	36(1)	24(1)	-17(1)	10(1)	-10(1)
C(39)	24(1)	17(1)	18(1)	-5(1)	8(1)	0(1)
C(40)	22(1)	23(1)	19(1)	-2(1)	6(1)	3(1)
C(41)	30(1)	22(1)	20(1)	-2(1)	10(1)	6(1)
C(42)	34(1)	21(1)	26(1)	-5(1)	16(1)	-4(1)
C(43)	27(1)	29(1)	30(1)	-13(1)	11(1)	-7(1)
C(44)	25(1)	25(1)	22(1)	-8(1)	6(1)	-4(1)
C(45)	35(1)	36(1)	20(1)	3(1)	10(1)	11(1)
C(46)	32(1)	50(2)	39(1)	-18(1)	12(1)	-19(1)
C(47)	31(1)	38(1)	31(1)	-12(1)	4(1)	-3(1)
C(48)	31(1)	67(2)	36(1)	-29(1)	12(1)	-15(1)
C(49)	35(1)	42(1)	34(1)	-22(1)	6(1)	-9(1)
C(50)	47(2)	38(1)	35(1)	-16(1)	-1(1)	-6(1)
C(51)	48(2)	30(1)	60(2)	-11(1)	-23(1)	6(1)

Table 5. Hydrogen coordinates ($\times 10^4$) and isotropic displacement parameters ($\text{\AA}^2 \times 10^3$) for ew1194.

	x	y	z	U(eq)
H(3A)	1248	7965	3439	22
H(4A)	517	7589	4831	24
H(5A)	557	5900	5834	22
H(10A)	959	4422	7188	30
H(10B)	314	3461	7448	30
H(10C)	-9	4479	6614	30
H(12A)	1788	2287	8228	24
H(14A)	546	-357	9431	26
H(16A)	433	922	6732	22
H(17A)	2205	503	10030	43
H(17B)	1107	649	10322	43
H(17C)	1685	1637	9842	43
H(18A)	2	-1335	8521	40
H(18B)	-55	-818	7453	40
H(18C)	-883	-504	8041	40
H(20A)	3479	1338	6378	25
H(22A)	3290	-740	5143	35
H(24A)	1100	1493	4830	28
H(25A)	4689	-898	6057	49
H(25B)	4630	-327	6778	49
H(25C)	5041	235	5807	49
H(26A)	1798	132	3696	57
H(26B)	861	99	4296	57
H(26C)	1648	-879	4538	57
H(30A)	1395	8543	1847	39
H(30B)	2387	8880	1353	39
H(30C)	2319	8644	2408	39
H(32A)	4463	4468	2629	24
H(34A)	4842	3252	667	32
H(36A)	2900	5717	295	26
H(37A)	5405	2254	2311	49
H(37B)	5519	2946	2922	49
H(37C)	6179	3098	2066	49
H(38A)	4132	4244	-844	49
H(38B)	3294	5154	-953	49
H(38C)	3059	3978	-513	49
H(40A)	2313	8079	-213	28

H(42A)	4774	9365	-1220	33
H(44A)	4743	7523	1371	28
H(45A)	2963	10060	-1941	51
H(45B)	2304	9115	-1745	51
H(45C)	3328	9084	-2215	51
H(46A)	6130	8457	850	59
H(46B)	6089	9344	-115	59
H(46C)	6390	8171	-22	59
H(47A)	912	5765	282	41
H(47B)	1032	5432	1348	41
H(48A)	5821	4988	3507	50
H(48B)	6739	5052	4094	50
H(49A)	3052	2738	2031	41
H(49B)	2171	2205	2614	41
H(50A)	9782	2754	2344	47
H(50B)	9052	3563	2603	47
H(51A)	4885	2494	5475	57
H(51B)	5310	3347	5804	57

Appendix 6

Crystallographic Data for $\text{Zr}(\text{LXL}-(\text{SiMe}_3)_2)\text{ClI}_2$

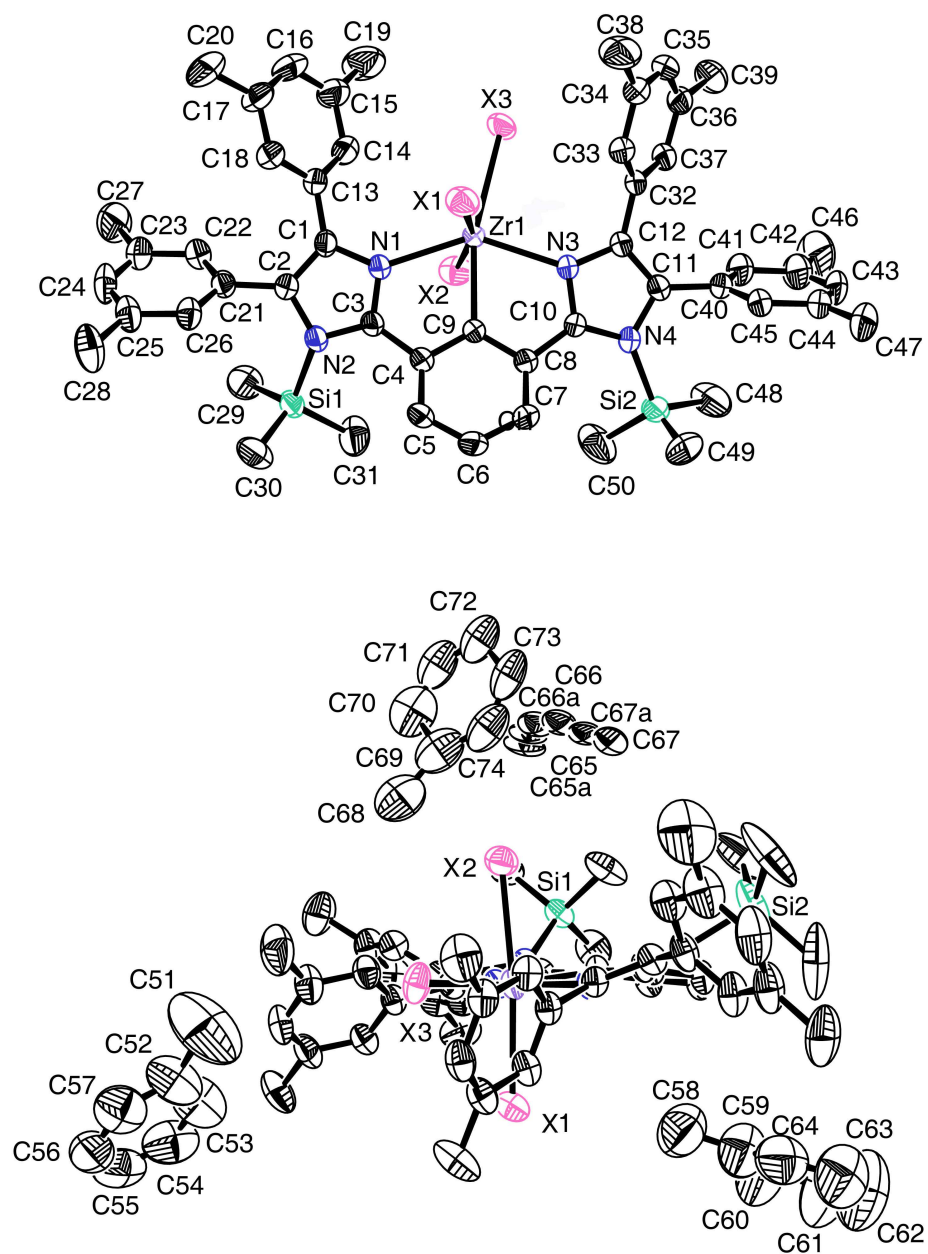


Figure A.6. 50 % thermal ellipsoid plot of $\text{Zr}(\text{LXL}-(\text{SiMe}_3)_2)\text{ClI}_2$.

Structure Determination.

Orange plates of **ew1705** were crystallized from a toluene solution with a trace of benzene at $-35\text{ }^{\circ}\text{C}$. A crystal of dimensions $0.42 \times 0.32 \times 0.22\text{ mm}$ was mounted on a standard Bruker SMART APEX CCD-based X-ray diffractometer equipped with a low-temperature device and fine-focus Mo-target X-ray tube ($\lambda = 0.71073\text{ \AA}$) operated at 1500 W power (50 kV, 30 mA). The X-ray intensities were measured at 225(2) K; the detector was placed at a distance 6.055 cm from the crystal. A total of 5190 frames were collected with a scan width of 0.5° in ω and 0.45° in ϕ with an exposure time of 10 s/frame. Indexing was performed by use of the CELL_NOW program which indicated that the crystal was a two-component, non-merohedral twin. The frames were integrated with the Bruker SAINT software package with a narrow frame algorithm. The integration of the data yielded a total of 437278 reflections to a maximum 2θ value of 57.06° of which 18123 were independent and 15077 were greater than $2\sigma(I)$. The final cell constants (Table 1) were based on the xyz centroids of 9322 reflections above $10\sigma(I)$. Analysis of the data showed negligible decay during data collection; the data were processed with TWINABS and corrected for absorption. The domains are related by a rotation of 171.6 degrees about the reciprocal $[0\ 1\ 0]$ axis. For this refinement, reflections from the dominant component as well as composite reflections were used. Merging of the data was performed in TWINABS and an HKLF 4 format file used for refinement. The structure was solved and refined with the Bruker SHELXTL (version 2008/3) software package, using the space group P2(1)/c with $Z = 4$ for the formula $\text{C}_{50}\text{H}_{57}\text{N}_4\text{Si}_2\text{ZrCl}_{0.43}\text{I}_{2.57} \cdot 2.25(\text{C}_7\text{H}_8) \cdot 0.25(\text{C}_6\text{H}_6)$. All non-hydrogen atoms were refined anisotropically with the hydrogen atoms placed in idealized positions. The halide

sites are site substitution disordered with contributions of both chloride and iodide. Full-matrix least-squares refinement based on F^2 converged at $R1 = 0.0614$ and $wR2 = 0.1709$ [based on $I > 2\sigma(I)$], $R1 = 0.0738$ and $wR2 = 0.1779$ for all data.

Sheldrick, G.M. SHELXTL, v. 2008/3; Bruker Analytical X-ray, Madison, WI, 2008.

Saint Plus, v. 7.34, Bruker Analytical X-ray, Madison, WI, 2006.

Sheldrick, G.M. CELL_NOW, v. 2008/2, Program for Indexing Twins and Other Problem Crystals, University of Gottingen: Gottingen, Germany, 2008.

Sheldrick, G.M. TWINABS, v. 2008/1. Program for Empirical Absorption Correction of Area Detector Data, University of Gottingen: Gottingen, Germany, 2008.

Table 1. Crystal data and structure refinement for ew1705.

Identification code	ew1705
Empirical formula	C _{67.25} H _{76.50} Cl _{10.43} I _{2.57} N ₄ Si ₂ Zr
Formula weight	1429.60
Temperature	225(2) K
Wavelength	0.71073 Å
Crystal system, space group	Monoclinic, P2(1)/c
Unit cell dimensions	a = 29.112(6) Å alpha = 90.00(3) deg. b = 11.854(2) Å beta = 99.39(3) deg. c = 21.331(4) Å gamma = 90.00(3) deg.
Volume	7263(3) Å ³
Z, Calculated density	4, 1.307 Mg/m ³
Absorption coefficient	1.330 mm ⁻¹
F(000)	2878

Crystal size	0.42 x 0.32 x 0.22 mm
Theta range for data collection	2.20 to 28.53 deg.
Limiting indices	-38<=h<=39, -15<=k<=15, -28<=l<=28
Reflections collected / unique	437278 / 18123 [R(int) = 0.0905]
Completeness to theta = 28.53	98.2 %
Absorption correction	Semi-empirical from equivalents
Max. and min. transmission	0.7585 and 0.6051
Refinement method	Full-matrix least-squares on F ²
Data / restraints / parameters	18123 / 297 / 802
Goodness-of-fit on F ²	1.145
Final R indices [I>2sigma(I)]	R1 = 0.0614, wR2 = 0.1709
R indices (all data)	R1 = 0.0738, wR2 = 0.1779
Largest diff. peak and hole	1.031 and -0.754 e.A ⁻³

Table 2. Atomic coordinates (x 10⁴) and equivalent isotropic displacement parameters (A² x 10³) for ew1705. U(eq) is defined as one third of the trace of the orthogonalized U_{ij} tensor.

	x	y	z	U(eq)
Zr(1)	7627(1)	7054(1)	2970(1)	35(1)
I(1)	8248(1)	5502(1)	2583(1)	54(1)
I(2)	6830(1)	8350(1)	3139(1)	56(1)
I(3)	7636(1)	6039(1)	4174(1)	54(1)
Cl(1)	8248(1)	5502(1)	2583(1)	54(1)
Cl(2)	6830(1)	8350(1)	3139(1)	56(1)
Cl(3)	7636(1)	6039(1)	4174(1)	54(1)
Si(1)	6347(1)	7842(1)	596(1)	45(1)
Si(2)	8440(1)	11645(1)	2997(1)	76(1)

C(1)	6804(2)	5616(4)	1909(2)	38(1)
C(2)	6555(2)	5847(4)	1325(2)	39(1)
C(3)	7085(2)	7166(3)	1574(2)	36(1)
C(4)	7424(2)	8076(4)	1577(2)	37(1)
C(5)	7532(2)	8639(4)	1049(2)	46(1)
C(6)	7876(2)	9455(4)	1134(2)	47(1)
C(7)	8101(2)	9740(4)	1740(2)	46(1)
C(8)	7990(2)	9176(4)	2267(2)	38(1)
C(9)	7666(2)	8293(4)	2189(2)	36(1)
C(10)	8211(2)	9283(4)	2932(2)	36(1)
C(11)	8607(2)	9768(4)	3862(2)	39(1)
C(12)	8460(1)	8681(4)	3896(2)	36(1)
C(13)	6749(2)	4650(4)	2325(2)	42(1)
C(14)	6699(2)	4799(5)	2951(3)	51(1)
C(15)	6628(3)	3875(5)	3332(3)	66(2)
C(16)	6604(2)	2802(5)	3064(3)	69(2)
C(17)	6647(2)	2636(4)	2439(3)	62(2)
C(18)	6724(2)	3560(4)	2065(3)	50(1)
C(19)	6546(4)	4074(8)	4003(4)	103(3)
C(20)	6602(3)	1470(5)	2127(4)	92(3)
C(21)	6201(2)	5161(4)	922(2)	41(1)
C(22)	5812(2)	4779(5)	1151(2)	49(1)
C(23)	5467(2)	4169(5)	764(3)	59(1)
C(24)	5526(2)	3958(5)	141(3)	65(2)
C(25)	5912(2)	4315(5)	-95(3)	56(1)
C(26)	6255(2)	4915(4)	302(2)	45(1)
C(27)	5039(3)	3776(8)	1015(4)	91(2)
C(28)	5973(3)	4074(7)	-769(3)	82(2)
C(29)	5740(2)	7507(6)	663(4)	70(2)
C(30)	6439(3)	7714(6)	-227(3)	75(2)
C(31)	6463(3)	9282(5)	924(4)	80(2)
C(32)	8608(2)	7883(4)	4425(2)	38(1)
C(33)	8812(2)	6867(4)	4313(2)	44(1)
C(34)	8962(2)	6116(4)	4811(2)	49(1)
C(35)	8906(2)	6425(5)	5419(2)	52(1)
C(36)	8709(2)	7456(4)	5548(2)	47(1)
C(37)	8559(2)	8167(4)	5041(2)	43(1)
C(38)	9170(3)	5001(5)	4689(4)	86(2)
C(39)	8663(3)	7814(6)	6208(3)	72(2)
C(40)	8926(2)	10448(4)	4330(2)	47(1)
C(41)	8770(2)	10902(5)	4863(3)	60(1)
C(42)	9072(3)	11593(6)	5275(3)	79(2)
C(43)	9514(3)	11787(6)	5159(3)	81(2)
C(44)	9678(2)	11330(5)	4636(3)	67(2)
C(45)	9374(2)	10652(5)	4220(3)	56(1)
C(46)	8894(4)	12111(9)	5846(4)	133(4)

C(47)	10166(3)	11537(8)	4521(4)	95(3)
C(48)	8499(5)	12580(5)	3689(4)	133(5)
C(49)	8940(4)	11842(10)	2571(5)	143(5)
C(50)	7863(4)	11943(6)	2524(4)	109(3)
C(51)	7435(7)	2922(12)	5578(7)	217(9)
C(52)	7476(4)	1742(8)	5340(5)	115(3)
C(53)	7415(4)	501(10)	4672(5)	126(4)
C(54)	7425(4)	474(10)	4469(6)	119(3)
C(55)	7494(3)	-402(9)	4864(7)	120(3)
C(56)	7568(3)	-219(9)	5535(6)	113(3)
C(57)	7562(4)	828(10)	5743(6)	114(3)
C(58)	9447(4)	8043(11)	2972(6)	140(4)
C(59)	9761(4)	8632(10)	2668(6)	121(3)
C(60)	9765(5)	8512(14)	2063(6)	161(5)
C(61)	10088(5)	9222(18)	1726(7)	194(7)
C(62)	10381(7)	9808(17)	2046(8)	205(7)
C(63)	10411(5)	9828(13)	2678(7)	152(5)
C(64)	10145(4)	9232(10)	3029(7)	125(3)
C(65)	4678(11)	9510(30)	250(20)	68(6)
C(66)	4974(16)	10270(30)	600(13)	69(6)
C(67)	5325(13)	10840(20)	370(20)	77(7)
C(65A)	4607(12)	9220(30)	-20(30)	77(7)
C(66A)	793(14)	9830(40)	513(17)	70(7)
C(67A)	5168(14)	10540(30)	495(17)	71(6)
N(1)	7129(1)	6464(3)	2067(2)	37(1)
N(2)	6725(1)	6863(3)	1113(2)	38(1)
N(3)	8198(1)	8380(3)	3315(2)	35(1)
N(4)	8442(1)	10166(3)	3242(2)	42(1)
C(68)	5478(14)	7220(30)	2498(17)	128(10)
C(69)	5314(10)	8400(30)	2350(16)	118(7)
C(70)	4802(10)	8400(30)	2217(16)	119(8)
C(71)	4616(10)	9380(30)	2205(14)	103(7)
C(72)	4757(10)	10420(30)	2312(12)	100(6)
C(73)	5262(10)	10480(30)	2449(12)	100(6)
C(74)	5471(10)	9480(30)	2388(15)	109(7)

Table 3. Bond lengths [Å] and angles [deg] for ew1705.

Zr(1)-C(9)	2.238(4)
Zr(1)-N(3)	2.319(3)
Zr(1)-N(1)	2.320(3)
Zr(1)-I(1)	2.7966(11)

Zr(1)-I(3)	2.8337(10)
Zr(1)-I(2)	2.8540(11)
Si(1)-C(30)	1.824(7)
Si(1)-N(2)	1.838(4)
Si(1)-C(29)	1.839(7)
Si(1)-C(31)	1.855(6)
Si(2)-N(4)	1.830(4)
Si(2)-C(48)	1.831(8)
Si(2)-C(50)	1.845(8)
Si(2)-C(49)	1.855(11)
C(1)-C(2)	1.365(6)
C(1)-N(1)	1.384(5)
C(1)-C(13)	1.473(6)
C(2)-N(2)	1.405(6)
C(2)-C(21)	1.473(6)
C(3)-N(1)	1.332(5)
C(3)-N(2)	1.364(5)
C(3)-C(4)	1.460(6)
C(4)-C(5)	1.389(6)
C(4)-C(9)	1.403(6)
C(5)-C(6)	1.384(7)
C(6)-C(7)	1.392(7)
C(7)-C(8)	1.392(6)
C(8)-C(9)	1.401(6)
C(8)-C(10)	1.464(6)
C(10)-N(3)	1.350(5)
C(10)-N(4)	1.357(5)
C(11)-C(12)	1.363(6)
C(11)-N(4)	1.411(6)
C(11)-C(40)	1.486(6)
C(12)-N(3)	1.392(5)
C(12)-C(32)	1.482(6)
C(13)-C(14)	1.379(7)
C(13)-C(18)	1.403(7)
C(14)-C(15)	1.399(8)
C(15)-C(16)	1.392(9)
C(15)-C(19)	1.508(10)
C(16)-C(17)	1.372(9)
C(17)-C(18)	1.395(8)
C(17)-C(20)	1.531(8)
C(21)-C(22)	1.380(7)
C(21)-C(26)	1.388(7)
C(22)-C(23)	1.392(7)
C(23)-C(24)	1.390(9)
C(23)-C(27)	1.510(9)
C(24)-C(25)	1.372(9)

C(25)-C(26)	1.395(7)
C(25)-C(28)	1.504(8)
C(32)-C(33)	1.380(7)
C(32)-C(37)	1.386(6)
C(33)-C(34)	1.400(7)
C(34)-C(35)	1.385(8)
C(34)-C(38)	1.493(8)
C(35)-C(36)	1.396(8)
C(36)-C(37)	1.385(7)
C(36)-C(39)	1.498(7)
C(40)-C(45)	1.383(8)
C(40)-C(41)	1.397(8)
C(41)-C(42)	1.402(8)
C(42)-C(43)	1.369(11)
C(42)-C(46)	1.529(12)
C(43)-C(44)	1.392(11)
C(44)-C(45)	1.401(7)
C(44)-C(47)	1.501(10)
C(51)-C(52)	1.500(15)
C(52)-C(57)	1.379(14)
C(52)-C(53)	1.437(15)
C(53)-C(54)	1.294(14)
C(54)-C(55)	1.333(15)
C(55)-C(56)	1.429(15)
C(56)-C(57)	1.319(14)
C(58)-C(59)	1.392(15)
C(59)-C(60)	1.299(15)
C(59)-C(64)	1.438(14)
C(60)-C(61)	1.526(19)
C(61)-C(62)	1.220(18)
C(62)-C(63)	1.34(2)
C(63)-C(64)	1.359(18)
C(65)-C(66)	1.380(9)
C(65)-C(67)#1	1.387(7)
C(66)-C(67)	1.381(9)
C(67)-C(65)#1	1.387(7)
C(65A)-C(67A)#1	1.33(4)
C(65A)-C(66A)	1.377(9)
C(66A)-C(67A)	1.384(9)
C(67A)-C(65A)#1	1.33(4)
C(68)-C(69)	1.49(2)
C(69)-C(74)	1.36(2)
C(69)-C(70)	1.47(2)
C(70)-C(71)	1.28(2)
C(71)-C(72)	1.31(2)
C(72)-C(73)	1.45(2)

C(73)-C(74)	1.34(2)
C(9)-Zr(1)-N(3)	70.73(14)
C(9)-Zr(1)-N(1)	71.41(14)
N(3)-Zr(1)-N(1)	141.80(13)
C(9)-Zr(1)-I(1)	95.62(12)
N(3)-Zr(1)-I(1)	94.33(10)
N(1)-Zr(1)-I(1)	84.42(10)
C(9)-Zr(1)-I(3)	163.65(11)
N(3)-Zr(1)-I(3)	95.69(9)
N(1)-Zr(1)-I(3)	122.50(9)
I(1)-Zr(1)-I(3)	94.43(3)
C(9)-Zr(1)-I(2)	83.23(12)
N(3)-Zr(1)-I(2)	98.59(10)
N(1)-Zr(1)-I(2)	81.81(10)
I(1)-Zr(1)-I(2)	65.82(3)
I(3)-Zr(1)-I(2)	90.11(4)
C(30)-Si(1)-N(2)	110.9(3)
C(30)-Si(1)-C(29)	110.6(3)
N(2)-Si(1)-C(29)	107.8(2)
C(30)-Si(1)-C(31)	113.2(4)
N(2)-Si(1)-C(31)	107.4(2)
C(29)-Si(1)-C(31)	106.7(3)
N(4)-Si(2)-C(48)	110.7(3)
N(4)-Si(2)-C(50)	107.5(3)
C(48)-Si(2)-C(50)	106.4(5)
N(4)-Si(2)-C(49)	107.1(4)
C(48)-Si(2)-C(49)	109.9(6)
C(50)-Si(2)-C(49)	115.2(5)
C(2)-C(1)-N(1)	108.5(4)
C(2)-C(1)-C(13)	127.8(4)
N(1)-C(1)-C(13)	123.7(4)
C(1)-C(2)-N(2)	107.7(4)
C(1)-C(2)-C(21)	129.7(4)
N(2)-C(2)-C(21)	122.4(4)
N(1)-C(3)-N(2)	111.6(4)
N(1)-C(3)-C(4)	118.7(4)
N(2)-C(3)-C(4)	129.6(4)
C(5)-C(4)-C(9)	121.4(4)
C(5)-C(4)-C(3)	126.4(4)
C(9)-C(4)-C(3)	112.1(4)
C(6)-C(5)-C(4)	119.0(4)
C(5)-C(6)-C(7)	120.8(4)
C(8)-C(7)-C(6)	119.9(4)
C(7)-C(8)-C(9)	120.2(4)
C(7)-C(8)-C(10)	128.2(4)

C(9)-C(8)-C(10)	111.1(4)
C(8)-C(9)-C(4)	118.3(4)
C(8)-C(9)-Zr(1)	121.2(3)
C(4)-C(9)-Zr(1)	119.5(3)
N(3)-C(10)-N(4)	112.2(4)
N(3)-C(10)-C(8)	117.8(4)
N(4)-C(10)-C(8)	130.0(4)
C(12)-C(11)-N(4)	107.8(4)
C(12)-C(11)-C(40)	130.0(4)
N(4)-C(11)-C(40)	121.9(4)
C(11)-C(12)-N(3)	109.0(4)
C(11)-C(12)-C(32)	126.2(4)
N(3)-C(12)-C(32)	124.3(4)
C(14)-C(13)-C(18)	119.6(5)
C(14)-C(13)-C(1)	121.5(4)
C(18)-C(13)-C(1)	118.8(4)
C(13)-C(14)-C(15)	120.8(5)
C(16)-C(15)-C(14)	118.6(6)
C(16)-C(15)-C(19)	121.9(6)
C(14)-C(15)-C(19)	119.3(6)
C(17)-C(16)-C(15)	121.6(5)
C(16)-C(17)-C(18)	119.5(5)
C(16)-C(17)-C(20)	122.4(6)
C(18)-C(17)-C(20)	118.1(6)
C(17)-C(18)-C(13)	119.9(5)
C(22)-C(21)-C(26)	119.7(4)
C(22)-C(21)-C(2)	120.7(4)
C(26)-C(21)-C(2)	119.5(4)
C(21)-C(22)-C(23)	121.0(5)
C(24)-C(23)-C(22)	118.0(5)
C(24)-C(23)-C(27)	121.4(5)
C(22)-C(23)-C(27)	120.5(6)
C(25)-C(24)-C(23)	122.2(5)
C(24)-C(25)-C(26)	118.8(5)
C(24)-C(25)-C(28)	121.7(5)
C(26)-C(25)-C(28)	119.5(6)
C(21)-C(26)-C(25)	120.3(5)
C(33)-C(32)-C(37)	119.4(4)
C(33)-C(32)-C(12)	120.3(4)
C(37)-C(32)-C(12)	120.3(4)
C(32)-C(33)-C(34)	120.9(5)
C(35)-C(34)-C(33)	118.2(5)
C(35)-C(34)-C(38)	120.7(5)
C(33)-C(34)-C(38)	121.1(5)
C(34)-C(35)-C(36)	122.1(5)
C(37)-C(36)-C(35)	117.8(4)

C(37)-C(36)-C(39)	119.8(5)
C(35)-C(36)-C(39)	122.4(5)
C(36)-C(37)-C(32)	121.6(5)
C(45)-C(40)-C(41)	120.7(5)
C(45)-C(40)-C(11)	118.9(5)
C(41)-C(40)-C(11)	120.4(5)
C(40)-C(41)-C(42)	118.7(6)
C(43)-C(42)-C(41)	119.8(7)
C(43)-C(42)-C(46)	121.8(7)
C(41)-C(42)-C(46)	118.3(8)
C(42)-C(43)-C(44)	122.3(5)
C(43)-C(44)-C(45)	117.8(6)
C(43)-C(44)-C(47)	121.7(6)
C(45)-C(44)-C(47)	120.6(7)
C(40)-C(45)-C(44)	120.7(6)
C(57)-C(52)-C(53)	116.3(10)
C(57)-C(52)-C(51)	122.6(11)
C(53)-C(52)-C(51)	121.1(11)
C(54)-C(53)-C(52)	120.8(12)
C(53)-C(54)-C(55)	122.0(12)
C(54)-C(55)-C(56)	119.9(10)
C(57)-C(56)-C(55)	118.0(11)
C(56)-C(57)-C(52)	122.8(11)
C(60)-C(59)-C(58)	121.3(12)
C(60)-C(59)-C(64)	117.1(12)
C(58)-C(59)-C(64)	120.6(12)
C(59)-C(60)-C(61)	120.8(12)
C(62)-C(61)-C(60)	118.7(15)
C(61)-C(62)-C(63)	119.8(17)
C(62)-C(63)-C(64)	126.7(13)
C(63)-C(64)-C(59)	115.1(13)
C(66)-C(65)-C(67)#1	129(3)
C(65)-C(66)-C(67)	124(3)
C(66)-C(67)-C(65)#1	107(3)
C(67A)#1-C(65A)-C(66A)	110(3)
C(65A)-C(66A)-C(67A)	120(3)
C(65A)#1-C(67A)-C(66A)	130(3)
C(3)-N(1)-C(1)	106.7(3)
C(3)-N(1)-Zr(1)	115.7(3)
C(1)-N(1)-Zr(1)	136.9(3)
C(3)-N(2)-C(2)	105.3(3)
C(3)-N(2)-Si(1)	125.6(3)
C(2)-N(2)-Si(1)	121.8(3)
C(10)-N(3)-C(12)	105.7(3)
C(10)-N(3)-Zr(1)	115.8(3)
C(12)-N(3)-Zr(1)	135.8(3)

C(10)-N(4)-C(11)	105.3(4)
C(10)-N(4)-Si(2)	128.4(3)
C(11)-N(4)-Si(2)	125.0(3)
C(74)-C(69)-C(70)	110(2)
C(74)-C(69)-C(68)	141(3)
C(70)-C(69)-C(68)	108(2)
C(71)-C(70)-C(69)	114(2)
C(70)-C(71)-C(72)	137(3)
C(71)-C(72)-C(73)	111(2)
C(74)-C(73)-C(72)	114(2)
C(73)-C(74)-C(69)	133(2)

Symmetry transformations used to generate equivalent atoms:

#1 -x+1,-y+2,-z

Table 4. Anisotropic displacement parameters ($\text{Å}^2 \times 10^3$) for ew1705. The anisotropic displacement factor exponent takes the form: $-2 \pi^2 [h^2 a^{*2} U_{11} + \dots + 2 h k a^* b^* U_{12}]$

	U11	U22	U33	U23	U13	U12
Zr(1)	43(1)	32(1)	28(1)	3(1)	-1(1)	-7(1)
I(1)	65(1)	45(1)	49(1)	0(1)	4(1)	12(1)
I(2)	68(1)	50(1)	53(1)	0(1)	16(1)	10(1)
I(3)	51(1)	74(1)	36(1)	19(1)	0(1)	-16(1)
Cl(1)	65(1)	45(1)	49(1)	0(1)	4(1)	12(1)
Cl(2)	68(1)	50(1)	53(1)	0(1)	16(1)	10(1)
Cl(3)	51(1)	74(1)	36(1)	19(1)	0(1)	-16(1)
Si(1)	50(1)	40(1)	40(1)	-1(1)	-9(1)	3(1)
Si(2)	120(2)	37(1)	57(1)	11(1)	-31(1)	-24(1)
C(1)	37(2)	33(2)	40(2)	-4(2)	-3(2)	-3(2)
C(2)	43(2)	34(2)	38(2)	-2(2)	1(2)	-5(2)
C(3)	44(2)	32(2)	31(2)	-3(2)	-1(2)	-1(2)
C(4)	44(2)	36(2)	29(2)	1(2)	0(2)	-4(2)
C(5)	63(3)	43(2)	29(2)	4(2)	-4(2)	-5(2)
C(6)	63(3)	45(3)	34(2)	8(2)	7(2)	-7(2)
C(7)	56(3)	39(2)	40(2)	6(2)	3(2)	-12(2)

C(8)	47(2)	34(2)	31(2)	0(2)	0(2)	-6(2)
C(9)	43(2)	35(2)	28(2)	2(2)	0(2)	-8(2)
C(10)	40(2)	33(2)	34(2)	2(2)	-2(2)	-9(2)
C(11)	40(2)	38(2)	35(2)	0(2)	-4(2)	-3(2)
C(12)	34(2)	39(2)	33(2)	2(2)	-2(2)	-5(2)
C(13)	40(2)	39(2)	43(2)	2(2)	-2(2)	-8(2)
C(14)	61(3)	43(3)	50(3)	-2(2)	7(2)	-11(2)
C(15)	89(4)	56(3)	54(3)	7(3)	14(3)	-15(3)
C(16)	86(4)	46(3)	76(4)	17(3)	18(3)	-16(3)
C(17)	71(4)	34(2)	78(4)	6(2)	5(3)	-7(2)
C(18)	55(3)	38(2)	53(3)	2(2)	0(2)	-3(2)
C(19)	162(9)	87(5)	67(5)	11(4)	39(5)	-24(6)
C(20)	131(7)	36(3)	107(6)	-1(3)	11(5)	-12(4)
C(21)	40(2)	37(2)	42(2)	-2(2)	-4(2)	1(2)
C(22)	47(3)	53(3)	45(3)	-3(2)	-2(2)	-4(2)
C(23)	50(3)	60(3)	61(3)	-2(3)	-4(2)	-13(2)
C(24)	52(3)	66(4)	69(4)	-25(3)	-11(3)	-13(3)
C(25)	55(3)	59(3)	50(3)	-18(2)	-6(2)	1(2)
C(26)	42(2)	43(2)	49(3)	-12(2)	2(2)	0(2)
C(27)	64(4)	115(7)	92(5)	7(5)	4(4)	-33(4)
C(28)	80(4)	103(6)	62(4)	-41(4)	2(3)	-5(4)
C(29)	56(3)	66(4)	85(4)	9(3)	-1(3)	15(3)
C(30)	96(5)	79(4)	46(3)	10(3)	-6(3)	4(4)
C(31)	79(4)	46(3)	103(5)	-15(3)	-25(4)	15(3)
C(32)	35(2)	40(2)	35(2)	3(2)	-4(2)	-9(2)
C(33)	52(3)	40(2)	38(2)	2(2)	-2(2)	-8(2)
C(34)	57(3)	38(2)	48(3)	3(2)	-5(2)	-6(2)
C(35)	58(3)	52(3)	42(2)	14(2)	-8(2)	-11(2)
C(36)	53(3)	51(3)	35(2)	0(2)	3(2)	-12(2)
C(37)	45(2)	47(2)	35(2)	0(2)	0(2)	-8(2)
C(38)	122(6)	45(3)	83(5)	2(3)	-7(4)	24(4)
C(39)	96(5)	81(4)	35(3)	-3(3)	2(3)	-10(4)
C(40)	57(3)	37(2)	41(2)	3(2)	-10(2)	-14(2)
C(41)	75(4)	54(3)	48(3)	-11(2)	0(3)	-15(3)
C(42)	111(6)	69(4)	52(3)	-14(3)	-7(3)	-27(4)
C(43)	98(5)	76(4)	57(4)	-3(3)	-20(3)	-49(4)
C(44)	67(4)	64(3)	60(3)	16(3)	-20(3)	-31(3)
C(45)	59(3)	58(3)	43(3)	9(2)	-11(2)	-22(2)
C(46)	196(12)	123(8)	77(6)	-56(6)	7(6)	-45(8)
C(47)	77(5)	111(6)	88(5)	18(5)	-16(4)	-54(5)
C(48)	252(13)	32(3)	84(5)	-4(3)	-66(7)	-5(5)
C(49)	161(10)	155(9)	99(7)	60(7)	-17(6)	-110(8)
C(50)	155(8)	55(4)	92(6)	-7(4)	-53(6)	31(5)
C(51)	360(20)	111(7)	163(13)	-55(8)	-24(15)	5(13)
C(52)	135(8)	89(5)	108(6)	-22(4)	-25(6)	7(6)
C(53)	138(8)	106(6)	114(6)	-21(5)	-33(6)	-5(6)

C(54)	97(6)	124(7)	132(7)	-52(5)	8(6)	-3(6)
C(55)	64(5)	93(5)	202(9)	-44(6)	20(6)	-12(4)
C(56)	63(4)	97(5)	180(8)	22(6)	24(6)	1(4)
C(57)	95(6)	120(6)	119(7)	-5(5)	-5(5)	2(6)
C(58)	141(9)	139(10)	153(10)	-32(8)	59(8)	-29(7)
C(59)	136(8)	125(8)	105(6)	-28(6)	24(6)	-30(6)
C(60)	153(10)	227(14)	96(6)	-12(8)	2(7)	-77(9)
C(61)	157(11)	312(18)	107(7)	-1(10)	0(7)	-102(11)
C(62)	211(15)	247(16)	152(9)	-30(12)	16(11)	-114(12)
C(63)	155(10)	152(10)	144(8)	-50(9)	8(8)	-54(8)
C(64)	106(7)	106(7)	155(8)	-38(6)	-1(6)	-11(5)
C(65)	72(13)	62(14)	70(16)	8(12)	10(13)	48(10)
C(66)	68(15)	59(13)	81(12)	24(10)	17(11)	37(11)
C(67)	69(15)	68(14)	96(15)	47(12)	18(12)	45(11)
C(65A)	79(13)	72(14)	77(17)	13(12)	1(13)	60(11)
C(66A)	71(14)	67(14)	74(13)	18(10)	15(11)	40(11)
C(67A)	68(16)	63(14)	86(13)	33(11)	27(11)	47(11)
N(1)	42(2)	33(2)	32(2)	-1(1)	-4(1)	-4(1)
N(2)	43(2)	35(2)	33(2)	-3(1)	-4(1)	-1(2)
N(3)	39(2)	34(2)	30(2)	-1(1)	-2(1)	-7(1)
N(4)	48(2)	37(2)	36(2)	-1(2)	-5(2)	-12(2)
C(68)	146(19)	168(14)	76(17)	-29(17)	33(16)	-2(15)
C(69)	127(12)	169(12)	64(13)	-15(14)	31(13)	2(12)
C(70)	127(12)	162(14)	61(13)	-20(15)	-3(14)	-23(11)
C(71)	98(12)	164(14)	47(11)	11(14)	11(11)	-19(10)
C(72)	109(12)	154(13)	41(11)	19(13)	21(11)	-12(12)
C(73)	107(12)	156(13)	41(10)	28(12)	23(11)	-21(11)
C(74)	98(13)	174(13)	59(13)	10(15)	25(12)	-13(10)

Table 5. Hydrogen coordinates ($\times 10^4$) and isotropic displacement parameters ($\text{Å}^2 \times 10^3$) for ew1705.

	x	y	z	U(eq)
H(5A)	7374	8467	640	56
H(6A)	7959	9822	778	57
H(7A)	8328	10311	1793	55
H(14A)	6712	5530	3124	62
H(16A)	6557	2176	3316	83
H(18A)	6760	3452	1639	60
H(19A)	6414	3400	4161	155
H(19B)	6331	4699	4009	155
H(19C)	6839	4252	4271	155
H(20A)	6592	898	2450	138
H(20B)	6867	1334	1915	138
H(20C)	6318	1438	1819	138
H(22A)	5779	4933	1574	59
H(24A)	5294	3558	-127	78
H(26A)	6524	5155	150	54
H(27A)	4802	3554	662	137
H(27B)	4921	4386	1247	137
H(27C)	5117	3137	1296	137
H(28A)	5704	3665	-984	124
H(28B)	6251	3623	-769	124
H(28C)	6004	4779	-989	124
H(29A)	5535	8073	439	106
H(29B)	5705	7499	1107	106
H(29C)	5660	6771	478	106
H(30A)	6341	6971	-387	113
H(30B)	6767	7817	-248	113
H(30C)	6258	8285	-484	113
H(31A)	6724	9607	758	121
H(31B)	6536	9242	1384	121
H(31C)	6190	9749	803	121
H(33A)	8849	6676	3897	53
H(35A)	9003	5924	5757	63
H(37A)	8420	8859	5116	52
H(38A)	9491	4975	4901	129
H(38B)	9159	4902	4235	129
H(38C)	8994	4403	4850	129
H(39A)	8801	8555	6293	107

H(39B)	8822	7276	6511	107
H(39C)	8336	7844	6249	107
H(41A)	8468	10746	4943	72
H(43A)	9714	12244	5442	97
H(45A)	9474	10333	3863	67
H(46A)	8667	11610	5984	200
H(46B)	8750	12834	5727	200
H(46C)	9153	12217	6190	200
H(47A)	10185	12280	4336	143
H(47B)	10250	10971	4231	143
H(47C)	10379	11494	4921	143
H(48A)	8298	12318	3979	200
H(48B)	8411	13341	3552	200
H(48C)	8820	12576	3903	200
H(49A)	8830	12133	2148	215
H(49B)	9094	11124	2539	215
H(49C)	9158	12373	2802	215
H(50A)	7641	11386	2621	163
H(50B)	7884	11908	2076	163
H(50C)	7762	12689	2628	163
H(51A)	7583	3441	5322	326
H(51B)	7587	2970	6017	326
H(51C)	7109	3117	5550	326
H(53A)	7366	2097	4378	151
H(54A)	7382	342	4028	143
H(55A)	7495	-1139	4702	144
H(56A)	7620	-828	5821	136
H(57A)	7618	957	6183	137
H(58A)	9142	8387	2871	210
H(58B)	9550	8068	3428	210
H(58C)	9431	7265	2830	210
H(60A)	9566	7982	1830	193
H(61A)	10061	9208	1281	233
H(62A)	10587	10244	1848	246
H(63A)	10639	10304	2903	183
H(64A)	10208	9213	3475	150
H(65)	4447	9195	456	82
H(66)	4933	10406	1022	82
H(67)	5529	11374	596	93
H(65A)	4358	8703	-39	93
H(66A)	4665	9761	888	84
H(67A)	5282	10900	880	85
H(68A)	5374	6974	2885	192
H(68B)	5816	7204	2557	192
H(68C)	5352	6732	2150	192
H(70)	4626	7733	2147	142

H(71)	4291	9342	2087	123
H(72)	4558	11048	2302	120
H(73)	5427	11144	2569	120
H(74)	5790	9550	2368	131

Appendix 7

Atomic Coordinates for Geometry Optimized Computational Structures

Coordinates for 4.18

atom	angstroms		
	x	y	z
Zr1	0.0000000000	0.0000000000	-0.8823561943
C2	0.0000000000	0.0000000000	1.4099289479
C3	0.0000000000	0.0000000000	4.1968827216
C4	0.0000000000	1.2123378404	2.1102336309
C5	0.0000000000	-1.2123378404	2.1102336309
C6	0.0000000000	-1.2198854790	3.5119964268
C7	0.0000000000	1.2198854790	3.5119964268
H8	0.0000000000	-2.1622203237	4.0539582761
H9	0.0000000000	2.1622203237	4.0539582761
H10	0.0000000000	0.0000000000	5.2861555206
C11	0.0000000000	2.3869596231	1.2358106649
C12	0.0000000000	-2.3869596231	1.2358106649
N13	0.0000000000	2.1404978516	-0.1175405091
N14	0.0000000000	3.6820599537	1.5433578761
N15	0.0000000000	-2.1404978516	-0.1175405091
N16	0.0000000000	-3.6820599537	1.5433578761
C17	0.0000000000	3.3848401988	-0.6967721886
H18	0.0000000000	3.5137149802	-1.7700268459
C19	0.0000000000	4.3158740447	0.3219434154
H20	0.0000000000	5.3972459112	0.2467058445
C21	0.0000000000	-3.3848401988	-0.6967721886
H22	0.0000000000	-3.5137149802	-1.7700268459
C23	0.0000000000	-4.3158740447	0.3219434154
H24	0.0000000000	-5.3972459112	0.2467058445
Cl25	2.5143418143	0.0000000000	-1.0200041157
Cl26	0.0000000000	0.0000000000	-3.5052382059
Cl27	-2.5143418143	0.0000000000	-1.0200041157

Coordinates for 4.18.S

	angstroms		
atom	x	y	z
Zr1	0.0000000000	0.0000000000	-0.8823561943
C2	0.0000000000	0.0000000000	1.4099289479
C3	0.0000000000	0.0000000000	4.1968827216
C4	0.0000000000	1.2123378404	2.1102336309
C5	0.0000000000	-1.2123378404	2.1102336309
C6	0.0000000000	-1.2198854790	3.5119964268
C7	0.0000000000	1.2198854790	3.5119964268
H8	0.0000000000	-2.1622203237	4.0539582761
H9	0.0000000000	2.1622203237	4.0539582761
H10	0.0000000000	0.0000000000	5.2861555206
C11	0.0000000000	2.3869596231	1.2358106649
C12	0.0000000000	-2.3869596231	1.2358106649
N13	0.0000000000	2.1404978516	-0.1175405091
N14	0.0000000000	3.6820599537	1.5433578761
N15	0.0000000000	-2.1404978516	-0.1175405091
N16	0.0000000000	-3.6820599537	1.5433578761
C17	0.0000000000	3.3848401988	-0.6967721886
H18	0.0000000000	3.5137149802	-1.7700268459
C19	0.0000000000	4.3158740447	0.3219434154
H20	0.0000000000	5.3972459112	0.2467058445
C21	0.0000000000	-3.3848401988	-0.6967721886
H22	0.0000000000	-3.5137149802	-1.7700268459
C23	0.0000000000	-4.3158740447	0.3219434154
H24	0.0000000000	-5.3972459112	0.2467058445
Cl25	2.5143418143	0.0000000000	-1.0200041157
Cl26	0.0000000000	0.0000000000	-3.5052382059
Cl27	-2.5143418143	0.0000000000	-1.0200041157

Coordinates for 4.19

	angstroms		
atom	x	y	z
Zr1	-0.0028929943	0.0004120173	-2.2675708844
C2	-0.0027393522	-0.0005373487	0.0274096637
C3	-0.0018420441	-0.0004060689	2.8134312532
C4	0.0023992750	-1.2134881049	0.7321312720
C5	-0.0073590622	1.2127086626	0.7319466940
C6	-0.0064038900	1.2198472302	2.1339364381
C7	0.0023149560	-1.2207628893	2.1341225920

H8	-0.0092200215	2.1544621338	2.6801433019
H9	0.0056063208	-2.1553345261	2.6803790976
H10	-0.0014811148	-0.0002734938	3.9009940424
C11	0.0083062205	-2.3802850319	-0.1553062478
C12	-0.0142999210	2.3800478557	-0.1549207846
N13	0.0194819147	-2.1383505179	-1.4945231098
N14	-0.0003577481	-3.7043589253	0.0960437403
N15	-0.0318520416	2.1392457184	-1.4938461980
N16	-0.0004102438	3.7042061677	0.0971664013
C17	0.0164361157	-3.3658352812	-2.1098219840
H18	0.0221302872	-3.4647956149	-3.1845364385
C19	0.0046657164	-4.3267921374	-1.1365037026
H20	-0.0003821396	-5.4023031916	-1.2040489760
C21	-0.0280636912	3.3666200921	-2.1085648940
H22	-0.0375727346	3.4667369707	-3.1832009224
C23	-0.0092072511	4.3271974532	-1.1348985769
H24	-0.0009579621	5.4026943355	-1.2021381935
B25	-0.0150458786	-4.5075409632	1.4730139865
H26	0.9880210248	-4.2305073230	2.1117683221
H27	-0.0229798016	-5.6936324476	1.1775438963
H28	-1.0201954903	-4.2135506094	2.1003500709
B29	0.0256570623	4.5070013357	1.4741424182
H30	1.0316959292	4.2065525042	2.0968247658
H31	-0.9764418352	4.2364499691	2.1174380948
H32	0.0397431976	5.6930708431	1.1786412519
C133	-2.5004636433	-0.0496028521	-2.3742480314
C134	0.0210771296	-0.0289325371	-4.8627996391
C135	2.4953110418	0.0789683306	-2.3437926551

Coordinates for 4.19.S

atom	angstroms		
	x	y	z
Zr1	0.0000000000	0.0000000000	-1.0795634613
C2	0.0000000000	0.0000000000	1.2151538541
C3	0.0000000000	0.0000000000	4.0011779344
C4	0.0000000000	1.2131927453	1.9197764562
C5	0.0000000000	-1.2131927453	1.9197764562
C6	0.0000000000	-1.2202867690	3.3217913326
C7	0.0000000000	1.2202867690	3.3217913326
H8	0.0000000000	-2.1547657004	3.8681460815
H9	0.0000000000	2.1547657004	3.8681460815
H10	0.0000000000	0.0000000000	5.0887411162

C11	0.0000000000	2.3807987367	1.0331599163
C12	0.0000000000	-2.3807987367	1.0331599163
N13	0.0000000000	2.1415053022	-0.3064905253
N14	0.0000000000	3.7048642756	1.2866693769
N15	0.0000000000	-2.1415053022	-0.3064905253
N16	0.0000000000	-3.7048642756	1.2866693769
C17	0.0000000000	3.3696782593	-0.9195670341
H18	0.0000000000	3.4709578340	-1.9941121982
C19	0.0000000000	4.3292101864	0.0552953882
H20	0.0000000000	5.4048276027	-0.0106765960
C21	0.0000000000	-3.3696782593	-0.9195670341
H22	0.0000000000	-3.4709578340	-1.9941121982
C23	0.0000000000	-4.3292101864	0.0552953882
H24	0.0000000000	-5.4048276027	-0.0106765960
B25	0.0000000000	4.5061579195	2.6639471214
H26	-1.0034166783	4.2185285929	3.2975038761
H27	0.0000000000	5.6930215503	2.3718783124
H28	1.0034166783	4.2185285929	3.2975038761
B29	0.0000000000	-4.5061579195	2.6639471214
H30	-1.0034166783	-4.2185285929	3.2975038761
H31	1.0034166783	-4.2185285929	3.2975038761
H32	0.0000000000	-5.6930215503	2.3718783124
C133	2.5002091320	0.0000000000	-1.1518325776
C134	0.0000000000	0.0000000000	-3.6574993737
C135	-2.5002091320	0.0000000000	-1.1518325776

Coordinates for 4.20

angstroms			
atom	x	y	z
Zr1	-0.0037425528	-0.0095120414	-2.1464446799
C2	0.0026111835	-0.0106778576	0.1575893184
C3	-0.0080894809	-0.0033957721	2.9326882170
C4	-1.2318423516	-0.0405811624	0.8456856721
C5	1.2265603658	0.0216941112	0.8563015497
C6	1.2167509993	0.0248585608	2.2579594443
C7	-1.2269741454	-0.0356107405	2.2476406242
H8	2.1326700477	0.0530518086	2.8403530313
H9	-2.1464715106	-0.0586566646	2.8241715502
H10	-0.0128662988	0.0003100271	4.0179673130
C11	-2.4091479432	-0.0891940440	-0.0695585964
C12	2.3973740596	0.0683959318	-0.0661485754
N13	-2.1230151183	-0.1310403222	-1.3757180503
N14	-3.7902853352	-0.1114453125	0.0814766228
N15	2.0952678475	0.1111528729	-1.3738249312
N16	3.7746352110	0.0965865695	0.0714605387

C17	-3.2817950763	-0.1908406000	-2.0912451933
H18	-3.2984034725	-0.2359863839	-3.1689672545
C19	-4.3128541151	-0.1814893053	-1.2161630210
H20	-5.3676983540	-0.2175247516	-1.4087307404
C21	3.2531201395	0.1803194738	-2.1001721670
H22	3.2446183749	0.2249278983	-3.1757897064
C23	4.2877733376	0.1745979876	-1.2323744897
H24	5.3413584696	0.2166303137	-1.4310540953
Si25	-5.0476732532	-0.0082888754	1.4144694401
Si26	5.0463083885	-0.0168782346	1.3908940043
Ci27	-0.3975489650	2.4292722183	-2.0128815255
Ci28	0.8472742946	0.0502279787	-4.4856894025
Ci29	-0.1164737349	-2.4757239535	-2.0269739873
C30	6.7217506780	-0.0667321117	0.5269859600
H31	6.8374365382	-0.9209619805	-0.1462545660
H32	7.4917366974	-0.1680795722	1.2995788193
H33	6.9559096348	0.8462264222	-0.0278780153
C34	4.8127602208	-1.6234458000	2.3256283346
H35	4.8748182000	-2.4771881669	1.6440652906
H36	3.8582412262	-1.6964072442	2.8526047649
H37	5.6064396661	-1.7407907516	3.0695936609
C38	4.9682746582	1.5277398101	2.4487922668
H39	4.0290495832	1.6411945658	2.9957933657
H40	5.0964271593	2.4232769376	1.8318303716
H41	5.7780646054	1.5209617070	3.1857978951
C42	-4.9317417604	-1.5327160594	2.4962171711
H43	-5.0470497677	-2.4405674989	1.8966287656
H44	-5.7368311478	-1.5279982638	3.2379724264
H45	-3.9884175495	-1.6194898857	3.0374055857
C46	-4.8366364099	1.6138743344	2.3249311409
H47	-3.8780449534	1.7120562517	2.8400368526
H48	-5.6253197966	1.7272402600	3.0757064514
H49	-4.9202043141	2.4562616083	1.6333854677
C50	-6.7341214181	-0.0052052034	0.5714881631
H51	-6.9492757455	-0.9236983875	0.0200517485
H52	-6.8834108382	0.8440598528	-0.0990420493
H53	-7.4965115528	0.0750446693	1.3541261985

Coordinates for 4.20.S

atom	angstroms		
	x	y	z
C1	0.0000000000	0.0000000000	0.6068359567
C2	0.0000000000	0.0000000000	3.3844022636
C3	0.0000000000	1.2254002599	1.3023206378

C4	0.0000000000	-1.2254002599	1.3023206378
C5	0.0000000000	-1.2206926192	2.7035053611
C6	0.0000000000	1.2206926192	2.7035053611
H7	0.0000000000	-2.1371974361	3.2836940784
H8	0.0000000000	2.1371974361	3.2836940784
H9	0.0000000000	0.0000000000	4.4695369965
C10	0.0000000000	2.3939027555	0.3815801665
C11	0.0000000000	-2.3939027555	0.3815801665
N12	0.0000000000	2.1088243400	-0.9295637969
N13	0.0000000000	-2.1088243400	-0.9295637969
C14	0.0000000000	3.2776714945	-1.6398460474
H15	0.0000000000	3.2946117288	-2.7182826265
C16	0.0000000000	-3.2776714945	-1.6398460474
H17	0.0000000000	-3.2946117288	-2.7182826265
N18	0.0000000000	-3.7671650315	0.5376604375
C19	0.0000000000	4.3029636603	-0.7571505221
H20	0.0000000000	5.3613481569	-0.9382186851
C21	0.0000000000	-4.3029636603	-0.7571505221
H22	0.0000000000	-5.3613481569	-0.9382186851
N23	0.0000000000	3.7671650315	0.5376604375
Zr24	0.0000000000	0.0000000000	-1.7072211783
Cl25	2.4665492786	0.0000000000	-1.5148858347
Cl26	-2.4665492786	0.0000000000	-1.5148858347
Cl27	0.0000000000	0.0000000000	-4.1947350828
Si28	0.0000000000	4.9724586528	1.9187545425
C29	1.5786256522	4.7679895174	2.9054868321
H30	1.6239185477	5.5193401871	3.7007924601
H31	2.4528974156	4.9175968166	2.2653895800
H32	1.6845991634	3.7875084927	3.3744492646
C33	-1.5786256522	4.7679895174	2.9054868321
H34	-1.6239185477	5.5193401871	3.7007924601
H35	-1.6845991634	3.7875084927	3.3744492646
H36	-2.4528974156	4.9175968166	2.2653895800
C37	0.0000000000	6.6844270730	1.1353410604
H38	0.0000000000	7.4233316839	1.9439187623
H39	-0.8864064497	6.8835691436	0.5278952201
H40	0.8864064497	6.8835691436	0.5278952201
Si41	0.0000000000	-4.9724586528	1.9187545425
C42	0.0000000000	-6.6844270730	1.1353410604
H43	-0.8864064497	-6.8835691436	0.5278952201
H44	0.0000000000	-7.4233316839	1.9439187623
H45	0.8864064497	-6.8835691436	0.5278952201
C46	-1.5786256522	-4.7679895174	2.9054868321
H47	-2.4528974156	-4.9175968166	2.2653895800
H48	-1.6845991634	-3.7875084927	3.3744492646
H49	-1.6239185477	-5.5193401871	3.7007924601

C50	1.5786256522	-4.7679895174	2.9054868321
H51	2.4528974156	-4.9175968166	2.2653895800
H52	1.6239185477	-5.5193401871	3.7007924601
H53	1.6845991634	-3.7875084927	3.37444492646

Coordinates for 4.21

	angstroms		
atom	x	y	z
Zr1	-0.0250000000	-0.0030000000	-2.1550000000
C2	-0.0070000000	0.0000000000	0.1700000000
C3	0.0270000000	0.0010000000	2.8950000000
C4	-0.0040000000	-1.2270000000	0.8220000000
C5	0.0100000000	1.2280000000	0.8210000000
C6	0.0260000000	1.2270000000	2.2060000000
C7	0.0120000000	-1.2250000000	2.2080000000
H8	0.0400000000	2.1600000000	2.7690000000
H9	0.0150000000	-2.1570000000	2.7720000000
H10	0.0400000000	0.0020000000	3.9850000000
C11	-0.0180000000	-2.3640000000	-0.1010000000
C12	0.0090000000	2.3630000000	-0.1050000000
N13	-0.0300000000	-2.1250000000	-1.4170000000
N14	-0.0200000000	-3.6920000000	0.0240000000
N15	-0.0060000000	2.1210000000	-1.4200000000
N16	0.0210000000	3.6910000000	0.0190000000
C17	-0.0400000000	-3.2780000000	-2.1480000000
H18	-0.0500000000	-3.2420000000	-3.2210000000
C19	-0.0340000000	-4.2910000000	-1.2240000000
H20	-0.0380000000	-5.3640000000	-1.2650000000
C21	-0.0040000000	3.2730000000	-2.1520000000
H22	-0.0150000000	3.2360000000	-3.2260000000
C23	0.0130000000	4.2870000000	-1.2300000000
H24	0.0220000000	5.3610000000	-1.2720000000
B25	-0.0110000000	-4.3730000000	1.1940000000
F26	0.9840000000	-4.0960000000	1.8070000000
F27	-0.0190000000	-5.5950000000	1.0040000000
F28	-0.9900000000	-4.0860000000	1.8280000000
B29	0.0400000000	4.3740000000	1.1870000000
F30	1.0310000000	4.0840000000	1.8010000000
F31	-0.9430000000	4.1010000000	1.8220000000
F32	0.0490000000	5.5940000000	0.9970000000
Cl33	-2.4460000000	0.0260000000	-2.3870000000
Cl34	-0.0350000000	0.0020000000	-4.5880000000
Cl35	2.3930000000	-0.0110000000	-2.4160000000

Coordinates for 4.21.S

atom	angstroms		
	x	y	z
Zr1	0.0000000000	0.0000000000	-1.6593602078
C2	0.0000000000	0.0000000000	0.6360227852
C3	0.0000000000	0.0000000000	3.4171489624
C4	0.0000000000	1.2164638177	1.3387690018
C5	0.0000000000	-1.2164638177	1.3387690018
C6	0.0000000000	-1.2216707365	2.7395047888
C7	0.0000000000	1.2216707365	2.7395047888
H8	0.0000000000	-2.1506228306	3.2955372190
H9	0.0000000000	2.1506228306	3.2955372190
H10	0.0000000000	0.0000000000	4.5039200366
C11	0.0000000000	2.3851407557	0.4412741023
C12	0.0000000000	-2.3851407557	0.4412741023
N13	0.0000000000	2.1293561438	-0.8883815375
N14	0.0000000000	3.7243922551	0.6556049021
N15	0.0000000000	-2.1293561438	-0.8883815375
N16	0.0000000000	-3.7243922551	0.6556049021
C17	0.0000000000	3.3412818826	-1.5353863398
H18	0.0000000000	3.4119794245	-2.6120178055
C19	0.0000000000	4.3245480063	-0.5927517525
H20	0.0000000000	5.3962297114	-0.6845177535
C21	0.0000000000	-3.3412818826	-1.5353863398
H22	0.0000000000	-3.4119794245	-2.6120178055
C23	0.0000000000	-4.3245480063	-0.5927517525
H24	0.0000000000	-5.3962297114	-0.6845177535
B25	0.0000000000	4.6023815811	1.9810014456
B26	0.0000000000	-4.6023815811	1.9810014456
Cl27	2.4953409219	0.0000000000	-1.6832452344
Cl28	0.0000000000	0.0000000000	-4.2302627253
Cl29	-2.4953409219	0.0000000000	-1.6832452344
F30	-1.1509325298	-4.3272338123	2.7318065112
F31	1.1509325298	-4.3272338123	2.7318065112
F32	0.0000000000	-5.9523657360	1.5676426569
F33	-1.1509325298	4.3272338123	2.7318065112
F34	1.1509325298	4.3272338123	2.7318065112
F35	0.0000000000	5.9523657360	1.5676426569

Coordinates for 4.22

atom	angstroms		
	x	y	z
Zr1	-0.0002875215	-0.0012335840	-2.2843189387
C2	0.0003211737	-0.0032979507	0.0399995832
C3	0.0002350603	-0.0008542995	2.8351366060
C4	1.2095651755	0.0020876690	0.7477727763
C5	-1.2090798118	-0.0065393728	0.7476546686
C6	-1.2144014846	-0.0064264490	2.1507025473
C7	1.2149299499	0.0040213987	2.1508182222
H8	-2.1306787064	-0.0113915244	2.7281737858
H9	2.1311637927	0.0098801027	2.7283616704
H10	0.0001743873	-0.0001264094	3.9199702439
C11	2.3645272102	0.0066682484	-0.1533091414
C12	-2.3643178561	-0.0101675863	-0.1531299899
N13	2.1648805169	0.0146615263	-1.4827093085
N14	3.7021608498	0.0016053118	0.0930020892
N15	-2.1651915431	-0.0208773473	-1.4824632645
N16	-3.7019464791	-0.0003376819	0.0934693036
C17	3.3955064080	0.0151054274	-2.0910478663
H18	3.5024027265	0.0207616143	-3.1638529548
C19	4.3586810224	0.0068888164	-1.1284578621
H20	5.4342268521	0.0042187614	-1.1910678267
C21	-3.3958244237	-0.0190590081	-2.0905254734
H22	-3.5031433282	-0.0265033991	-3.1632968142
C23	-4.3587454645	-0.0060451484	-1.1277670692
H24	-5.4342674365	-0.0002051610	-1.1902685149
C25	4.3778105021	-0.0105727409	1.3842079837
H26	4.1289673583	0.8815662577	1.9601491033
H27	5.4519265077	-0.0214911732	1.2088995565
H28	4.1097193917	-0.9018943211	1.9524671830
C29	-4.3772811597	0.0186334958	1.3846884134
H30	-4.1032735049	0.9093340320	1.9510348575
H31	-4.1342202458	-0.8739289266	1.9624535976
H32	-5.4513012907	0.0362626795	1.2094189095
Cl33	0.0267235239	-2.4606655445	-2.1489816556
Cl34	0.0132351940	0.0108423514	-4.7675792292
Cl35	-0.0398907256	2.4574927365	-2.1352348787

Coordinates for 4.22.S

	angstroms		
atom	x	y	z
Zr1	0.0000000000	0.0000000000	-1.1420938878
C2	0.0000000000	0.0000000000	1.1828753089
C3	0.0000000000	0.0000000000	3.9784332868
C4	0.0000000000	1.2092614701	1.8908090723
C5	0.0000000000	-1.2092614701	1.8908090723
C6	0.0000000000	-1.2146142188	3.2939009593
C7	0.0000000000	1.2146142188	3.2939009593
H8	0.0000000000	-2.1308130121	3.8715176199
H9	0.0000000000	2.1308130121	3.8715176199
H10	0.0000000000	0.0000000000	5.0632789270
C11	0.0000000000	2.3645127085	0.9900643216
C12	0.0000000000	-2.3645127085	0.9900643216
N13	0.0000000000	2.1646919413	-0.3397217950
N14	0.0000000000	3.7018955848	1.2365063496
N15	0.0000000000	-2.1646919413	-0.3397217950
N16	0.0000000000	-3.7018955848	1.2365063496
C17	0.0000000000	3.3960811283	-0.9477238362
H18	0.0000000000	3.5032078299	-2.0206075852
C19	0.0000000000	4.3586973668	0.0154862818
H20	0.0000000000	5.4342294048	-0.0468793307
C21	0.0000000000	-3.3960811283	-0.9477238362
H22	0.0000000000	-3.5032078299	-2.0206075852
C23	0.0000000000	-4.3586973668	0.0154862818
H24	0.0000000000	-5.4342294048	-0.0468793307
C25	0.0000000000	4.3773801481	2.5277958544
H26	-0.8917185537	4.1190278833	3.1000685192
H27	0.0000000000	5.4515757592	2.3527778949
H28	0.8917185537	4.1190278833	3.1000685192
C29	0.0000000000	-4.3773801481	2.5277958544
H30	-0.8917185537	-4.1190278833	3.1000685192
H31	0.8917185537	-4.1190278833	3.1000685192
H32	0.0000000000	-5.4515757592	2.3527778949
C133	2.4607622045	0.0000000000	-1.0016946927
C134	0.0000000000	0.0000000000	-3.6255751756
C135	-2.4607622045	0.0000000000	-1.0016946927

Coordinates for 4.23

	angstroms		
atom	x	y	z
Zr1	-0.0265728637	0.0007622980	-2.2540706883
C2	-0.0112556621	0.0160440005	0.0620349353
C3	-0.0120062864	0.0108613469	2.8569375364
C4	1.1979735555	0.0056672723	0.7761056835
C5	-1.2279185850	0.0234234620	0.7713262249
C6	-1.2263233810	0.0244038291	2.1737142561
C7	1.2041965796	0.0005648763	2.1773983748
H8	-2.1394393635	0.0374044320	2.7521773577
H9	2.1187590748	-0.0105377101	2.7539770708
H10	-0.0142894522	0.0085954320	3.9411515357
C11	2.3520574476	0.0024743257	-0.1339673583
C12	-2.4003415210	0.0381847894	-0.1193849678
N13	2.1301823910	-0.0041326159	-1.4511424064
N14	3.7199444429	0.0118380577	0.0597133470
N15	-2.2142102315	0.0725375911	-1.4344708526
N16	-3.7710305096	0.0244099995	0.1087451377
C17	3.3412505638	0.0030629072	-2.1085920948
H18	3.3909479798	0.0008151904	-3.1849607803
C19	4.3406285029	0.0124404770	-1.1988030100
H20	5.4099491046	0.0183752917	-1.3039050678
C21	-3.4359772067	0.0881450629	-2.0627187204
H22	-3.5285349552	0.1201273303	-3.1360238210
C23	-4.4175415247	0.0584589192	-1.1321515095
H24	-5.4888045039	0.0563788220	-1.2138245163
C25	4.4608561131	0.0187354938	1.2845222055
C26	-4.4897217035	-0.0456211192	1.3437648061
Cl27	-0.4916241396	-2.4081742518	-2.1708958826
Cl28	1.0033065191	-0.1321714886	-4.5018978347
Cl29	-0.3206246908	2.4326431800	-2.3024153878
F30	-4.2605472545	1.0264954233	2.1165555778
F31	-4.1536968220	-1.1355626761	2.0480968705
F32	-5.8031085187	-0.1008025280	1.0927512291
F33	4.1742290322	1.0943852276	2.0314629070
F34	4.2030503940	-1.0698137526	2.0238412879
F35	5.7693496702	0.0397164799	1.0115632292

Coordinates for 4.23.S

	angstroms		
atom	x	y	z
Zr1	0.0000000000	0.0000000000	-1.6564473246
C2	0.0000000000	0.0000000000	0.6603482122
C3	0.0000000000	0.0000000000	3.4441318717
C4	0.0000000000	1.2190342917	1.3631041702
C5	0.0000000000	-1.2190342917	1.3631041702
C6	0.0000000000	-1.2204002722	2.7653296922
C7	0.0000000000	1.2204002722	2.7653296922
H8	0.0000000000	-2.1359777099	3.3443842363
H9	0.0000000000	2.1359777099	3.3443842363
H10	0.0000000000	0.0000000000	4.5284596077
C11	0.0000000000	2.3752059014	0.4422306370
C12	0.0000000000	-2.3752059014	0.4422306370
N13	0.0000000000	2.1373583891	-0.8706013214
N14	0.0000000000	3.7555212180	0.6007306608
N15	0.0000000000	-2.1373583891	-0.8706013214
N16	0.0000000000	-3.7555212180	0.6007306608
C17	0.0000000000	3.3278469992	-1.5575672763
H18	0.0000000000	3.3641176530	-2.6348874118
C19	0.0000000000	4.3460497569	-0.6712846654
H20	0.0000000000	5.4123374966	-0.8008051906
C21	0.0000000000	-3.3278469992	-1.5575672763
H22	0.0000000000	-3.3641176530	-2.6348874118
C23	0.0000000000	-4.3460497569	-0.6712846654
H24	0.0000000000	-5.4123374966	-0.8008051906
C25	0.0000000000	4.5528599332	1.7914988777
C26	0.0000000000	-4.5528599332	1.7914988777
Cl27	2.4510830465	0.0000000000	-1.4380350632
Cl28	0.0000000000	0.0000000000	-4.1288037946
Cl29	-2.4510830465	0.0000000000	-1.4380350632
F30	-1.0825526008	-4.3197816609	2.5452522187
F31	1.0825526008	-4.3197816609	2.5452522187
F32	0.0000000000	-5.8486877511	1.4521444510
F33	-1.0825526008	4.3197816609	2.5452522187
F34	1.0825526008	4.3197816609	2.5452522187
F35	0.0000000000	5.8486877511	1.4521444510

Coordinates for 4.24

	angstroms		
atom	x	y	z
Zr1	-0.0024653149	-0.0233913954	-2.2274004216
C2	0.0001231212	-0.0225509700	0.0938390331
C3	0.0002617404	-0.0250010524	2.8942792252
C4	1.2020212696	-0.0259633540	0.8054174219
C5	-1.2021326738	-0.0209952260	0.8053262355
C6	-1.2143021121	-0.0215375167	2.2056073068
C7	1.2149193216	-0.0275766399	2.2056238423
H8	-2.1416540943	-0.0195184408	2.7737170116
H9	2.1424030310	-0.0309768329	2.7735980097
H10	0.0002712090	-0.0258348917	3.9788465886
C11	2.3536148570	-0.0272380554	-0.0884966178
C12	-2.3555297559	-0.0204251471	-0.0864279338
N13	2.1851021884	-0.0250960505	-1.4183622202
N14	3.6790994824	-0.0279800892	0.1846322309
N15	-2.1910587975	-0.0199683676	-1.4165440963
N16	-3.6804191230	-0.0254495748	0.1902863744
C17	3.4367626209	-0.0228313170	-1.9940020473
H18	3.5694429240	-0.0194821957	-3.0638468774
C19	4.3801871532	-0.0249976934	-1.0101839815
H20	5.4564192591	-0.0255684059	-1.0448839165
C21	-3.4442091559	-0.0266413471	-1.9886145202
H22	-3.5809844894	-0.0287747131	-3.0579165447
C23	-4.3847129838	-0.0294703504	-1.0022821820
H24	-5.4609255707	-0.0327127004	-1.0343332000
C125	-0.0175611689	-2.4780393758	-2.0752238386
C126	0.0699757108	-0.0233977361	-4.7054405916
C127	-0.0168386467	2.4315910794	-2.0784233643
H28	-4.0862208215	-0.0273471103	1.1118030420
H29	4.0872606265	-0.0289601210	1.1053864328

Coordinates for 4.24.S

	angstroms		
atom	x	y	z
Zr1	0.0000000000	0.0000000000	-0.9729966652
C2	0.0000000000	0.0000000000	1.3478387209
C3	0.0000000000	0.0000000000	4.1477357766
C4	0.0000000000	1.2020284135	2.0586416224
C5	0.0000000000	-1.2020284135	2.0586416224
C6	0.0000000000	-1.2146922257	3.4589508747
C7	0.0000000000	1.2146922257	3.4589508747
H8	0.0000000000	-2.1420841266	4.0272490794
H9	0.0000000000	2.1420841266	4.0272490794
H10	0.0000000000	0.0000000000	5.2323888513
C11	0.0000000000	2.3540827615	1.1655479268
C12	0.0000000000	-2.3540827615	1.1655479268
N13	0.0000000000	2.1879151155	-0.1646133343
N14	0.0000000000	3.6794143067	1.4409991078
N15	0.0000000000	-2.1879151155	-0.1646133343
N16	0.0000000000	-3.6794143067	1.4409991078
C17	0.0000000000	3.4402822944	-0.7382164645
H18	0.0000000000	3.5756759345	-1.8077752722
C19	0.0000000000	4.3826722666	0.2471007217
H20	0.0000000000	5.4592415103	0.2139246676
C21	0.0000000000	-3.4402822944	-0.7382164645
H22	0.0000000000	-3.5756759345	-1.8077752722
C23	0.0000000000	-4.3826722666	0.2471007217
H24	0.0000000000	-5.4592415103	0.2139246676
Cl25	2.4543468665	0.0000000000	-0.8157162078
Cl26	0.0000000000	0.0000000000	-3.4521083645
Cl27	-2.4543468665	0.0000000000	-0.8157162078
H28	0.0000000000	-4.0864002344	2.3626214984
H29	0.0000000000	4.0864002344	2.3626214984